The Design, Synthesis, and Microbiological Investigation of Tobramycin Catecholate Conjugates

By

Joseph Rebizant

A Thesis submitted to the Faculty of Graduate Studies of

The University of Manitoba

In partial fulfillment of the requirement of the degree of

MASTER OF SCIENCE

Department of Chemistry

University of Manitoba

Winnipeg, Manitoba, Canada

Abstract

With the ever-growing threat of multi-drug resistant (MDR) bacteria to the public health, there is a mounting need for the development of novel therapeutics to combat them. Sideromycins are an emerging approach to develop new therapeutics by covalently linking siderophore ligands to antibiotics. This allows these sideromycins to exploit the siderophore uptake mechanism that are fundamental to bacteria, allowing the antibiotic to transverse the bacterial membrane and bypass resistant factors, analogous to a Trojan Horse. Aminoglycosides are a class of broad-spectrum antibiotics that inhibit protein synthesis and are usually reserved for severe bacterial infections, especially those that are caused by Gram-negative bacteria. A common form of resistance against aminoglycoside that develop in clinically isolated Gram-negative bacteria, especially in *Pseudomonas aeruginosa* strains, is outer membrane impermeability to aminoglycosides. In theory, conjugation of aminoglycosides with a siderophore moiety will allow the aminoglycoside increased access to their intercellular target by exploiting the siderophore uptake system and bypassing impermeability resistance factors. In this study, a new series of aminoglycoside-siderophore conjugates are synthesized by conjugating the aminoglycoside tobramycin to 3,4-dihydroxybenzoic acid, a siderophore ligand, resulting in tobramycin-catecholate (TOB-CAT) conjugates. To elucidate the significance of the catecholate to the activity of the TOB-CAT conjugates, methoxy protected tobramycin-catecholate (TOB-mCAT) conjugates were also synthesized, where the added methoxy groups block the binding capabilities of the catecholate component. *In vitro* antibacterial studies in MHB show that these TOB-CAT conjugates have *P. aeruginosa* specific activity, reaching tobramycin susceptibility breakpoints in three *P. aeruginosa* clinically isolated strains. These studies also showed that the TOB-mCAT conjugates have no activity against the tested Gram-negative strains, indicating the

catecholate for the activity observed by the TOB-CAT conjugates. *In vitro* antibacterial studies in iron deficient cation-adjusted MHB (ID-CAMHB) show a total loss of significant activity of the TOB-CAT conjugates against *P. aeruginosa* clinical isolates. *In vitro* combination studies indicate that both the TOB-CAT and TOB-mCAT conjugates are capable of synergizing legacy antibiotics, particularly novobiocin and rifampicin, against Gram-negative bacterial strains in MHB. These combination results, along with results from an NPN outer membrane against PAO1 bacterial cells assay, suggest that both the TOB-CAT and TOB-mCAT conjugates have an outer membrane permeabilization mode of action.

Acknowledgements

I would first like acknowledge my supervisor Dr. Schweizer for his knowledge, support, and guidance throughout my project. The skills and qualities I have learned from this experience I will carry with me forever.

I would also like to thank the rest of my committee members, Dr. Rebecca Davis, and Dr. Ayush Kumar, for taking the time to guide me on my project and giving me valuable advice on my work.

A special thanks to our collaborators Dr. George Zhanel and Dr. Ayush Kumar who contributed to this research.

I wish to thank the members of the Schweizer Research Group, especially Dr. Ronald Domalaon, Dr. Shiv Dhiman, and Dr. Ayan Mukherjee for their mentorship and guidance with my project. I would like to thank Danyel Ramirez and Danzel Ramirez for advising me in the microbiology lab. All the members of the group created a positive working atmosphere, and I will cherish their friendship forever.

I am grateful for the constant support from my friends and family, especially my mother Marlene Rebizant, my father Ken Rebizant, and my girlfriend Nicole Muchow. They inspire me to be the best version of myself everyday.

Table of Contents

Abstract ..... **i**

Acknowledgements ..... **iii**

Table of Contents ..... **iv**

List of Abbreviations ..... **viii**

Chapter 1: Background and Introduction **1**

1.1 Introduction 1

1.2 Aminoglycosides 3

1.2.1 History of Aminoglycosides 3

1.2.2 Classification of Aminoglycosides 4

1.2.3 Mechanism of Action 7

1.2.4 Mechanism of Resistance 12

1.2.5 Aminoglycoside Toxicity 16

1.3 Siderophores 19

1.3.1 Introduction to Siderophores 19

1.3.2 The Discovery of Siderophores 20

1.3.3 Siderophore Classification 21

1.3.4 The Iron Tug of War 25

1.3.5 Siderophore Secretion 28

1.3.6 Mechanism for Iron-Siderophore Uptake 31

1.3.7 Evolutionary and Social Aspects of Siderophores 33

1.4 Sideromycins 37

1.4.1 The Trojan Horse Approach 37

1.4.2 Introduction to Sideromycins 38

1.4.3 Natural Occurring Sideromycins 40

1.4.4 Synthetic Sideromycins 44

1.4 References 49

Chapter 2: Thesis Objectives 60
2.1 The Thesis Purpose 60
2.2 The Thesis Objectives 61
2.3 Thesis Organization 62
Chapter 3: Design and Synthesis of Conjugates 63
3.1 Chemical Synthesis 63
3.1.1 Synthesis of the Active Tobramycin-Catechol Conjugates 63
3.1.2 Synthesis of the Control Tobramycin-Catechol Conjugates 68
3.2 Discussion 71
3.2.1 Rationalization of Component Selection 71
3.2.2 Obstacles Encountered During Synthesis 74
3.3 References 83
Chapter 4: Microbiology Studies 87
4.1 Antibacterial Activity 87
4.1.1 Antimicrobial Activity of Active Compounds in MHB 87
4.1.2 Antimicrobial Activity of Active Compounds in ID-CAMHB 89
4.1.3 Antimicrobial Activity of Control Compounds in MHB 91
4.1.4 Antimicrobial Activity of Active Compounds in ID-CAMHB 92
4.2 Combination Studies 94
4.2.1 Combination Studies of Active Compounds Against Wild-type Gram-negative Strains 94
4.2.2 Combination Studies of Active Compounds Against Gram-negative Clinical Isolates 104
4.2.3 Combination Studies of Control Compounds Against Wild-type Gram-negative Strains 110
4.2.4 Combination Studies of Active Compounds Against Gram-negative Clinical Isolates 115
4.3 Discussion 121
4.3.1 The Effects of the Catechol Group on the Antibacterial Activity of the Active Conjugates 121

4.3.2 The Effects of The Catechol Group on the Adjuvant Activity of the Active Conjugates 124

4.3.3 The Effects of the Alkyl Tether Length on the Adjuvant Activity of the Conjugates 130

4.3.4 The Effects of ID-CAMHB on the Activity of the Active Conjugates 132

4.3 References 135

Chapter 5: Mechanistic Studies 137

5.1 Membrane Permeabilization 137

5.1.1 NPN Outer Membrane Permeabilization Assay 137

5.1.2 Synergy of Rifampicin and Novobiocin Against Gram-negative Bacteria 139

5.2 Discussion 142

5.2.1 Possible Modes of Action of Active Conjugates 142

5.3 References 148

Chapter 6: Conclusion and Future Work 151

6.1 General Conclusion 151

6.2 Future Work 152

6.2.1 Future Studies 152

6.2.2 Future Synthetic Work 153

6.3 References 156

Chapter 7: Supporting Information 157

7.1 Experimental Section 157

7.1.1 Synthetic Chemistry 157

7.2 Microbiology 182

7.2.1 Bacterial Isolates 182

7.2.2 Minimum Inhibitory Concentration Determination 182

7.2.3 Antibacterial Combination Screening 181

7.2.4 Outer membrane Permeabilization Assay 182

7.3 References 184

7.4 Tables 186
7.5 NMR Spectra.....187
7.6 Mass Spectra 223

List of Abbreviations

ABC	ATP-binding cassette
ACC	aminoglycoside N-acetyltransferases
AME	aminoglycoside modifying enzyme
ANT	aminoglycoside O-nucleotidyltransferases
APH	aminoglycoside O-phosphotransferases
aq	aqueous
ATCC	American Type Culture Collection
Boc	tert-butyloxycarbonyl
Boc)2O	di-tert-butyl dicarbonate
CAN-ICU	Canadian National Intensive Care Unit
CANWARD	Canadian Ward Surveillance
cat.	catalyst
CAT	catecholate
CDC	Centers for Disease Control
CE	common era
CLSI	Clinical and Laboratory Standards Institute
DBP	dibasic peptides

DCM	dichloromethane
DHBS	2,3-dihydroxybenzoylserine
DIPEA	*N*,*N*-diisopropylethylamine
DMF	dimethyl formamide
EDPI	energy dependent phase I
EDPII	energy dependent phase I
EIN	Emerging Infectious Network
EPI	efflux pump inhibitors
Et_3N	triethylamine
FDA	Food and Drug Administration
FDC	Cefiderocol
Fe-S	iron-sulfur
FIC	fractional inhibitory concentration
FICI	fractional inhibitory concentration index
Fpn	ferroprotein
GNAT	GCN5-related N-acetyltransferase
HATU	Hexafluorophosphate Azabenzotriazole Tetramethyl Uronium
HBTU	Hexafluorophosphate benzotriazole Tetramethyl Uronium

ICUs	intensive care units
ID-CAMHB	iron deficient cation adjusted Mueller-Hinton broth
IDSA	Infectious Diseases Society of America
IM	inner membrane
Lcn-2	lipocalin 2
IL	interleukin
J	coupling constant (in NMR)
LPS	lipopolysaccharide
mCAT	methoxy protected catecholate
McC	Microcin C
MATE	multidrug and toxic compound extrusion
MDR	multidrug-resistant
MeOH	methanol
MFS	major facilitator superfamily
MHB	Mueller-Hinton broth
MIC	minimum inhibitory concentration
MIN	minocycline
NEB	nebramine

NMP	1-naphthylmethyl piperazine
NPN	1-N-phenylnaphthylamine
OM	outer-membrane
OMP	outer-membrane protein
OMR	outer-membrane receptor
PAR	paroxetine
PBP	periplasmic binding proteins
PDR	pandrug-resistant
PMB	p-Methoxybenzyl
PMB-Cl	p-methoxybenzyl chloride
PMBN	polymyxin B nonapeptide
ppm	parts per million
RIF	rifampicin
RND	resistance-nodulation-division
ROS	reactive oxygen species
ROSET	rotational surveillance and energy transfer
SerRS	seryl-tRNA synthetase
SMR	small multidrug resistance

SPC	sugar phosphate cyclase
RMT	16S rRNA methyltransferase
rt	room temperature
TBAHS	tetrabutylammonium hydrogen sulfate
TBDMS	tert-butyldimethylsilyl
TBDMSCl	tert-butyldimethylsilyl chloride
TBTU	tetrafluoroborate benzotriazole **T**etramethyl **U**ronium
tBu	tert-buty
THF	tetrahydrofuran
TOB	tobramycin
WHO	World Health Organization
WT AB	wild-type *Acinetobacter baumannii*
WT EC	wild-type *Escherichia coli*
XDR	extensively drug-resistant
2-DOS	2-deoxystreptamine
δ	chemical shift in parts per million
ψ	membrane potential

Chapter 1: Background and Introduction

1.1 INTRODUCTION

The rapid emergence of antibiotic resistant bacteria is a persisting and growing challenge the world faces in modern medicine[1]. The IDSA Emerging Infectious Network (EIN) conducted a survey in 2011 of infectious-disease specialists which found that more than 60% of the participants had seen a pandrug-resistant (PDR), untreatable bacterial infection in the past year[1]. This rise in emerging antibiotic resistant bacteria can be attributed to several factors: the misuse and overuse of antibiotics in both medicine and agriculture, along with the inadequate research and development of novel antibiotics by pharmaceutical companies[1]. This has created an urgent need for the development of novel therapeutics to combat these multi-drug resistant (MDR) bacterial infections[1]. MDR pathogens are defined as having acquired non-susceptibility to at least one agent in three or more antimicrobial categories, and PDR pathogens have acquired non-susceptibility to all known agents in all antimicrobial categories[2]. If no significant novel treatments are found by 2050, a review cited by the Centers for Disease Control (CDC) and the World Health Organization (WHO), "Antimicrobial Resistance: Tackling a crisis for the health and wealth of nations", has estimated that we could potentially see MDR bacterial infections causing 10 million annual deaths globally[3].

In the pre-antibiotic era, countless lives were lost due to uncontrolled bacterial infections that could be treated today[4]. Antibiotics are one of the most successful forms of chemotherapy in the history of medicine that work to kill or inhibit the growth of bacteria[5]. There is evidence to suggest that ancient humans had some knowledge for treating bacterial infection; from the ancient Egyptians applying moldy bread on wounds to trace amounts of tetracyclines being

found in the skeletal remains of ancient Sudanese Nubia dating back to 350–550 CE[5,6]. Penicillin is considered to be the first antibiotic discovered, where in 1928 the bacteriologist Alexander Fleming returned to his laboratory after a vacation and noticed on one of his leftover agar plates there was bacterial growth inhibited around a mold colony[5,7]. He isolated the mold and identified it as part of the genus *Penicillium*, and thus he named the active agent penicillin[5,7]. This was the spark that ignited the field of antibiotic research, revolutionizing medicine. Since then, 22 different classes of antibiotics have been discovered[5,8]. These classes categorize antibiotics based on similarities in chemical structure and mode of action. One of the most prescribed and well-known class of antibiotics is the β-lactams[9]. Members of this class contain a β-lactam ring and inhibit the formation of peptidoglycan, a component of the bacterial cell wall, by binding to penicillin binding proteins[9].

Aminoglycosides are a broad-spectrum class of antibiotics that act to inhibit protein synthesis[10]. They are among the first agents to be used for routine clinical use and have been a cornerstone of antibacterial chemotherapy since the streptomycin was introduced in 1944[10]. Widespread use of aminoglycosides as a first-line agent against bacterial infections led to the evolution of bacterial resistance to them[10]. Along with the growing resistance, there are several adverse effects that accompanies aminoglycoside use, which include nephrotoxicity and ototoxicity[10–12]. These factors led to a shift away from aminoglycosides, in favour of third-generation cephalosporins, carbapenems and fluoroquinolones in the 1980's, due to lower toxicity and broader activity[10]. Now, with the increasing resistance growing to these antibiotics there has been a renewed interest in aminoglycosides for the development of novel agents and use in combination therapy to treat MDR bacterial infections[10].

With the ever-growing threat of antibiotic resistance bacteria there is a growing need of novel therapeutics to combat them. This research uses the "Trojan Horse" strategy to develop and explore aminoglycoside-siderophores to treat resistant bacterial infections. In theory, these aminoglycoside-siderophore conjugates will be able to exploit the Fe^{3+}-siderophore uptake system, increasing the concentration of the conjugate in the bacterial cytoplasm. This will allow greater access of the conjugate to their inner target and bypass outer membrane impermeability resistant mechanisms that are common in clinically isolated Gram-negative bacteria. This will hopefully open up a pathway to modify aminoglycosides to restore their antibacterial activity against MDR pathogens that were once resistant. To test this premise, active tobramycin-catecholate (TOB-CAT) were synthesized and were tested against a variety of strains of bacteria for antibacterial and adjuvant activity.

1.2 AMINOGLYCOSIDES

1.2.1 History of Aminoglycosides

Aminoglycosides are a group of polycationic antibiotics produced naturally or derived semi-synthetically from natural products produced by the Actinomycetes[10]. The actinomycetes are an extremely diverse group of Gram-positive bacteria, being ubiquitous in both aquatic and terrestrial environments[13]. They are one of the largest bacterial phyla with over 350 known genera to date[13]. The Actinomycetes have yielded many clinically essential molecules, with approximately two thirds of all known antibiotics derived from them, with the most significant species being *Streptomyces*[13].

Inspired by the discovery of penicillin in 1928, the first aminoglycoside was isolated from a strain of *Streptomyces griseus* in 1944 in a planned screening for antimicrobial substances[14]. This aminoglycoside came to be known streptomycin, of which has our knowledge and understanding of aminoglycosides have become based around[10,14]. Streptomycin unlike many antibiotics at the time was found to have a broad range of antibiotic activity, having activity against most Gram-negative bacteria, few Gram-positive bacteria, and against *Mycobacterium tuberculosis*[15]. In the proceeding years several other aminoglycosides were introduced to the clinical world, including neomycin (1949, *Streptomyces fradiae*), kanamycin (1957, *Streptomyces kanamyceticus*), gentamicin (1963, Micromonospora purpurea), and tobramycin (1967, *Streptomyces tenebrarius*)[10,14]. Aminoglycosides are isolated primarily from two groups of Actinomycetes, the *Streptomyces* (Aminoglycosides with the -mycin suffix) and the *Micromonospora* (Aminoglycosides with the -micin suffix)[14]. The other semisynthetic aminoglycosides are derivatives of naturally formed aminoglycosides, like netilmicin (derived from sisomicin) and amikacin (derived from kanamycin)[14]. These analogs were designed to overcome common resistance mechanism employed by bacteria[10,14]. As a class, aminoglycosides with their broad activity have been an effective agent employed to deal with life threatening infections for decades[10,14].

1.2.2 Classification of Aminoglycosides

Aminoglycosides are poly cationic amino sugar molecules[10,16]. Aminoglycosides typically consists of one central aminocyclitol ring linked to one or more amino sugars via a pseudoglycosidic linkages[16]. Aminocyclitol rings are amino polyhydroxy cycloalkanes that are a component of a variety of natural and biologically active products derived from

microorganisms[17]. Enzymes known as sugar phosphate cyclases (SPCs) form aminocyclitols from simple sugar units, typically forming six-membered rings[17]. The aminocyclitol that is typical in aminoglycosides is the 2-deoxystreptamine (2-DOS) ring[10,16,17].

2-Deoxystreptamine is a cyclohexane with two amines substituted at the 1 and 3 carbon position, and three alcohol groups substituted at the 4, 5, and 6 carbon position[10,16,17]. Aminoglycosides are classified into 4 general groups based off their structure: (1) 4-mono-substituted-2-DOS ring; (2) 4,5-disubstituted-2-DOS ring; (3) 4,6-disubsituted-2-DOS ring; (4) aminoglycosides without DOS ring[10,16].

Most aminoglycosides are in the 4,5-disubstituted- and 4,6-disubsituted-2-DOS ring classes, with few belonging in the other two groups[10,16]. The 4,5-disubstitued-2-DOS aminoglycosides have two glycosides substituted at the 4 and 5 position of the 2-DOS centre ring[10,16]. This class includes aminoglycosides such as neomycin B, ribostamycin, and paromomycin (Figure 1a). The 4,6-disubstituted-2-DOS aminoglycosides have two glycosides substituted at the hydroxy groups located at the 4 and 6 positions of the 2-DOS centre ring[10,16]. The accepted nomenclature for these two classes of aminoglycosides is to refer to the amino sugar attached to the 4-carbon position of the 2-DOS as ring I, the 2-DOS as ring II, and the amino sugar ring attached at the 5 or 6 position of the 2-DOS as ring III[16]. Numbering wise; ring I is the primed ring, ring II is not primed, and ring III is a double primed ring (Figure 1)9.

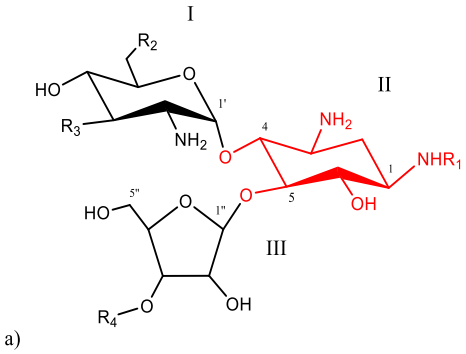

4,5-Disubstituted 2-DOS AGs

Antibiotic	R_1	R_2	R_3	R_4
Ribostamycin	H	NH_2	OH	H
Paromomycin	H	OH	OH	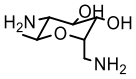
Neomycin B	H	NH_2	OH	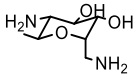
Lividomycin A	H	OH	H	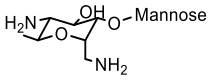

4,6-Disubstituted 2-DOS AGs

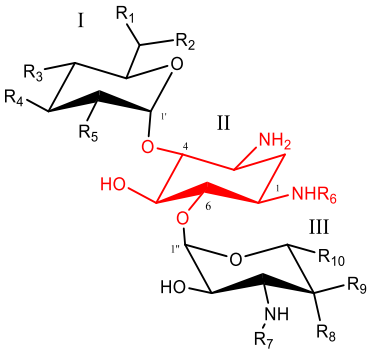

Antibiotic	R_1	R_2	R_3	R_4	R_5	R_6	R_7	R_8	R_9	R_{10}
Kanamycin A	H	NH_2	OH	OH	OH	H	H	H	OH	CH_2OH
Kanamycin B	H	NH_2	OH	OH	NH_2	H	H	H	OH	CH_2OH
Tobramycin	H	NH_2	OH	H	NH_2	H	H	H	OH	CH_2OH
Dibekacin	H	NH_2	H	H	NH_2	H	H	H	OH	CH_2OH
Gentamicin B	H	NH_2	OH	OH	OH	H	CH_3	OH	CH_3	H
Arbekacin	H	NH_2	H	H	NH_2	AHB	H	H	OH	CH_2OH
Amikacin	H	NH_2	OH	OH	OH	AHB	H	H	OH	CH_2OH

Figure 1. Structures of representative aminoglycosides of the a) 4,5-disubstituted 2-DOS and b) 4,6-disubstituted 2-DOS classes. The 2-DOS ring (ring II) is highlighted in red[16].

Few aminoglycosides fall in the 4-mono-substituted-2-DOS ring and aminoglycosides without DOS ring classes[16]. The 4-mono substituted-2-DOS ring aminoglycosides have only one amino sugar bound to the hydroxy group at the 4-position of the aminocyclitol ring[16]. Among this group are aminoglycosides such as neamine and apramycin (Figure 2)[16]. The aminoglycosides that do not have DOS rings typically contain a different aminocyclitol, most prominently streptamine. Streptamine is the same as 2-DOS, however it has a hydroxyl group in

the 2 position, where 2-DOS does not[16]. Among this group of aminoglycosides are spectinomycin and the cornerstone of aminoglycosides, streptomycin (Fig. 2)[16].

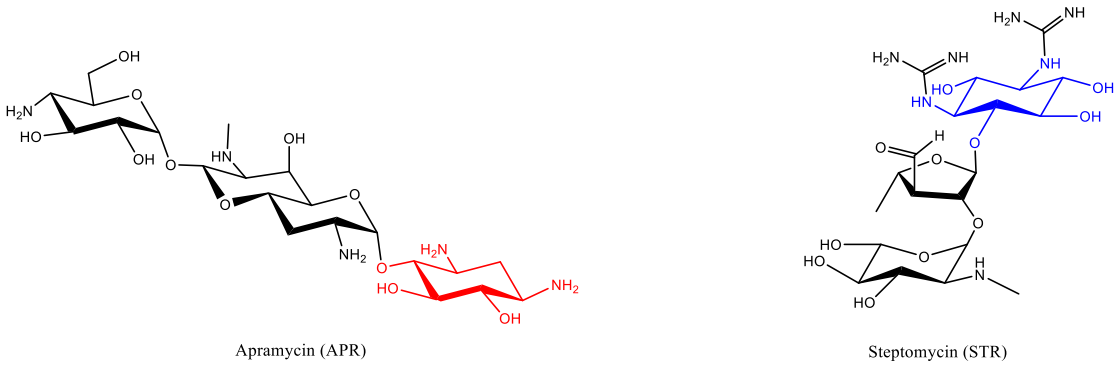

Figure 2. The structures of representative aminoglycosides from 4-monosubstituted 2-DOS and non-2-DOS classes of aminoglycosides. The 2-DOS ring is highlighted in red and the streptamine ring is highlighted in blue[16].

1.2.3 Mechanism of Action

1.2.3.1 Cell Entry of Aminoglycosides

Aminoglycosides enter the cell in three distinct stages. The first stage is the ionic binding to the outer membrane of the cell and the "self promoted uptake", the last two steps are the energy-dependent phases I and II (EDPI and EDPII)[10,18].

The uptake of aminoglycosides into the bacterial cell initiates with the primary ionic binding of the molecule and the "self promoted uptake" of the molecule[10,18]. The cationic aminoglycosides electrostatically bind themselves to the anionic components of bacterial outer membranes[10,18]. In Gram-negative bacteria these are primarily the lipopolysaccharides (LPS) and in Gram-positive it is primarily the teichoic acid that are used as the initial binding sites[10,18]. This

adsorption is instantaneous, reversible and concentration dependent[18]. Once adsorbed to the outer membrane aminoglycosides then work to cross the outer membrane into the periplasm[10,18].

Molecules that are below a size exclusion limit are able to pass through porins, however polycation molecules, including aminoglycosides, have another method to cross the outer membrane termed the self promoted uptake mechanism[10,18]. The LPS of Gram-negative bacteria bind and form cross-bridges with divalent cations (Ca^{2+}/Mg^{2+}) to stabilize the outer membrane[10,18]. Aminoglycosides, at physiological pH, are able to interact with these divalent cation binding sites of the LPS and displace the cations[18]. The displacement of the stabilizing cations results in the disruption of the outer membrane and an increased permeability to the aminoglycoside[18]. Studies suggest aminoglycosides are capable of using both the self promoted uptake mechanism and by using porins to cross the outer membrane, the pathway of which depends on the organism[18]. In vitro interaction data for *Pseudomonas aeruginosa* have shown that aminoglycosides use the self promoted uptake pathway, while liposome swelling data have shown that aminoglycosides enter the periplasm of *Escherichia coli* through porin channels[18].

Once the aminoglycosides are in the periplasm, two energy dependent phases (EDPI and EDPII) facilitate the entry of the molecules into the cytoplasm in an electron transport-mediated process, that is still not well understood to this day[18]. EDPI is a slow rate of energy uptake, with the duration and the rate of the uptake dependent on the concentration of aminoglycoside and independent of any carrier proteins[10,18]. It is suggested that during EDPI, aminoglycosides transverse the cytoplasmic membrane in response to the membrane potential ($\Delta\psi$) of the protonmotive force (PMF) of the cell, with a minimum threshold potential required before uptake occurs[18]. Since the generation of the $\Delta\psi$ is oxygen-dependent, aminoglycosides lack activity against anaerobic bacteria[18]. Following EDPI is the third phase, EDPII, which is an accelerated

linear rate of the accumulation of aminoglycosides across the cytoplasmic membrane[18]. Despite being energy dependent, EDPII exhibits diffusion kinetics across the cytoplasmic membrane[18].

1.2.3.2 Inhibition of Protein Synthesis

Aminoglycosides have two modes of action that kill bacteria, the first being the inhibition of protein synthesis that dominates at lower concentrations, < 4μg/mL in *P. aeroginosa*[19]. Aminoglycosides accomplish this by binding to the A-site located on the 16S ribosomal RNA (rRNA) of the 30S ribosomal subunit (Figure 3a)[20,21]. There are four bases in the rRNA A-site that interact with the incoming tRNA: A1408, A1492, A1493, and G1494[20,21]. This region termed the decoding region is where the recognition between the codon and anticodon occurs. Studies show that aminoglycosides bind to this decoding region and interfere with the accurate recognition between the rRNA and the conjugate tRNA[20,21]. The outcome of which is error prone protein translation, producing assembled polypeptides with incorrect amino acids that are released and cause damage to the cell[20,21]. It is also postulated that this interaction can block the translocation of the tRNA from the A-site to the peptidyl-tRNA site (P-site)[20,21].

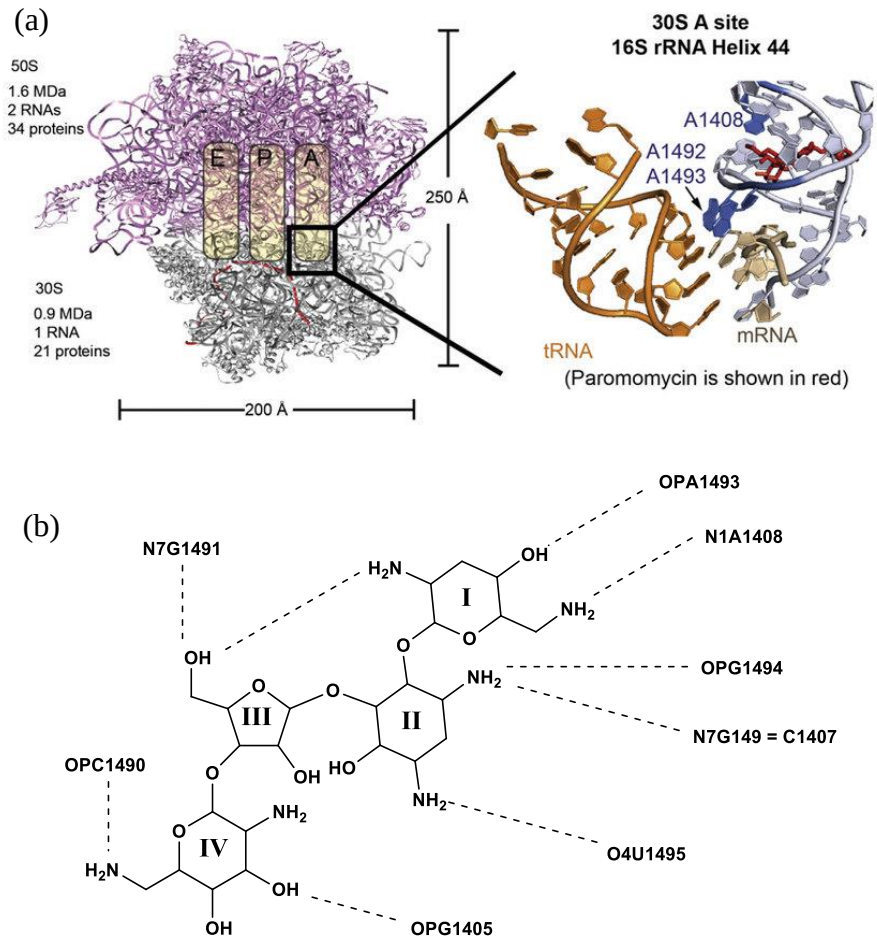

Figure 3. (a) A rendered model of the bacterial ribosome indicating the location where aminoglycosides bind and the detailed interaction of paromomycin (red), 16s rRNA of the 44 helix (white) and the tRNA (orange)[22].(b) The molecular structure of paromomycin and its atomic interactions with nucleotides of 16s rRNA[16].

Different classes of aminoglycosides will bind to the A-site of the ribosome at slightly different regions, depending on their specific structural complementarity with the region[20,21]. Recent structural studies have been conducted for the mode of interactions of paromomycin, a representative aminoglycoside of the neomycin class, with an RNA mimic of the A-site region (Figure 3b)[20,21]. Once bound to the paromomycin a distinct structure is stabilized between

nucleotides A1408, A1492 and 1493, with bases A1408 and A1493 forming a noncanonical base pair[20,21]. Nucleotide A1492 does not have any base pairing and forms a bulge in the A-site with the other nucleotides that paromomycin binds[20,21]. This bulge creates a pocket where ring II of paromomycin sits and ring I binds to the universally conserved base pairs U1406:U1496 and C1407:G1494 of the RNA[20,21]. Rings III and IV have nonspecific interactions in the major groove of the rRNA. Similar aminoglycosides will bind similarly to paromomycin. Ring I and II of gentamicin Cla and tobramycin have similar interactions as does paromomycin, with the ring III differing due to structural changes[20,21].

1.2.3.3 Disruption of the Outer Membrane in Gram-Negative Bacteria

The second mode of action that aminoglycosides exhibit is their disruption of the outer membrane, this mechanism dominates at higher concentrations[19]. Studies using tobramycin against *P. aeruginosa* have shown that membrane disruption occurs at concentrations of ≥ 8μg/mL[19]. As mentioned previously with their "self promoted uptake" mechanism, aminoglycosides are able to displace the divalent cations that stabilize the out membrane of Gram-negative bacteria, resulting in its disruption[19]. This mechanism has been modeled in *P. aeruginosa*, shown to be a rapid mechanism of killing in contrast with the protein inhibition mechanism[19]. This ability of aminoglycosides to disrupt the outer membrane have made them good candidates for combination therapy with antibiotics that have intracellular targets[19].

1.2.4 Mechanisms of Aminoglycoside Resistance

There are a few main mechanisms of resistance to aminoglycosides that bacteria have developed; (1) modification of the aminoglycosides by aminoglycoside modifying enzymes (AMEs), (2) modification of the binding site on the ribosome, (3) decreased permeability of the aminoglycosides, and (4) increased efflux out of the cell[10].

One of the most common of these mechanisms are the use of AMEs[10]. Located on plasmids, AMEs are thought to originate through horizontal gene transfers from actinomycetes of whom would naturally carry these genes since they utilize aminoglycosides[10]. There are three groups that have categorized more than 100 known different AMEs, the aminoglycoside N-acetyltransferases (ACCs), aminoglycoside O-phosphotransferases (APHs), and aminoglycoside O-nucleotidyltransferases (ANTs)[10]. These subgroups further divided based on the position on the aminoglycoside that they modify into different classes[10]. ACCs are part of the GCN5-related N-acetyltransferase (GNAT) super family and make up the largest group of AMEs[10]. These enzymes modify the amino or hydroxy groups that are at various positions on the core aminoglycoside structure[10]. These modifications lead to a decrease in the binding affinity of the aminoglycoside to its target, this as a result lowers the activity of the enzyme[10].

Posttranscriptional modification of the aminoglycoside binding site occurs through the action of 16S rRNA methyltransferases (RMTs)[10]. These enzymes methylate specific rRNA nucleotides at the target site preventing aminoglycosides from binding effectively[10]. The RMTs are divided into two general classes based upon the nucleotide that they methylated[10]. One of the classes methylate the N7 position of nucleotide G^{1405} which cause resistance 4,6-disubstituted aminoglycosides[10]. The other class methylates the N1 position of nucleotide A^{1408} which causes

resistance to both 4,6- and 4,5-disubstituted aminoglycosides[10]. This posttranscriptional methylation is commonly seen in Actinomycetes that produce aminoglycosides, which include Streptomyces and Micromonospora, of which contain these mechanisms to be naturally resistant to their metabolites[10]. However, in 2003, the first reported clinical case of a pathogen having an RMT was from an isolated *P. aeruginosa* strain in Japan[10].

Aminoglycosides having an internal main target of the ribosome make them more susceptible to changes in the permeability[10,23]. As previously mentioned, AGs have shown to have two different uptake mechanisms in Gram-negative bacteria, through porin channels and through the self-promoted uptake mechanism[19,23]. Both of which can be inhibited through changes of the bacterial membrane either with alterations of the LPS or changes in expression of porins[23]. During the self promoted uptake mechanism, the polycationic aminoglycosides are able to displace the divalent cations that bind to the negative LPS which stabilizes the bacterial outer membrane[10,23]. Gram-negative bacteria have several known two-component systems that respond to the presence of cationic metals or antimicrobial molecules by attaching a 4-amino-4-deoxy-L-arabinose sugar to the LPS[23]. The attachment of this positively charged arabinose to the LPS reduces the net negative charge on the outer membrane, effectively decreasing the affinity of aminoglycosides for the outer membrane[23].

Porins are large water-filled transmembrane protein channels located on the cytoplasm that allow for diffusion of small hydrophilic molecules across the membrane[23]. The porins have a β-barrel structure forms the water-filled channel across the cytoplasmic membrane[23]. Porins are known to mediate the movement of antibiotics across the outer membrane of Gram-negative bacteria, and therefore the expression of the porins can be linked to antibiotic resistance[23]. One of the most well studied porins is OmpF in *Escherichia coli*, which mediates the transport of β-

lactam and fluoroquinolone antibiotics into the cell[23]. As a result, OmpF mutant strains have been shown to be resistant to β-lactam antibiotics[16]. Despite there being evidence for porins involvement in the transportation of some antibiotics, liked β-lactams, across the cytoplasmic membrane, the involvement of porins in the transportation of aminoglycosides is still unknown in Gram-negative bacteria[23]. It is hypothesized that OmpF could be involved in kanamycin resistance through the downregulation of the porin, however the results are inconclusive[23]

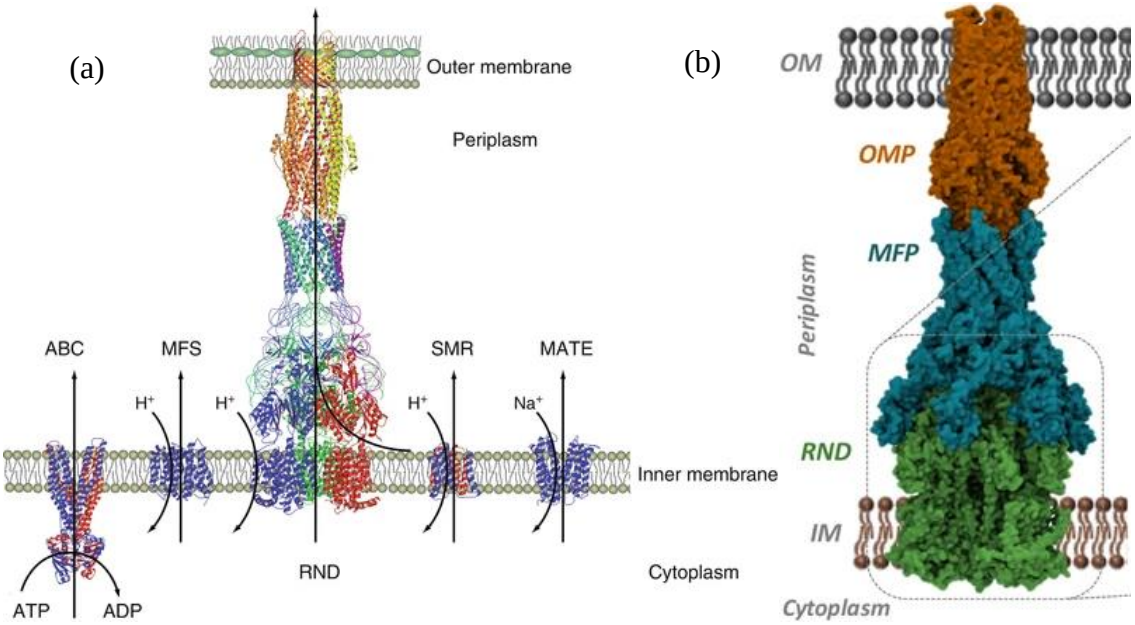

Figure 4. (a) The crystal structures of proteins from five major drug efflux superfamilies; ABC, SMR, MATE, MFS and RND pumps[24]. (b) Structure of the RND tripartite, displaying the three components (RND, MFP, and OMP) that comprise the efflux system[25].

The last main mechanism of resistance that bacteria have evolved in order to deal with aminoglycoside antibiotics are the presence of efflux pumps[10]. Gram-negative bacteria contain multiple multi-drug efflux pumps belonging to several families[26]. These are five major drug

efflux pump superfamilies: ABC (ATP-binding cassette), SMR (small multidrug resistance), MATE (multiple antibiotic and toxin extrusion), MFS (major facilitator superfamily), and RND (Resistance-Nodulation-Division) (Figure 4a)[24,26]. Multidrug efflux pumps are an important form of intrinsic resistance in Gram-negative bacteria, with the upregulation of these providing an increased resistance to a broad spectrum of drugs. Most efflux pumps are located in the cytoplasmic membrane and rapidly pump out drugs only into the periplasm[26]. RND pumps, with few exceptions, are primarily the only pumps that exist in a tripartite form extending from the inner membrane to the outer membrane[26]. The tripartite is comprise of three components: the RND cytoplasmic membrane antiporter, the membrane fusion protein (MFP), and an outer-membrane protein (OMP) (Figure 4b)[25]. This allows the pump to extrude molecules from both the cytoplasm and the periplasm out into the environment[26]. Among these RND pumps, the AcrAB-TolC complex in *E. coli* and it's homolog MexAB-OprM in *P. aeruginosa* are the most well known examples among Gram-negative bacteria[27].

There are few efflux pumps able to pump out aminoglycosides due to its polycationic, hydrophilic structure[27]. *E. coli* have AcrD, a close homolog to AcrB which forms the AcrAD-TolC complex much like the AcrAB-TolC complex, however the AcrAD-TolC complex is capable of extruding aminoglycoside antibiotics[27]. As a member of the RND family efflux pumps, the AcrAD-TolC exist in a tripartite form crossing the inner and outer membrane[26]. The three proteins making the AcrAD-TolC assembly are ArcD the RND drug-proton antiporter, AcrA the MFP in the periplasm connecting the AcrD and TolC proteins and the OMP, TolC[27]. This tripartite complex of AcrAD-TolC allows for aminoglycosides to be pumped directly into the bacteria's environment rather than pumped into periplasm alone, making it more effective for bacterial resistance17.

Similarly, *P. aeruginosa* have the RND pump system MexXY, that is shown to be involved in the natural resistance of PAO1 to aminoglycosides, tetracycline, and erythromycin[28–30]. It is thought that only ribosome inhibitors upregulate the production of MexXY proteins because the MexXY substrate, ofloxacin, does not induce upregulation of the proteins[28,30]. The MexXY efflux system is comprised of three proteins with analogous functions as the AcrAD-TolC systems in *E. coli*[28–31]. The MexY functions as the RND cytoplasmic membrane antiporter and the MexX functions as the MFP[28,29,31]. MexXY is capable of complexing with two OMPs, OprM or OprA, to form a continuous channel through the outer and cytoplasmic membrane[31]. *P. aeruginosa* clinical isolates from cystic fibrosis (CF) patients have an upregulation of the MexXY efflux system and this is a major determinant of aminoglycoside resistance[28–30].

1.2.5 Toxicity of Aminoglycosides

The major draw back of utilizing aminoglycosides is the potential for nephro- and ototoxicity in patients[10]. A clinical review of 144 published trials around the world covering approximately 10,000 aminoglycoside treated patients from 1975-1982 determined that there was a frequency of 8.7%-14.0% of nephrotoxicity[32]. Approximately 5% of the administered aminoglycoside are retained by the epithelial cell lining of the proximal tubules of the nephrons in the kidneys[11]. The aminoglycosides accumulate and are localized in lysosomal and endosomal vacuoles, and the Golgi apparatus of the cells[11]. Once accumulated, they induce a morphological change in the lysosomes of the cell comparative to the lysosomal accumulation of myeloid bodies[11]. This is followed by tubular dysfunction including the release of brush-border and lysosomal enzymes, decreased reabsorption of proteins, wasting of K^+, Mg^{2+}, Ca^{2+} and glucose[11]. These signs progress into the development of nonoliguric renal failure and a hypoosmotic fall in

creatine clearance[11]. Histopathological studies strongly support that the functional toxicity of aminoglycosides is due primarily to tubular necrosis. However, the specific mechanism of the tubular necrosis has not yet been elucidated[11]. The tubular necrosis might not be due to a single mechanism but due to the simultaneous multiple alteration of the tubular cells[11]. The nephrotoxicity induced by aminoglycosides is reversible, and recovery is observed once the administration of the aminoglycosides is halted[11].

The same survey mentioned prior calculated an average frequency of cochlear and vestibular toxicity amongst patients administered aminoglycosides of 2.4-13.9% and 1.4-3.5%, respectively[32]. Aminoglycoside's ototoxicity can target both main structures of the inner ear; the vestibular system, responsible for spatial orientation and maintain the body's balance, and the cochlea, responsible for the transduction of auditory signals[33,34]. Damage to the cochlea can cause permanent and bilateral high-frequency sensorineural hearing loss[12]. While damage to the vestibular system can cause disequilibrium and oscillopsia (loss of vestibular ocular-reflex), however this vestibular hypofunction is often reversible[12]. In vitro studies have supported the hypothesis for an iron-aminoglycoside complex mediated reactive oxygen species (ROS)-induced cell damage[12]. The amine nitrogen and deprotonated alcoholic oxygens of the terminal amine sugar ring of aminoglycosides are capable of chelating metal ions, like iron atoms, from biomolecules[12]. Thus, forming chelated iron-aminoglycoside complexes of which are redox-active and capable of inducing the formation of ROS[12]. These ROS damage the hair cells inducing apoptosis[12]. A loss of cochlear hair cells results in sensory transmission hearing loss since these cells are terminally differentiated and do not regenerate[12]. Unlike the cochlear hair cells, the vestibular hair cells have the potential to regenerate and therefore vestibulotoxicity is considered temporary[12].

Despite aminoglycoside induced nephrotoxicity and ototoxicity being independent from one another, there might be an underlying mechanism in common to the uptake of aminoglycoside into the cell lines[12]. The uptake of aminoglycoside into these different human cells seems to be related to the cationic structure of aminoglycosides[11]. The positively charged aminoglycosides are attracted to the acidic phospholipids located in the cellular membrane of cells through electrostatic interactions[11]. Phosphatidylserine is an acidic phospholipid found plentifully in the cells of the brush border in the proximal tubules of nephrons, and studies have shown that neomycin has induced the externalization of phosphatidylserine to the apical surface of cochlear hair cells[11,35]. Once the aminoglycosides are at the cell surface, they likely attach to a transmembrane protein called megalin[11]. Megalin is an endocytic receptor and is a member of the low-density lipoprotein receptor family that has been observed to be expressed in renal proximal tubule epithelium and the epithelial of the inner ear using immunohistochemistry[36,37]. Megalin has been shown to be involved in the binding and the endocytosis of polybasic molecules, including aminoglycosides and polymyxin B[38]. Aminoglycosides are endocytosed into endosomes in the cells by megalin, from here aminoglycosides may cause aggregate formation and ROS damage[11,12].

There has been much effort in reducing the nephrotoxic and ototoxic effects of aminoglycosides in order to make them more clinically applicable[11]. One of these approaches was to decrease the accumulation of aminoglycosides in the cells of the tissues[11]. This approach would be looking at reducing the uptake of aminoglycosides in the cells or increasing the release of aminoglycosides from the cells[11]. Typically, it is easier to reduce the uptake of a drug or molecule into the target cell, this is done usually by using competing inhibitors[11]. Kinetic studies on the uptake of aminoglycosides into the tubular cells of the kidneys have displayed saturation

kinetics, effectively aminoglycosides can inhibit their own reabsorption, allowing much of the drug to pass through the lumen[11]. This was used to explain findings of early animal studies that seemed to show that a single daily dose of gentamicin was significantly less nephrotoxic than the same dose divide into three separate injections throughout the day, which was the more conventional method for the administration of aminoglycosides since their inception[11,39].

This led to several studies looking at how different dosing regimes affect the efficacy and toxicity of the administered aminoglycoside[11]. The findings generally followed that a single daily dose showed a significant increase in clinical and bacteriological efficacy, with a reduced frequency in nephrotoxicity and ototoxicity as compared to a multiple daily dose[40–43]. With these studies it was observed that the bactericidal activity and clinical outcomes are positively correlated with peak the concentration of aminoglycosides, and that nephrotoxicity is related to prolonged exposure to the drug[41]. It also seems that aminoglycosides using the single-daily dose have a post-antibiotic effect, where bacterial growth is inhibited even after the concentration is decreased below the MIC[41]. These observations seem to be attributed to a transiently high serum concentration followed by a very low serum concentration during the single-daily dose regime[41]. Due to these studies, the single-daily dose regime has been widely accepted and utilized[11,41].

1.3 SIDEROPHORES

1.3.1 Introduction of Siderophores

Iron is an essential nutrient in all living organisms as it used in many metabolic pathways necessary for life[44–46]. Even though iron is one of the most abundant elements on the earth it is not readily bioavailable in aerobic environments[47]. In our oxygen rich environment, the soluble

ferrous iron (Fe^{2+}) gets oxidized to the insoluble ferric iron (Fe^{3+}), which makes it far less accessible to microorganisms[46]. For optimal growth, bacteria require an iron concentration of 10^{-5}-10^{-7}M, while ferric iron has a typical solubility of 10^{-17}M at a neutral pH in a natural environment[47]. Consequently, microorganisms, fungi and plants have evolved mechanism to scavenge iron from soil, aqueous environments, and other living organisms or hosts[47]. One of the most prominent of these mechanisms evolved is the production, secretion, and uptake of siderophores[44–47]. Siderophores are low molecular-weight (500-1500 Daltons) organic compounds that chelate ferric (Fe^{3+}) ions in the environment[46,48]. The genes for siderophore biosynthesis, secretion, and uptake are regulated by iron levels in the environment and are upregulated during iron starvation[46,47]. Once siderophores complex ferric (Fe^{3+}) ions, they have specific uptake mechanisms that recognize and transport the complex into the bacterial cell[47].

1.3.2 Discovery of Siderophores

Mycobactin, ferrochrome, and coprogen were among the first isolated siderophores from 1949-1952 and were identified as growth factors (Figure 5)[46]. These findings sparked a new interest in these growth factors, delving into the structure of the compounds along with their properties[46]. Studies characterized the coordination groups of the mycobactin and determine that it forms complexes with ferric iron (Fe^{3+})[46]. In 1956, Garibaldi and Neilands, demonstrated that by growing the organism *Ustilago sphaerogena* in iron-deficient medium the production of ferrichrome A was enhanced. This established the connection between the regulation of these growth factors and organism's environment, suggesting that the growth factors are important for iron acquisition[46]. Several hydroxyamates were characterized as these iron-binding growth factors by the mid 1960's[46]. Since 1970, these growth factors were termed siderophores, "sidero-

" from the Greek word for "iron" and "-phore" the Greek word for "carrier"[46,47]. Over 270 siderophores have since been structurally characterized, most using catechol, hydroxamate, or carboxylate function binding groups[46].

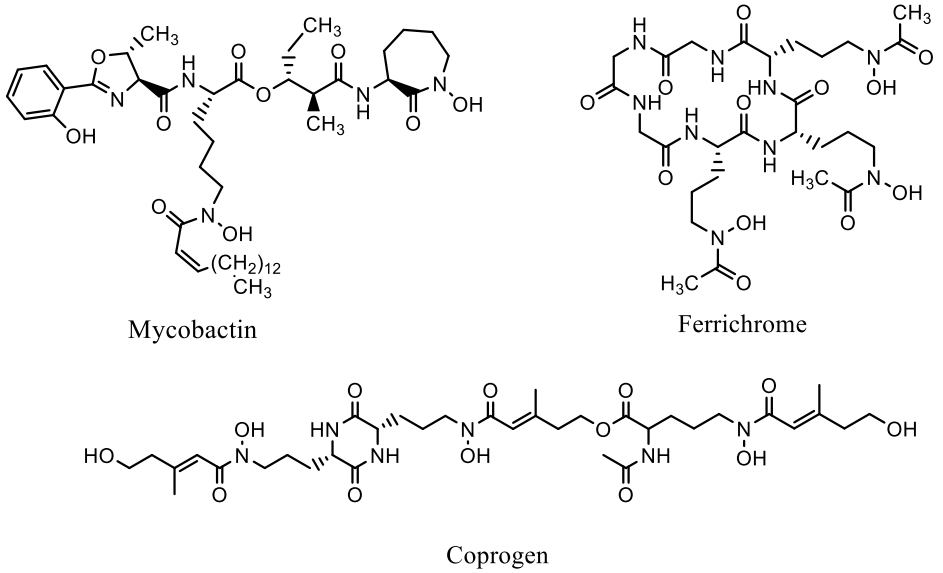

Figure 5. The molecular structure of Mycobactin, Ferrichrome, and Coprogen.

1.3.3 Classification of Siderophore

Siderophores posses a higher affinity for ferric iron (Fe^{3+}) than ferrous iron (Fe^{2+})[46]. This was selected for because ferric iron (Fe^{3+}) is not only the more abundant iron ion in natural environments but also because it would be difficult to have ligands that are selective for ferrous iron (Fe^{2+}) over other dipositive cations that are of biological importance to microorganisms[46]. Negatively charged oxygen atoms are the donor atoms that have the strongest affinity for ferric iron (Fe^{3+}), the higher electron density around the oxygen provides a greater interaction[46]. Charged oxygen atom are the most common donor atoms that siderophores employ with nitrogen

or sulphur sometimes being used however they have less affinity for ferric iron (Fe^{3+})[46]. Siderophores utilize these donor atoms using bidentate binding ligands, each containing two donor atoms, that coordinate ferric iron (Fe^{3+}) in a thermodynamically favourable octahedral geometry[46,47].

The most common bidentate binding ligands that are utilized in siderophores are catechols, hydroxamates, α-hydroxycarboxylates, and hydroxyphenyloxazolone[46]. A catecholate binding ligand is a dihydroxybenzene with the two hydroxy substituents ortho to each other (Figure 6)[46,47]. Once deprotonated, these two ortho hydroxy groups have high electron density give catecholates high affinity for ferric iron (Fe^{3+})[46,47]. Alterations to the structure of which withdraws electron density can make the alcohols more acidic, and therefore increase the affinity for ferric iron (Fe^{3+})[49].

Hydroxamate binding ligands are amides where there is an additional hydroxy group attached to the nitrogen centre (Figure 6)[46,47]. Like amides, hydroxamate moieties have two mesomeric forms, one form creates high electron density on the carbonyl oxygen[46]. This oxygen with the deprotonated hydroxy group creates the bidentate that has high affinity for ferric iron (Fe^{3+})[46,47]. This affinity can be enhanced with conjugated side chains which would increase electron density on the carbonyl oxygen[47].

α-Hydroxycarboxylates binding ligands contain a carboxylate moiety and an alcohol on the α carbon to the carboxylate (Figure 6)[46,50]. The deprotonated oxygens from the carboxylate and alcohol moieties are the donor atoms in the bidentate ligand[46,50]. The pKa of the alcohol can be

decreased by intramolecular hydrogen bonding that stabilizes the conjugate anion, increasing the affinity for ferric iron (Fe^{3+})[46].

Hydroxyphenyloxazolone binding ligands coordinate ferric iron (Fe^{3+}) through a phenol alcohol and a nitrogen atom from a neighbouring oxazolone ring (Figure 6)[46]. The alcohol gets deprotonated forming a phenolate anion and a resonance form of oxazolone ring puts a positive charge on the oxygen and a negative charge on the nitrogen[46]. The phenolate anion and the nitrogen anion provide the electron density for coordinating ferric iron (Fe^{3+})[46]. Increasing the acidity of the phenol alcohol and stability of the resonance form of oxazolone ring will increase the affinity for ferric iron (Fe^{3+})[46].

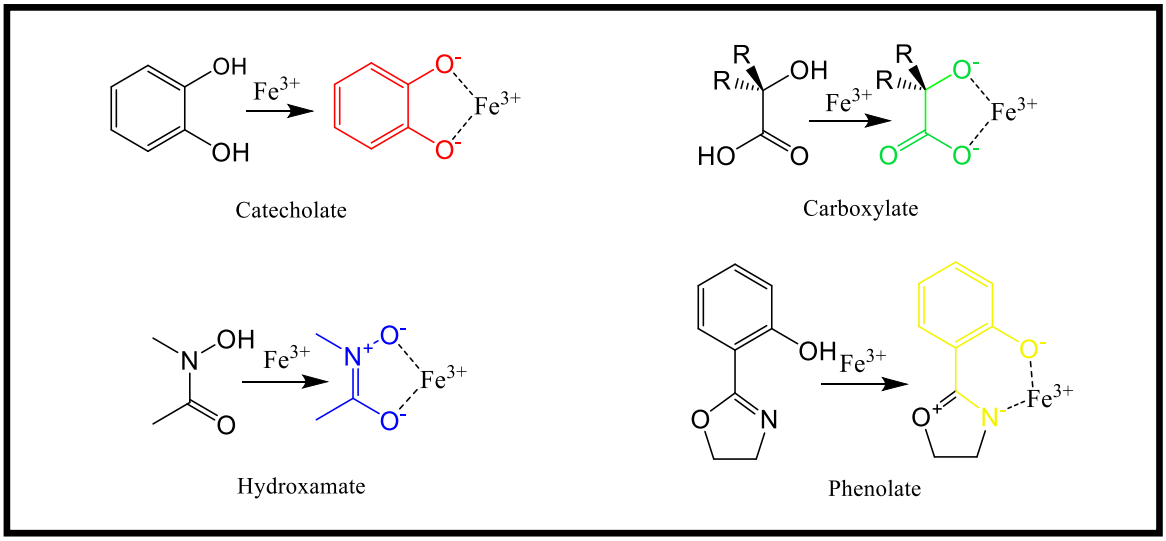

Figure 6. Structures of common siderophore binding ligands[46].

These four types of binding ligands are what define the main categories of bacterial siderophores: catecholates, hydroxamates, carboxylate, phenolates[51]. Bacterial siderophores that

utilize more than one type of binding ligand are called mixed siderophores. Some examples of bacterial siderophores from these groups are Enterobactin (Catecholate), Ferrichrome (Hydroxamate), Staphyloferrin A (Carboxylate), Pyochelin (Phenolate) and Pyoverdine (Mixed) (Figure 7)[46,47,51]. Often a single siderophore contains three binding ligands, so they bind in a 1:1 ratio with ferric iron (Fe^{3+})[46,51]. Siderophores with less than three binding ligands can form complexes with multiple siderophore molecules[46,51]. Some other siderophore ligands include α-aminocarboxylates and α-hydroxyimidazoles[46]. These ligands are less commonly utilized by bacterial siderophores and are similar to the previously mentioned ligands, apart from them having a nitrogen and oxygen donor atoms instead of two oxygen atoms[46].

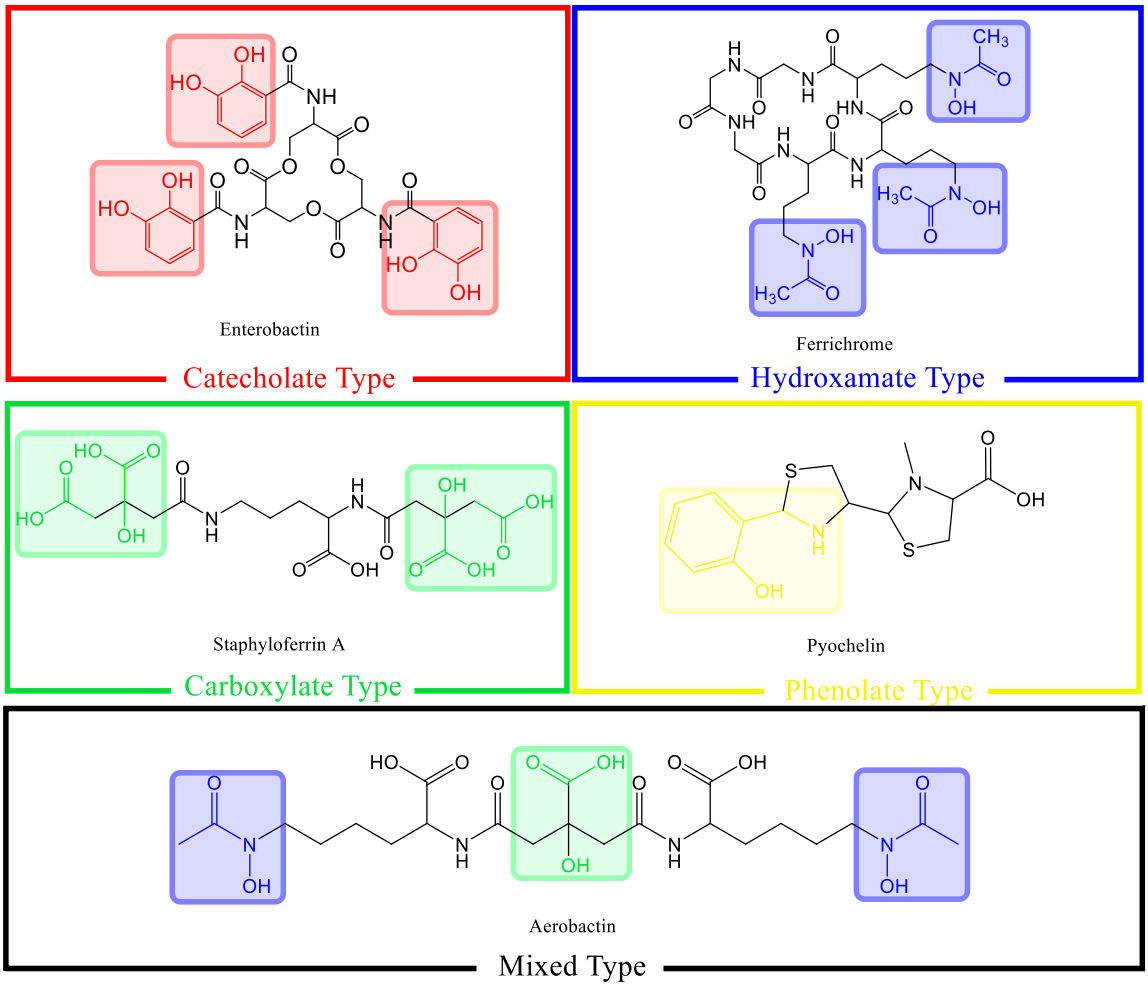

Figure 7. Structures of representative siderophores from the five main classes of siderophores with the binding ligands highlighted[46,47,51].

1.3.4 The Iron Tug of War

Iron is the most abundant metal ion in the human body and is indispensable for essential functions[51,52]. The bioavailability of iron is under strict regulation in mammalian hosts controlling the absorption, transport, and storage[51,52]. A small fraction of the body's iron comes from the diet, most coming from recycled red blood cells[52]. Ferric (Fe^{3+}) and ferrous (Fe^{2+}) iron are both important for oxygen transport, cellular respiration, and DNA transport in the body once

complexed to heme, iron-sulfur (Fe-S) clusters and ribonucleotides reductases[52]. Iron is so tightly regulated because of these fundamental functions and the ROS toxicity that is induced by high concentrations of it[52]. Most of the iron present in the host are bound to protein, like transferrin and lactoferrin[51,52].

Transferrin is the prominent iron-binding protein found in the plasma and lymphatic system which transport iron from between cells[52,53]. In healthy individuals' transferrin has an approximate 33% iron saturation, during states of iron depletion or anemia this iron saturation can drop below 10%[54,55]. Lactoferrin on the other hand is the primary iron-binding protein in air-way secretions, and is stored in neutrophil granules[54,56]. Like transferrin, lactoferrin transports extracellular iron between cells, usually being less than 10% saturated with iron[54,56].Lactoferrin aids in bactericidal activity by depriving pathogens of iron and by assisting in the generation of ROS for oxidative killing[52,54].

In response to inflammation caused by a bacterial infection the host employs a nutritional immune response[52]. This is a primary line of defence that vertebrate immune systems have evolved in which the host sequesters trace minerals in order to starve invading pathogens and inhibit their growth[52,57]. Iron is one of these minerals that the host targets during nutritional immunity because it is fundamental to the microorganisms' biological process[52,57]. One such mechanism the host employs in order to hinder iron is accessibility is the expression of the protein hepcidin, which is induced at the onset of infection by hepatic interleukin (IL)-6[52,57,58]. Hepcidin is a 25-amino acid peptide hormone produced in the liver and is released into systematic circulation[57]. Hepcidin binds to the iron exporter, ferroportin (Fpn), expressed on macrophages, duodenal epithelia, and iron-storing hepatocytes[52,57,58]. This induces the internalization and degradation of the Fpn[52]. The down regulation of Fpn traps iron in

macrophages and iron-storing hepatocytes, and prevents iron absorption in the intestines[52,59]. This initiates hypoferremia in the body to starve extracellular bacteria[52,59].

The basal expression of iron-binding proteins, lactoferrin and transferrin, creates a low free iron environment (approx. 10^{-24} M) that is much lower than the sufficient iron levels to support bacterial growth (10^5-10^6 M iron per cell)[52]. The host environment can be further depleted of iron during infection by the aforementioned induced nutritional immunity[52,57]. In order for bacteria to establish an infection in this environment they have evolved mechanisms for stealing iron from the host proteins[52]. One weapon in the bacterial arsenal is the synthesis, secretion and uptake of siderophores[44,52]. As mentioned siderophores are small organic molecules able to chelate ferric iron (Fe^{3+}) selectively[44,46,52]. These bacterial siderophores have a higher affinity for iron than host iron-binding proteins and are able to strip the iron from them[52]. Bacteria also have outer membrane receptors able to chelate iron from transferrin and are able to transport host iron bound heme protein into their cytoplasm through a receptor uptake mechanism[52]. These weapons that bacteria have evolved have allowed them to steal iron from their host and establish an infection.

In response to bacterial siderophores, mammalian hosts have evolved proteins called lipocalins which are capable of binding and sequestering siderophores[52]. They are a diverse group of proteins sharing a core structure[52]. One such lipocalin, lipocalin 2 (Lcn-2), can use ionic and cation-π interactions to bind specifically to the catecholate iron-siderophore complexes[52]. Lcn-2 is capable of binding both unbound siderophore and iron-siderophore complexes, however the protein has a higher affinity for the complex[52]. Since Lcn-2 does not bind iron directly, they do not compete against bacterial siderophores or host iron-binding proteins[52]. Lcn-2 is expressed throughout the body on a basal level, major sources being the gut and liver, and is upregulated

during inflammation[52]. Lcn-2 and other lipocalins are thus bactericidal agent since they are able to prevent bacteria from acquiring sufficient iron for growth[52].

Bacteria have thus developed strategies to evade the binding of lipocalins, one strategy being the modification of siderophores[52]. Bacteria are capable of modifying a targeted siderophore to be unrecognizable to the lipocalin and upregulate the exertion of the modified molecule while down regulating the targeted siderophore[52]. For example, Lcn2 binds to the iron-enterobactin complex rendering it useless to the bacteria[52]. To work around Lcn2, bacteria upregulate the release of 2,3-dihydroxybenzoylserine (DHBS), a cleaved linear product of enterobactin, and downregulate the exportation of enterobactin[52]. The cleaved modification of DHBS prevents the binding of Lcn2 and allowing DHBS to act as a "stealth siderophore"[52].

This war between host and pathogen over iron availability has led to the co-evolution of multiple mechanism used to try to gain a step above each other. Siderophores are only a small aspect of this larger war between the host and bacteria in this war for iron. Genes associated with the biosynthesis of siderophores can he be a predictive marker of high or low virulence[44,48,52].

1.3.5 Siderophore Secretion

Despite the biosynthesis of siderophores and their mechanism of iron acquisition being researched extensively, little is still known about their secretion systems[60]. Given the size and charge of most siderophore molecules, it is unlikely that they passively diffuse across the membrane[60]. Thus, it can be assumed that siderophores must rely on exporters to be secreted into the environment[60]. The siderophore export systems identified in the past decades have been part of two superfamilies: the ABC transporters and the Major Facilitator Superfamily (MFS)

transporters[60,61]. The first identified pump was an ABC transporter in *Mycobacterium smegmatis*, ExiT, that exports exochelin[60,61]. Other transporters include, IroC which exports enterobactin and salmochelin in *Salmonella enterica*, and PvdE and PchHI, which export pyoverdine and pyochelin respectively[60]. These exporters transport newly synthesized siderophores from the cytoplasm into the periplasm, additional transporters are needed to transport siderophores across the outer membrane.

One of the most extensively studied export system of siderophores is that of enterobactin in *E. coli*[61,62]. In 2002, the MFS transporter EntS was discovered to be a primary exporter of enterobactin[61,62]. This provided some of the first conclusive evidence for siderophore export mechanisms in Gram-negative bacteria[62]. TolC outer membrane channel was then later shown to be involved in the exportation of enterobactin from the periplasm to the culture medium[62,63]. Then in 2014, an investigation into the role of TolC-dependent RND-type drug efflux systems on the exportation of enterobactin across the outer membrane was conducted[62]. In this study, several RND efflux pump genes were deleted, *entS, tolC, acrB, acrD, mdtABC, acrEF,* and *mdtEF* genes, to create various mutants and observe how these deletions affect the release of enterobactin[62]. The results of this study showed that AcrB, AcrD, and MdtABC are required for the secretion of enterobactin[62].

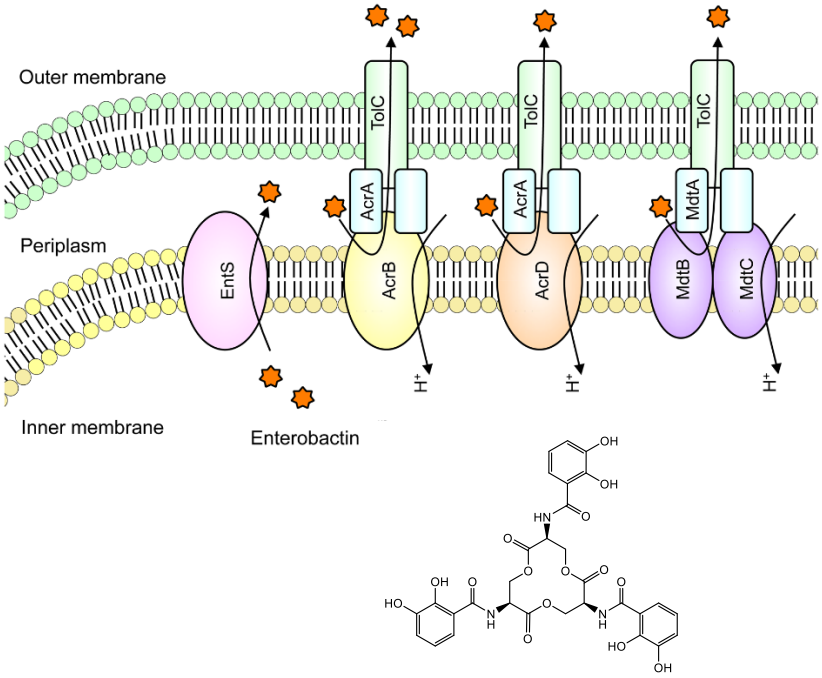

Figure 8. Illustration of proteins involved in the mechanism for the exportation of enterobactin in *E. coli*[62].

These findings are important for establishing a model for siderophore secretion in Gram-negative bacteria. From the evidence shown so far, it seems that there are semi-specific transporters of the ABC and MFS families that export new siderophores across the inner membrane[60,61]. Once in the periplasm, the siderophores are transported out non-specifically into the environment through RND efflux pumps[62,63]. For enterobactin's case in *E. coli*, enterobactin is transported into the periplasm by EntS and from there seems to be exported out by AcrB, AcrD, and MdtABC through the TolC channel (Figure 8)[62,63] .

1.3.6 Mechanism for Iron-Siderophore Uptake

Once siderophores complexes with iron in the environment they must be taken up by the bacteria using their iron uptake mechanism[64]. In general, there are two stages for Gram-negative bacteria to uptake the iron-siderophore complex. The first being the iron-siderophore complex must be recognized by a specific outer membrane receptor (OMR) which additionally transports the complex across the outer membrane into the periplasm. The second step is the iron must cross the inner membrane into the cytoplasm using a second transport protein[64].

OMRs are very diverse proteins, that are specific to the species of bacteria and the class of siderophore the recognize[51]. For example, in *Pseudomonas aeruginosa* the OMR responsible for the transportation of pyoverdine and pyochelin complexes are FpvA and FptA respectively, and FepA which is responsible for the transportation of enterobactin complex in *E. coli*[51,64]. The energy for the internalization process of the siderophore complex by the OMRs is provided by the TonB-dependent energy transduction system, consisting of TonB, ExbB, and ExbD[51,64–66]. The current model of this protein interaction is the Rotational Surveillance and Energy Transfer model (ROSET)[51,66]. According to the ROSET model the inner membrane proteins ExbB and ExbD use the proton motive force in the periplasm from cellular respiration to drive the TonB protein to physically rotate in the inner membrane[51,66]. This rotation of the TonB protein causes a conformational change in the OMR which promotes the internalization of the siderophore-iron complex into the periplasm[51,66]. This pathway across the inner membrane of having a specific OMR that recognizes the siderophore complex and is driven to internalize the complex by the TonB-ExbB-ExbD transduction system is conserved amongst Gram-negative bacteria with few exceptions[51,66].

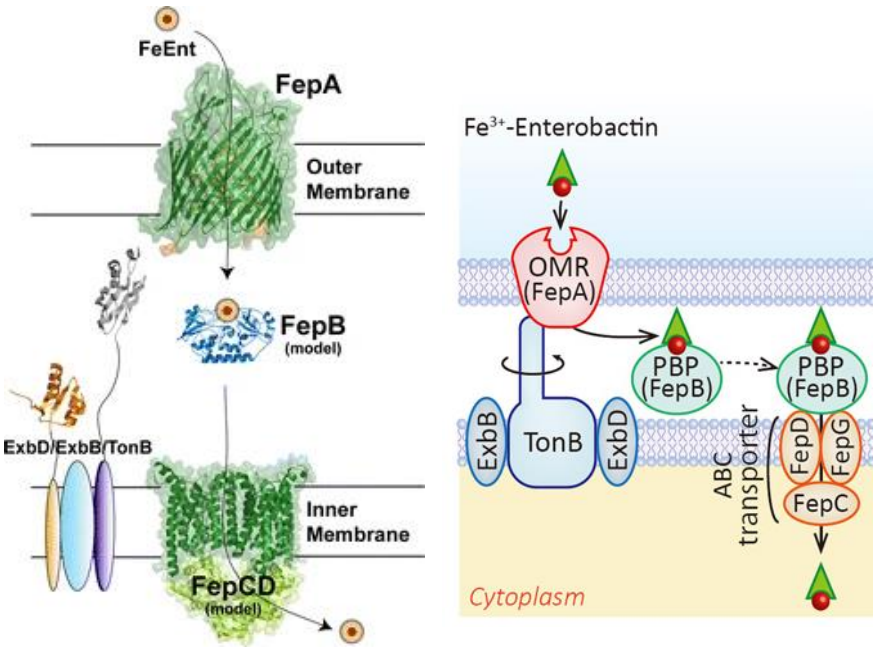

Figure 9. Two representations of the Fe^{3+}-enterobactin uptake mechanism in *E. coli* showing the proteins involved. One on the left highlighting the protein conformations and structural interactions53, while to the right the rotational action of the TonB protein is highlighted[51].

The translocation of iron-siderophore complexes across the inner membrane is not well conserved in many Gram-negative bacteria, except for in most cases it utilizes ABC transporters[68]. Once siderophore complex cross the inner membrane and enter the periplasm they are bound to periplasmic binding proteins (PBP)[51,69]. There are generally two different pathways seen from here, the PBPs take the siderophore complex directly to inner membrane transporters which transports the whole complex, or the PBPs will separate the siderophore complex and only transport the iron in the cytoplasm and will secret the siderophore back into the environment (Figure 10)[51]. In the case of the siderophore enterobactin, once its complex

enters the periplasm it binds to the PBP FepB (Figure 9)[51,69]. FepB shuttles the complex to the ABC transporter protein system, FepCDG, on the inner membrane which transports the complex into the cytoplasm (Figure 9)[51,69]. From here proteins reduce the complex which release the iron from the enterobactin (Figure 9)[51,69]. In the case of pyoverdine in *P. aeruginosa*, the siderophore complex is bound and reduced first by the PBPs FpvC and FpvF (Figure 10)[51,69]. The separated pyoverdine is transported to the outer membrane and secreted out in the environment, the iron is transported to the cytoplasm by the ABC transporter complex FpvDE (Figure 10)[51,69].

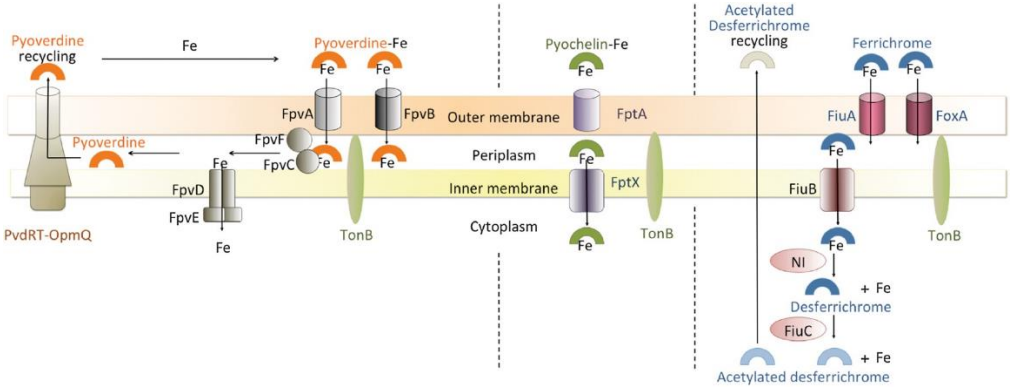

Figure 10. An illustration comparing the different uptake pathways of pyoverdine (left), pyochelin (middle), and ferrichrome (right) in *P. aeruginosa.* Highlighting the differences between the pathways once the siderophore complex reaches the periplasm[69].

1.3.7 Evolutionary and Social Aspects of Siderophores

One large flaw with the use of siderophores is the fact that once they are secreted into the environment, they can diffuse to far away from the bacteria that produced them[70,71]. This brings up the question as to why bacteria would waste the energy to produce and secrete siderophores

when they might not gain the value from them, especially since many bacteria also have membrane-bound uptake mechanisms[70,71]. There are evolutionary advantages of siderophores when looking at the single cell and group of cells perspective[70].

Studies have created mathematical models to explain the evolutionary advantage of siderophores from the single cell perspective[71]. From these models it seems that in unstructured (or less viscous) environments membrane-bound iron uptake systems are greater than siderophore uptake systems for motile cells[70,71]. This is likely because the unstructured media allows large siderophore diffusion and easier accessibility of iron by membrane-bound systems[70]. However, in sessile bacteria, siderophores allow them to access iron from a further distance away than their membrane-bound systems would be able to reach (Figure 11b&d)[70,71]. The largest advantage seems to be that siderophores are capable of solubilizing clumps of iron resources not immediately next to the cell (Figure 11c)[70,71]. This frees up iron and increases the accessibility of the nutrient to cells that secrete them, while cells that rely on membrane-bound systems have to come into contact with the clump (Figure 11c)[70,71]. This factor is important when considering why bacteria that have greater siderophore expression are usually hyper virulent[70]. Since most iron in the body is attached to proteins, siderophores allow bacteria to strip iron from these proteins in an area rather than only direct contact through membrane bound systems[52,70,71].

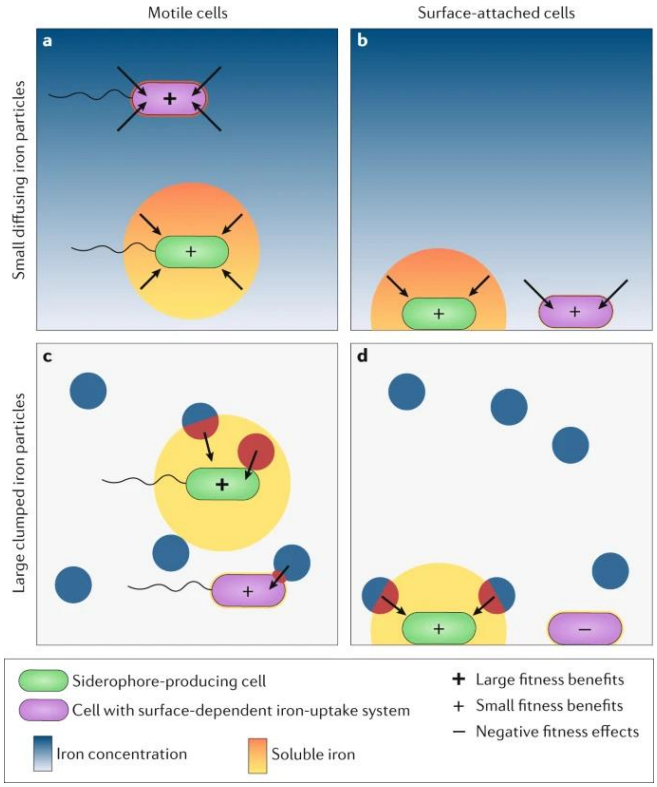

Figure 11. Depiction comparing the benefits and negative effects between siderophore-producing (green) and membrane-bound (purple) iron uptake systems on a single cell in differing iron environments and differing mobility of the cell[70].

Since most of the time bacteria grow in large populations and not as single cells, it is important to consider the cooperative aspects of siderophores to evaluate their evolutionary importance[70]. Bacterial cells in a colony do not have to just rely on their own siderophores, as they can utilized the siderophores secreted by their neighbours[70]. This sharing of siderophores is important to minimize the loss of a producer's siderophores to diffusion[70]. The higher the bacterial density of a colony the higher the availability of soluble iron to the colony[70]. This cooperative social behaviour of sharing siderophores provides a direct benefit to both the producer and the receiver, as a result provides an increase fitness (Figure 12)[70].

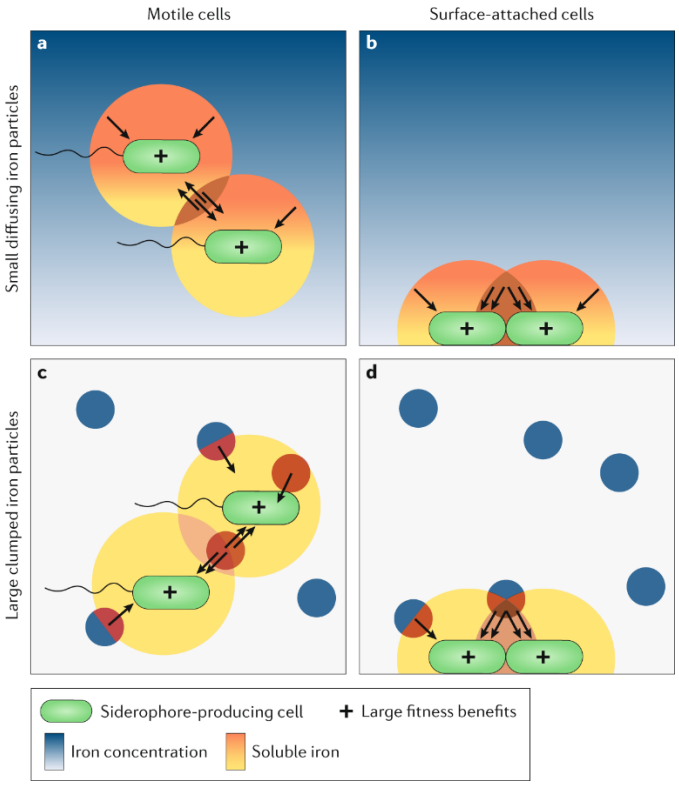

Figure 12. Illustration depicting the sharing social interaction between two siderophore-producing cells in differing iron environments and differing mobility of the cells[70].

It is unknown if it was either the self-directed benefits or the indirect group benefits of siderophores which caused their evolutionary pressure[70]. The evolution of siderophores might have been initially selected for the benefits it provides to the single cell over membrane bound system, with other regulatory mechanisms evolving later to fine tune the benefits to surrounding bacteria[70]. Bacteria have also evolved ways to exploit this cooperative behaviour from other siderophore producing bacteria[70]. Some bacteria will express the receptor for some siderophores they don't produce, effectively receiving the advantage of the siderophore pool while not wasting the energy producing siderophores to replenish it[70,72]. This "cheating" behaviour is observed in *Pseudomonas* strains with the siderophore pyoverdine[70,72].

1.4 SIDEROMYCINS

1.4.1 Trojan Horse Approach

The Trojan Horse strategy was designed as a way to bypass the impermeable cellular membranes of Gram-negative bacteria[73]. This method is a strategy focused on "smuggling" antibiotics in Gram-negative cells by exploiting their natural mechanisms[73]. In Greek mythology, Greek soldiers hid in a giant wooden horse so they could sneak their way into the city of Troy and when the Trojan's guard was down, the Greeks killed them inside their city[73]. This approach uses an antibiotic, analogous to the Greek soldiers, conjugated to a physiologically relevant molecule, analogous to the Trojan Horse[73]. Not only is this method a novel approach for researchers to infiltrate bacterial membranes, but bacteria also utilize the same strategy in their war against other bacteria[74,75]. One such example is Microcin C (McC), which is a peptide-nucleotide antibiotic that inhibits protein synthesis using a specific peptide to gain entry to the cell[74,75]. There is now an ever-growing interest to use siderophores to smuggle antibiotics inside Gram-negative bacteria.

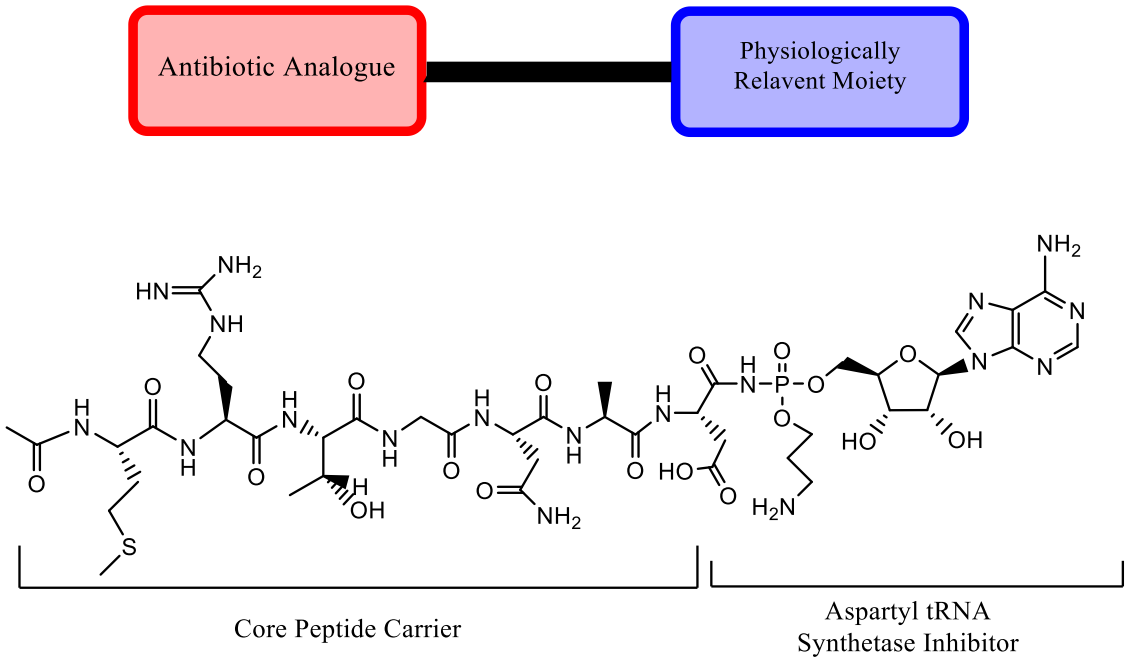

Figure 13. A simplified schematic depicting the necessary components for a "Trojan Horse" drug (top). The molecular structure of McC (bottom) outlining the core peptide carrier necessary for the transportation of McC into target cells and the aspartyl tRNA synthetase inhibitor responsible for killing the target cell[74,75].

1.4.2 Introduction to Sideromycins

An emerging approach to combat the antibiotic crisis is sideromycins[76]. Sideromycins are compounds that covalently link antibiotics to siderophore or siderophore-like moieties (Figure 14)[76–78]. Naturally occurring sideromycins have been identified as early as the 1940's and now designing synthetic sideromycins is growing field[78,79]. A frequent problem antibiotic therapy, especially for Gram-negative bacteria, is that outer membrane reduces the MIC of antibiotic to a point where the concentration in the body becomes toxic[76,78]. These siderophore-antibiotic conjugates were designed to improve the amount of an antibiotic that gets to its bacterial target

and bypass bacterial resistance mechanisms[76–78,80]. By exploiting the active bacterial iron uptake mechanism these conjugates greatly increase the antibiotic efficacy, in some cases lowering the minimal inhibitory concentration (MIC) by 100-fold than that of the respective antibiotic alone[76,80].

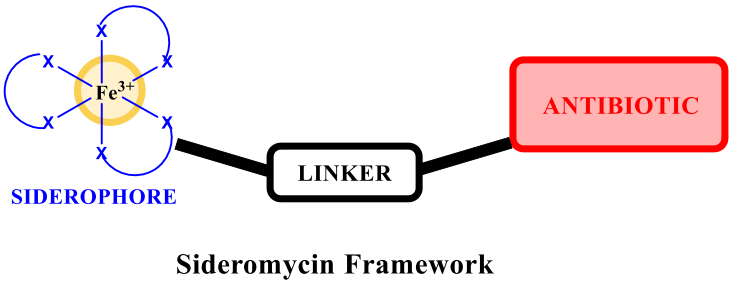

Figure 14. The generic structural framework of sideromycin molecules[76].

Designing these conjugates can be tricky as you must make sure the siderophore can still be recognized by both the OMR and the ABC transporter complex of the inner membrane in Gram-negative bacteria[76,78]. This means that the complex the synthetic sideromycin makes with ferric iron (Fe^{3+}) must be similar enough to the complex formed by the original siderophore. Also, the linker that connects the antibiotic and siderophore components must be chosen to be stable in a host environment, but also be able to ideally release the antibiotic component intracellularly due to enzymatic action[76,78].

1.4.3 Natural Occurring Sideromycins

The term sideromycins was coined after discovering naturally occurring ferric iron (Fe^{2+}) conjugated to antibiotics in the 1940s and 1950s[76]. Sideromycins were discovered before siderophores, and their activity was found to be antagonized by siderophores[76]. This was determined to be due to the competition for the iron uptake system that the two shared[76]. These antibiotics were first isolated in various species of *Actinomyces,* some of these products being albomycin, ferrimycin, and daunomycin (Figure 15)[81].

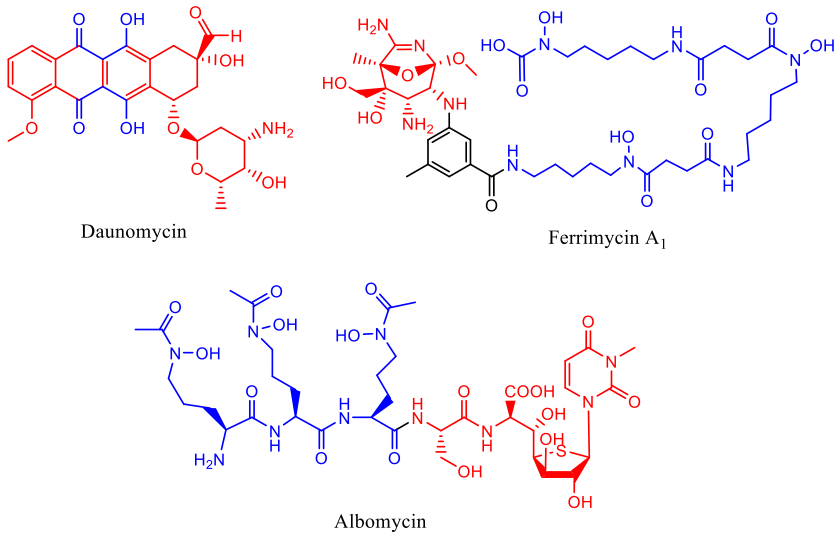

Figure 15. The molecular structures of the natural sideromycins; daunomycin, ferrimycin and albomycin[81]. The siderophore component (blue) and antibiotic component (red) of the structures are highlighted[81].

The most well studied naturally occurring sideromycin is albomycin[76,78,79]. This antibiotic was isolated by Gause and Brazhnikova from a species of streptomycetes, *Actinomyces subtropicus*, in 1951[79]. Albomycin was found to be effective at inhibiting the growth of various Gram-positive and Gram-negative strains[79]. It showed inhibition of the growth of staphylococci that was resistant to penicillin, tetracycline, streptomycin, and erythromycin[79]. Albomycin showed approximately a ten times lower MIC than penicillin against staphylococci[79]. The antibiotic has been shown to be non-toxic in animal and clinical trials[79]. Given these results Albomycin was used clinically in the Soviet Union by the 1940s[76,79].

Despite this great focus on Albomycin in the 1940s and 1950s it took until the 1980s for the structure of the antibiotic to be discovered, using chemical synthesis[78]. There are two main components of Albomycin like any sideromycin: the siderophore-like component and the antibiotic component or the "warhead" (Figure 16)[76,78]. The siderophore component is made from a serine linked to three N^5-acetyl-N^5-hydroxy-L-ornithine molecules through peptide linkages[82]. This structure forms a tri-hydroxamate iron-chelating ligand that is similar to ferrichrome[78]. The antibiotic component is a 4'-thio (N4-carbamoyl-3-methyl) cytidine moiety, a nucleoside analogous antibiotic[83]. There are three variations of albomycin that differ based off the substituents on the C4 of the cytidine component: Albomycin δ_1 (R=O), Albomycin δ_2 (R=$NCONH_2$), and Albomycin ε (R=NH) (Figure 16)[83].

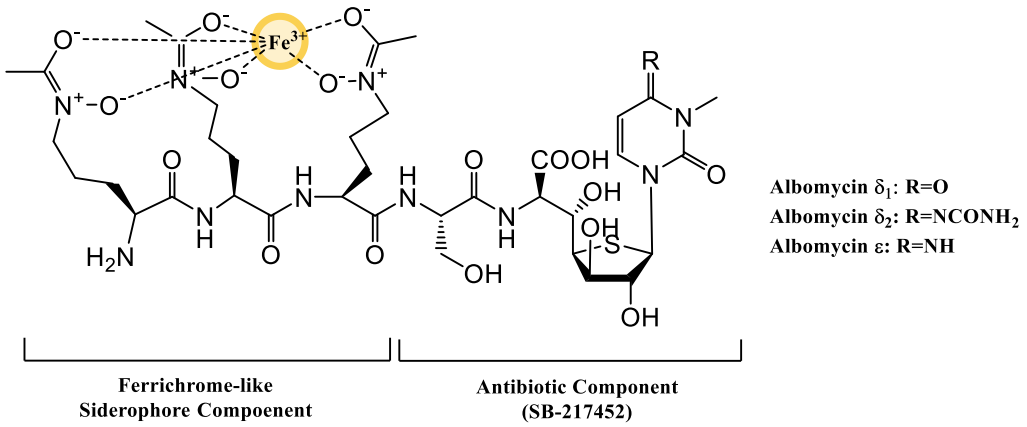

Figure 16. The molecular structure of the Albomycin conjugates highlighting the ferrichrome-like siderophore moiety and the active antibiotic component (SB-217452)[84]

Iron forms a complex with the ferrichrome-like component of albomycin and gets internalized by a Fe^{3+}-hydroxamate uptake system (Figure 17)[78]. In *E. coli*, this iron-complex binds to the TonB-dependent OMR FhuA, the binding of which stimulates its internalization into the periplasm[78]. Once in the periplasm, the Fe^{3+}-albomycin complex binds to FhuD the periplasmic subunit of FhuBC, an ABC transporter on the inner membrane of the cell[78,84]. Once transported into the cytoplasm by the FhuBCD complex, the Fe^{3+} of the complex gets reduced to Fe^{2+} and dissociates from the complex[78,84]. Then the siderophore component of albomycin gets cleaved off at the serine linker by the peptidase PepN, releasing the thioribosyl pyrimidine component (SB-217452)[84].

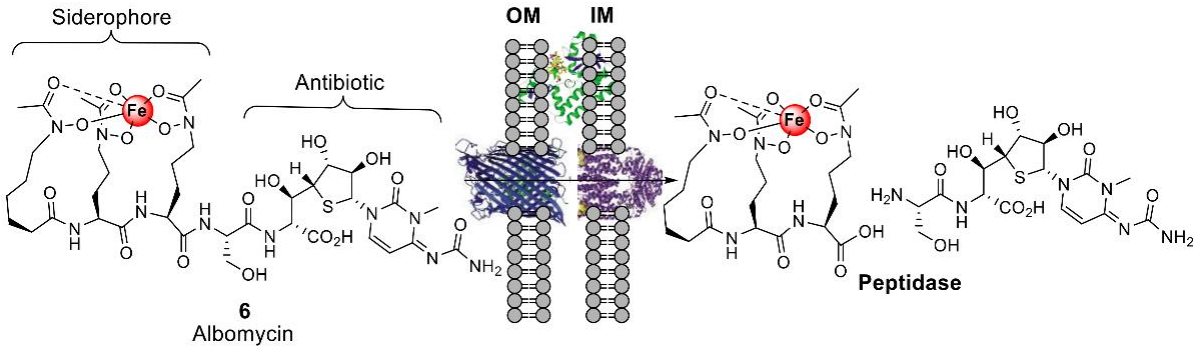

Figure 17. A schematic diagram showing the transportation of albomycin into Gram-negative bacteria[78]. Albomycin is actively transported across the outer (OM) and inner membrane (IM) using TonB-dependent and ABC transporter proteins[78]. Once in the cytoplasm albomycin is cleaved by a peptidase separating the siderophore and antibiotic components[78].

The seryl-linked thioribosyl pyrimidine was shown to inhibit the seryl-tRNA synthetase (SerRS) in Staphylococcus aureus at low concentrations[84]. Molecular modeling studies of the complex formed by SB-217452 and SerRS shows that the N4 carbamoyl modified cytosine of SB-217452 mimics the adenine of seryl-AMP (Figure X.)[84]. SerRSs are involved in protein translation by catalyzing the transfer of L-serine to the tRNA (Ser), using seryl-AMP as a substrate[84]. The inhibition of seryl-tRNA results in serine not being able to be added to growing peptide chains, blocking protein synthesis and results in the death of the cell[84]. When SB-217452 is added directly to bacterial culture the inhibition of growth is not observed. This shows that the activity of albomycin is dependent on the siderophore component for its entry into the target cells[84].

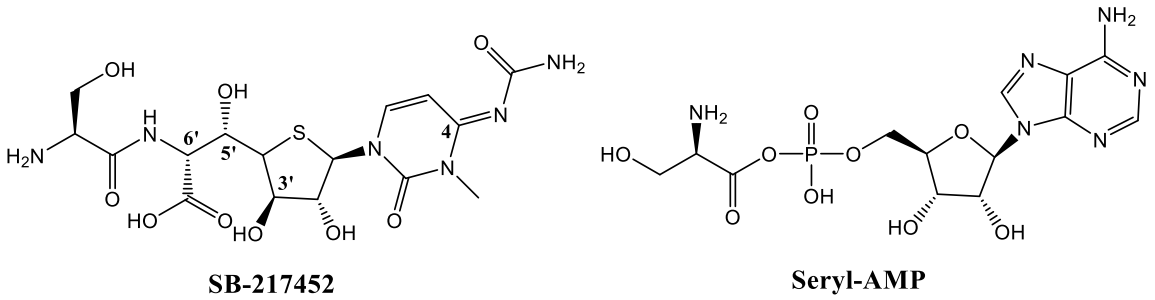

Figure 18. The molecular structure of SB-217452 (SerRS inhibitor) and Seryl-AMP (SerRS substrate) highlighting their similar framework[84].

1.4.4 Synthetic Sideromycins

Synthetic and semi-synthetic sideromycins have been reported as early as the 1970s[78]. Where known antibiotics are attached to natural occurring siderophore-like moieties via a relatively small linker[78]. This strategy is an attempt to increase the concentration of the antibiotic that makes it inside the cell, increasing the efficacy of the drug[78]. In 1977, Zahner et al. reported the synthesis of a sulfonamide antibiotic that was covalently linked to a ferrioxamine B analogue of which showed limited activity in Gram-positive *Staphylococcus aureus*[78]. Another notable attempt to make an effective synthetic sideromycin was done by Ohi, who synthesized ureidopenicillins covalently linked to catechol moieties[78]. These conjugates displayed a 30-60-fold decrease in the MICs compared to piperacillin against *P. aeruginosa*[78]. This work led to the focused research into catechol-β-lactam antibiotic conjugates in the 1980s and 1990s (GR69153, M-14659, and S-9096), finally leading to the development of cefiderocol[78,85].

Cefiderocol is the first sideromycin to advance into late-stage development and has been approved by the FDA for clinical use (Figure 19)[86]. It's an injectable cephalosporin-siderophore

synthesized and developed by Shingo & Co., Ltd., Japan[87]. Cephalosporins are β-lactam antibiotics, and as such their activity occurs due to the inhibition of the formation of bacterial cell walls[87]. Their target, penicillin-binding proteins (PBPs), is more difficult to reach in Gram-negative bacteria due to the low permeability of their outer membrane[87]. However, cefiderocol can penetrate the outer membrane with the siderophore component exploiting their siderophore uptake mechanism[87]. Cefiderocol was developed to treat serious Gram-negative bacterial infections showing potent activity against carbapenem-resistant and MDR Enterobacterials, and non-fermentative Gram-negative bacilli[87].

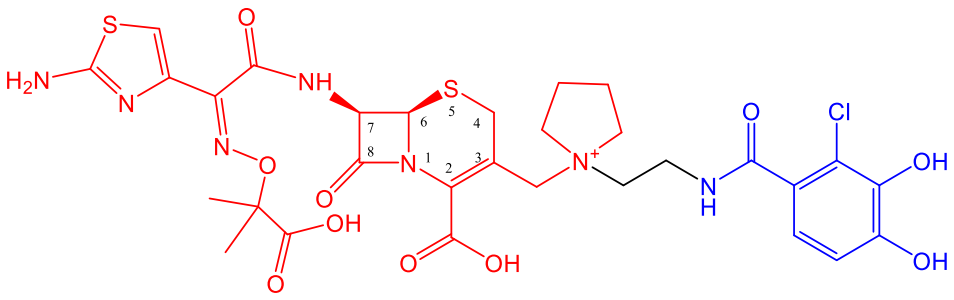

Cefiderocol

Figure 19. The molecular structure of cefiderocol highlighting the cephalosporin β-lactam component (red) and the catecholate siderophore component (blue)[87,88].

Cefiderocol has structurally stability against a variety of Ambler class A, C, and D β-lactamases, and is the first agent with activity against class B β-lactamases[87]. The resistance against β-lactamases and the siderophore component give cefiderocol enhanced activity against resistant bacteria[85,87]. Cefiderocol has microbiological activity superior or equal to that of

ceftazidime-avibactam and meropenem against Gram-negative bacilli and is more potent than both ceftazidime-avibactam and meropenem against *Actinetobacter baumanii* (including MDR isolates), and all resistant phenotypes of *Pseudomonas aeruginosa*[87].

Cefiderocol has a unique chemical structure of which has aspects of both ceftazidime and cefepime, third- and fourth- generation cephlasporins[85,87]. Cefiderocol has at its 7-position an amino-acyl group with an aminothiazole ring and a carboxypropyl-oxyimino attached to the alpha position, similar to ceftazidime (Figure 20)[87]. These components increase the functionality of cefiderocol[87]. Both the aminothiazole ring and the carboxypropyl-oxyimino group provide enhanced activity against Gram-negative bacilli, the latter gives stability against the hydrolysis by β-lactamases[87]. At the 3-position cefiderocol has a pyrrolidine ring attached by a one carbon linker, similar to cefepime (Figure 20)[87]. The zwitterionic properties of this pyrrolidine ring increases the water solubility[87]. However, unlike cefepime, cefiderocol has a 2-chloro-3,4-dihydroxybenzoic acid attached to the pyrrolidine ring is through an amide linker[87]. This unique structure gives cefiderocol the resistance to β-lactamases and the increased uptake into the periplasm by the catechol moiety[87].

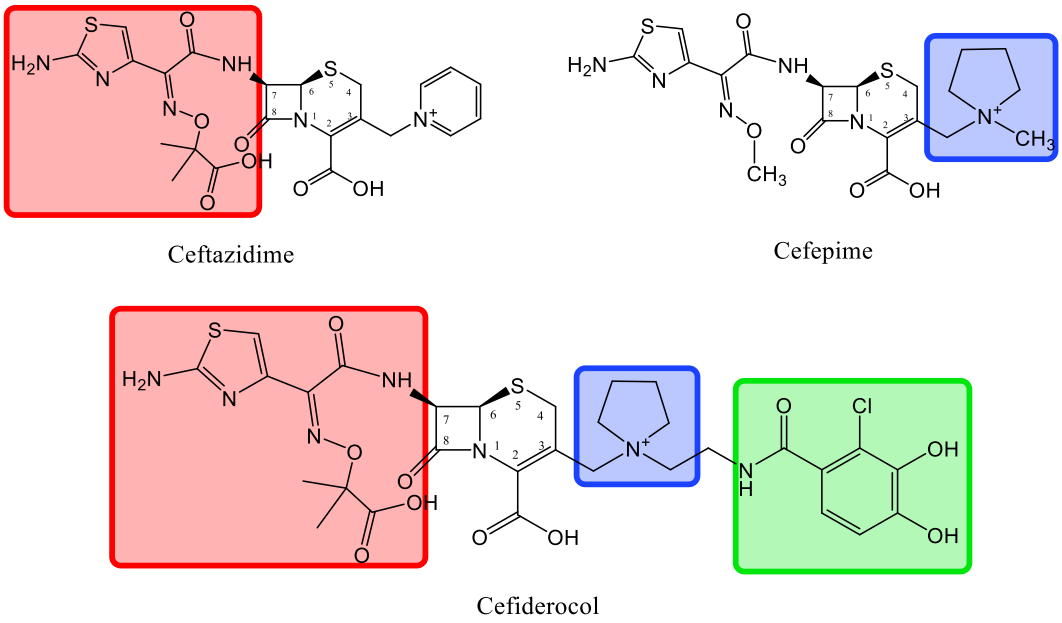

Figure 20. Diagram highlighting the structural activity relationship of cefiderocol to both ceftazidime and cefepime[87,88]. Attached to the 7-position the aminothiazole ring and the carboxypropyl-oxyimino group (red) come from ceftazidime. Attached to the 3-position the pyrrolidine ring (blue) comes from cefepime[87,88]. Cefiderocol then has a catecholate siderophore group (green) attached to the pyrrolidine ring[87,88].

Most β-lactamases antibiotics cross the outer membrane and enter the periplasm by passive diffusion through porin channels[87]. Due to the catechol binding ligand cefiderocol takes advantage of the iron uptake system of bacteria and increases its concentration into the periplasm compared to passive diffusion[87]. The catechol ligand forms a complex with Fe^{3} and binds to the OMR on bacteria, like PiuA in *P. aeruginosa*, which delivers the drug into the periplasm (Figure 21)[87]. Once in the periplasm, cefiderocol gets separated from the Fe^{3+} and binds to penicillin binding proteins (PBPs) and inhibit peptidoglycan synthesis, causing cell death (Figure 21)[87]. Like other oxyimino-cephalosporins, cefiderocol primarily binds to PBP_3[87]. Cefiderocol's ability

to utilize active transport into the periplasm and resist hydrolysis from a variety of β-lactamases makes it an innovate weapon against resistant bacteria[87].

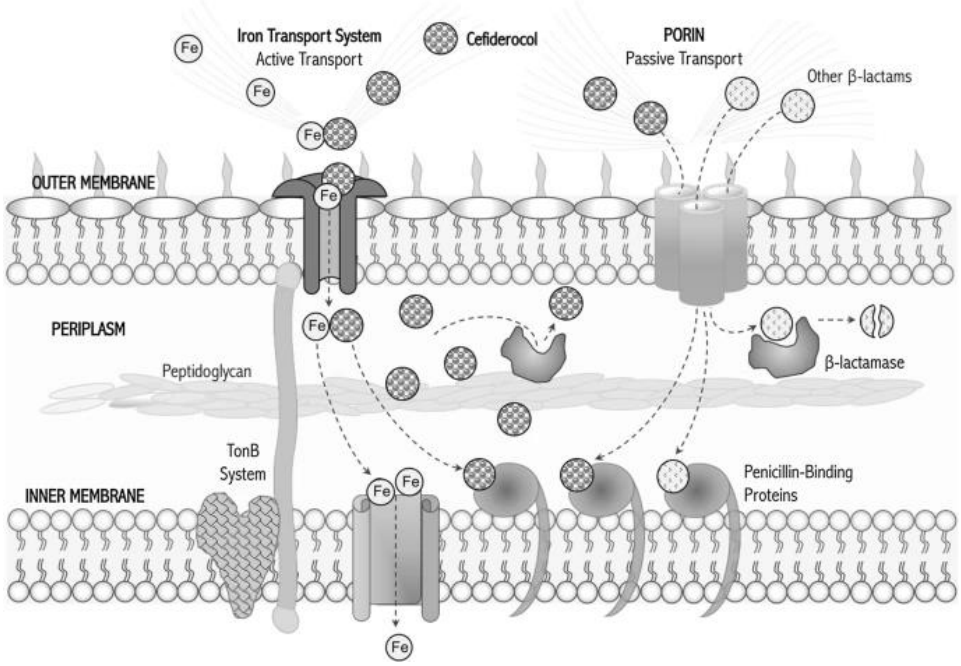

Figure 21. Diagram depicting the internalization and action of cefiderocol in Gram-negative bacteria[87].

1.5 REFERENCES

1. Ventola, C. L. The antibiotic resistance crisis: part 1: causes and threats. *P T* **40**, 277–283 (2015).

2. Magiorakos, A.-P. *et al.* Multidrug-resistant, extensively drug-resistant and pandrug-resistant bacteria: an international expert proposal for interim standard definitions for acquired resistance. *Clin Microbiol Infect* **18**, 268–81 (2012).

3. O'Neill J. Review on Antimicrobial Resistance Antimicrobial Resistance: Tackling a crisis for the health and wealth of nations. *London: Review on Antimicrobial Resistance* (2014).

4. Mohr, K. I. History of Antibiotics Research. in *How to Overcome the Antibiotic Crisis : Facts, Challenges, Technologies and Future Perspectives* (eds. Stadler, M. & Dersch, P.) 237–272 (Springer International Publishing, 2016). doi:10.1007/82_2016_499.

5. Aminov, R. I. A brief history of the antibiotic era: lessons learned and challenges for the future. *Front Microbiol* **1**, 134 (2010).

6. Wainwright, M. Moulds in Folk Medicine. *Folklore* **100**, 162–166 (1989).

7. Gaynes, R. The Discovery of Penicillin—New Insights After More Than 75 Years of Clinical Use. *Emerg Infect Dis* **23**, 849–853 (2017).

8. Coates, A. R. M., Halls, G. & Hu, Y. Novel classes of antibiotics or more of the same? *Br J Pharmacol* **163**, 184–94 (2011).

9. Bush, K. & Bradford, P. A. β-Lactams and β-Lactamase Inhibitors: An Overview. *Cold Spring Harb Perspect Med* **6**, (2016).

10. Krause, K. M., Serio, A. W., Kane, T. R. & Connolly, L. E. Aminoglycosides: An Overview. *Cold Spring Harb Perspect Med* **6**, a027029 (2016).

11. Mingeot-Leclercq, M. P. & Tulkens, P. M. Aminoglycosides: nephrotoxicity. *Antimicrob Agents Chemother* **43**, 1003–1012 (1999).

12. Guthrie, O. W. Aminoglycoside induced ototoxicity. *Toxicology* **249**, 91–96 (2008).

13. Takahashi, Y. & Nakashima, T. Actinomycetes, an Inexhaustible Source of Naturally Occurring Antibiotics. *Antibiotics (Basel)* **7**, 45 (2018).

14. Begg, E. J. & Barclay, M. L. Aminoglycosides--50 years on. *Br J Clin Pharmacol* **39**, 597–603 (1995).

15. Schatz, A. *et al.* The Classic: Streptomycin, a Substance Exhibiting Antibiotic Activity against Gram-Positive and Gram-Negative Bacteria. *Clin Orthop Relat Res* **437**, (2005).

16. Magnet, S. & Blanchard, J. S. Molecular Insights into Aminoglycoside Action and Resistance. *Chem Rev* **105**, 477–498 (2005).

17. Mahmud, T. Progress in aminocyclitol biosynthesis. *Curr Opin Chem Biol* **13**, 161–170 (2009).

18. Taber, H. W., Mueller, J. P., Miller, P. F. & Arrow, A. S. Bacterial uptake of aminoglycoside antibiotics. *Microbiol Rev* **51**, 439–457 (1987).

19. Bulitta, J. B. *et al.* Two mechanisms of killing of Pseudomonas aeruginosa by tobramycin assessed at multiple inocula via mechanism-based modeling. *Antimicrob Agents Chemother* **59**, 2315–2327 (2015).

20. François, B. *et al.* Crystal structures of complexes between aminoglycosides and decoding A site oligonucleotides: role of the number of rings and positive charges in the specific binding leading to miscoding. *Nucleic Acids Res* **33**, 5677–5690 (2005).

21. P, K. L., Jalal, H. & Shahriar, M. Aminoglycosides: Perspectives on Mechanisms of Action and Resistance and Strategies to Counter Resistance. *Antimicrob Agents Chemother* **44**, 3249–3256 (2000).

22. Tsai, A. *et al.* The Impact of Aminoglycosides on the Dynamics of Translation Elongation. *Cell Rep* **3**, 497–508 (2013).

23. Garneau-Tsodikova, S. & Labby, K. J. Mechanisms of Resistance to Aminoglycoside Antibiotics: Overview and Perspectives. *Medchemcomm* **7**, 11–27 (2016).

24. Murakami, S. Structures and Transport Mechanisms of RND Efflux Pumps. in *Efflux-Mediated Antimicrobial Resistance in Bacteria* 3–28 (Springer International Publishing, 2016). doi:10.1007/978-3-319-39658-3_1.

25. Ramaswamy, V. K., Vargiu, A. v., Malloci, G., Dreier, J. & Ruggerone, P. Molecular Rationale behind the Differential Substrate Specificity of Bacterial RND Multi-Drug Transporters. *Sci Rep* **7**, 8075 (2017).

26. Nikaido, H. Structure and mechanism of RND-type multidrug efflux pumps. *Adv Enzymol Relat Areas Mol Biol* **77**, 1–60 (2011).

27. Ramos, A. J. & Hiroshi, N. Aminoglycosides Are Captured from both Periplasm and Cytoplasm by the AcrD Multidrug Efflux Transporter of Escherichia coli. *J Bacteriol* **187**, 1923–1929 (2005).

28. Jeannot, K., Sobel, M. L., el Garch, F., Poole, K. & Plésiat, P. Induction of the MexXY efflux pump in Pseudomonas aeruginosa is dependent on drug-ribosome interaction. *J Bacteriol* **187**, 5341–6 (2005).

29. Hocquet, D. *et al.* MexXY-OprM efflux pump is necessary for a adaptive resistance of Pseudomonas aeruginosa to aminoglycosides. *Antimicrob Agents Chemother* **47**, 1371–5 (2003).

30. Morita, Y., Tomida, J. & Kawamura, Y. MexXY multidrug efflux system of Pseudomonas aeruginosa. *Front Microbiol* **3**, 408 (2012).

31. Singh, M., Sykes, E. M. E., Li, Y. & Kumar, A. MexXY RND pump of Pseudomonas aeruginosa PA7 effluxes bi-anionic β-lactams carbenicillin and sulbenicillin when it partners with the outer membrane factor OprA but not with OprM. *Microbiology (N Y)* **166**, 1095–1106 (2020).

32. Kahlmeter, G. & Dahlager, J. I. Aminoglycoside toxicity – a review of clinical studies published between 1975 and 1982. *Journal of Antimicrobial Chemotherapy* **13**, 9–22 (1984).

33. Baloh, R. W., Honrubia, V. & Kerber, K. A. Baloh and Honrubia's Clinical Neurophysiology of the Vestibular System. in (Oxford University Press, 2013). doi:10.1093/med/9780195387834.003.0001.

34. Driver, E. C. & Kelley, M. W. Development of the cochlea. *Development* **147**, dev162263 (2020).

35. Goodyear, R. J., Gale, J. E., Ranatunga, K. M., Kros, C. J. & Richardson, G. P. Aminoglycoside-induced phosphatidylserine externalization in sensory hair cells is regionally restricted, rapid, and reversible. *J Neurosci* **28**, 9939–9952 (2008).

36. Zheng, G. *et al.* Organ distribution in rats of two members of the low-density lipoprotein receptor gene family, gp330 and LRP/??2MR, and the receptor-associated protein (RAP). *J Histochem Cytochem* **42**, 531–542 (1994).

37. Hosokawa, S., Hosokawa, K., Ishiyama, G., Ishiyama, A. & Lopez, I. A. Immunohistochemical localization of megalin and cubilin in the human inner ear. *Brain Res* **1701**, 153–160 (2018).

38. Nagai, J., Tanaka, H., Nakanishi, N., Murakami, T. & Takano, M. Role of megalin in renal handling of aminoglycosides. *American Journal of Physiology-Renal Physiology* **281**, F337–F344 (2001).

39. Reiner, N. E., Bloxham, D. D. & Thompson, W. L. Nephrotoxicity of gentamicin and tobramycin given once daily or continuously in dogs *†. *Journal of Antimicrobial Chemotherapy* **4**, 85–101 (1978).

40. Ali, M. Z. & Goetz, M. B. A Meta-Analysis of the Relative Efficacy and Toxicity of Single Daily Dosing versus Multiple Daily Dosing of Aminoglycosides. *Clinical Infectious Diseases* **24**, 796–809 (1997).

41. Bailey, T. C., Little, J. R., Littenberg, B., Reichley, R. M. & Dunagan, W. C. A Meta-Analysis of Extended-Interval Dosing versus Multiple Daily Dosing of Aminoglycosides. *Clinical Infectious Diseases* **24**, 786–795 (1997).

42. Blaser, J. & König, C. Once-daily dosing of aminoglycosides. *European Journal of Clinical Microbiology and Infectious Diseases* **14**, 1029–1038 (1995).

43. Barza, M., Ioannidis, J. P., Cappelleri, J. C. & Lau, J. Single or multiple daily doses of aminoglycosides: a meta-analysis. *BMJ* **312**, 338–345 (1996).

44. Page, M. G. P. The Role of Iron and Siderophores in Infection, and the Development of Siderophore Antibiotics. *Clinical Infectious Diseases* **69**, S529–S537 (2019).

45. Martínez, J. L., Delgado-Iribarren, A. & Baquero, F. Mechanisms of iron acquisition and bacterial virulence. *FEMS Microbiol Rev* **6**, 45–56 (1990).

46. Hider, R. C. & Kong, X. Chemistry and biology of siderophores. *Nat Prod Rep* **27**, 637–657 (2010).

47. Khan, A., Singh, P. & Srivastava, A. Synthesis, nature and utility of universal iron chelator – Siderophore: A review. *Microbiol Res* **212–213**, 103–111 (2018).

48. Marcus, M. & A, M. M. Siderophore-Based Iron Acquisition and Pathogen Control. *Microbiology and Molecular Biology Reviews* **71**, 413–451 (2007).

49. Liu, B., Zhou, C., Zhang, Z., Roland, J. D. & Lee, B. P. Antimicrobial property of halogenated catechols. *Chemical Engineering Journal* **403**, 126340 (2021).

50. Bermejo, E., Carballo, R., Castiñeiras, A. & Lago, A. B. Coordination of α-hydroxycarboxylic acids with first-row transition ions. *Coord Chem Rev* **257**, 2639–2651 (2013).

51. Wilson, B. R., Bogdan, A. R., Miyazawa, M., Hashimoto, K. & Tsuji, Y. Siderophores in Iron Metabolism: From Mechanism to Therapy Potential. *Trends Mol Med* **22**, 1077–1090 (2016).

52. Golonka, R., Yeoh, B. S. & Vijay-Kumar, M. The Iron Tug-of-War between Bacterial Siderophores and Innate Immunity. *J Innate Immun* **11**, 249–262 (2019).

53. Brock, J. H. Iron-binding Proteins. *Acta Paediatr* **78**, 31–43 (1989).

54. Good, M., Kolls, J. K. & Empey, K. M. 123-Neonatal Pulmonary Host Defense. in *Fetal and Neonatal Physiology* 1265–1296 (2022).

55. Mietzner, T. A. & Morse, S. A. The Role of Iron-Binding Proteins in the Survival of Pathogenic Bacteria. *Annu Rev Nutr* **14**, 471–493 (1994).

56. Bezwoda, W. R. & Mansoor, N. Lactoferrin from human breast milk and from neutrophil granulocytes. Comparative studies of isolation, quantitation, characterization and iron binding properties. *Biomedical Chromatography* **3**, 121–126 (1989).

57. Hennigar, S. R. & McClung, J. P. Nutritional Immunity: Starving Pathogens of Trace Minerals. *Am J Lifestyle Med* **10**, 170–173 (2016).

58. Rishi, G., Wallace, D. F. & Subramaniam, V. N. Hepcidin: regulation of the master iron regulator. *Biosci Rep* **35**, e00192 (2015).

59. Ganz, T. & Nemeth, E. Hepcidin and iron homeostasis. *Biochim Biophys Acta* **1823**, 1434–1443 (2012).

60. Crouch, M.-L. v, Castor, M., Karlinsey, J. E., Kalhorn, T. & Fang, F. C. Biosynthesis and IroC-dependent export of the siderophore salmochelin are essential for virulence of Salmonella enterica serovar Typhimurium. *Mol Microbiol* **67**, 971–983 (2008).

61. Furrer, J. L., Sanders, D. N., Hook-Barnard, I. G. & McIntosh, M. A. Export of the siderophore enterobactin in Escherichia coli: involvement of a 43 kDa membrane exporter. *Mol Microbiol* **44**, 1225–1234 (2002).

62. Horiyama, T. & Nishino, K. AcrB, AcrD, and MdtABC multidrug efflux systems are involved in enterobactin export in Escherichia coli. *PLoS One* **9**, e108642–e108642 (2014).

63. Bleuel, C. *et al.* TolC is involved in enterobactin efflux across the outer membrane of Escherichia coli. *J Bacteriol* **187**, 6701–6707 (2005).

64. Hannauer, M., Barda, Y., Mislin, G. L. A., Shanzer, A. & Schalk, I. J. The ferrichrome uptake pathway in Pseudomonas aeruginosa involves an iron release mechanism with acylation of the siderophore and recycling of the modified desferrichrome. *J Bacteriol* **192**, 1212–1220 (2010).

65. Higgs, P. I., Larsen, R. A. & Postle, K. Quantification of known components of the Escherichia coli TonB energy transduction system: TonB, ExbB, ExbD and FepA. *Mol Microbiol* **44**, 271–281 (2002).

66. Klebba, P. E. ROSET Model of TonB Action in Gram-Negative Bacterial Iron Acquisition. *J Bacteriol* **198**, 1013–1021 (2016).

67. Chu, B. C. *et al.* Siderophore uptake in bacteria and the battle for iron with the host; a bird's eye view. *BioMetals* **23**, 601–611 (2010).

68. Chakraborty, R. *Iron Uptake in Bacteria with Emphasis on E. coli and Pseudomonas*. (Springer Netherlands, 2013).

69. Mislin, G. L. A. & Schalk, I. J. Siderophore-dependent iron uptake systems as gates for antibiotic Trojan horse strategies against Pseudomonas aeruginosa. *Metallomics* **6**, 408–420 (2014).

70. Kramer, J., Özkaya, Ö. & Kümmerli, R. Bacterial siderophores in community and host interactions. *Nat Rev Microbiol* **18**, 152–163 (2020).

71. Leventhal, G. E., Ackermann, M. & Schiessl, K. T. Why microbes secrete molecules to modify their environment: the case of iron-chelating siderophores. *J R Soc Interface* **16**, 20180674 (2019).

72. Butaitė, E., Baumgartner, M., Wyder, S. & Kümmerli, R. Siderophore cheating and cheating resistance shape competition for iron in soil and freshwater Pseudomonas communities. *Nat Commun* **8**, 414 (2017).

73. Tillotson, G. S. Trojan Horse Antibiotics-A Novel Way to Circumvent Gram-Negative Bacterial Resistance? *Infect Dis* **9**, 45–52 (2016).

74. Severinov, K. & Nair, S. K. Microcin C: biosynthesis and mechanisms of bacterial resistance. *Future Microbiol* **7**, 281–289 (2012).

75. Dong, S.-H. *et al.* Biosynthesis of the RiPP trojan horse nucleotide antibiotic microcin C is directed by the N-formyl of the peptide precursor. *Chem Sci* **10**, 2391–2395 (2018).

76. Braun, V., Pramanik, A., Gwinner, T., Köberle, M. & Bohn, E. Sideromycins: tools and antibiotics. *Biometals* **22**, 3–13 (2009).

77. Lin, Y.-M., Ghosh, M., Miller, P. A., Möllmann, U. & Miller, M. J. Synthetic sideromycins (skepticism and optimism): selective generation of either broad or narrow spectrum Gram-negative antibiotics. *BioMetals* **32**, 425–451 (2019).

78. Negash, K. H., Norris, J. K. S. & Hodgkinson, J. T. Siderophore-Antibiotic Conjugate Design: New Drugs for Bad Bugs? *Molecules* **24**, 3314 (2019).

79. Gause, G. F. Recent studies on albomycin, a new antibiotic. *Br Med J* **2**, 1177–1179 (1955).

80. Möllmann, U., Heinisch, L., Bauernfeind, A., Köhler, T. & Ankel-Fuchs, D. Siderophores as drug delivery agents: application of the “Trojan Horse” strategy. *BioMetals* **22**, 615–624 (2009).

81. Knüsel, F. & Nüesch, J. Mechanism of Action of Sideromycins. *Nature* **206**, 674–676 (1965).

82. Dolence, E. K., Lin, C. E., Miller, M. J. & Payne, S. M. Synthesis and siderophore activity of albomycin-like peptides derived from N5-acetyl-N5-hydroxy-L-ornithine. *J Med Chem* **34**, 956–968 (1991).

83. Ushimaru, R. & Liu, H. Biosynthetic Origin of the Atypical Stereochemistry in the Thioheptose Core of Albomycin Nucleoside Antibiotics. *J Am Chem Soc* **141**, 2211–2214 (2019).

84. Travin, D. Y., Severinov, K. & Dubiley, S. Natural Trojan horse inhibitors of aminoacyl-tRNA synthetases. *RSC Chem Biol* **2**, 468–485 (2021).

85. Sato, T. & Yamawaki, K. Cefiderocol: Discovery, Chemistry, and In Vivo Profiles of a Novel Siderophore Cephalosporin. *Clinical Infectious Diseases* **69**, S538–S543 (2019).

86. Saisho, Y., Katsube, T., White, S., Fukase, H. & Shimada, J. Pharmacokinetics, Safety, and Tolerability of Cefiderocol, a Novel Siderophore Cephalosporin for Gram-Negative Bacteria, in Healthy Subjects. *Antimicrob Agents Chemother* **62**, e02163-17 (2018).

87. Zhanel, G. G. *et al.* Cefiderocol: A Siderophore Cephalosporin with Activity Against Carbapenem-Resistant and Multidrug-Resistant Gram-Negative Bacilli. *Drugs* **79**, 271–289 (2019).

88. Aoki, T. *et al.* Cefiderocol (S-649266), A new siderophore cephalosporin exhibiting potent activities against Pseudomonas aeruginosa and other gram-negative pathogens including multi-drug resistant bacteria: Structure activity relationship. *Eur J Med Chem* **155**, 847–868 (2018).

Chapter 2: Thesis Objectives

2.1 THE PURPOSE OF THE THESIS

The purpose of this work is to explore how the "Trojan Horse" strategy can be used to develop novel therapeutics from aminoglycoside antibiotics. I hypothesize that this "Trojan Horse" model of sideromycins can be expanded to aminoglycoside antibiotics by making aminoglycoside-siderophore conjugates to increase their efficacy against MDR pathogens. There has never been aminoglycoside-siderophore conjugates synthesized previously, so this work represents a new embarkment into the unknown to obtain a better understanding of the effects of siderophore conjugation to antibiotics. As mentioned previously aminoglycosides have both an inner cellular target, the ribosome, and an outer cellular target, permeabilizing the cellular membrane. In theory these aminoglycoside-siderophore conjugates would be able to exploit the Fe^{3+}-siderophore uptake system, in affect increasing the concentration of the antibiotic in the cytoplasm and periplasm. This would hopefully increase its efficacy, allowing more of the conjugate to reach its inner cellular target, and bypass resistance mechanism. The theoretical increase in concentration delivered inside the cell as compared to unmodified tobramycin will hopefully also help reduce the concentration dependent toxicity of tobramycin. To test this premise, active tobramycin-catecholate (TOB-CAT) conjugates and control methoxy protected tobramycin-catecholate (TOB-mCAT) conjugates were synthesized and were tested against a variety of strains of bacteria for antibacterial and adjuvant activity.

2.1 STUDY OBJECTIVES

The ever-growing threat of antibiotic resistance bacteria makes the development of novel interventions a priority to public health. The aim of the work described in this thesis is utilize the emerging "Trojan Horse" strategy to develop and explore novel therapeutics against MDR bacteria. The study objectives include:

1) To design and synthesize aminoglycoside-siderophore conjugates. Utilizing tobramycin as the aminoglycoside component and 3,4-dihydroxybenzoic acid as a catecholate siderophore component.

2) To assess the antibacterial activity and adjuvant activity of the newly synthesized active conjugates by determining their minimum inhibitory concentration (MIC) and fractional inhibitory concentration (FIC) index in *in vitro* studies against various bacterial strains.

3) To carry out mechanistic studies to determine a possible mode of action for these newly synthesized active conjugates.

4) To explore the structural activity relationships of the siderophore component of the newly synthesized active conjugates by synthesizing control conjugates with the Fe^3 catecholate binding ligand blocked and then evaluate the antibacterial and adjuvant properties of the control conjugates.

2.2 THESIS ORGANIZATION

Chapter 1 introduces the emerging threat of antibacterial resistance, and a comprehensive review of aminoglycoside antibiotics, siderophores and sideromycins

Chapter 3 outlines the steps for the chemical synthesis of the tobramycin-catecholate active and control conjugates, along with a discussion about the protocol and the obstacles that have been overcome.

Chapter 4 outlines the results from the microbiological assays against various strains of bacteria. These include the determination of the MIC and FIC index for both the active and control tobramycin-siderophore conjugates to test their antibacterial and adjuvant activity. The MIC and FIC index were determined for the active conjugates in the both MHB and ID-CAMHB.

Chapter 5 outlines the data relevant from the mechanistic studies and discuss possible modes of action of the active compounds.

Chapter 6 summarize the outcomes from the studies and discusses what steps should be taken to explore future work.

Chapter 7 contains the supporting information for chapters 3, 4, and 5.

Chapter 3: Synthesis of Conjugates

3.1 CHEMICAL SYNTHESIS

3.1.1 Synthesis of the Active Tobramycin-Catechol Conjugates

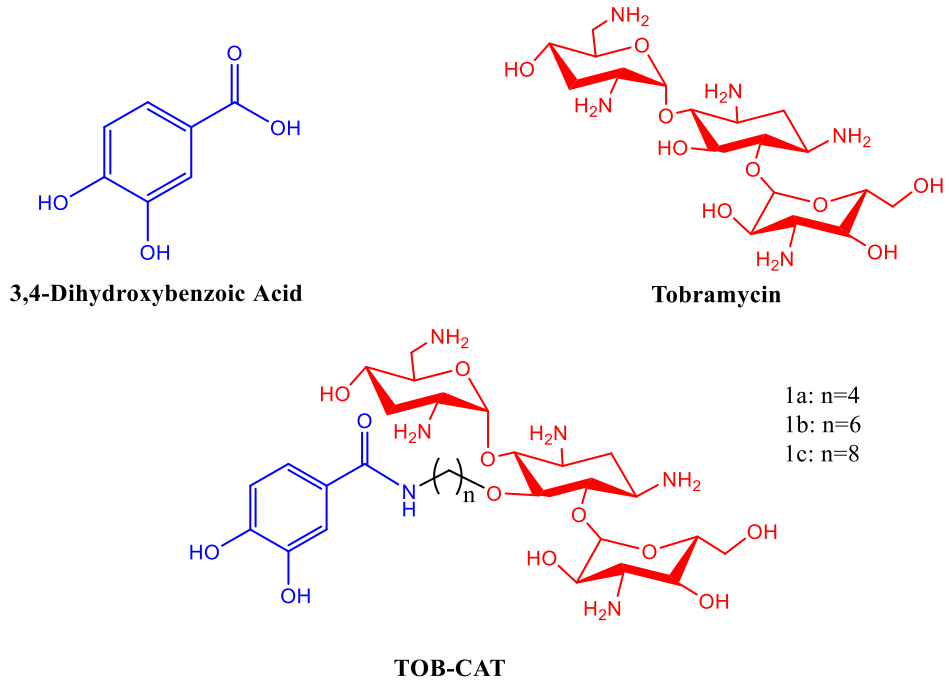

Figure 22. Structures of the synthesized TOB-CAT conjugates as well as the independent components of tobramycin and 3,4-dihydroxybenzoic acid.

A series of TOB-CAT conjugates **1a-c** were prepared with a varying carbon length linker joining the tobramycin to the catecholate binding group (Figure 22). Tobramycin was selected as the aminoglycoside representative because our group has a great deal of experience working with it and it being a 4,6-disubstituted DOS aminoglycoside it has a similar structure to commonly prescribed aminoglycosides[1–5]. A catecholate binding ligand was chosen to be the siderophore component of our conjugates because it is one of the most common binding ligands that are

incorporated in natural siderophores, like in enterobactin, and has seen success by being incorporated in cefiderocol[6,7]. The carbonyl carbon of a 3,4-dihydroxybenzoic acid was linked to the C5 position of tobramycin using an alkane chain[4].

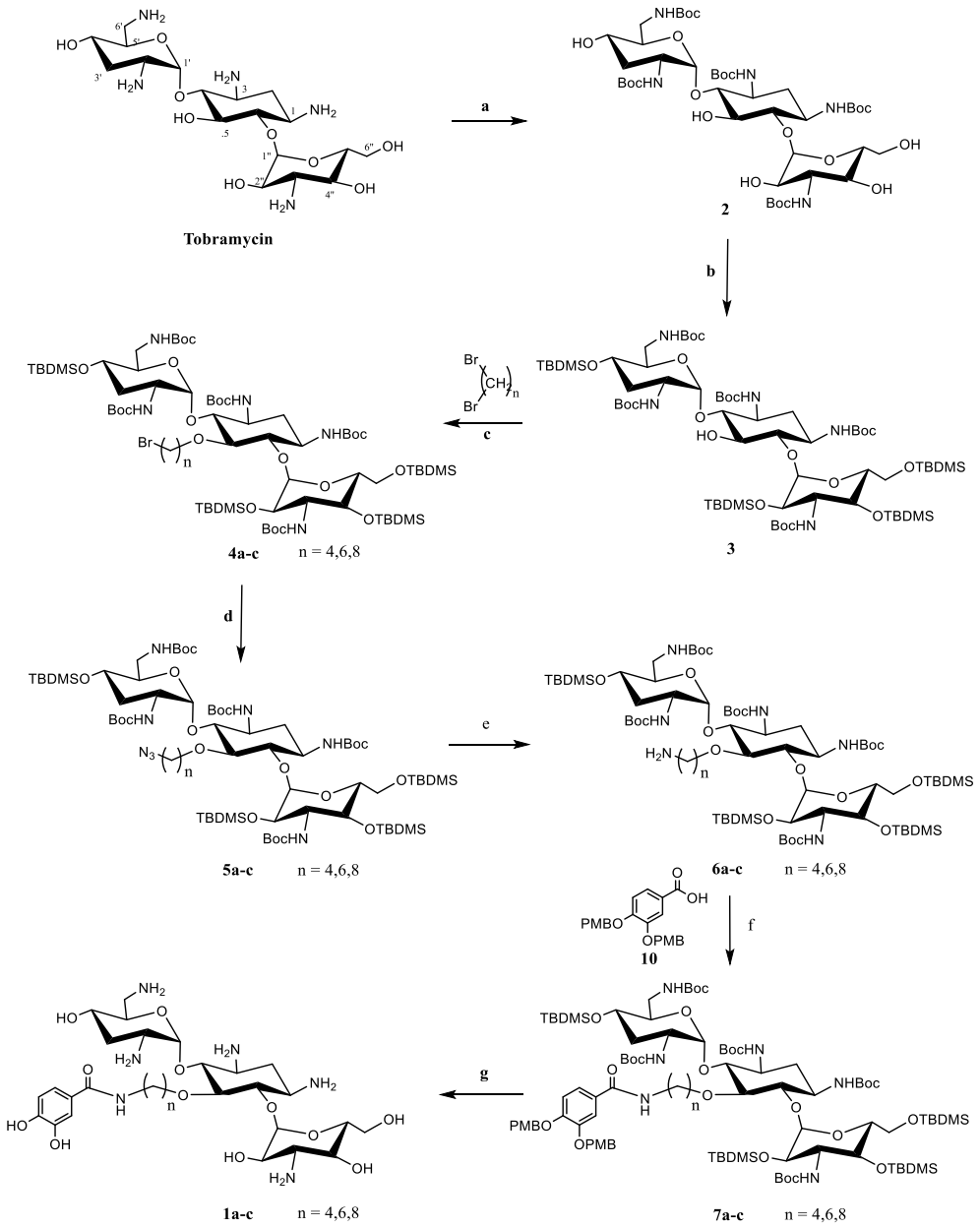

Scheme 1. Synthesis for compounds **1a-c**. Reagents and conditions: (a) $(Boc)_2O$, Et_3N, $MeOH/H_2O$ (2:1), rt to 55ºC, 16hr, 96%. (b) TBDMSCl, 1-methylimidazole, DMF, N_2 atmosphere, rt, 4 days, 92%. (c) Dibromoalkane, KOH, TBAHS, hydrated toluene, rt, overnight, 60-74%. (d) NaN_3, Dry DMF, N_2 atmosphere, 90ºC, 3-6hrs, 92-95%. (e) $Pd(OH)_2$, MeOH, H_2 atmosphere, 88-92%. (f) Mukaiyama Reagent, Et_3N, Dry THF, 90C, 5hrs, 21-41%. (g) HCl:MeOH (2:3), rt, 1hr, 21-45%.

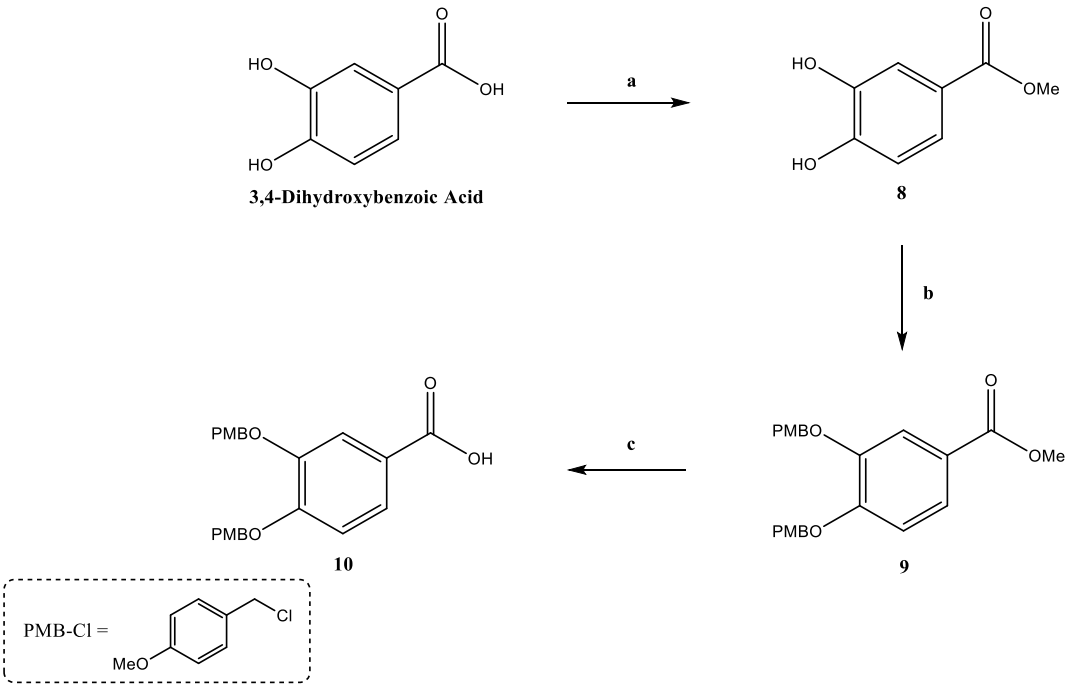

Scheme 2. Synthesis of compound **10**. Reagents and conditions: (a) H_2SO_4 (Cat.), MeOH, reflux, 16hrs, 92%. (b) PMB-Cl, K_2CO_3, 18-Crown-6, Dry DMF, 55°C, 16hrs, 89%. (c) 2M aq NaOH sol., THF:MeOH (1.3:1), reflux, 2hrs, 95%.

The synthesis of TOB-CAT conjugates **1a-c** (Scheme 1) were performed as follows. To create the Boc-protected tobramycin intermediate **2**, tobramycin was treated with di-tert-butyl dicarbonate ($(Boc)_2O$) and triethylamine (Et_3N)[1,4]. Treating **2** with TBDMSCl and 1-methylimidazole causes all the hydroxyl groups, except for the C5 positioned hydroxyl group, silyl protected, yielding intermediate **3**[1,4]. Intermediates **4a-c** are formed by reacting compound **3** with 1,*n*-dibromoalkane in basic conditions with hydrated toluene[1,4]. The bromine, at the end of the bromoalkylated intermediates **4a-c**, are substituted with an azide using NaN_3 to form the **5a-c** intermediates[4]. Intermediates **6a-c** are formed using $Pd(OH)_2$ to reduce the azides of compounds **5a-c** to amines[4]. Compounds **6a-c** were further coupled to a PMB protected 3,4-

dihydroxybenzoic acid, compound **10**, using Mukaiyama reagent and Et_3N to form intermediates **7a-c**[8]. After the amide coupling, intermediates **7a-c** are treated with HCl:MeOH (2:3 *v*/*v*) which deprotects the Boc, TBDMS, and PMB protecting groups in one step to form the final TOB-CAT conjugates, compounds **1a-c**[1,9,10].

In order to couple the catechol moiety to tobramycin, the 3,4-dihyrdoxybenzoic acid must be prepped by protecting the hydroxyl groups prior. The preparation of 3,4-dihydroxybenzoic acid to compound **10** (Scheme 2) were performed as follows[9]. 3,4-dihydroxybenzoic acid was treated with MeOH and H_2SO_4 forming a methyl ester intermediate **8**[9]. Next, the hydroxyl groups of compound **8** is protected using PMB-Cl and 18-Crown-6 in basic conditions, using K_2CO_3, to form intermediate **9**[9]. The final step in this preparation is the hydrolysis of the methyl ester using a 2M NaOH aq solution with a THF:MeOH (1.3:1 *v*/*v*) solvent to form the PMB protected 3,4-dihydroxybenzoic acid **10**[9].

3.1.2 Synthesis of the Control Tobramycin-Catechol Conjugates

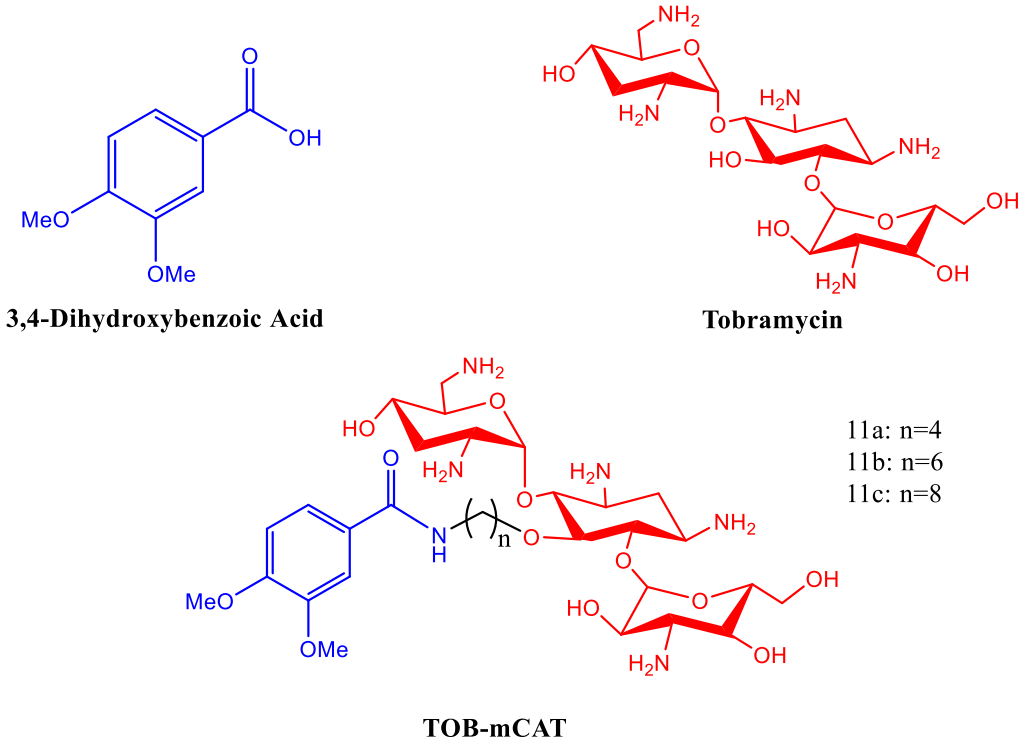

Figure 23. Structures of the synthesized TOB-mCAT conjugates as well as the independent components of tobramycin and 3,4-dihydroxybenzoic acid.

In order to study the effects of the catecholate group on activity of conjugates **1a-c** a control compound of similar structure must be synthesized to compare activity. To create a successful control compound, the goal is to isolate and change only the structural aspect that you are interested in comparing to the active compounds without compromising the rest of the structure. A series of TOB-mCAT conjugates **11a-c** were prepared with a varying carbon length linker joining tobramycin to a methoxy protected catecholate (Figure 23). So, where the TOB-CAT conjugates link 3,4-dihydroxybenzoic acid to tobramycin, the TOB-mCAT conjugates link 3,4-dimethoxybenzoic acid to tobramycin. The 3,4-dimethoxybenzoic acid has the catecholate

the hydroxy groups protected with methoxy groups. These methoxy groups prevent possible binding to the Fe^{3+} while being small enough to not drastically change structure of the molecule as compared to the TOB-CAT conjugates. Similar to the TOB-CAT conjugates, the aminoglycoside being used for the TOB-mCAT compounds is tobramycin and is connected at the C5 position to the carbonyl carbon of 3,4-dimethoxybenzoic acid via carbon linker.

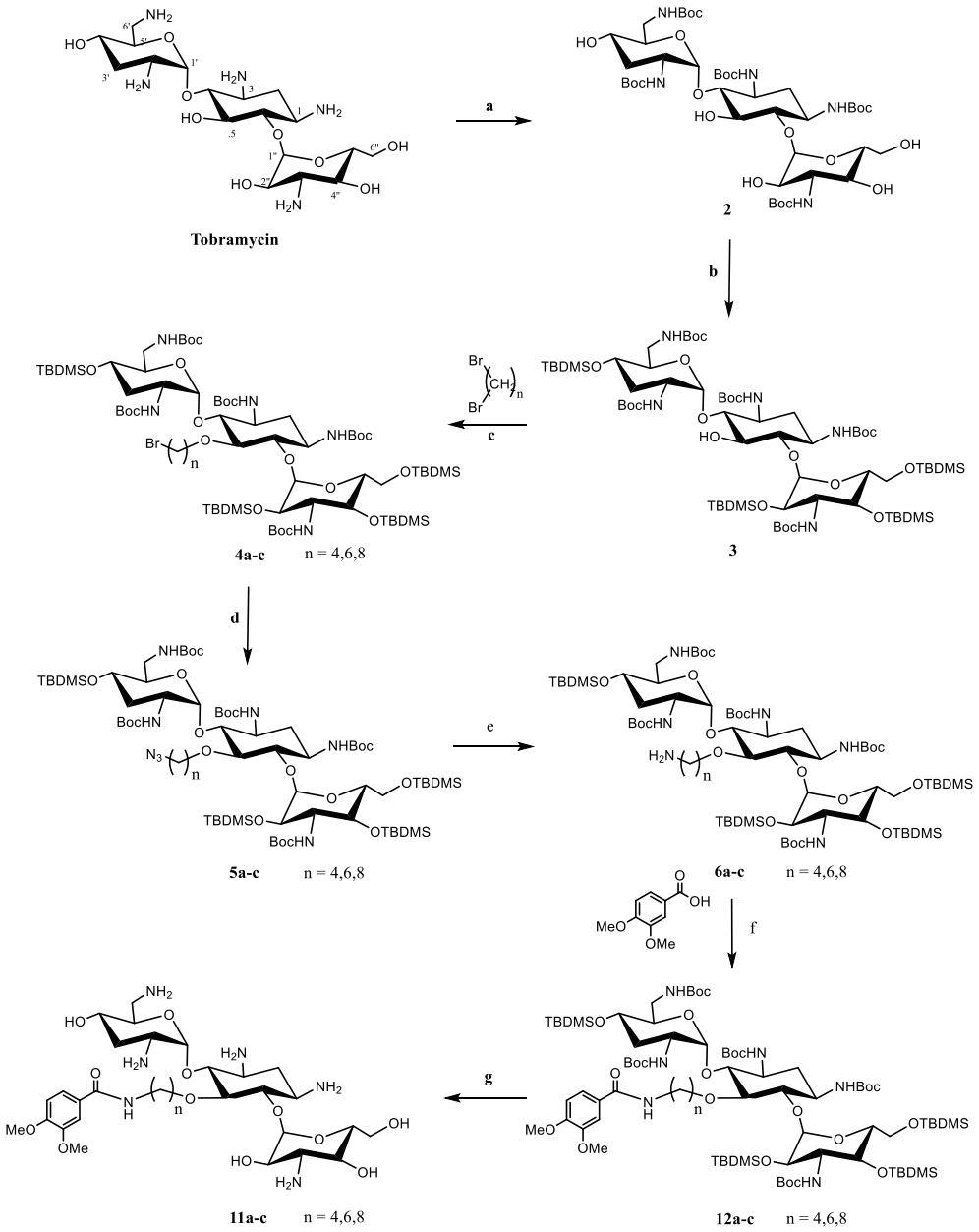

Scheme 3. Synthesis for compounds **11a-c**. Reagents and conditions: (a) $(Boc)_2O$, Et_3N, $MeOH/H_2O$ (2:1), rt to 55°C, 48hr, 96%. (b) TBDMSCl, 1-methylimidazole, DMF, N_2 atmosphere, rt, 4 days, 92%. (c) Dibromoalkane, KOH, TBAHS, hydrated toluene, rt, overnight, 60-74%. (d) NaN_3, Dry DMF, N_2 atmosphere, 90°C, 3-6hrs, 92-95%. (e) $Pd(OH)_2$, MeOH, H_2 atmosphere, 88-92%. (f) Mukaiyama Reagent, Et_3N, Dry THF, 90°C, 5hrs, 54-64%. (g) HCl:MeOH (2:3), rt, 1hr, 36-48%.

The synthesis protocol for the TOB-mCAT conjugates is virtually the same as the protocol for the synthesis of the TOB-CAT conjugates with the exception of using 3,4-dimethoxybenzoic acid instead of compound **10** during the amide coupling. The synthesis of TOB-mCAT conjugates **11a-c** (Scheme 3) were performed as follows. Tobramycin is reacted with di-tert-butyl dicarbonate ($(Boc)_2O$) and triethylamine (Et_3N) to form the Boc-protected intermediate **2**, protecting the amines of tobramycin. Protecting the hydroxyls, all except the one positioned at C5, with silyl ether protecting groups is done by reacting **2** with TBDMSCl and 1-methylimidazole, yielding the fully protected intermediate **3**. Then reacting **3** with 1,*n*-dibromoalkane in basic conditions with hydrated toluene results in the formation of intermediates **4a-c**. A substitution reaction is carried out with NaN_3 to substitute the bromine of conjugates **4a-c** with an azide to form conjugates **5a-c**. This azide on the **5a-c** conjugates is then reduced to an amine using $Pd(OH)_2$ in a H_2 environment to form the **6a-c** conjugates. These conjugates are then used in an amide coupling reaction using Mukaiyama reagent and Et_3N to link **6a-c** to 3,4-dimethoxybenzoic acid, resulting in the formation of compounds **7a-c**. The final step in this synthesis was the deprotection of the TBDMS and Boc protecting groups of **7a-c** using HCl:MeOH (2:3 *v*/*v*) which results in the formation of the TOB-mCAT conjugates **11a-c**

3.2 DISCUSSION

3.2.1 Rationalization of Component Selection

As mentioned previously I chose tobramycin as the aminoglycoside antibiotic component of these conjugates. Tobramycin was chosen because it is a 4,6-disubstituted 2-DOS aminoglycoside, of which is one of the larger classes of clinically used aminoglycosides, making

tobramycin a relatively good representative of clinically used aminoglycosides[6]. Also, our research group has extensive experience studying tobramycin and a have a method to selectively protect all amine and hydroxyl groups except the hydroxyl at the C5 position, allowing a location for alkylation and subsequent attachment of the catecholate group[1–4].

Tobramycin, like other aminoglycosides, have two modes of action: the inhibition of protein synthesis and the destabilization of the cellular membrane[11,12]. The membrane destabilization should remain with these conjugates as nothing is interfering with the polycationic structure of tobramycin when alkylating the hydroxyl at the C5 position[11,12]. However, predicting the effect of alkylating the C5 hydroxyl on the rRNA binding capabilities of tobramycin is more difficult. The C5 position is part of the highly conserved DOS ring of aminoglycosides, which is needed for protein inhibition[5]. This hydroxyl group forms a hydrogen bond to a water molecule of which through another molecule makes a hydrogen bond with the G_{1491} nucleotide in the A site on the 16S ribosomal RNA of *E. coli* (Figure 24)[5,13]. This interaction may not be crucial to the overall RNA binding of tobramycin because there are far more interactions from the other the anime and hydroxyl groups of tobramycin that are involved in RNA binding[5]. Also, the 4,5-disubstituted-2-DOS ring aminoglycosides are substituted at the C5 hydroxyl position, and these aminoglycosides are still able to interact with the RNA[5]. So, tobramycin is a reasonable choice for the antibiotic component, and it is reasonable to assume the antibiotic activity will be conserved after conjugation.

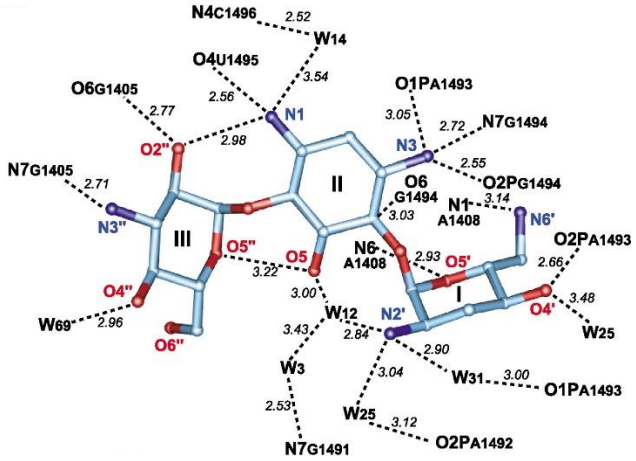

Figure 24. (a) A model of tobramycin displaying the hydrogen bonds (dashed lines) its functional groups form with *E. coli* rRNA[13].

For the siderophore component of these conjugates a catecholate moiety was chosen. Along with hydroxamate and carboxylate ligands, catecholate binding ligands are among the most common ligands that are incorporated in siderophores[6]. Catecholate moieties generally have a higher affinity for Fe^{3+} than other binding ligands, they are easy to conjugate in theory, and their use was put in practice with the development of cefiderocol[6,9]. For the active compounds 3,4-dihydroxybenzoic acid was used to add the catecholate group because the carboxylic acid moiety lends itself to be easily attached by amide coupling.

The control compounds needed to have a similar structure to the active compounds with the catechol moiety being inhibited. So, for the control compounds I chose to use 3,4-dimethoxybenzoic acid instead of the 3,4-dihydroxybenzoic acid. This is because the methoxy groups block the catechol function and are small enough additions to not compromise the original structures established from the active compounds. These factors make compounds **11a-c** viable as control compounds to test and compare to the TOB-CAT (**1a-c**) conjugates.

3.2.2 Obstacles Encountered During Synthesis

3.2.2.1 Catechol Protecting Groups

One of the obstacles that was encountered during the synthesis of the TOB-CAT was determining what protecting group to use for the 3,4-dihydroxybenzoic acid hydroxyl groups at the C3 and C4 positions. These hydroxyl groups need to be protected prior to the amide coupling step because the conditions of the amide coupling also promotes ester formation with any free hydroxyl groups, which would create side products.

One of the first attempts was to use silyl ether protection, using the same protocol as the protection of compound **2** (Figure 25)[1,4]. This produced multiple products, one of which was the successful protection of the two hydroxyl groups on the aromatic ring while leaving the acid moiety free. So, the protection of the 3,4-dihydroxybenzoic acid was fairly easy and in theory the deprotection would be easy as well because it would get deprotected along with the Boc and other TBDMS protecting groups in one step. However, while trying to couple this TBDMS-protected 3,4-dihydroxybenzoic acid to **6a-c** the TBDMS groups would deprotect and the target molecule was unable to be recovered. Despite changing the reaction conditions, the target molecule was still unable to be recovered. TBDMS is a fairly bulky protecting group, two TBDMS groups next to each other likely induce significant strain due to steric hindrance likely adding to their instability.

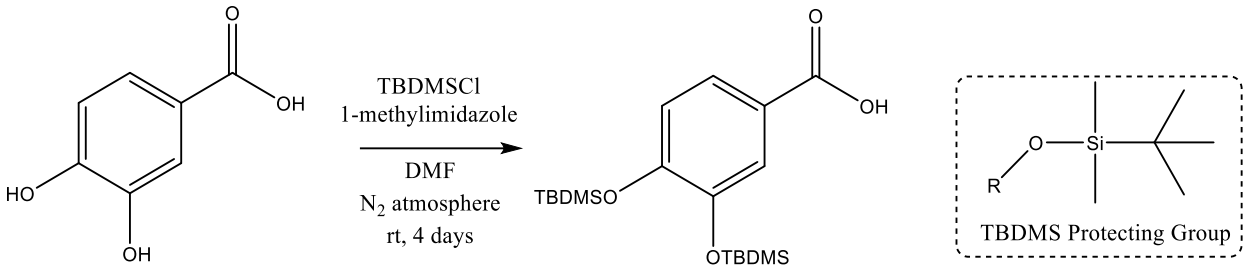

Figure 25. The TBDMS protection of 3,4-dihydroxybenzoic acid protocol.

The next protecting group that was considered was a methyl ether protecting group. This would have been done by conjugating 3,4-dimethoxybenzoic acid instead of 3,4-dihydroxybenzoic acid, as was done for the synthesis of **11a-c** (Scheme 3). Methyl ether protection are very stable so this would be well suited to use for the amide coupling reaction, evident from the synthesis of **11a-c** (Scheme 3). However, the stability of the methyl ethers would require a second deprotection step because the Boc and TBDMS deprotection step would not be able to deprotect the methyl ether. Commonly methyl ethers are deprotected by a BBr_3-asssisted cleavage reaction[14–16]. Our compounds have another ether linkages that connects the alkyl linker to the C5 position of tobramycin that might also get cleaved by the BBr_3 reaction[14–16]. Due to the possibility of cleaving the target molecule and the additional deprotection step, the methyl ether protection was passed on.

The next protecting group that was considered was a benzyl ether protecting group. Benzyl ether protection is generated by using William Ether Synthesis, where the hydroxyl group is initially deprotonated in basic conditions and then undergoes a S_N2 reaction with a benzyl halide[17]. These protecting groups are then often deprotected with palladium-catalyzed hydrogenation[18]. However, benzyl ethers are unstable in acidic conditions, so it's possible that it can be deprotected during the acidic deprotection of the Boc and TBDMS protecting groups[9]. P-

methoxybenzyl chloride (PMB-Cl) was chosen as the benzyl halide because its ether is slightly more reactive than an ordinary benzyl ether, owing to the electron donation from the methoxy group, making it easier to deprotect. PMB-Cl is also the benzyl halide used to protect the catecholate in the synthesis of cefiderocol, showing that PMB protection is able to withstand amide coupling conditions as well as being acid liable[9]. Our protection followed a standard Williamson Ether Synthesis mechanism using PMB-Cl with K_2CO_3 and 18-Crown-6 to generate the ether (Scheme 3). The PMB protecting group is then deprotected in the same acidic conditions that deprotect the Boc and TBDMS groups. PMB protection was then kept for the final protocol because it has a fairly simple protection step (Scheme 3) and gets deprotected in the same step as TBDMS and Boc (Scheme 1).

3.2.2.2 Amide Coupling Protocol

Another obstacle that had to be overcame during this synthesis was figuring out how to attach the catechol component to the tobramycin component. A few mechanisms were thought of including amide coupling and “Click Chemistry”, as our research group has experience with both. Ultimately amide coupling was discussed to be the first attempt, this is because the structure of 3,4-dihydroxybenzoic acid lends itself to be coupled to the amine of **6a-c**. Furthermore, this will allow the linker to be a simple alkane chain, unlike the 1,2,3 triazole linker that would be incorporated by Click Chemistry[19]. 1,2,3 triazole containing compounds have been shown to have biological activity[20–22]. When the purpose of this work is to elucidate the effects of the introducing catecholate groups to tobramycin, the introduction of other possible biological active structures, like 1,2,3 triazole, should be avoided where possible.

Amide bond formation usually involves the union of a carboxylic acid and an amine[23]. This unification does not happen spontaneously at room temperature, requiring high temperature to eliminate the water[23]. Organisms' biological systems utilize enzymes to catalyze this reaction at physiological temperatures[23]. For chemical synthesis, the carboxylic acid needs to first be activated by a coupling agent to convert the -OH of the acid to a good leaving group, followed by the treatment of the desired amine[23]. The coupling agents activate the carboxylic acid by generating active compounds such as acid chlorides, anhydrides, carbonic anhydrides, or active esters[23]. There are many coupling agents that have slightly different mechanism of activating the carboxylic acid[23]. The question now is which coupling agent to use for the coupling of the tobramycin conjugate to 3,4-dihydroxybenzoic acid.

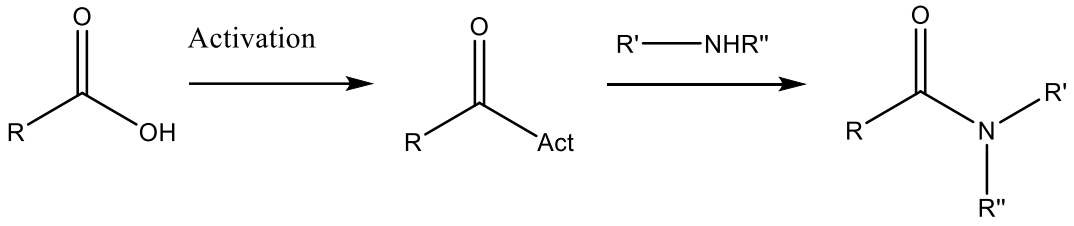

Figure 26. General outline for the amide coupling between a carboxylic acid and an amine.

The first coupling agent that was tried in the amide formation protocol was HATU, a guanidinium salt (Figure 28)[23,24]. In theory, this protocol initially starts with reacting the carboxylic acid (3,4-dimethoxybenzoic acid) with HATU and DIPEA to allow for the activated 7-azabenzotriazole (OAt) ester to be formed [23]. This is followed by the addition of the tobramycin amine intermediate (**6a-c**), which reacts with the activated OAt ester in a S_N1

mechanism to form the amide conjugate (**7a-c**). This mechanism is simplified in (Figure 27). Despite the theorized protocol being relatively straight forward, the desired **7a-c** conjugates were not formed. I tried changing the reaction time and temperature, however no amide coupling occurred and if left the mixture long enough I would get some deprotection of the protecting groups. I also tried changing the coupling agents to TBTU and HBTU, however I still could not get these guanidium coupling agents to work (Figure 28).

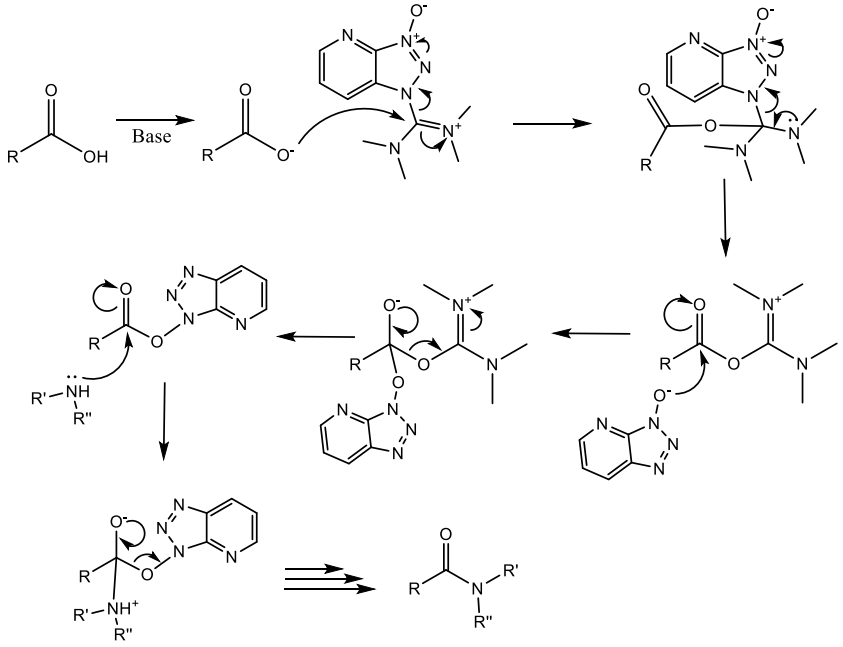

Figure 27. The carboxylic acid activation process and amide coupling mechanism using the guanidinium salt HATU[23]

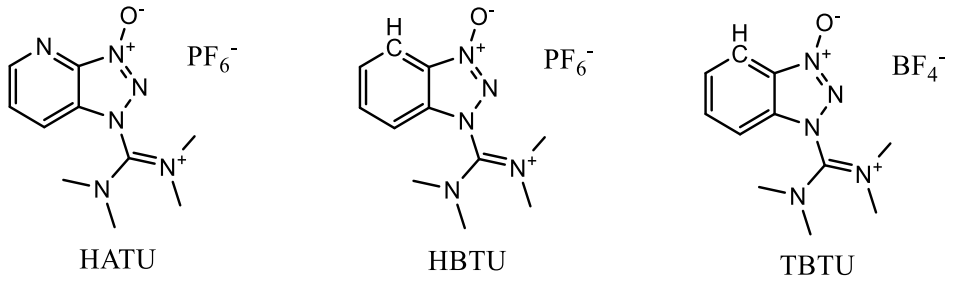

Figure 28. The molecular structures of the guanidinium salts HATU, HBTU, and TBTU[23].

The next coupling agent I tried using was N-methyl-2-chloropyridinium iodide (Mukaiyama's Reagent), which is part of the halo-pyridinium class of coupling agents[23]. Mukaiyama used N-methyl-2-chloropyridinium iodide to synthesize esters, amides and lactones[25]. However, it is not typically used for peptide synthesis because refluxing the reaction mixture is typically needed due to the insolubility of the agent[25].

The protocol follows the typical amide coupling outline where the carboxylic acid is first reacted with the Mukaiyama Reagent and a weak base. Then the activated ester is subjected to the desired amine which reacts in a S_N2 mechanism forming the target amide and a N-Methyl-2-pyridone side product (Figure 29)[26]. In this case, **10** was preactivated with Mukaiyama's reagent and triethylamine (Et_3N) in dry THF and an N_2 atmosphere to generate the activated ester intermediate[25,26]. Then compounds **6a-c** would be added to the reaction mixture and refluxed so it could react with the preactivated ester[25,26]. This method of amide coupling was found to work even though the yields are not ideal. I implemented this method for both the synthesis of the **1a-c** and the **11a-c** conjugates, with higher yields occurring for the reaction with 3,4-dimethoxybenzoic acid than the reaction with **10.** This difference in yield is likely due to the

large PMB protecting groups on **10** causing more significant steric hindrance than the methoxy groups on 3,4-dimethoxybenzoic.

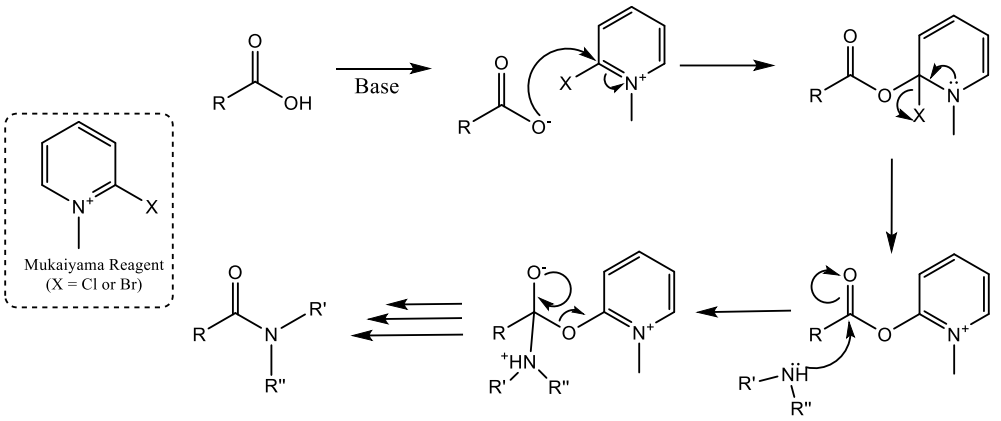

Figure 29. The carboxylic acid activation process and amide coupling mechanism using Mukaiyama Reagent[26]

3.2.2.3 Nebramine Formation

Nebramine is a 4-mono substituted-2-DOS ring aminoglycoside that is the product from the hydrolysis of tobramycin[1]. Our group has extensive experience synthesizing nebramine conjugates which typically requires a tobramycin conjugate to be subjected to MeOH:HCl (4:3) and heated at 70 °C overnight to get the hydrolysis to occur[1]. However, a problem that I was running into was the formation of the nebramine versions of my **1a-c** and **11a-c** conjugates when performing the deprotection with HCl:MeOH (2:3) (Figure 31). Even though this reaction was conducted at room temperature and only for the duration of an hour, the hydrolysis of tobramycin was still occurring producing the nebramine version of the conjugates along with a monosaccharide, kanosamine (Figure 30)[27].

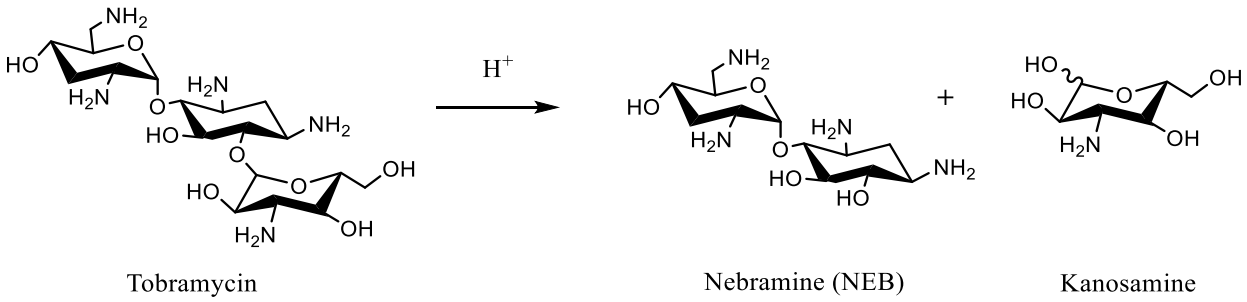

Figure 30. The hydrolysis of tobramycin in an acidic solution yielding nebramine and kanosamine[27].

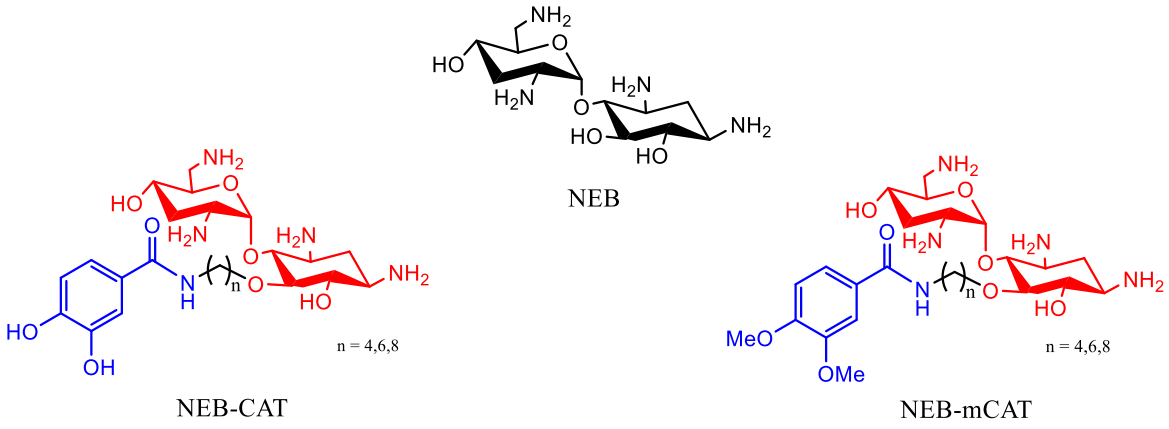

Figure 31. The molecular structure of nebramine (NEB), nebramine catecholate (NEB-CAT) and nebramine methoxy protected catecholate (NEB-mCAT) conjugates formed during the deprotection step.

The nebramine and kanosamine formed from this hydrolysis act as impurities when trying to isolate **1a-c** and **11a-c** from the reaction mixture[27]. Since nebramine and tobramycin are significantly polar molecules their conjugates elute close together and overlap when conducting a reverse phase column. In order to get a significantly pure final product I have to conduct multiple

reverse phase columns during the purification process. The formation of nebramine causes this deprotection step to have a relatively low yield, due both the product loss from the hydrolysis and the product loss during the purification steps.

The deprotection of the Boc and TBDMS protecting groups can be done in two consecutive steps, first deprotecting the TBDMS followed by the deprotection of Boc. This method would require more purification steps, with the product after the first deprotection step would have to be completely pure in order to reduce the side products for the final purification step. As a result, the overall yield for the consecutive step deprotection may be similar to the overall yield of the one-step deprotection.

An attempt was made to improve on the purification step after the one-step deprotection of Boc and TBDMS. After the reaction, the solid product was washed with a 10% NH_3 solution to neutralize the positive charge on the conjugates. This neutralized conjugate was then purified using a reverse phase chromatography on the Biotage auto-column with a 10% NH_3 in H_2O/MeOH. This allowed for a relatively easily separation of target conjugate from the nebramine and kanosamine impurities. The purified conjugate then needs to be washed with dilute HCl to recreate the HCl salt form of the target conjugate.

3.3 REFERENCES

1. Ammeter, D., Idowu, T., Zhanel, G. G. & Schweizer, F. Development of a nebramine-cyclam conjugate as an antibacterial adjuvant to potentiate β-lactam antibiotics against multidrug-resistant P. aeruginosa. *The Journal of Antibiotics* **72**, 816–826 (2019).

2. Guchhait, G. *et al.* Amphiphilic Tobramycins with Immunomodulatory Properties. *Angewandte Chemie* **127**, 6376–6380 (2015).

3. Domalaon, R., Yang, X., Lyu, Y., Zhanel, G. G. & Schweizer, F. Polymyxin B3–Tobramycin Hybrids with Pseudomonas aeruginosa-Selective Antibacterial Activity and Strong Potentiation of Rifampicin, Minocycline, and Vancomycin. *ACS Infectious Diseases* **3**, 941–954 (2017).

4. Lyu, Y. *et al.* Amphiphilic Tobramycin–Lysine Conjugates Sensitize Multidrug Resistant Gram-Negative Bacteria to Rifampicin and Minocycline. *Journal of Medicinal Chemistry* **60**, 3684–3702 (2017).

5. Magnet, S. & Blanchard, J. S. Molecular Insights into Aminoglycoside Action and Resistance. *Chemical Reviews* **105**, 477–498 (2005).

6. Hider, R. C. & Kong, X. Chemistry and biology of siderophores. *Natural Product Reports* **27**, 637–657 (2010).

7. Zhanel, G. G. *et al.* Cefiderocol: A Siderophore Cephalosporin with Activity Against Carbapenem-Resistant and Multidrug-Resistant Gram-Negative Bacilli. *Drugs* **79**, 271–289 (2019).

8. Pandey, K., Muthyala, M. K., Choudhary, S. & Kumar, A. Imidazolium salt-supported Mukaiyama reagent: an efficient condensation reagent for amide bond formation. *RSC Advances* **5**, 13797–13804 (2015).

9. Aoki, T. *et al.* Cefiderocol (S-649266), A new siderophore cephalosporin exhibiting potent activities against Pseudomonas aeruginosa and other gram-negative pathogens including multi-drug resistant bacteria: Structure activity relationship. *European Journal of Medicinal Chemistry* **155**, 847–868 (2018).

10. Williams, A. L., Dandepally, S. R. & Kotturi, S. v. A p-methoxybenzyl (PMB) protection/deprotection approach toward the synthesis of 5-phenoxy-4-chloro-N-(aryl/alkyl) thiophene-2-sulfonamides. *Molecular Diversity* **14**, 697–707 (2010).

11. Krause, K. M., Serio, A. W., Kane, T. R. & Connolly, L. E. Aminoglycosides: An Overview. *Cold Spring Harb Perspect Med* **6**, a027029 (2016).

12. Serio, A. W., Magalhães, M. L., Blanchard, J. S. & Connolly, L. E. Aminoglycosides: Mechanisms of Action and Resistance. in *Antimicrobial Drug Resistance: Mechanisms of Drug Resistance, Volume 1* (eds. Mayers, D. L., Sobel, J. D., Ouellette, M., Kaye, K. S. & Marchaim, D.) 213–229 (Springer International Publishing, 2017). doi:10.1007/978-3-319-46718-4_14.

13. Vicens, Q. & Westhof, E. Crystal Structure of a Complex between the Aminoglycoside Tobramycin and an Oligonucleotide Containing the Ribosomal Decoding A Site. *Chemistry & Biology* **9**, 747–755 (2002).

14. Punna, S., Meunier, S. & Finn, M. G. A Hierarchy of Aryloxide Deprotection by Boron Tribromide. *Organic Letters* **6**, 2777–2779 (2004).

15. Kosak, T. M., Conrad, H. A., Korich, A. L. & Lord, R. L. Ether Cleavage Re-Investigated: Elucidating the Mechanism of BBr3-Facilitated Demethylation of Aryl Methyl Ethers. *European Journal of Organic Chemistry* **2015**, 7460–7467 (2015).

16. Benton, F. L. & Dillon, T. E. The Cleavage of Ethers with Boron Bromide. I. Some Common Ethers. *J Am Chem Soc* **64**, 1128–1129 (1942).

17. Ouellette, R. J. & Rawn, J. D. 17 - Ethers and Epoxides. in *Organic Chemistry (Second Edition)* (eds. Ouellette, R. J. & Rawn, J. D.) 507–536 (Academic Press, 2018). doi:https://doi.org/10.1016/B978-0-12-812838-1.50017-7.

18. Yamamoto, Y. *et al.* Facile Hydrogenative Deprotection of N-Benzyl Groups Using a Mixed Catalyst of Palladium and Niobic Acid-on-Carbon. *ACS Omega* **5**, 2699–2709 (2020).

19. Thirumurugan, P., Matosiuk, D. & Jozwiak, K. Click Chemistry for Drug Development and Diverse Chemical–Biology Applications. *Chemical Reviews* **113**, 4905–4979 (2013).

20. Jakopec, S. *et al.* Ferrocene conjugates linked by 1,2,3-triazole and their Zn(II) and Cu(II) complexes: Synthesis, characterization and biological activity. *Applied Organometallic Chemistry* **36**, e6575 (2022).

21. Lauria, A. *et al.* 1,2,3-Triazole in Heterocyclic Compounds, Endowed with Biological Activity, through 1,3-Dipolar Cycloadditions. *European Journal of Organic Chemistry* **2014**, 3289–3306 (2014).

22. el Malah, T., Nour, H. F., Satti, A. A. E., Hemdan, B. A. & El-Sayed, W. A. Design, Synthesis, and Antimicrobial Activities of 1,2,3-Triazole Glycoside Clickamers. *Molecules* **25**, 790 (2020).

23. Valeur, E. & Bradley, M. Amide bond formation: beyond the myth of coupling reagents. *Chemical Society Reviews* **38**, 606–631 (2009).

24. Carpino, L. A. *et al.* The Uronium/Guanidinium Peptide Coupling Reagents: Finally the True Uronium Salts. *Angewandte Chemie International Edition* **41**, 441–445 (2002).

25. Pandey, K., Muthyala, M. K., Choudhary, S. & Kumar, A. Imidazolium salt-supported Mukaiyama reagent: an efficient condensation reagent for amide bond formation. *RSC Advances* **5**, 13797–13804 (2015).

26. Mukaiyama, T. New Synthetic Reactions Based on the Onium Salts of Aza-Arenes [New synthetic methods (29)]. *Angewandte Chemie International Edition in English* **18**, 707–721 (1979).

27. Brandl, M. & Gu, L. Degradation of tobramycin in aqueous solution. *Drug Development and Industrial Pharmacy* **18**, 1423–1436 (1992).

Chapter 4: Microbiological Studies

4.1 ANTIMICROBIAL STUDIES

4.1.1 Antimicrobial Activity of Active Compounds in MHB

The antibacterial activity of compounds **1a-c** was evaluated *in vitro* using the minimum inhibitory concentrations (MIC) against a panel of clinically relevant pathogens, comprised of Gram-negative wild and clinical isolate bacterial strains (Table 1). Antibacterial assays were carried out in Muller Hinton Broth (MHB). For the wild type strains, conjugates **1a-c** demonstrated some potent antibacterial activity against *P. aeruginosa* PAO1 (PAO1) (MIC 4-8 μg/mL) and less potent activity against *E. coli ATCC* 25922 and *Acinetobacter baumannii* ATCC 17978 (MIC ≥8 μg/mL). When compared to tobramycin (TOB), compounds **1a-c** have significantly less activity in all the wild type strains. The conjugates were also tested against a panel of clinically relevant Gram-positive wild type strains; however, no significant antibacterial activity was observed.

This *P. aeruginosa* specific activity that was observed for conjugates **1a-c** against the wild type strains becomes more apparent when taking a look at the clinical isolates. Compounds **1a-c** have potent activity against the *P. aeruginosa* clinical isolates (MIC 1-≤128 μg/mL) and no activity against the Enterobacteriaceae and *A. baumannii* clinical isolates (MIC ≥128 μg/mL). In almost all cases **1a-c** have significantly increased activity against the *P. aeruginosa* clinical isolates when compared to TOB, with the conjugates reaching TOB susceptibility breakpoints in *P. aeruginosa* 259-96918 (PA259), *P. aeruginosa* 260-97103 (PA260) and *P. aeruginosa* 101243 (PA101243). However, in all of the Enterobacteriaceae and *A. baumannii* clinical isolates, **1a-c** have significantly lower activity than TOB.

From the activity data of the *P. aeruginosa* clinical isolates, it seems like conjugate **1c** is the most active conjugate out of the three. Conjugate **1c** has notably a 256-fold, 64-fold, and a 64-fold increase in activity as compared to TOB against PA259, PA260, and *P. aeruginosa* 262-101856 (PA260) respectively.

Table 1. Antibacterial studies of TOB-CATs (**1a-c**) and tobramycin (TOB) against a panel of Gram-negative wild type and clinical isolates in MHB.

	Minimum Inhibitory Concentration (MIC) (μg/mL)				
Bacterial Strains	**TOB**	**FDC**	**1a**	**1b**	**1c**
Wild Type Strains					
***P. aeruginosa* PAO1**	0.5	0.25	8	4	8
***A. baumannii* ATCC 17978**	0.5	1	>128	8	>128
***E. coli ATCC* 25922**	2	0.25	64	32	128
Clinical Isolate Strains					
***P. aeruginosa* 100036**	128	0.125	16	16	8
***P. aeruginosa* 259-96918**	256	>8	4	4	1
***P. aeruginosa* 260-97103**	128	1	2	4	2
***P. aeruginosa* 262-101856**	1024	1	32	64	16
***P. aeruginosa* 264-104354**	128	1	32	128	16
***P. aeruginosa* 101243**	128	0.5	4	4	4
***A. baumannii* AB027**	64	>8	>128	>128	>128
***A. baumannii* LAC-4**	32	4	>128	>128	>128
***E. coli* 94474**	32	2	>128	>128	>128
***E. coli* 107115**	8	2	>128	>128	>128
***Enterococcus cloacae* 121187**	32	2	>128	>128	>128

4.1.2 Antimicrobial Activity of Active Compounds in ID-CAMHB

The antibacterial activity of conjugates **1a-c** were evaluated *in vitro* by measuring the MIC against clinically relevant Gram-negative bacteria by broth microdilution assays tested in iron deficient cation adjusted Mueller-Hilton broth (ID-CAMHB), which mimic the iron (Fe^{3+}) deficient conditions present during acute infections (Table 2). Using the methods provided by the CLSI, the produced ID-CAMHB media should contain 0.00 – 0.18 mg/L of iron, which is less than the 0.60 – 1.70 mg/L normal iron concentration range in human serum. TOB and cefiderocol (FDC) MIC data from microdilution broth assays were used to compare to the MICs of **1a-c** (Table 2).

The MIC results for conjugates **1a-c** against wild type Gram-negative strains have shown a significant decrease in activity in the ID-CAMHB (MIC ≥64 μg/mL). This decrease in activity is most prominently seen in PAO1, where there is an 8-fold or greater decrease in activity of **1a-c** as compared to their MICs in MHB (Table 2). Furthermore, the activity of **1a-c** has a larger decrease in activity as compared to TOB in ID-CAMHB than the conjugates did in regular MHB, this being a greater than 64-fold decrease. It is also evident that **1a-c** have far less activity than the FDA approved sideromycin FDC, with **1a-c** having at least a 128-fold decrease in activity as compared to FDC in ID-CAMHB.

Looking at the MIC results from the clinical isolates in ID-CAMHB we can see that **1a-c** have lost their significant antibacterial activity that they had in MHB. As the MICs for PA259, PA260, and PA260 that were 1-4 μg/mL in MHB are now >16 μg/mL in ID-CAMHB. This represents at least a 4-16-fold decrease in the activity of **1a-c** when they were subjected to the ID-CAMHB media. The *P. aeruginosa* specific activity that was once seen in the MHB media is

now lost in ID-CAMHB, where **1a-c** have MICs of >16 μg/mL against strains PA259, PA260, PA101243, and PA260, and MICs of >128 μg/mL for all other clinical isolates.

Table 2. Antibacterial activity of TOB-CATs (**1a-c**), tobramycin (TOB), and cefiderocol (FDC) against a panel of Gram-negative wild type and clinical isolate bacterial strains in ID-CAMHB.

	Minimum Inhibitory Concentration (MIC) (μg/mL)				
Bacterial Strains	**TOB**	**FDC**	**1a**	**1b**	**1c**
Wild Type Strains					
***P. aeruginosa* PAO1**	1	0.031	64	64	>128
***A. baumannii* ATCC 17978**	0.5	0.5	>128	64	>128
***E. coli ATCC* 25922**	0.5	0.031	64	64	128
Clinical Isolate Strains					
***P. aeruginosa* 100036**	>128	0.063	>16	>16	>16
***P. aeruginosa* 259-96918**	>128	0.125	>16	>16	>16
***P. aeruginosa* 260-97103**	128	0.063	>16	>16	>16
***P. aeruginosa* 262-101856**	>128	0.125	>128	>128	>128
***P. aeruginosa* 264-104354**	>128	0.063	>128	>128	>128
***P. aeruginosa* 101243**	128	0.125	>16	>16	>16
***A. baumannii* AB027**	128	8	>128	>128	>128
***A. baumannii* LAC-4**	128	2	>128	>128	>128
***E. coli* 94474**	32	0.25	>128	>128	>128
***E. coli* 107115**	8	0.5	>128	>128	>128
***E. cloacae* 121187**	32	0.25	>128	>128	>128

4.1.3 Antimicrobial Activity of Control Compounds in MHB

The antibacterial activity of the TOB-mCAT conjugates (**11a-c**) was determined *in vitro* by microdilution broth assays measuring the MICs in MHB against wild type and clinical isolate Gram-negative bacteria (Table 3). TOB and FDC MIC data from microdilution broth assays were used to compare to the MICs of **11a-c** (Table 3).

The MIC results for **11a-c** against both the wild type and clinical isolate Gram-negative strains show that the control compounds have no measurable antibacterial activity as compared to **1a-c** in MHB. Conjugates **11a-c** have MICs of >128 μg/mL against the wild type and clinical isolate strains. When looking at the strains where **1a-c** had the most significant activity against (PA259, PA260, and PA101243), we can see that compounds **11a-c** display >32-fold decease in activity. These results seem to suggest that the catechol binding ligand is critical for the activity of **1a-c**.

Table 3. Antibacterial activities of TOB-mCATs (**11a-c**), tobramycin (TOB), and cefiderocol (FDC) against a panel of Gram-negative wild type and clinical isolate bacterial strains in MHB

	Minimum Inhibitory Concentration (MIC) (μg/mL)				
Bacterial Strains	**TOB**	**FDC**	**11a**	**11b**	**11c**
Wild Type Strains					
***P. aeruginosa* PAO1**	0.5	0.25	>128	>128	>128
***A. baumannii* ATCC 17978**	0.5	1	>128	>128	>128
***E. coli ATCC* 25922**	2	0.25	>128	>128	>128
Clinical Isolate Strains					
***P. aeruginosa* 100036**	128	0.125	>128	>128	>128
***P. aeruginosa* 259-96918**	256	>8	>128	>128	>128
***P. aeruginosa* 260-97103**	128	1	>128	>128	>128
***P. aeruginosa* 262-101856**	1024	1	>128	>128	>128
***P. aeruginosa* 264-104354**	128	1	>128	>128	>128
***P. aeruginosa* 101243**	128	0.5	>128	>128	>128
***A. baumannii* AB027**	64	>8	>128	>128	>128
***A. baumannii* LAC-4**	32	4	>128	>128	>128
***E. coli* 94474**	32	2	>128	>128	>128
***E. coli* 107115**	8	2	>128	>128	>128
***E. cloacae* 121187**	32	2	>128	>128	>128

4.1.4 Antimicrobial Activity of Control Compounds in ID-CAMHB

The antibacterial activity of conjugates **11a-c** were evaluated *in vitro* by measuring the MIC against clinically relevant Gram-negative bacteria by broth microdilution assays tested in ID-CAMHB, to mimic the iron (Fe^{3+}) deficient conditions present during acute infections (Table 4). TOB and FDC MIC data from microdilution broth assays were used to compare to the MICs of **11a-c**.

As expected, the MIC results of conjugates **11a-c** show no activity against the wild type and clinical isolate Gram-negative bacterial strains, having MICs of >128 μg/mL for every strain. Since **1a-c** saw a decrease in activity in ID-CAMHB as compared to the activity in MHB, it makes sense that we don't observe an increased activity of **11a-c** in ID-CAMHB from their activity in MHB. Even though in ID-CAMHB **1a-c** has no significant activity, we are still able to see that **11a-c** conjugates have a lower activity in the wild type strains, where **1a** and **1b** have an MIC of 64 μg/mL against some strains while **11a-c** have MIC of >128 μg/mL against the same strains. This shows that the catechol binding ligand is vital to the activity of the **1a-c** conjugates despite the dampening effects of the ID-CAMHB media on their activity.

Table 4. Antibacterial activities of TOB-mCATs (**11a-c**), tobramycin (TOB), and cefiderocol (FDC) against a panel of Gram-negative wild type and clinical isolate bacterial strains in ID-CAMHB

	Minimum Inhibitory Concentration (MIC) (μg/mL)				
Bacterial Strains	**TOB**	**FDC**	**11a**	**11b**	**11c**
Wild Type Strains					
***P. aeruginosa* PAO1**	1	0.031	>128	>128	>128
***A. baumannii* ATCC 17978**	0.5	0.5	>128	>128	>128
***E. coli ATCC* 25922**	0.5	0.031	>128	>128	>128
Clinical Isolate Strains					
***P. aeruginosa* 100036**	>128	0.063	>128	>128	>128
***P. aeruginosa* 259-96918**	>128	0.125	>128	>128	>128
***P. aeruginosa* 260-97103**	128	0.063	>128	>128	>128
***P. aeruginosa* 262-101856**	>128	0.125	>128	>128	>128
***P. aeruginosa* 264-104354**	>128	0.063	>128	>128	>128
***P. aeruginosa* 101243**	128	0.125	>128	>128	>128
***A. baumannii* AB027**	128	8	>128	>128	>128
***A. baumannii* LAC-4**	128	2	>128	>128	>128
***E. coli* 94474**	32	0.25	>128	>128	>128
***E. coli* 107115**	8	0.5	>128	>128	>128
***E. cloacae* 121187**	32	0.25	>128	>128	>128

4.2 COMBINATION STUDIES

4.2.1 Combination Studies of Active Compounds Against Wild-type Gram-negative strains

To assess the adjuvant properties of the TOB-CAT conjugates (**1a-c**), checkerboard assays were conducted to determine their synergistic effects with a panel of 9 different antibiotics (across different antibiotic classes) against Gram-negative wild type and clinical isolate strains. The fractional inhibitory concentration (FIC) index, which is a numerical

quantification of the interaction between antibiotic and the tested conjugate, was calculated as described in Supplementary Information 7.2.2. Calculated FIC indices of >4, 0.5-4, and 0.5 indicate antagonism, no interaction, and synergy, respectively. To assess the adjuvant activity of compounds **1a-c** and **11a-c** at constant concentrations to one another, a "Relative MIC" for the antibiotics is also reported. This is the MIC of the antibiotic at a stated concentration of **1a-c** and **11a-c**.

Compounds **1a-c** showed synergy with minocycline, aztreonam, levofloxacin, rifampicin, and novobiocin against PAO1 (Table 5). With the greatest synergy of compounds **1a-c** seen with rifampicin (FIC index = 0.156 - 0.313), minocycline (FIC index = 0.25 - 0.313), and novobiocin (FIC index = 0.375 - 0.5). From the data (Table 5), compound **1c** seems to be the most synergistic with the selected antibiotics against PAO1.

Table 5. Combination Studies of Compounds **1a-c** Against Wild-Type *P. aeruginosa* PAO1.

Antibiotics	$MIC_{Antibiotic}$ (μg/mL)	$MIC_{Conjugates}$ (μg/mL)	FIC Index	Relative $MIC_{Antibiotic}$ [a] (μg/mL)	Fold Potentiation[b]
Compound 1a					
Aztreonam	8	16	0.375	1	8-Fold
Levofloxacin	0.25	16	0.500	0.0625	4-Fold
Minocycline	16	16	0.313	1	16-Fold
Novobiocin	512	16	0.375	64	8-Fold
Rifampicin	32	16	0.156	1	32-Fold
Compound 1b					
Aztreonam	4	16	0.500	1	4-Fold
Levofloxacin	0.5	16	0.500	0.125	4-Fold
Minocycline	32	16	0.250	2	16-Fold
Novobiocin	512	16	0.500	128	4-Fold
Rifampicin	32	16	0.313	2	16-Fold
Compound 1c					
Aztreonam	4	8	0.500	0.250	16-Fold
Levofloxacin	0.25	8	0.500	0.0313	8-Fold
Minocycline	8	8	0.313	0.5	16-Fold
Novobiocin	512	8	0.375	8	64-Fold
Rifampicin	32	8	0.188	0.0625	512-Fold

[a]Relative MIC of antibiotic was determined in the presence of 4 μg/mL of compounds **1a**, **1b** and **1c**. [b]Fold potentiation is calculated by $\frac{MIC_{Antibioitc}}{Relative\ MIC_{Antibioitc}}$, where values of ≤ 1 are reported as 0-Fold.

Compounds **1a-c** showed synergy with the β-lactam antibiotic aztreonam (FIC index = 0.375 – 0.5). To further investigate the possible synergy of compounds **1a-c** with β-lactam antibiotics, four more β-lactam antibiotics were selected to study. The β-lactam antibiotic family is broken down into multiple classes of which differ based off their chemistry around the β-lactam ring. The four additional antibiotics were selected across these different classes in order

to produce a diverse representative data of the β-lactam antibiotic family. These additional β-lactams are ceftazidime, piperacillin, imipenem, and meropenem of which represents the cephalosporin, penicillin, and carbapenem classes of β-lactams, respectfully. Along with aztreonam, a monobactam, these antibiotics cover the diverse β-lactam family fairly well.

Despite that all three TOB-CAT (**1a-c**) conjugates displayed synergy with aztreonam against PAO1 (Table 5), they had virtually no interaction with ceftazidime, piperacillin, meropenem and imipenem. That is with the exception of compound **1a** showing synergy with meropenem (FIC index = 0.375) against PAO1. Compound **1a** also seem to have the greatest adjuvant activity with these β-lactams as it has relatively lower FIC indices than compound **1b** and **1c**.

Table 6. Combination Studies of Compounds **1a-c** with β-lactam Antibiotics Against Wild-Type *P. aeruginosa* PAO1.

Antibiotics	$MIC_{Antibiotic}$ (μg/mL)	$MIC_{Conjugates}$ (μg/mL)	FIC Index	Relative $MIC_{Antibiotic}$[a] (μg/mL)	Fold Potentiation[b]
Compound 1a					
Ceftazidime	2	8	0.625	0.25	8-Fold
Piperacillin	4	8	0.750	1	4-Fold
Meropenem	1	8	0.375	0.125	8-Fold
Imipenem	2	8	0.750	1	2-Fold
Compound 1b					
Ceftazidime	2	16	0.625	1	2-Fold
Piperacillin	4	16	0.750	2	2-Fold
Meropenem	1	16	0.625	0.125	8-Fold
Imipenem	2	16	1.000	1	2-Fold
Compound 1c					
Ceftazidime	2	8	0.750	0.5	4-Fold
Piperacillin	4	8	0.750	2	2-Fold
Meropenem	1	8	0.750	0.25	4-Fold
Imipenem	2	8	1.000	1	2-Fold

[a]Relative MIC of antibiotic was determined in the presence of 4 μg/mL of compounds **1a**, **1b** and **1c**. [b]Fold potentiation is calculated by $\frac{MIC_{Antibioitc}}{Relative\ MIC_{Antibioitc}}$, where values of ≤ 1 are reported as 0-Fold.

Compounds **1a-c** showed synergy with aztreonam, rifampicin, and novobiocin against WT EC (Table 7). In addition, compound **1b** also displays synergy with levofloxacin, and compound **1c** shows synergy with minocycline. With the strongest synergy interaction of compounds **1a-c** occurring with rifampicin (FIC index = 0.063 – 0.375) and novobiocin (FIC index = 0.047 – 0.250). From the data of the combination study, compound **1c** is the most synergistic, displaying synergy with novobiocin (FIC index = 0.047), rifampicin (FIC index = 0.063), aztreonam (FIC index = 0.188), and minocycline (FIC index = 0.313).

Table 7. Combination Studies of Compounds **1a-c** Against Wild-Type *E. coli* ATCC 25922

Antibiotics	$MIC_{Antibiotic}$ (μg/mL)	$MIC_{Conjugates}$ (μg/mL)	FIC Index	Relative $MIC_{Antibiotic}$[a] (μg/mL)	Fold Potentiation[b]
Compound 1a					
Aztreonam	1	64	0.188	0.0625	16-Fold
Levofloxacin	0.0156	64	0.504	0.00781	2-Fold
Minocycline	1	64	0.750	1	0-Fold
Novobiocin	64	64	0.188	4	16-Fold
Rifampicin	4	64	0.188	0.25	16-Fold
Compound 1b					
Aztreonam	0.5	32	0.500	0.125	4-Fold
Levofloxacin	0.03125	32	0.275	0.00781	4-Fold
Minocycline	1	32	0.750	0.5	2-Fold
Novobiocin	64	32	0.250	2	32-Fold
Rifampicin	4	32	0.375	0.5	8-Fold
Compound 1c					
Aztreonam	0.5	128	0.188	0.125	4-Fold
Levofloxacin	0.0156	128	0.508	0.00781	2-Fold
Minocycline	1	128	0.313	0.25	4-Fold
Novobiocin	64	128	0.047	0.25	256-Fold
Rifampicin	4	128	0.063	0.0625	64-Fold

[a]Relative MIC of antibiotic was determined in the presence of 8 μg/mL of compounds **1a**, **1b** and **1c**. [b]Fold potentiation is calculated by $\frac{MIC_{Antibioitc}}{Relative\ MIC_{Antibioitc}}$, where values of ≤ 1 are reported as 0-Fold.

Compounds **1a-c** were also tested with the additional panel of β-lactam antibiotics as they showed synergy with aztreonam against WT EC (Table 7). Apart from compounds **1a** and **1c** with piperacillin, the TOB-CAT conjugates displayed virtually no synergy with the β-lactam antibiotics against WT EC (Table 8), despite them showing synergy with aztreonam. Compounds

1a and **1c** have slight synergy with piperacillin, having FIC indices of 0.313 and 0.156 respectively. Unlike the first panel of antibiotics tested (Table 7), there doesn't seem to be a better performing conjugate with these additional β-lactams against WT EC.

Table 8. Combination Studies of Compounds **1a-c** with β-lactam Antibiotics Against Wild-Typ *E. coli* ATCC 25922

Antibiotics	$MIC_{Antibiotic}$ (μg/mL)	$MIC_{Conjugates}$ (μg/mL)	FIC Index	Relative $MIC_{Antibiotic}$[a] (μg/mL)	Fold Potentiation[b]
Compound 1a					
Ceftazidime	4	64	0.750	4	0-Fold
Piperacillin	4	64	0.313	1	4-Fold
Meropenem	0.0156	64	1.004	0.0313	0-Fold
Imipenem	0.0625	64	2.004	0.0625	0-Fold
Compound 1b					
Ceftazidime	4	32	1.000	4	0-Fold
Piperacillin	4	32	0.750	2	2-Fold
Meropenem	0.0156	32	1.008	0.0313	0-Fold
Imipenem	0.0625	32	1.008	0.0625	0-Fold
Compound 1c					
Ceftazidime	4	128	0.563	2	2-Fold
Piperacillin	4	128	0.156	0.5	8-Fold
Meropenem	0.0156	128	2.002	0.0313	0-Fold
Imipenem	0.125	128	1.002	0.0625	2-Fold

[a]Relative MIC of antibiotic was determined in the presence of 8 μg/mL of compound **1a**, **1b** and **1c**. [b]Fold potentiation is calculated by $\frac{MIC_{Antibioitc}}{Relative\ MIC_{Antibioitc}}$, where values of ≤ 1 are reported as 0-Fold

Since the MICs of **1a-c** against WT AB are uncertain, as we can only say that it is above 128 μg/mL, the FIC indices are expressed as a range. When discussing these FIC indices ranges, we will be focusing on the upper limit of the range because the upper limit must be < 0.5 for the

interaction between the conjugate and antibiotic to be synergistic. Compounds **1a-c** showed good synergy with rifampicin (FIC index = 0.094 – 0.250) and novobiocin (FIC index = 0.156 - 0.250) against WT AB (Table 9). From these three conjugates, compound **1c** has the greater synergy and fold potentiation of rifampicin and novobiocin. Interestingly, despite **1b** having the greatest antibacterial activity against WT AB, it has lower synergy of rifampicin than **1c** which displayed no significant antibacterial activity (>128 μg/mL) against WT AB.

Table 9. Combination Studies of Compounds **1a-c** Against Wild-Type *A. baumannii* ATCC 17978.

Antibiotics	$MIC_{Antibiotic}$ (μg/mL)	$MIC_{Conjugates}$ (μg/mL)	FIC Index	Relative $MIC_{Antibiotic}$ [a] (μg/mL)	Fold Potentiation[b]
Compound 1a					
Aztreonam	64	>128	0.500<x≤0.531	32	2-Fold
Levofloxacin	0.125	>128	0.500<x≤0.563	0.0625	2-Fold
Minocycline	32	>128	0.500<x≤0.625	32	0-Fold
Novobiocin	32	>128	0.125<x≤0.250	8	4-Fold
Rifampicin	4	>128	0.125<x≤0.250	1	4-Fold
Compound 1b					
Aztreonam	64	>128	0.250<x≤0.375	32	2-Fold
Levofloxacin	0.125	>128	0.500<x≤0.563	0.125	0-Fold
Minocycline	32	>128	0.500<x≤0.563	16	2-Fold
Novobiocin	16	>128	0.031<x≤0.156	2	8-Fold
Rifampicin	4	>128	0.031<x≤0.156	0.5	8-Fold
Compound 1c					
Aztreonam	64	>128	1.000<x≤1.125	64	0-Fold
Levofloxacin	0.125	>128	1.000<x≤1.125	0.125	0-Fold
Minocycline	32	>128	1.000<x≤1.125	32	0-Fold
Novobiocin	16	>128	0.125<x≤0.188	2	8-Fold
Rifampicin	4	>128	0.031<x≤0.094	0.125	16-Fold

[a]Relative MIC of antibiotic was determined in the presence of 8 μg/mL of compound **1a**, **1b** and **1c**. [b]Fold potentiation is calculated by $\frac{MIC_{Antibioitc}}{Relative\ MIC_{Antibioitc}}$, where values of ≤ 1 are reported as 0-Fold

Despite compounds **1a-c** not showing any synergy with aztreonam against WT AB, they were still tested with the additional panel of β-lactam antibiotics to give a better perception on the β-lactam synergy of compounds **1a-c** in Gram-negative strains. Not surprisingly there was little synergy observed of the β-lactam antibiotics by **1a-c**, however, there was slight synergy of ceftazidime, piperacillin, and meropenem by compound **1b** (all having an FIC index = 0.375).

Table 10. Combination Studies of Compounds **1a-c** with β-lactam Antibiotics Against Wild-Type *A. baumannii* ATCC 17978.

Antibiotics	$MIC_{Antibiotic}$ (μg/mL)	$MIC_{Conjugates}$ (μg/mL)	FIC Index	Relative $MIC_{Antibiotic}$ [a] (μg/mL)	Fold Potentiation[b]
Compound 1a					
Ceftazidime	16	>128	0.500<x≤0.563	8	2-Fold
Piperacillin	32	>128	0.500<x≤0.531	16	2-Fold
Meropenem	0.25	>128	0.500<x≤0.625	0.125	2-Fold
Imipenem	0.0625	>128	1.000<x≤1.002	0.0625	0-Fold
Compound 1b					
Ceftazidime	16	>128	0.250<x≤0.375	8	2-Fold
Piperacillin	32	>128	0.250<x≤0.375	16	2-Fold
Meropenem	0.5	>128	0.250<x≤0.375	0.25	2-Fold
Imipenem	0.0625	>128	0.500<x≤0.625	0.0313	2-Fold
Compound 1c					
Ceftazidime	16	>128	0.500<x≤0.531	28	2-Fold
Piperacillin	32	>128	0.500<x≤0.625	32	0-Fold
Meropenem	0.25	>128	1.000<x≤1.002	0.25	0-Fold
Imipenem	0.0625	>128	1.000<x≤1.002	0.0625	0-Fold

[a]Relative MIC of antibiotic was determined in the presence of 8 μg/mL of compound **1a**, **1b** and **1c**. [b]Fold potentiation is calculated by $\frac{MIC_{Antibioitc}}{Relative\ MIC_{Antibioitc}}$, where values of ≤ 1 are reported as 0-Fold.

There are a few interesting points to note in the overview of the combination studies of **1a-c** against the wild-type Gram negative strains (Figure 32). Firstly, **1a-c** display good synergy with the main panel of five antibiotics against both PAO1 and WT EC, with some synergy of piperacillin with **1a** and **1c** against WT EC. Secondly, against WT AB synergy of rifampicin and novobiocin is mainly observed with **1a-c**, and **1c** displays synergy with aztreonam, ceftazidime, piperacillin, and meropenem against WT AB. Novobiocin and rifampicin were the antibiotics that synergized the most with **1a-c** against all three strains.

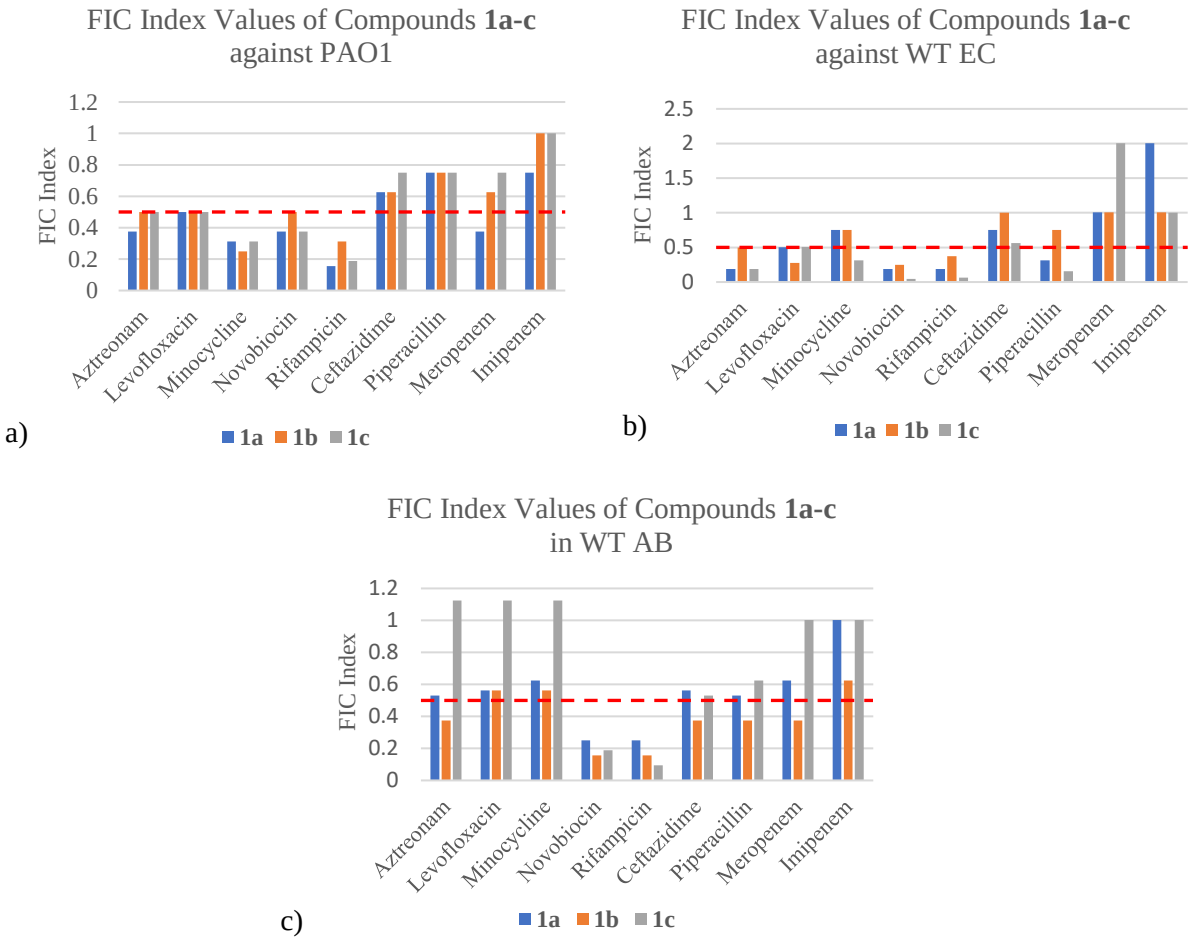

Figure 32. Bar graphs displaying the FIC indices of compounds **1a-c** with 9 selected antibiotics against a) PAO1, b) WT EC, and c) WT AB. FIC index values less than and equal to 0.5 (represented by the red dashed line) indicate a synergistic interaction.

4.2.2 Combination Studies of Active Compounds Against Gram-negative Clinical Isolates

Checkerboard assays were conducted to assess the adjuvant properties of compounds **1a-c** with 5 selected antibiotics (aztreonam, levofloxacin, minocycline, novobiocin, and rifampicin) against selected clinical isolate strains of *P. aeruginosa.* Strains PA259, PA260, and PA101243 were selected for these combination studies as compounds **1a-c** displayed strong antibacterial

activity on their own (Table 1). It is difficult to measure the synergy of **1a-c** in these clinical isolates, as the MIC in these strains are already relatively low and so the solo antibacterial activity of these conjugates takes over in the combination study.

Compounds **1a-c** all showed synergy with minocycline (FIC index = 0.281 – 0.500) against PA260, with some of the compounds showing synergy with novobiocin, levofloxacin, and rifampicin (Table 11). Compound **1a** showed the most synergy, having synergistic interactions with levofloxacin (FIC index = 0.313), minocycline (FIC index = 0.281), and rifampicin (FIC index = 0.500). However, **1c** showed the highest potentiation of the antibiotics at a concentration of 1 μg/mL, notably novobiocin and rifampicin being potentiated 16-fold.

Table 11. Combination Studies of Compounds **1a-c** Against *P. aeruginosa* PA260

Antibiotics	$MIC_{Antibiotic}$ (μg/mL)	$MIC_{Conjugates}$ (μg/mL)	FIC Index	Relative $MIC_{Antibiotic}$[a] (μg/mL)	Fold Potentiation[b]
Compound 1a					
Aztreonam	64	4	0.750	128	0-Fold
Levofloxacin	32	4	0.313	16	2-Fold
Minocycline	16	4	0.281	8	2-Fold
Novobiocin	512	4	0.531	256	2-Fold
Rifampicin	16	4	0.500	4	4-Fold
Compound 1b					
Aztreonam	64	4	0.504	64	0-Fold
Levofloxacin	32	4	0.504	16	2-Fold
Minocycline	16	4	0.500	8	2-Fold
Novobiocin	512	4	0.750	512	0-Fold
Rifampicin	16	4	0.500	16	0-Fold
Compound 1c					
Aztreonam	64	2	0.750	16	4-Fold
Levofloxacin	32	2	0.625	4	8-Fold
Minocycline	16	2	0.375	4	4-Fold
Novobiocin	512	2	0.500	32	16-Fold
Rifampicin	16	2	0.563	1	16-Fold

[a]Relative MIC of antibiotic was determined in the presence of 1 μg/mL of compound **1a**, **1b** and **1c**. [b]Fold potentiation is calculated by $\frac{MIC_{Antibioitc}}{Relative\ MIC_{Antibioitc}}$, where values of ≤ 1 are reported as 0-Fold

The MICs of **1a-c** determined from their combination studies against PA259 (Table 12) were higher than the expected MICs of Table 1. Due to this, there is uncertainty with the MICs, and they can only be stated as being >4 μg/mL until further studies are done. Compounds **1a-c** displayed little synergy with the selected antibiotics against PA259, with only **1a** and **1c** having synergistic interactions with rifampicin (Table 12). Compounds **1a** and **1c** have FIC indices with

upper limits of 0.500 and 0.375, respectively, with rifampicin. Compounds **1a** and **1c,** at a concentration of 4 μg/mL, have a 16-fold and 32-fold potentiation of rifampicin against PA259.

Table 12. Combination Studies of Compounds **1a-c** Against *P. aeruginosa* PA259

Antibiotics	$MIC_{Antibiotic}$ (μg/mL)	$MIC_{Conjugates}$ (μg/mL)	FIC Index	Relative $MIC_{Antibiotic}$[a] (μg/mL)	Fold Potentiation[b]
Compound 1a					
Aztreonam	32	>4	1.000<x≤1.008	64	0-Fold
Levofloxacin	512	>4	0.500<x≤1.000	256	2-Fold
Minocycline	32	>4	0.500<x≤0.750	8	4-Fold
Novobiocin	2048	>4	0.500<x≤1.000	1024	2-Fold
Rifampicin	16	>4	0.250<x≤0.500	1	16-Fold
Compound 1b					
Aztreonam	32	>4	1.000<x≤1.008	32	0-Fold
Levofloxacin	512	>4	0.500<x≤1.000	256	2-Fold
Minocycline	32	>4	0.500<x≤1.000	16	2-Fold
Novobiocin	2048	>4	1.000<x≤1.008	2048	0-Fold
Rifampicin	16	>4	0.125<x≤0.625	4	8-Fold
Compound 1c					
Aztreonam	32	>4	2.000<x≤2.008	64	0-Fold
Levofloxacin	512	>4	0.500<x≤0.750	256	2-Fold
Minocycline	32	>4	0.250<x≤0.750	8	4-Fold
Novobiocin	2048	>4	0.250<x≤0.750	512	4-Fold
Rifampicin	32	>4	0.125<x≤0.375	1	32-Fold

[a]Relative MIC of antibiotic was determined in the presence of 4 μg/mL of compound **1a**, **1b** and **1c**. [b]Fold potentiation is calculated by $\frac{MIC_{Antibioitc}}{Relative\ MIC_{Antibioitc}}$, where values of ≤ 1 are reported as 0-Fold.

Compounds **1a-c** display good synergy with novobiocin (FIC index = 0.250 – 0.375) and rifampicin (FIC index = 0.375 – 0.500) against PA101243 in MHB (Table 13). Conjugate **1a**

shows the best synergy out of the three compounds, having FIC indices of 0.250 and 0.375 with novobiocin and rifampicin, respectively. Compound **1c,** at a concentration of 2 μg/mL, has the highest potentiation of novobiocin and rifampicin with a 32- and 16-fold increase in the activity of the respective antibiotics.

Table 13. Combination Studies of Compounds **1a-c** against PA101243

Antibiotics	$MIC_{Antibiotic}$ (μg/mL)	$MIC_{Conjugates}$ (μg/mL)	FIC Index	Relative $MIC_{Antibiotic}$[a] (μg/mL)	Fold Potentiation[b]
Compound 1a					
Aztreonam	16	8	1.000	16	0-Fold
Levofloxacin	2	8	0.625	1	4-Fold
Minocycline	8	8	0.500	2	4-Fold
Novobiocin	128	8	0.250	4	32-Fold
Rifampicin	4	8	0.375	0.5	8-Fold
Compound 1b					
Aztreonam	16	8	1.008	16	0-Fold
Levofloxacin	2	8	0.625	1	2-Fold
Minocycline	4	8	1.008	4	0-Fold
Novobiocin	128	8	0.375	16	8-Fold
Rifampicin	8	8	0.500	2	4-Fold
Compound 1c					
Aztreonam	16	4	1.016	16	0-Fold
Levofloxacin	2	4	0.625	0.5	4-Fold
Minocycline	4	4	1.000	2	2-Fold
Novobiocin	64	4	0.375	2	32-Fold
Rifampicin	8	4	0.375	0.5	16-Fold

[a]Relative MIC of antibiotic was determined in the presence of 4 μg/mL of **1a-b** and 2 μg/mL of **1c.** [b]Fold potentiation is calculated by $\frac{MIC_{Antibioitc}}{Relative\ MIC_{Antibioitc}}$, where values of ≤ 1 are reported as 0-Fold.

There are a few interesting points to note in the overview of the combination studies of **1a-c** against the clinically isolated Gram-negative strains (Figure 33). The adjuvant potency of **1a-c** seems to be lower against the clinical isolates than the wild-type strains, likely due to the low MIC values against the clinical strains. We see synergy of novobiocin and rifampicin against PA260 and PA101243, with some synergy of rifampicin against PA259. The greatest synergy of rifampicin and novobiocin occurs against PA101243, where all three conjugates synergized the antibiotics. Against PA260, synergy of aztreonam, levofloxacin and minocycline were also reached with some of the conjugates.

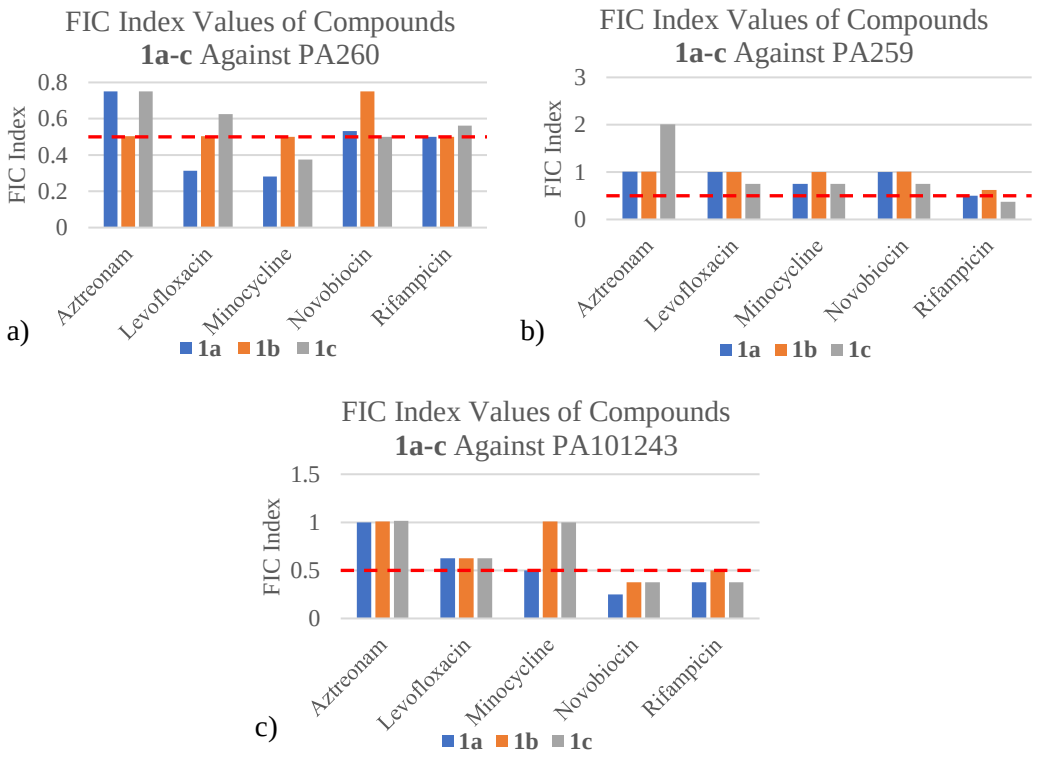

Figure 33. Bar graphs displaying the FIC indices of compounds **1a-c** with 5 selected antibiotics against a) PA260, b) PA259, and c) PA101243. FIC index values less than and equal to 0.5 (represented by the red dashed line) indicate a synergistic interaction.

4.2.3 Combination Studies of Control Compounds Against Wild-type Gram-negative Strains

To assess the effect of the catechol group on the adjuvant properties of **1a-c** against wild-type Gram-negative strains similar combination studies must likewise be conducted with the control compounds **11a-c** for comparison. The combination studies consisted of checkerboard assays being conducted to determine their synergistic effects with a panel of 5 different antibiotics (across different antibiotic families) against wild-type Gram-negative strains. The control compounds were not tested with the additional panel of beta-lactam antibiotics

(ceftazidime, piperacillin, imipenem, and meropenem) due to no significant synergy being observed with the active compounds. The FIC index was then calculated to quantify and determine if the interaction between **11a-c** and the chosen antibiotics is synergistic.

Despite their low antibacterial activity, compounds **11a-c** showed synergy with novobiocin against PAO1, having FIC index values of 0.375, 0.250, and 0.125, respectively (Table 14). However, **11c** shows additional synergy with aztreonam (FIC index = 0.313), minocycline (FIC index = 0.188) and rifampicin (FIC index = 0.313) against PAO1. It is evident that against PAO1 **11c** has the best adjuvant activity, not only because of synergizing multiple antibiotics but also because of higher potentiation of the minocycline, novobiocin and rifampicin (8-, 32-, and 8-fold respectively) at a concertation of 8 μg/mL.

Table 14. Combination Studies of Compounds **11a-c** Against Wild-type *P. aeruginosa* PAO1

Antibiotics	$MIC_{Antibiotic}$ (μg/mL)	$MIC_{Conjugates}$ (μg/mL)	FIC Index	Relative $MIC_{Antibiotic}$[a] (μg/mL)	Fold Potentiation[b]
Compound 11a					
Aztreonam	4	>128	0.500<x≤0.531	2	2-Fold
Levofloxacin	2	>128	0.500<x≤0.508	1	2-Fold
Minocycline	8	>128	0.500<x≤0.563	4	2-Fold
Novobiocin	512	>128	0.250<x≤0.375	256	2-Fold
Rifampicin	16	>128	0.500<x≤0.531	8	2-Fold
Compound 11b					
Aztreonam	4	>128	0.500<x≤0.563	2	2-Fold
Levofloxacin	1	>128	0.500<x≤0.531	1	2-Fold
Minocycline	8	>128	0.500<x≤0.531	4	2-Fold
Novobiocin	512	>128	0.125<x≤0.250	64	16-Fold
Rifampicin	16	>128	0.500<x≤0.531	8	2-Fold
Compound 11c					
Aztreonam	4	>128	0.250<x≤0.313	1	4-Fold
Levofloxacin	2	>128	0.500<x≤0.531	0.5	4-Fold
Minocycline	8	>128	0.125<x≤0.188	1	8-Fold
Novobiocin	512	>128	0.063<x≤0.125	32	32-Fold
Rifampicin	16	>128	0.250<x≤0.313	2	8-Fold

[a]Relative MIC of antibiotic was determined in the presence of 8 μg/mL of compound **11a**, **11b** and **11c**. [b]Fold potentiation is calculated by $\frac{MIC_{Antibioitc}}{Relative\ MIC_{Antibioitc}}$, where values of ≤ 1 are reported as 0-Fold.

Compounds **11a-c** display good synergy with novobiocin against WT EC, having FIC index values of 0.313, 0.250, and 0.125, respectively (Table 15). In addition, **11b** and **11c** also show synergy with rifampicin, having FIC indices of 0.281 and 0.375, respectively. It is evident that **11c** works as the most effective adjuvant against WT EC from the Table 15 data, and that there is a general trend of increasing carbon linker length and adjuvant activity.

Table 15. Combination Studies of Compounds **11a-c** against *E. coli* ATCC 25922.

Antibiotics	$MIC_{Antibiotic}$ (μg/mL)	$MIC_{Conjugates}$ (μg/mL)	FIC Index	Relative $MIC_{Antibiotic}$[a] (μg/mL)	Fold Potentiation[b]
Compound 11a					
Aztreonam	0.5	>128	1.000<x≤1.125	0.5	0-Fold
Levofloxacin	0.00195	>128	1.000<x≤1.125	0.00195	0-Fold
Minocycline	0.5	>128	1.000<x≤1.002	1	2-Fold
Novobiocin	128	>128	0.250<x≤0.313	32	4-Fold
Rifampicin	4	>128	0.500<x≤0.625	2	2-Fold
Compound 11b					
Aztreonam	0.5	>128	0.500<x≤0.508	0.25	2-Fold
Levofloxacin	0.00195	>128	1.000<x≤1.125	0.00195	0-Fold
Minocycline	0.5	>128	1.000<x≤1.125	1	0-Fold
Novobiocin	128	>128	0.125<x≤0.250	32	4-Fold
Rifampicin	8	>128	0.250<x≤0.281	2	4-Fold
Compound 11c					
Aztreonam	0.5	>128	1.000<x≤1.125	0.5	0-Fold
Levofloxacin	0.000977	>128	1.000<x≤1.125	0.000977	0-Fold
Minocycline	0.5	>128	0.500<x≤0.531	0.25	2-Fold
Novobiocin	128	>128	0.063<x≤0.125	8	16-Fold
Rifampicin	4	>128	0.250<x≤0.375	2	2-Fold

[a]Relative MIC of antibiotic was determined in the presence of 8 μg/mL of compound **11a**, **11b** and **11c**. [b]Fold potentiation is calculated by $\frac{MIC_{Antibioitc}}{Relative\ MIC_{Antibioitc}}$, where values of ≤ 1 are reported as 0-Fold.

Compounds **11b** and **11c** display synergy with novobiocin and rifampicin against WT AB (Table 16). **11b** has a FIC index of 0.375 for both rifampicin and novobiocin, and **11c** has an FIC index of 0.250 for both rifampicin and novobiocin. Compound **11c** displays the highest adjuvant activity against WT AB having the lowest FIC for rifampicin and novobiocin, as well as having the highest fold potentiation of the antibiotics at concentration of 8 μg/mL.

Table 16. Combination Studies of Compounds **11a-c** Against *A. baumannii* ATCC 17978

Antibiotics	$MIC_{Antibiotic}$ (μg/mL)	$MIC_{Conjugates}$ (μg/mL)	FIC Index	Relative $MIC_{Antibiotic}$[a] (μg/mL)	Fold Potentiation[b]
Compound 11a					
Aztreonam	64	>128	0.500<x 0.625	64	0-Fold
Levofloxacin	0.125	>128	1.000<x≤1.125	0.125	0-Fold
Minocycline	8	>128	1.000<x≤1.125	8	0-Fold
Novobiocin	16	>128	0.500<x≤0.531	8	2-Fold
Rifampicin	4	>128	0.500<x≤0.531	2	2-Fold
Compound 11b					
Aztreonam	64	>128	1.000<x≤1.125	64	0-Fold
Levofloxacin	0.125	>128	1.000<x≤1.125	0.125	0-Fold
Minocycline	8	>128	0.500<x≤0.502	4	2-Fold
Novobiocin	16	>128	0.250<x≤0.375	8	2-Fold
Rifampicin	4	>128	0.250<x≤0.375	2	2-Fold
Compound 11c					
Aztreonam	64	>128	0.500<x≤0.625	64	0-Fold
Levofloxacin	0.125	>128	1.000<x≤1.125	0.125	0-Fold
Minocycline	8	>128	0.500<x≤0.502	4	2-Fold
Novobiocin	16	>128	0.125<x≤0.250	4	4-Fold
Rifampicin	2	>128	0.125<x≤0.250	0.5	4-Fold

[a]Relative MIC of antibiotic was determined in the presence of 8 μg/mL of **11a-c** of compound **11a**, **11b** and **11c**. [b]Fold potentiation is calculated by $\frac{MIC_{Antibioitc}}{Relative\ MIC_{Antibioitc}}$, where values of ≤ 1 are reported as 0-Fold.

There are a few interesting points to note in the overview of the combination studies of **11a-c** against the wild-type Gram-negative strains (Figure 34). Like with **1a-c**, we observe synergy of rifampicin and novobiocin with **11a-c** against the three wild-type strains, however the level of synergy is not as strong as that with **1a-c**. Across these three strains it seems like **11c** has the highest adjuvant potency because it synergizes novobiocin and rifampicin in all three strains, as well as synergizing aztreonam and minocycline in PAO1.

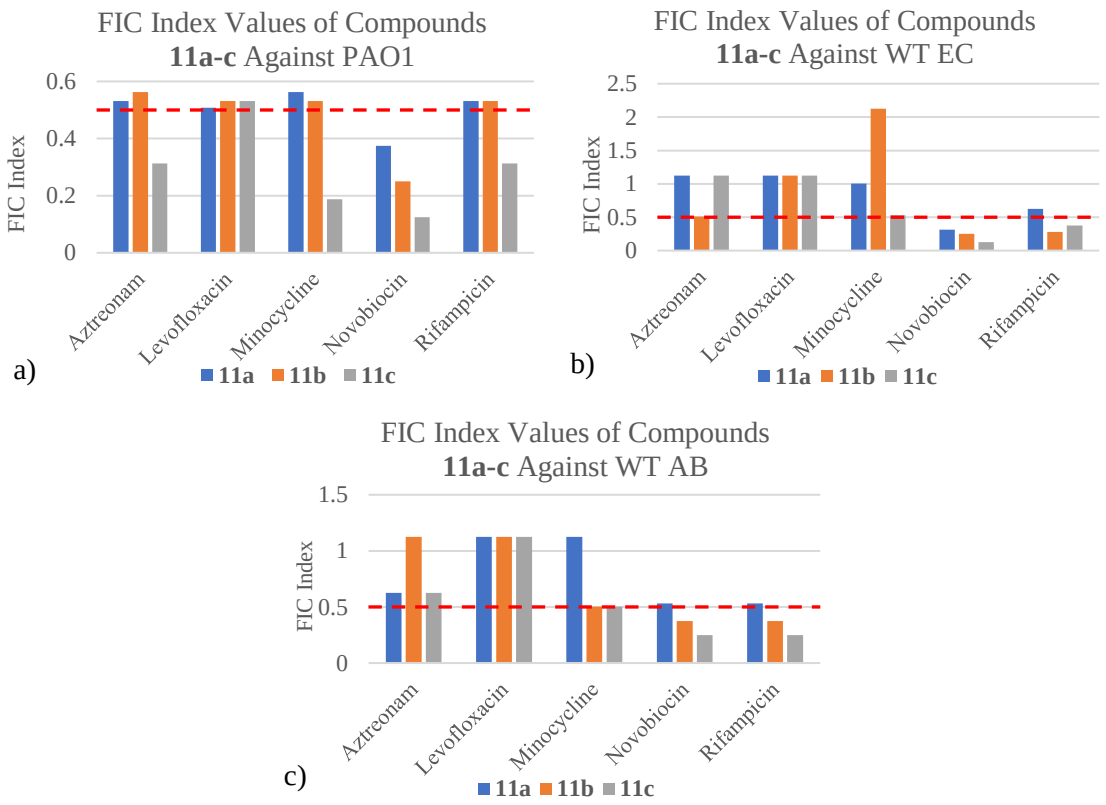

Figure 34. Bar graphs displaying the FIC indices of compounds **1a-c** with 5 selected antibiotics against a) PAO1, b) WT EC, and c) WT AB. FIC index values less than and equal to 0.5 (represented by the red dashed line) indicate a synergistic interaction.

4.2.4 Combination Studies of Active Compounds Against Gram-negative Clinical Isolates

Checkerboard assays were conducted to assess the adjuvant properties of compounds **11a-c** with 5 selected antibiotics (aztreonam, levofloxacin, minocycline, novobiocin, and rifampicin) against selected clinical isolate strains of *P. aeruginosa.* Strains PA259, PA260, and PA101243 were selected for these combination studies in order to compare with the combination studies conducted with **1a-c** against these aforementioned strains (Table 11-13). For Tables 17-19 the Relative $MIC_{Antibitotic}$ was reported at a concentration of 16 μg/mL for compound **11a-c.**

Compounds **11a-c** all synergize well with novobiocin (FIC indices = 0.094 – 0.250) against PA260, with **11b** and **11**c displaying additional synergistic interactions (Table 17). Conjugate **11b** also displays synergy with levofloxacin (FIC index = 0.313), while displaying a stronger synergistic interaction with novobiocin than **11a**. Compound **11c** displays the strongest interactions with antibiotics out of the three conjugates, synergizing with all the tested antibiotics against PA260. Most notably, **11c** had strong synergy with novobiocin (FIC index = 0.094) and levofloxacin (FIC index = 0.156), and at a concentration of 16 μg/mL was able to potentiate the activity of all the tested antibiotics by 8-Fold (64-Fold for novobiocin).

Table 17. Combination Studies of Compounds **11a-c** Against *P. aeruginosa* PA260

Antibiotics	$MIC_{Antibiotic}$ (μg/mL)	$MIC_{Conjugates}$ (μg/mL)	FIC Index	Relative $MIC_{Antibiotic}$ [a] (μg/mL)	Fold Potentiation[b]
Compound 11a					
Aztreonam	128	>128	0.500<x≤0.625	64	2-Fold
Levofloxacin	32	>128	0.500<x≤0.625	8	2-Fold
Minocycline	8	>128	0.500<x≤0.625	4	2-Fold
Novobiocin	512	>128	0.125<x≤0.250	64	8-Fold
Rifampicin	16	>128	0.500<x≤0.563	8	2-Fold
Compound 11b					
Aztreonam	128	>128	0.500<x≤0.625	64	2-Fold
Levofloxacin	16	>128	0.250<x≤0.313	8	4-Fold
Minocycline	8	>128	0.500<x≤0.531	4	2-Fold
Novobiocin	512	>128	0.125<x≤0.188	32	16-Fold
Rifampicin	16	>128	0.500<x≤0.516	8	2-Fold
Compound 11c					
Aztreonam	128	>128	0.125<x≤0.250	16	8-Fold
Levofloxacin	32	>128	0.125<x≤0.156	4	8-Fold
Minocycline	8	>128	0.125<x≤0.250	1	8-Fold
Novobiocin	256	>128	0.031<x≤0.094	4	64-Fold
Rifampicin	16	>128	0.125<x≤0.250	2	8-Fold

[a]Relative MIC of antibiotics was determined in the presence of 16 μg/mL of **11a-c.** [b]Fold potentiation is calculated by $\frac{MIC_{Antibioitc}}{Relative\ MIC_{Antibioitc}}$, where values of ≤ 1 are reported as 0-Fold.

Compounds **11a-c** showed almost no synergy with the five selected antibiotics against PA259 (Table 18). Only **11c** displayed good synergy with novobiocin (FIC index = 0.375) and rifampicin (FIC index = 0.188), while **11a** and **11b** showed no synergy.

Table 18. Combination Studies of Compounds **11a-c** Against *P. aeruginosa* PA259

Antibiotics	$MIC_{Antibiotic}$ (μg/mL)	$MIC_{Conjugates}$ (μg/mL)	FIC Index	Relative $MIC_{Antibiotic}$ [a] (μg/mL)	Fold Potentiation[c]
Compound 11a					
Aztreonam	64	>128	1.000<x≤1.002	32	0-Fold
Levofloxacin	512	>128	1.000<x≤1.002	512	0-Fold
Minocycline	32	>128	1.000<x≤1.002	32	0-Fold
Novobiocin	2048	>128	1.000<x≤1.125	1024	2-Fold
Rifampicin	32	>128	0.500<x≤0.504	16	2-Fold
Compound 11b					
Aztreonam	64	>128	1.000<x≤1.002	64	0-Fold
Levofloxacin	512	>128	1.000<x≤1.002	512	0-Fold
Minocycline	32	>128	1.000<x≤1.002	32	0-Fold
Novobiocin	2048	>128	0.500<x≤0.563	1024	2-Fold
Rifampicin	32	>128	0.500<x≤0.508	16	2-Fold
Compound 11c					
Aztreonam	32	>128	0.500<x≤0.625	16	2-Fold
Levofloxacin	512	>128	1.000<x≤1.002	512	0-Fold
Minocycline	32	>128	0.500<x≤0.531	16	2-Fold
Novobiocin	2048	>128	0.250<x≤0.375	512	4-Fold
Rifampicin	32	>128	0.125<x≤0.188	4	8-Fold

[a]Relative MIC of antibiotics was determined in the presence of 16 μg/mL of **11a-c.** [b]Fold potentiation is calculated by $\frac{MIC_{Antibioitc}}{Relative\ MIC_{Antibioitc}}$, where values of ≤ 1 are reported as 0-Fold.

Compounds **11a-c** display no synergy with the selected antibiotics against PA101243 (Table 19). Even though we observed no synergy of the antibiotics with **11a-c**, we observe more potentiation of the antibiotics as the carbon linker of the adjuvant increases in size. Compound **11c** has the lowest FIC index values and shows the most potentiation of antibiotic activity.

Table 19. Combination Studies of Compounds **11a-c** Against *P. aeruginosa* PA101243

Antibiotics	$MIC_{Antibiotic}$ (μg/mL)	$MIC_{Conjugates}$ (μg/mL)	FIC Index	Relative $MIC_{Antibiotic}$[a] (μg/mL)	Fold Potentiation[c]
Compound 11a					
Aztreonam	16	>128	1.000<x≤1.002	16	0-Fold
Levofloxacin	1	>128	1.000<x≤1.002	2	0-Fold
Minocycline	4	>128	1.000<x≤1.002	8	0-Fold
Novobiocin	128	>128	1.000<x≤1.002	128	0-Fold
Rifampicin	4	>128	1.000<x≤1.002	4	0-Fold
Compound 11b					
Aztreonam	8	>128	1.000<x≤1.002	16	0-Fold
Levofloxacin	1	>128	1.000<x≤1.002	2	0-Fold
Minocycline	4	>128	1.000<x≤1.002	4	0-Fold
Novobiocin	128	>128	0.500<x≤0.625	64	2-Fold
Rifampicin	8	>128	1.000<x≤1.002	8	0-Fold
Compound 11c					
Aztreonam	8	>128	0.500<x≤0.502	8	0-Fold
Levofloxacin	2	>128	0.500<x≤0.563	1	2-Fold
Minocycline	4	>128	1.000<x≤1.002	4	0-Fold
Novobiocin	128	>128	0.500<x≤0.563	64	2-Fold
Rifampicin	2	>128	0.500<x≤0.625	1	2-Fold

[a]Relative MIC of antibiotics was determined in the presence of 16 μg/mL of **11a-c.** [b]Fold potentiation is calculated by $\frac{MIC_{Antibioitc}}{Relative\ MIC_{Antibioitc}}$, where values of ≤ 1 are reported as 0-Fold.

There are a few interesting points to note in the overview of the combination studies of **11a-c** against the wild-type Gram-negative strains (Figure 35). It is quite evident that **11c** is the most potent adjuvant from the TOB-mCAT conjugates. **11c** was able to synergize novobiocin and rifampicin against both PA260 and PA259, while also synergizing aztreonam levofloxacin, and minocycline against PA260. The only other synergy observed is by **11a** and **11b** with

novobiocin, and by **11b** with levofloxacin, both against PA260. There was no synergy of the antibiotics observed against PA101243.

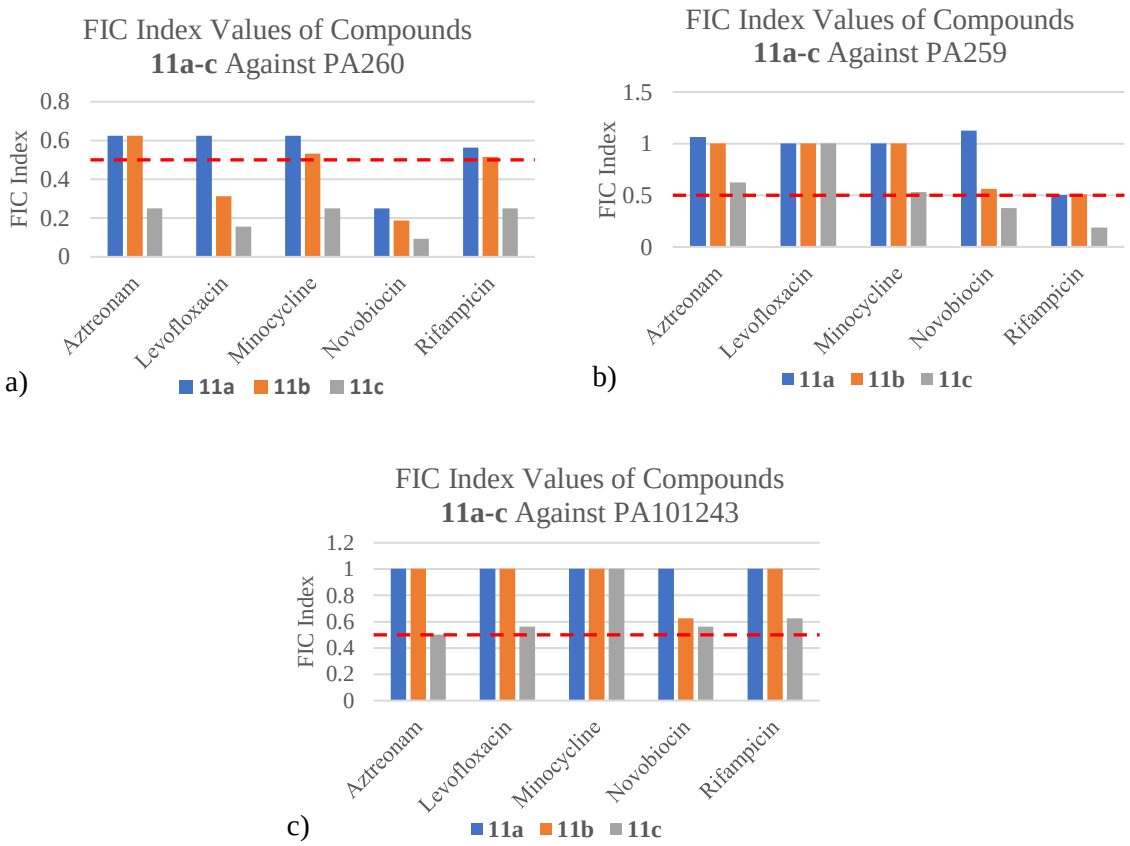

Figure 35. Bar graphs displaying the FIC indices of compounds **1a-c** with 5 selected antibiotics against a) PA260, b) PA259, and c) PA101243. FIC index values less than and equal to 0.5 (represented by the red dashed line) indicate a synergistic interaction.

4.3 DISCUSSION

4.3.1 The Effects of the Catechol Group on the Antibacterial Activity of the Active Conjugates

The first notable observation from the antibacterial activity data of **1a-c** (Table 1) is the clear *P. aeruginosa* specific activity of the conjugates. Against the wild-type Gram-negative strains, we observe moderate activity (MIC = 4-8 μg/mL) against PAO1 and low activity against WT EC and WT AB (MIC = 8 - >128 μg/mL). This comes to an 8-16-fold reduction in activity against PAO1, an 8- >256-fold reduction in activity against WT AB, and a 16-64-fold reduction in activity against WT EC as compared to the activity of tobramycin against these wild-type strains. However, when looking at the activity against the clinical isolates we can see **1a-c** having a 1-256-fold increase in activity against the *P. aeruginosa* strains but displaying no activity (MIC = >128 μg/mL) against the *A. baumannii* and Enterobacteriaceae strains. Compounds **1a-c** were able to reach the 4 μg/mL susceptibility breakpoint of tobramycin against PA260, PA259, and PA101243.

The clinical isolates tested have developed some mechanism of resistance to tobramycin compared to their wild-type counterparts. This is evident from tobramycin's 4-2048-fold reduced activity when tested against these clinical strains (Table 1). The antibacterial results show that the modifications to tobramycin that make **1a-c**, allow the conjugates to bypass these mechanisms in the *P. aeruginosa* clinical isolates, making some of these strains susceptible to **1a-c**. The two main components that were added in these modifications were the alkyl linker chain and the catechol group from the 3,4-dihydroxybenzoic acid added. The question then becomes, what part of these modification is responsible for antibacterial activity against the *P. aeruginosa* clinical strains.

In order to work out which part of the modification is responsible for this *P. aeruginosa* specific antibacterial activity we will be looking at similar tobramycin modified conjugates as well as the TOB-mCAT control conjugates, **11a-c**. Our research group has experience attaching a variety of components to tobramycin through the simple alkyl chain that was used to make **1a-c**. The first conjugates being considered are tobramycin tethered to 1-naphthylmethyl piperazine (TOB-NMP), paroxetine (TOB-PAR), and to dibasic peptides (TOB-DBP)(Figure 36)[1]. These conjugates have tobramycin connected to efflux pump inhibitors (EPI), which is important because the efflux inhibitors don't add additional antibacterial activity on their own[1]. If the carbon tether plays a role in the activity of **1a-c** we should also observe similar results with these conjugates. However, there was no significant activity against Gram-negative bacteria (MIC = ≥ 32 μg/mL) observed with the EPI conjugates[1].

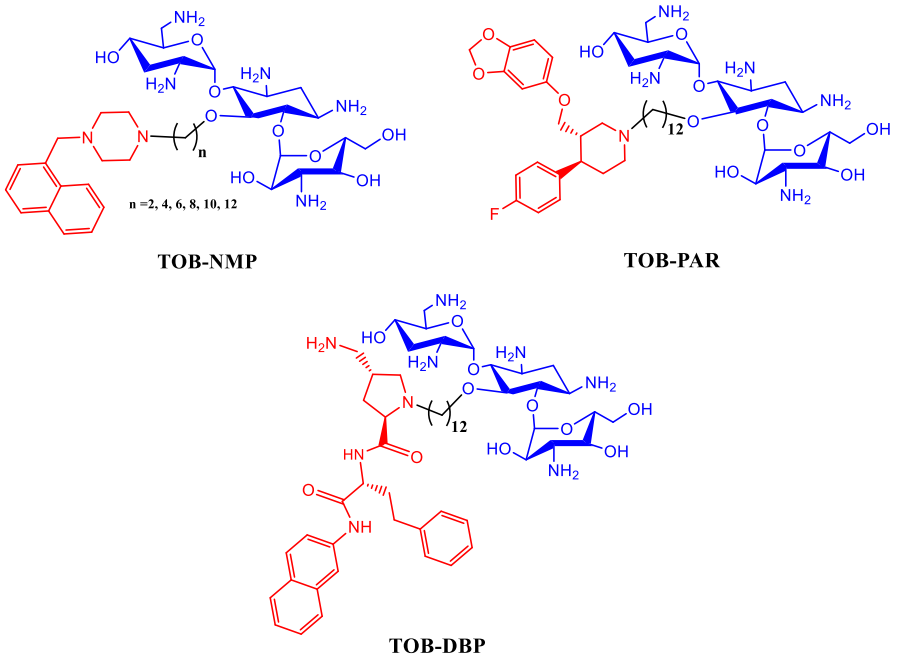

Figure 36. The molecular structures of the tobramycin-linked efflux pump inhibitor (EPI) conjugates; TOB-NMP, TOB-PAR, and TOB-DBP.

Another example of a similar tobramycin conjugate made by our research group that can be used for comparison is the amphiphilic lysine tobramycin conjugates. These conjugates have tobramycin connected to a 10-chloro-9-anthraldehyde and a lysine via an alkyl chain (Figure 37)[2]. This structure is again similar as **1a-c** and the EPI tobramycin conjugates, where the 10-chloro-9-anthraldehyde and lysine don't have much antibacterial activity on their own[2]. Again, if the activity of these conjugates is similar to that of **1a-c** then the carbon tether may play some role in the activity of **1a-c**. However, these amphiphilic lysine tobramycin conjugates have low antibacterial activity against Gram-negative bacteria (MIC = ≥ 16 μg/mL) and moderate to low activity against *P. aeruginosa* clinical isolates (MIC = 8 - ≥ 512 μg/mL)[2].

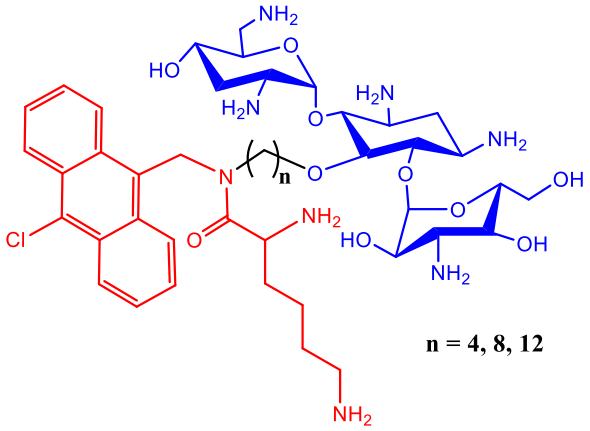

Amphiphilic Lysine Tobramycin Conjugates

Figure 37. The molecular structure of the amphiphilic lysine tobramycin conjugates

The most effective comparison to figure out which modification is responsible for the antibacterial activity of **1a-c** is comparing it to the control TOB-mCAT conjugates, **11a-c**. The **11a-c** conjugates are the most structurally similar to **1a-c**, having tobramycin tethered to a 3,4-dimethoxybenzoic acid via an alkyl chain rather than the 3,4-dihydroxybenzoic acid. This

substitution of the 3,4-dimethoxybenzoic acid results in a conjugate with the exact same structure with only the catechol component being modified slightly. The addition of the methoxy group of the **11a-c** block any of the metal ion complex formation capabilities of the oxygen atoms from the catechol group that may have been present with **1a-c** (Figure 23). We see a complete loss of any antibacterial activity (MIC = ≥ 128 μg/mL) of **11a-c** against both the wild-type and clinically isolated Gram-negative strains as compared to **1a-c** (Table 3). This provides the most prominent evidence supporting that the unhindered catechol group of **1a-c** plays an important role in the antibacterial activity observed from the conjugates, and not another structural aspect from the modification.

4.3.2 The Effects of The Catechol Group on the Adjuvant Activity of the Active Conjugates

It seems quite clear that the catechol moiety plays a vital role in the antibacterial activity of the **1a-c** conjugate. However, the effect of the catecholate on the adjuvant activity of **1a-c** is not so clear cut because, unlike in the antibacterial activity assays, both the **1a-c** and **11a-c** displayed synergistic interactions with the panel of antibiotics. This suggests that the metal chelation property of the added catecholate does not play a vital role in the synergistic interaction but may result in enhancing the interaction.

In the combination studies, both **1a-c** and **11a-c** were tested with a panel five antibiotics, consisting of aztreonam, levofloxacin, minocycline, novobiocin, and rifampicin, against the Gram-negative wild-type strains (PAO1, WT EC, and WT AB). Additionally, **1a-c** were tested with an additional panel of β-lactam antibiotics, consisting of ceftazidime, piperacillin, meropenem, and imipenem, against the wild-type Gram-negative strains. The most notable result

observed from these combination studies against the wild-type strains is that **1a-c** were all capable of synergizing novobiocin and rifampicin against all three strains (Figure 38). Additionally, **1a-c** were all capable of synergizing the five antibiotics against PAO1. Conjugates **11a-c** also show synergy with novobiocin and rifampicin against some of the wild-type strains, most prominently **11c** of which synergizes novobiocin and rifampicin for all three wild-type strains (Table 14-16).

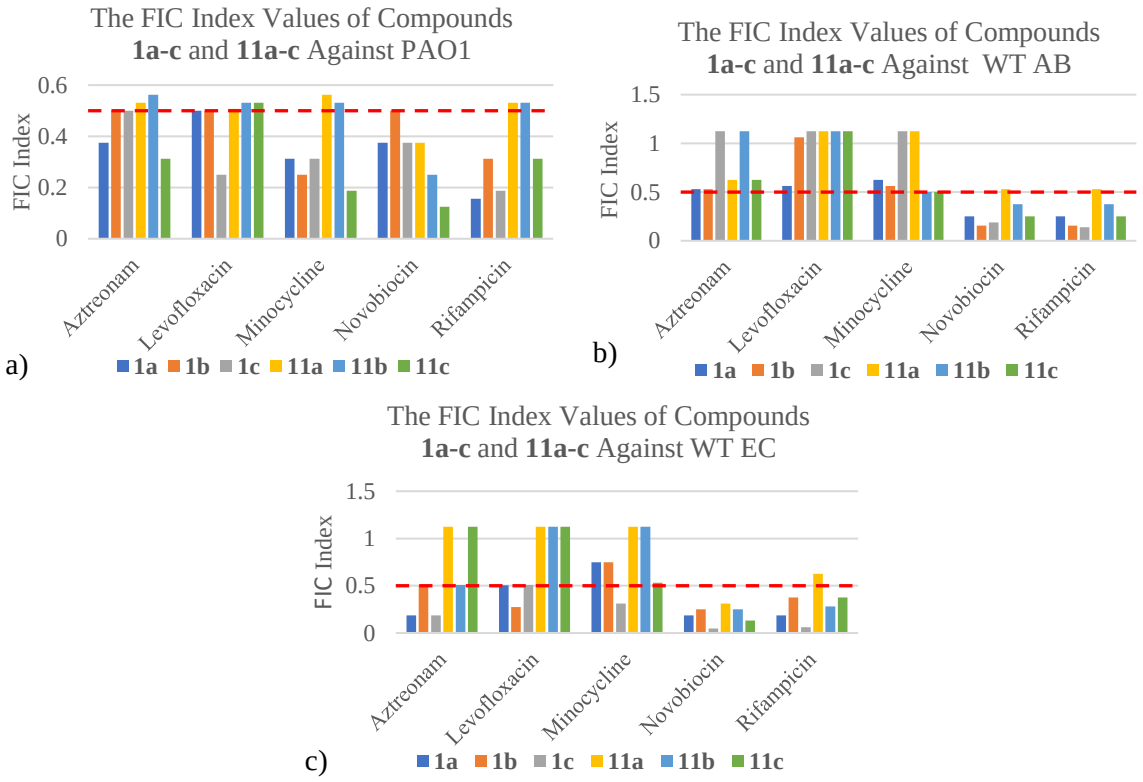

Figure 38. Bar graphs displaying the FIC indices of compounds **1a-c** and **11a-c** with 5 selected antibiotics against a) PAO1, b) WT EC, and c) WT AB. FIC index values less than and equal to 0.5 (represented by the red dashed line) indicate a synergistic interaction.

At first glance, it might seem that **11a-c** are relatively comparable to **1a-c** due to these control conjugates being able to also synergize the tested antibiotics. However, just looking at the FIC index values to determine synergy does not give the full picture of the adjuvant properties of these conjugates. This is due do to **11a-c** not having stand-alone antibacterial activity while conjugates **1a-c** have good antibacterial activity at low concentrations. So, the antibacterial activity of **1a-c** ends up taking over before more significant synergy can take place.

Another way to represent the data from these combination studies is to look at the potentiation of the antibiotics at a set concentration for all conjugates (Figure 39). When the data is represented this way, it is clear that **1a-c** are able to have more favourable interactions with the antibiotics than **11a-c**. **1a-c** are able to potentiate all the antibiotics greater than **11a-c** against these wild-type strains. The difference in how the data is represented is best exemplified when looking at the interactions of **1c** and **11c** with rifampicin against PAO1. Despite rifampicin being synergized by both **1c** (FIC index = 0.189) and **11c** (FIC index = 0.313), **1c** potentiates rifampicin 512-fold while **11c** only potentiates rifampicin by 4-fold at a concentration of 4 μg/mL. This supports that the catecholate group has a significant impact on the adjuvant properties of **1a-c** against wild-type Gram-negative bacteria.

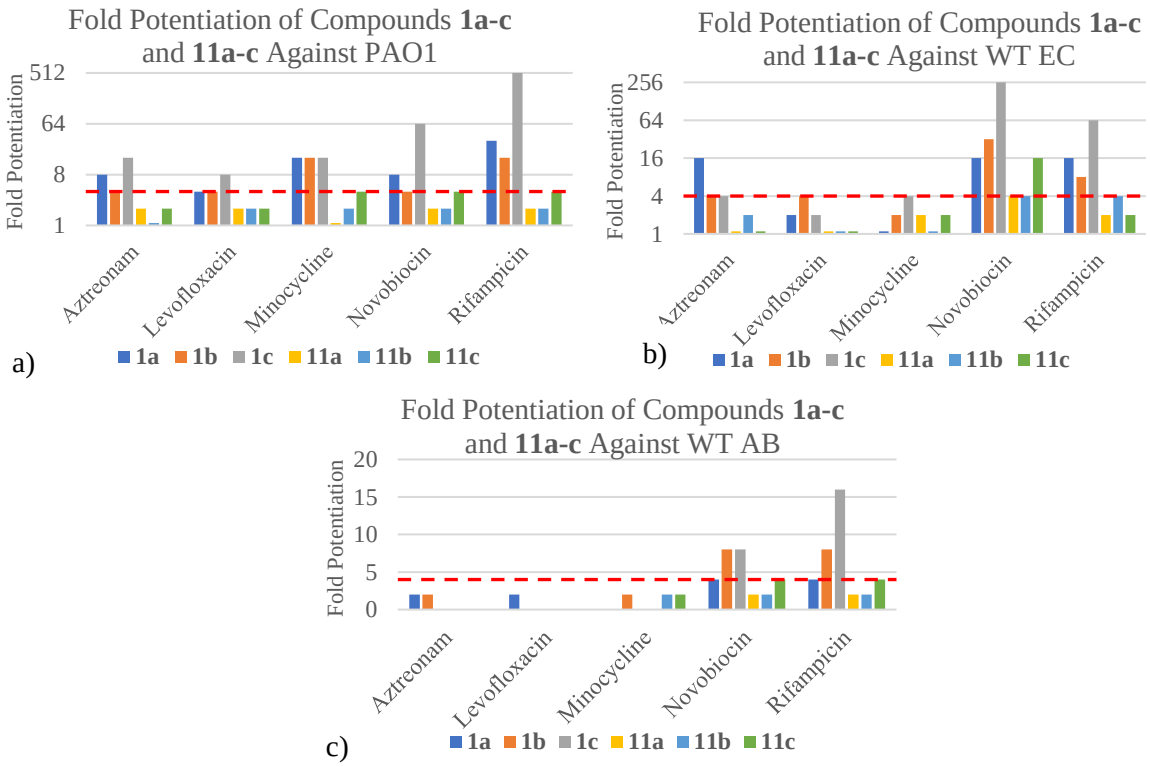

Figure 39. Bar graphs displaying the fold potentiation of the 5 selected antibiotics by compounds **1a-c** and **11a-c** against a) PAO1, b) WT EC, and c) WT AB. Fold potentiation values of greater than and equal to 4-fold (represented by the red dashed line) indicate a significant antibiotic potentiation. Concentrations of compounds **1a-c** and **11a-c** were kept at 4 μg/mL for PA01, and 8 μg/mL for WT EC and WT AB.

The combination studies of **1a-c** and **11a-c** against the three *P. aeruginosa* clinical isolates **1a-c** reached the 4 μg/mL susceptibility break point (PA260, PA259, and PA101243) display similar results as those conducted on the wild-type strains. When just looking at the FIC index values, **11a-c** have comparable interactions with the antibiotics as the **1a-c** conjugates (Figure 40). Compound **11c** in particular, even outperforms **1a-c** in some cases, most notably against PA260, where **11c** synergizes every antibiotic and has lower FIC indices (FIC indices = 0.094 –

0.250) than every other conjugate. These results are again deceiving because the antibacterial activity of **1a-c** (MIC = 1-4 μg/mL) is much higher than that of **11a-c** (MIC = >16 μg/mL). As a result, we get outcomes like **11c** synergizing rifampicin at a concentration of 16 μg/mL and **1c** not synergizing rifampicin, even though it kills the PA260 strain at 2 μg/mL.

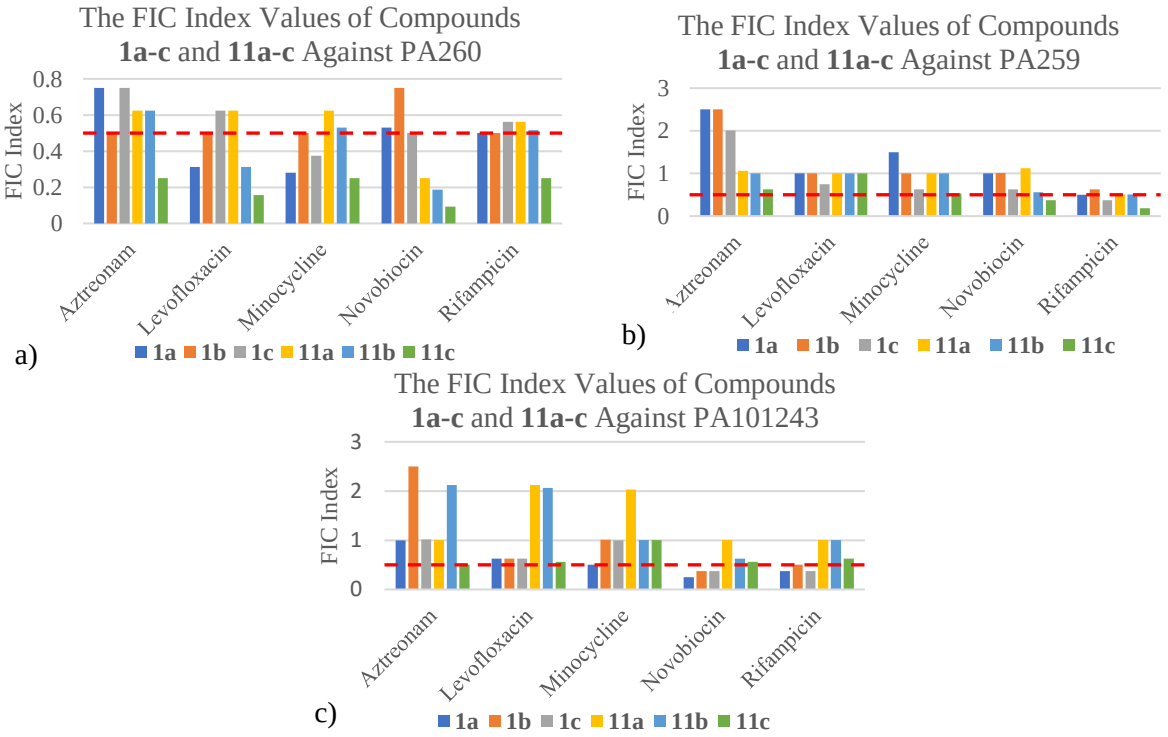

Figure 40. Bar graphs displaying the FIC indices of compounds **1a-c** and **11a-c** with 5 selected antibiotics against a) PA260, b) PA259, and c) PA101243. FIC index values less than and equal to 0.5 (represented by the red dashed line) indicate a synergistic interaction.

Again, if the data from the combination studies is represented as the potentiation of the antibiotics by a constant concentration of either **1a-c** and **11a-c** a more diverging picture is seen (Figure 41). When represented this way, it is clear that **1a-c** are capable of potentiating the

antibiotics against the clinical isolates far greater than **11a-c.** In almost every scenario the **1a-c** outperformed their **11a-c** counterpart, with **1c** being the best overall. This is most evident against PA260, where **1c** was able to significantly potentiate (≥ 4-Fold) every antibiotic, while no other conjugate was able to reach significant potentiation the antibiotics, except for **1a** with rifampicin.

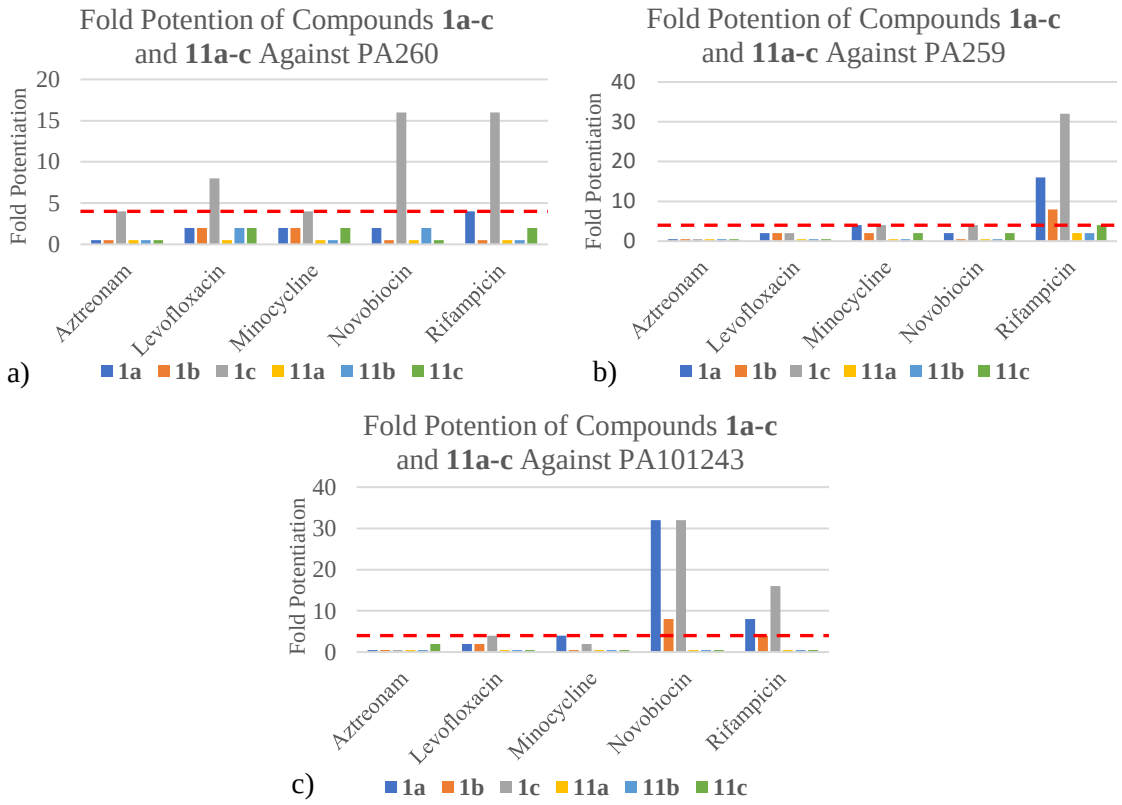

Figure 41. Bar graphs displaying the fold potentiation of the 5 selected antibiotics by compounds **1a-c** and **11a-c** against a) PA260, b) PA259, and c) PA101243. Fold potentiation values of greater than and equal to 4-fold (represented by the red dashed line) indicate a significant antibiotic potentiation. Concentrations of compounds **1a-c** and **11a-c** were kept at 1 μg/mL for PA260, 4 μg/mL for PA259, and 2 μg/mL for PA101243.

The catecholate group is evidently not solely responsible for the adjuvant properties of **1a-c** as synergy with the panel of antibiotics is observed in both **1a-c** and **11a-c** against the Gram-negative bacteria. Despite some instance of comparable synergy between the active and control conjugates, at a constant concentration compounds **1a-c** clearly potentiate the antibiotics to a much greater degree than **11a-c**. This difference in drug potentiation must be due to the only change in the conjugates structure, that being the unhindered catechol group of **1a-c**.

4.3.3 The Effects of the Alkyl Tether Length on the Adjuvant Activity of the Conjugates

Not only was the presence of the catecholate group observed to effect adjuvant and antibacterial properties of the conjugates, but the length of the carbon tether was also observed to be a significant factor in the antibacterial and adjuvant potency. This observation makes sense since increasing tether length increases the hydrophobicity of the conjugates and studies have shown that increasing the hydrophobicity of membrane-active compounds to a threshold increases their antimicrobial activity[2,3]. The high hydrophobicity is important for the penetration of these compounds across the bacterial membrane[2,3].

It is evident that both the antibacterial and adjuvant properties of **1a-c** are affected by the carbon tether length. Interestingly, the activity of **1a-c** does not only increase linearly with the increasing hydrophobicity of the conjugates (**1c** > **1b** > **1a**), but also in a rather consistent order of the 8-carbon tether being the most active followed by the 4-carbon tether and then the 6-carbon tether (**1c** > **1a** > **1b**)**.** These two orders of **1a-c** activity are fairly consistent for both antibacterial and adjuvant activity, and what's constant in both orders is that **1c** displays the greatest activity.

Similarly, we observe a trend in adjuvant activity and tether length with the **11a-c** conjugates. This trend is a fairly linear correlation with increasing tether length and increasing adjuvant activity. Conjugate **11c** clearly shows the highest adjuvant potency in most tested scenarios with **11a** shows the lowest adjuvant potency (**11c** > **11b** > **11a**).

From the microbiological assays it is evident that the tether length has an influence on the antibacterial and adjuvant activity. The tether length likely works to increase the hydrophobicity of the conjugates to meet some threshold, a sweet spot of hydrophobicity that gives the conjugates optimal activity[2,3]. This however is a balancing act, as increasing the hydrophobicity of a membrane-active compound can also increase the hemolysis in erythrocytes[3]. The 8-carbon tether conjugates, **1c** and **11c**, seem to be closer to the optimal level of hydrophobicity than the other conjugates giving rise to the trend in activity.

A surprising and unique finding of the microbiology studies, related to the tether length, is that **1b** had a much greater antibacterial activity against WT AB than **1a** or **1c**. Even both **1a** and **1c** had an MIC of >128 μg/mL against WT AB, of which usually have a greater activity, **1b** displayed an MIC of 8 μg/mL. Since the only difference between the **1a-c** conjugates is the tether length, this large increase in activity of **1b** must be influenced by the 6-carbon length tether. This suggests that the 6-carbon tether might be the perfect length for the hydrophobicity threshold to be reached against WT AB.

4.3.3 The Effects of ID-CAMHB on the Activity of the Active Conjugates

The purpose of testing the conjugates in ID-CAMHB was to mimic the environment during a bacterial infection of a host. In theory **1a-c** would have an increased antibacterial activity in ID-CAMHB as compared to regular MHB because the catecholate group would have increased the conjugates uptake across the outer membrane via the exploitation of the bacteria siderophore uptake system. This phenomenon is observed by cefiderocol as its antibacterial activity increases up to 64-fold in ID-CAMHB (Table 2) as compared to MHB (Table 1). Unfortunately, the same was not observed when **1a-c** was tested in ID-CAMHB, in fact the opposite was observed. Conjugates **1a-c** had, in some scenarios, greater than a 16-fold decrease in antibacterial activity with none of the conjugates displaying significant activity in either the wild-type or clinical Gram-negative strains. The question then becomes, what could have caused this decrease in activity?

One possibility for this decrease in activity may be that the bacterial siderophores are out competing the iron binding of **1a-c** in the ID-CAMHB media. During iron starvation bacterial growth slows down and the expression of genes for the biosynthesis and uptake of siderophores have been shown to increase in *P. aeruginosa* and other bacteria[4,5]. Many of the siderophores these bacteria will produce, and release are hexadentate, like enterobactin, desferrichrome, and pyoverdine, while **1a-c** are bidentate molecules[6]. The changes in entropy associated with formation of these siderophore complexes are greater for hexadentate ligands than for tetradentate or bidentate molecules[6,7]. The close proximity of the binding ligands of the hexadentate bacterial siderophores allow the formation of these high affinity coordination hexadentate complexes[6,7]. While **1a-c** require three conjugates to be close enough to form a hexadentate complex, or water molecules will fill up these positions resulting in a less stable

complex[6]. Therefore, the ID-CAMHB may stimulate the production and release of bacterial siderophores that out compete **1a-c** for iron, due to their better binding affinity, causing this observed decline in activity in ID-CAMHB.

Cefiderocol, despite being a bidentate molecule for iron, displays increased activity against Gram-negative bacteria in ID-CAMHB. At first glance this may seem contradictory to the aforementioned hypothesis to why **1a-c** lost its activity in ID-CAMHB; however, **1a-c** have a slightly different catecholate structure that might account for this discrepancy. The catecholate moiety in cefiderocol is a 2-chloro-3,4-dihydroxybenzoic acid, while **1a-c** just have a 3,4-dihydroxybenzoic acid catecholate group[8]. Studies have shown that the iron chelating capabilities of these catecholates increases with the decreasing pKa values of their hydroxy groups[8]. Chlorine is an electron withdrawing group, the addition of it to the catecholate increases the acidity of the hydroxy groups due to the inductive effect[8]. It may be that even though cefiderocol is a bidentate molecule, the chloro-catecholate gives the conjugate enough binding affinity to compete with the bacterial siderophores in ID-CAMHB. This would allow cefiderocol to maintain activity in this media unlike **1a-c**, of which can't compete with the bacterial siderophores.

Another cause for the drop activity of **1a-c** in ID-CAMHB from MHB may have to do with the addition of Ca^{2+}, Mg^{2+}, and Zn^{2+} used to adjust the cation concentration. This would have a two-fold effect on the activity of **1a-c**, it might hinder the activity of the tobramycin component and these cations can interfere with the iron chelating of the catecholate moiety[9–12]. Higher concentrations of divalent cations reduce the activity of aminoglycoside against Gram-negative bacteria[10–12]. Aminoglycosides disrupt the divalent cation cross bridge between the LPS of Gram-negative bridge by displacing the cations[10–12]. The binding site of the LPS thus is in

equilibrium with the binding of divalent cations and the aminoglycoside, thus high concentrations of divalent cations will cause a higher likelihood of cations binding.

Catecholate groups are actually able to bind other divalent cations, like Ca^{2+}, Mg^{2+}, and Zn^{2+}, with relatively good affinity[9]. Thus, by increasing the concentrations of these other divalent cations we are reducing the chances of a successful iron-catecholate complex from forming. If the theorized mechanism of action for **1a-c** occurs, the increase in other divalent cations may decrease the activity of these conjugates. These two effects from increasing the cation concentration might account for the decrease in activity in ID-CAMHB from MHB.

4.3 REFERENCES

1. Lyu, Y. *et al.* Amphiphilic Tobramycin–Lysine Conjugates Sensitize Multidrug Resistant Gram-Negative Bacteria to Rifampicin and Minocycline. *Journal of Medicinal Chemistry* **60**, 3684–3702 (2017).

2. Lyu, Y., Domalaon, R., Yang, X. & Schweizer, F. Amphiphilic lysine conjugated to tobramycin synergizes legacy antibiotics against wild-type and multidrug-resistant Pseudomonas aeruginosa. *Peptide Science* **111**, e23091 (2019).

3. Chen, Y. *et al.* Role of peptide hydrophobicity in the mechanism of action of alpha-helical antimicrobial peptides. *Antimicrob Agents Chemother* **51**, 1398–1406 (2007).

4. Klebba, P. E. *et al.* Iron Acquisition Systems of Gram-negative Bacterial Pathogens Define TonB-Dependent Pathways to Novel Antibiotics. *Chem Rev* **121**, 5193–5239 (2021).

5. Ochsner, U. A., Wilderman, P. J., Vasil, A. I. & Vasil, M. L. GeneChip® expression analysis of the iron starvation response in Pseudomonas aeruginosa: identification of novel pyoverdine biosynthesis genes. *Molecular Microbiology* **45**, 1277–1287 (2002).

6. Hider, R. C. & Kong, X. Chemistry and biology of siderophores. *Natural Product Reports* **27**, 637–657 (2010).

7. Raymond, K. N., Allred, B. E. & Sia, A. K. Coordination Chemistry of Microbial Iron Transport. *Acc Chem Res* **48**, 2496–2505 (2015).

8. Aoki, T. *et al.* Cefiderocol (S-649266), A new siderophore cephalosporin exhibiting potent activities against Pseudomonas aeruginosa and other gram-negative pathogens

including multi-drug resistant bacteria: Structure activity relationship. *European Journal of Medicinal Chemistry* **155**, 847–868 (2018).

9. Xu, Z. Mechanics of metal-catecholate complexes: the roles of coordination state and metal types. *Sci Rep* **3**, 2914 (2013).

10. Zimelis, V. M. & Jackson, G. G. Activity of Aminoglycoside Antibiotics against Pseudomonas aeruginosa: Specificity and Site of Calcium and Magnesium Antagonism. *The Journal of Infectious Diseases* **127**, 663–669 (1973).

11. Ramirez-Ronda, C. H., Holmes, R. K. & Sanford, J. P. Effects of divalent cations on binding of aminoglycoside antibiotics to human serum proteins and to bacteria. *Antimicrob Agents Chemother* **7**, 239–245 (1975).

12. Hancock, R. E. W. Aminoglycoside uptake and mode of action—with special reference to streptomycin and gentamicin: I. Antagonists and mutants. *Journal of Antimicrobial Chemotherapy* **8**, 249–276 (1981).

Chapter 5: Mechanistic Studies

5.1 MEMBRANE PERMEABILIZATION

5.1.1 NPN Outer Membrane Permeabilization Assay

In order to gain an insight into the mechanism of action of the TOB-CAT conjugates (**1a-c**) we performed a membrane permeabilization assay against *P. aeruginosa* PAO1. Using a well-recognized outer membrane permeability assay using NPN (1-N-phenylnapthylamine) we were able to demonstrate that **1a** is able to permeabilize the outer membrane of PAO1 bacteria[1,2]. NPN is a small molecule fluorescent probe, that fluoresces strongly when it binds to phospholipids, weakly fluoresces in aqueous solutions and does not effectively transfer the outer membrane[1]. This property of NPN can be used to determine when the outer membrane of bacteria is permeabilized[1]. Only when the outer membrane is compromised will NPN transverse into the periplasmic space and have access to phospholipids, where NPN will bind and fluoresce[1].

Polymyxin B nonapeptide (PMBN) is a modified analog of the lipopeptide antibiotic polymyxin B, discovered as a natural product from *Paenibacillus polymyxa*[3–6]. Polymyxin B is a kno[a)] uter membrane permeabilizer of Gram-negative bacteria and is used clinically as a last-resort therapy for life-threatening infections from drug resistant Gram-negative bacteria, including *P. aeruginosa*[3–6]. PMBN has the N-terminal fatty amino acid segment removed from polymyxin B, truncating the molecule[4,5]. As a result of losing the hydrophobic tail, PMBN loses the antimicrobial activity of PMB, but preserves its outer membrane permeabilizing action[5–7]. PMBN was used as a positive control for the NPN assays conducted and as a comparative marker for clinically relevant membrane permeabilization of PAO1[2].

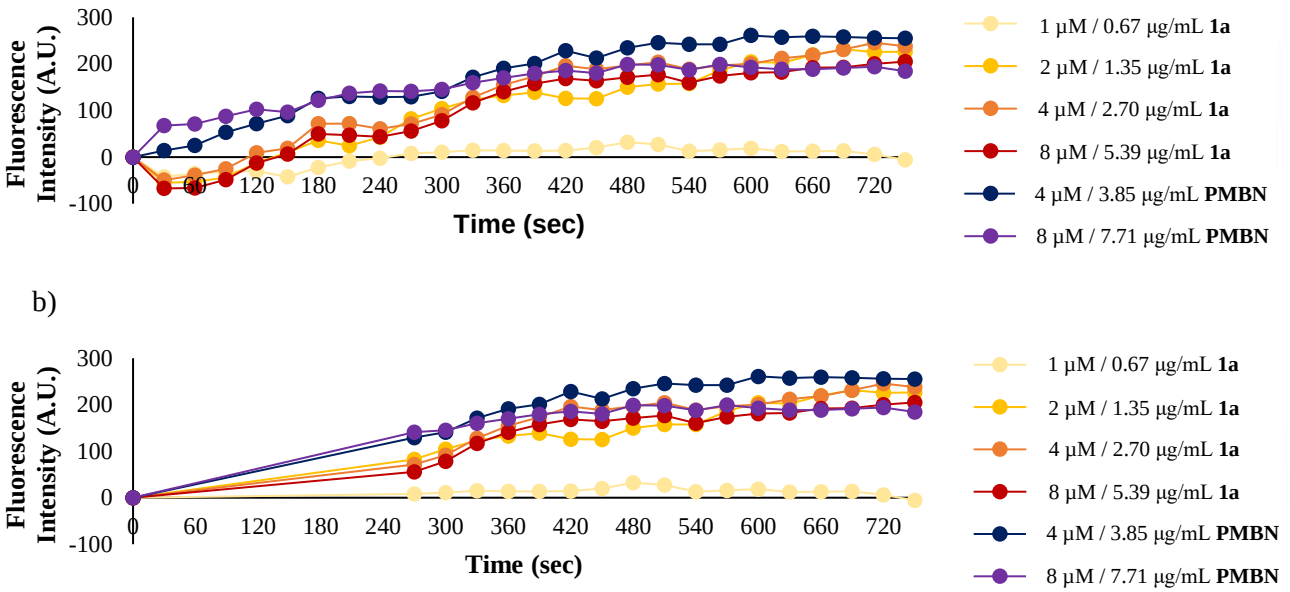

Figure 42. The permeabilization of the outer membrane by **1a** was measured by the change in fluorescence from the accumulation of 1-N-phenylnaphthylamine (NPN) in PAO1 cells. Graph a) depicts the change in fluorescence from 0-750sec and b) depicts the change in fluorescence from 270-750sec. Polymyxin B nonapeptide (PMBN) was used as a positive control.

The conducted NPN assay display that **1a** permeabilizes the outer membrane of PAO1 in a concentration-dependent manner (Figure 42). The results show that **1a** at concentrations of 2-8 µM shows similar levels of membrane permeabilization as 4-8 µM of PBMN. An interesting observation from the data is that there appears to be a threshold concentration of **1a** of which needs to be met before any membrane permeabilization occurs. Concentration of 2-8 µM **1a** all have similar intensities despite the concentration increasing, while **1a** at a concentration of 1 µM displays almost no activity. This suggest that there is a threshold concentration of **1a**,

approximately 2 μM, that must be met before the conjugate has any outer membrane permeabilization activity

From the NPN assay data we also observe a negative absorbance during approximately the first 120 seconds of Figure 42a. This negative absorbance is likely a result of interference caused by the absorbance of the aromatic catechol that is part of **1a**. Carbonyl chromophores that contain an aromatic ring are capable of absorbing UV light in the 350nm region[8]. The excitation wavelength used to excite the NPN molecules during the assay is 350nm and the emitted wavelength being monitored is 420 nm (Supplementary Information 7.2.4). Since an untreated PAO1 cell suspension with NPN was used as a negative control to establish the baseline fluorescence, the interference of **1a** was not accounted for in the baseline measurements. When running the NPN assay for the **1a** treated sample, the aromatic catechol absorbs some of the 350nm light without emitting light at 420nm. Thus, when compared to the baseline data would result in a net negative fluorescence at the beginning of the assay (before NPN penetrates the outer membrane) which is what is observed (Figure 42).

5.1.2 Synergy of Rifampicin and Novobiocin Against Gram-negative Bacteria

Rifampicin and novobiocin are both antibiotics that have intracellular targets and have their antibacterial activity against Gram-negative bacteria severely reduced due their inability to transverse the outer membrane[9,10]. Given this they are sometimes used in combination therapy against Gram-negative bacteria, often paired with an outer membrane-active antibiotic like colistin or PMB[9,10]. The membrane-active antibiotic allows rifampicin and novobiocin to

penetrate the outer membrane and reach their designated target, resulting in a synergistic interaction against Gram-negative bacteria[9,10].

Looking at how **1a-c** and **11a-c** interact in combination with rifampicin and novobiocin against Gram-negative bacteria might give insight into their mechanism of action. Against wild-type strains (PAO1, WT EC, WT AB) we observed good synergy of novobiocin (FIC indices = 0.047-0.500) and rifampicin (FIC indices = 0.063-0.375) by **1a-c** (Figure 43). Some additional synergy was observed in the clinical strain by **1a-c**, especially against PA101243, where FIC indices of 0.250-0.375 and 0.375-0.500 were observed for novobiocin and rifampicin, respectively. Conjugates **11a-c** were able to also synergize the wild-type and clinical strains, however there were less instances and often to a lesser degree than **1a-c** (Figure 43). These synergistic interactions suggest that the conjugates were able to enhance the cellular uptake of rifampicin and novobiocin, likely through the permeabilization of the outer membrane.

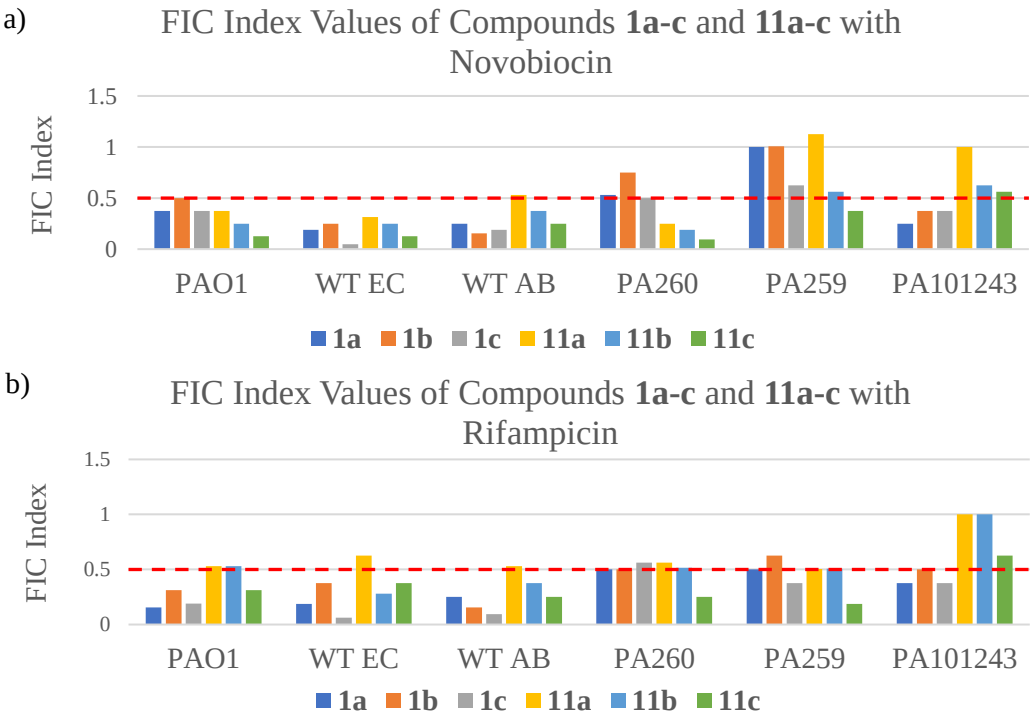

Figure 43. Bar graphs displaying the FIC indices of compounds **1a-c** and **11a-c** with (a) novobiocin and (b) rifampicin against wild-type (PAO1, WT EC, and WT AB) and clinically isolated (PA260, PA259, and PA101243) Gram-negative bacteria. FIC index values less than and equal to 0.5 (represented by the red dashed line) indicate a synergistic interaction.

5.2 DISCUSSION

5.2.1. Possible Modes of Action of the Antibacterial Effects of Active Conjugates

5.2.1.1 Polymyxin B Like Membrane Permeabilization Mechanism Model

The results from the NPN assay and the combination studies with rifampicin and novobiocin suggest that both **1a-c** and **11a-c** effect the outer membrane of Gram-negative bacteria. Compound **1a** displayed similar membrane permeabilization activity against PAO1 as PMBN in the NPN assays, and since **1b** and **1c** only differ in the carbon linker length it is safe to assume would display comparable activities. To elucidate **1a-c**'s mechanism of action we should compare structural similarities with similar molecules. Due to the similar membrane permeabilization activity of PMBN and PMB would be a good comparison.

Both polymyxin B and PMBN contain a polycationic peptide ring of which has been shown to interact with the LPS of the outer membrane of Gram-negative bacteria in a similar way as tobramycin or other aminoglycosides[4–6]. The polycation ring displaces the divalent cations that bridge and stabilize the LPS which causes rearrangement in the outer leaflet resulting in membrane permeability[3–6]. The leading model for the antibacterial activity of PMB is linked to the fatty acyl chain that inserts itself into the hydrophobic domain of the outer membrane[3–6]. This insertion acts to weaken the packing of the lipid A fatty acyl chains, resulting in the degradation of the outer membrane integrity and the movement of PMB into the periplasm[3–6]. Once in the periplasm, polymyxin B degrades the physical integrity of the phospholipid bilayer releasing the cellular contents[3–6].

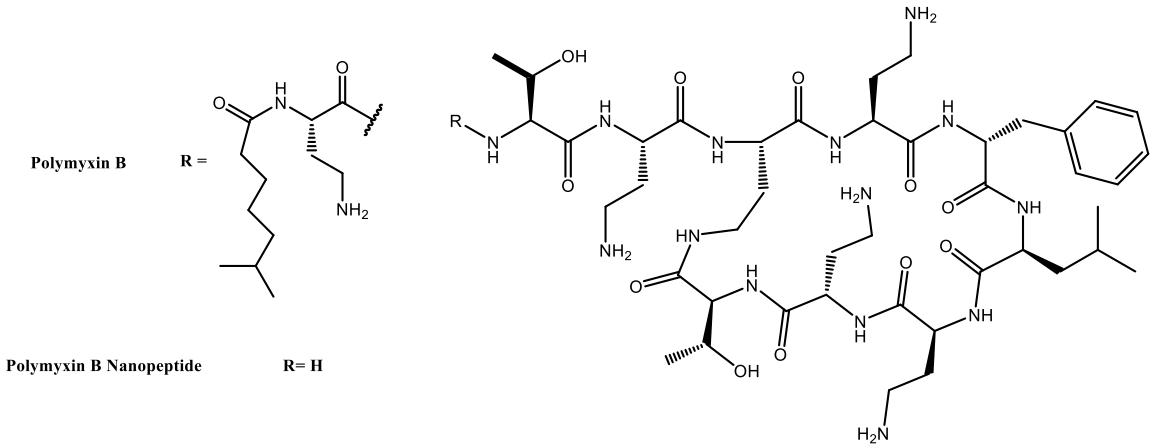

Figure 44. The molecular structure of Polymyxin B and Polymyxin B Nonapeptide (PMBN).

The structure of PMB can be simplified into two components: a large networked polycationic component and a long hydrophobic tail component (Figure 45). Comparing this simplified model of PMB to the structures of **1a-c** we start to see some similarities. The tobramycin component of **1a-c** is similar to the cyclic peptide of PMB, and the carbon tether and aromatic ring of **1a-c** are similar to the hydrophobic tail of PMB.

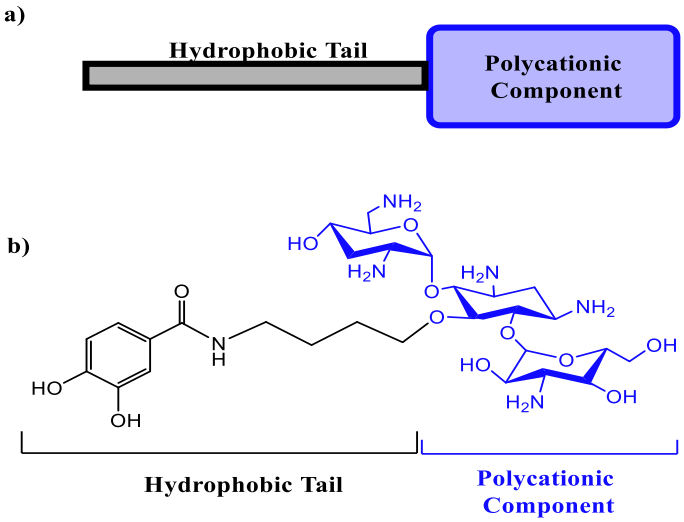

Figure 45. A depiction of a) a simplified schematic of the major components that make PMB and b) the molecular structure of **1a** with the polycationic and hydrophobic components labeled to relate to the simplified schematic of PMB

The results of the NPN assay and combination studies exhibit that the tobramycin of **1a-c** has likely retained its ability to displace the bridging cations and permeabilize the outer membrane of Gram-negative bacteria. The carbon tether and 3,4-dihydroxybenzoic acid of **1a-c** may insert itself into the outer membrane and interact with the hydrophobic region of lipid A, much like the lipophilic tail of PMB. Even though there is no direct evidence supporting this interaction, we do observe greater antibacterial activity of **1a-c** against the clinical isolates as compared to tobramycin (Table 1). However, **11a-c** of which has a more hydrophobic tail component, with the methylation of the catechol hydroxy groups, has no significant antibacterial activity. This indicates that the antibacterial activity of **1a-c** is due to more factors then just having a similar structure to PMB.

5.2.1.2 Chelation of Metal Ions Mechanism to Membrane Permeabilization Model

Initially TOB-CAT hybrids were synthesized to exploit the iron-siderophore uptake mechanism of bacteria, bypassing the impermeable outer membrane and any membrane associated resistant mechanism, increasing their cellular concentration and efficacy. In theory, the antibacterial activity of these TOB-CAT conjugates should increase when tested in iron deficient environments because the bacterial uptake of iron is greater in such conditions[11]. However, we found that **1a-c** have no significant activity against Gram-negative bacteria in the ID-CAMHB. This suggests that the addition of the catecholates to tobramycin may not have resulted in its intended mechanism of action.

Despite **1a-c** not having any activity in iron deficient media, **1a-c** was observed to have greater antibacterial activity as compared to tobramycin and the control conjugates, **11a-c**, in MHB. Even though the catecholate may not be assisting **1a-c** in exploiting the siderophore uptake mechanism of the bacteria, it is evident that it plays a significant role in the direct antibacterial activity. It may be that the catecholate of these conjugates are sequestering divalent cations that are necessary for the bacterial strains to thrive, in a nutritional immunity type mechanism of action[12,13]. Studies show that the MIC value of just a catecholate (1,2-dihydroxybenzoic acid), is too high to account for the antibacterial activity of which is observed with **1a-c**[12,14].

Chelators are often used in combination with antibiotics as adjuvants. Zinc chelators are often paired with β-lactam antibiotics to increase activity because zinc is needed for bacterial metallo-β-lactamases to hydrolyze β-lactam antibiotics[15]. Tetracycline antibiotics can be combined with iron chelators to increase activity because iron can often block the magnesium

binding location of tetracycline that is needed for their activity[16]. Aminoglycosides are not directly inhibited by divalent cations, however the concentrations of cations such as Ca^{2+} and Mg^{2+} can reduce their binding to the LPS[17,18]. Even though catecholates have a higher binding affinity for iron, they are capable of binding calcium and magnesium[19]. The attached catecholate may be able to bind Ca^{2+} and Mg^{2+} destabilizing the outer membrane of *P. aeruginosa*, while maintaining the antibacterial activity of tobramycin.

This may explain why we observe a decrease in the antibacterial activity of **1a-c** against Gram-negative bacteria in ID-CAMHB. The higher concentration of Ca^{2+}, Mg^{2+}, and Zn^{2+} would reduce the activity of not only the tobramycin component, but it will also reduce the chelating property of the catechol. The increased cations would compete against the polycationic tobramycin for binding to the LPS and reduce the effectiveness of the catechol component chelating the Ca^{2+} and Mg^{2+} at inducing membrane permeabilization.

5.2.1.3 Exploiting the Siderophore Uptake Mechanism of Bacteria Model

Lastly, the antibacterial activity of **1a-c** may in fact be due to the conjugates exploiting the iron-uptake mechanism of the bacteria. This would explain why we see **1a-c** maintain good antibacterial activity against the MDR *P. aeruginosa* strains that are resistant to tobramycin. It is likely these strains have changes to their outer membrane that resist the self-promoted uptake tobramycin. Thus, it might be that **1a-c** can bypass these outer membrane resistant mechanisms that inhibit tobramycin, by using the channels proteins that transport iron-siderophore complexes across the outer membrane. The methylation of the catechol hydroxy groups of **11a-c** block the

iron complexing capabilities of the conjugates, explaining why no significant antibacterial activity is observed against the tested Gram-negative bacteria.

As with the aforementioned membrane permeabilization by metal chelation model, the ability of **1a-c** to use the iron-siderophore specific channels would be hindered by an increase in divalent cation concentration. The higher concentrations of Ca^{2+} and Mg^{2+} and the lower concentration of Fe^{3+} in the ID-CAMHB media make it less likely for **1a-c** to form a complex with Fe^{3+}. Since it's harder for the conjugates to form iron complexes, the activity of the conjugates would lower as well. This is supported by the results observed from the antibacterial assays in ID-CAMHB. None of these models are very conclusive and require more experimental studies to better understand the mechanism of action of **1a-c**.

5.3 REFERENCES

1. Muheim, C. *et al.* Increasing the permeability of Escherichia coli using MAC13243. *Sci Rep* **7**, 17629 (2017).

2. Yang, X. *et al.* A Tobramycin Vector Enhances Synergy and Efficacy of Efflux Pump Inhibitors against Multidrug-Resistant Gram-Negative Bacteria. *Journal of Medicinal Chemistry* **60**, 3913–3932 (2017).

3. Trimble, M. J., Mlynárčik, P., Kolář, M. & Hancock, R. E. W. Polymyxin: Alternative Mechanisms of Action and Resistance. *Cold Spring Harb Perspect Med* **6**, a025288 (2016).

4. Tsubery, H., Ofek, I., Cohen, S. & Fridkin, M. Structure−Function Studies of Polymyxin B Nonapeptide: Implications to Sensitization of Gram-Negative Bacteria. *Journal of Medicinal Chemistry* **43**, 3085–3092 (2000).

5. Ayoub Moubareck, C. Polymyxins and Bacterial Membranes: A Review of Antibacterial Activity and Mechanisms of Resistance. *Membranes (Basel)* **10**, 181 (2020).

6. Akhoundsadegh, N., Belanger, C. R. & Hancock, R. E. W. Outer Membrane Interaction Kinetics of New Polymyxin B Analogs in Gram-Negative Bacilli. *Antimicrob Agents Chemother* **63**, e00935-19 (2019).

7. Antibacterial synergism of polymyxin B nonapeptide and hydrophobic antibiotics in experimental gram-negative infections in mice.

8. Sisa, M., Bonnet, S. L., Ferreira, D. & van der Westhuizen, J. H. Photochemistry of flavonoids. *Molecules* **15**, 5196–245 (2010).

9. May, J. M. *et al.* The Antibiotic Novobiocin Binds and Activates the ATPase That Powers Lipopolysaccharide Transport. *J Am Chem Soc* **139**, 17221–17224 (2017).

10. Wehrli, W. Rifampin: Mechanisms of Action and Resistance. *Reviews of Infectious Diseases* **5**, S407–S411 (1983).

11. Ochsner, U. A., Wilderman, P. J., Vasil, A. I. & Vasil, M. L. GeneChip® expression analysis of the iron starvation response in Pseudomonas aeruginosa: identification of novel pyoverdine biosynthesis genes. *Molecular Microbiology* **45**, 1277–1287 (2002).

12. Paterson, J. R. *et al.* Insights into the Antibacterial Mechanism of Action of Chelating Agents by Selective Deprivation of Iron, Manganese, and Zinc. *Appl Environ Microbiol* **88**, e0164121–e0164121 (2022).

13. Haque, H. & Russell, A. D. Effect of chelating agents on the susceptibility of some strains of gram-negative bacteria to some antibacterial agents. *Antimicrob Agents Chemother* **6**, 200–206 (1974).

14. Thompson, M. G., Corey, B. W., Si, Y., Craft, D. W. & Zurawski, D. v. Antibacterial activities of iron chelators against common nosocomial pathogens. *Antimicrob Agents Chemother* **56**, 5419–5421 (2012).

15. Schnaars, C. *et al.* Synthesis and Preclinical Evaluation of TPA-Based Zinc Chelators as Metallo-β-lactamase Inhibitors. *ACS Infectious Diseases* **4**, 1407–1422 (2018).

16. Faure, M. E., Cilibrizzi, A., Abbate, V., Bruce, K. D. & Hider, R. C. Effect of iron chelation on anti-pseudomonal activity of doxycycline. *International Journal of Antimicrobial Agents* **58**, 106438 (2021).

17. Ramirez-Ronda, C. H., Holmes, R. K. & Sanford, J. P. Effects of divalent cations on binding of aminoglycoside antibiotics to human serum proteins and to bacteria. *Antimicrob Agents Chemother* **7**, 239–245 (1975).

18. Hancock, R. E. W. Aminoglycoside uptake and mode of action—with special reference to streptomycin and gentamicin: I. Antagonists and mutants. *Journal of Antimicrobial Chemotherapy* **8**, 249–276 (1981).

19. Xu, Z. Mechanics of metal-catecholate complexes: the roles of coordination state and metal types. *Sci Rep* **3**, 2914 (2013).

Chapter 6: Conclusion and Future Work

6.1 GENERAL CONCLUSION

In this work, we have successfully synthesized tobramycin-catecholate based conjugates (TOB-CAT) in order to explore the utilization of conjugating siderophore moieties to antibiotics to exploit the siderophore-iron uptake mechanism of bacteria and restore antibacterial activity of aminoglycosides against once resistant pathogens. These conjugates displayed specific antibacterial activity against wild-type and clinical isolate *P. aeruginosa* strains. It was determined, by testing the antibacterial activity of the methoxy protected control conjugates (TOB-mCAT), that the catecholate is critical for the observed antibacterial activity of TOB-CAT conjugates. Surprisingly, the TOB-CAT conjugates lost all their significant activity when tested in iron deficient media.

The combination studies showed that both the TOB-CAT and TOB-mCAT conjugates were capable of synergizing multiple legacy antibiotics of which include aztreonam, minocycline, levofloxacin, novobiocin, and rifampicin against wild-type Gram-negative pathogens and MDR *P. aeruginosa* strains. There were few instances of synergy observed with the TOB-CAT conjugates with β-lactam antibiotics including piperacillin, ceftazidime, and meropenem against wild-type Gram-negative pathogens. The greatest synergistic interactions observed were with the TOB-CAT conjugates and novobiocin and rifampicin. The adjuvant activity of the conjugates seems to be dependent on the increasing carbon tether link and the presence of the catecholate.

The mechanism of the tobramycin-catecholate conjugates is not fully understood from the studies carried out. The results from the NPN assays show that the TOB-CAT conjugates permeabilizes outer membranes of PAO1 on par with PMBN. This membrane permeabilization action of the tobramycin-catecholate is also supported by the high synergistic interaction displayed of TOB-CAT and TOB-mCAT conjugates with novobiocin and rifampicin. The polycationic and lipophilic components of the TOB-CAT and TOB-mCAT conjugates seem to be important for their membrane permeabilization activity. The catecholate of TOB-CAT conjugates may enhance the membrane permeabilization or helps the conjugate across the outer membrane using the siderophore uptake system, however the impact of the catecholate is not conclusive.

6.2 FUTURE WORK

6.2.1 Future Studies

This thesis and research have demonstrated that tobramycin-catecholate conjugates have high antibacterial activity against *P. aeruginosa* wild type and clinical strains and are able to revive the activity of multiple legacy antibiotics against Gram-negative bacteria. For additional microbiology testing, more combination studies could be done with additional clinical *P. aeruginosa* strains. Furthermore, additional combination studies should be conducted in the ID-CAMHB to see if adjuvant activity of TOB-CAT and TOB-mCAT conjugates will be preserved in that environment. Even though the TOB-mCAT conjugates have no antibacterial activity they still synergized antibiotics in combination studies in MHB. Similarly, the TOB-CAT conjugates may synergize antibiotics in ID-CAMHB even though they showed no antibacterial activity.

To further understand the mechanism of action of these conjugates there are more tests that should be conducted. In order to see if the ribosomal binding of the tobramycin component of the TOB-CAT conjugates is preserved, A-site binding assays can be conducted with PAO1 rRNA[1]. After the disappointing results from the antibacterial assays in ID-CAMHB with TOB-CAT, I think it is important to conduct iron binding assays to make sure that the attached catechol still maintains its ability to complex iron. These additional studies will shed light on mechanism of action of the TOB-CAT conjugates providing insight on how the Trojan Horse method using catecholates can be further explored.

6.2.1 Future Synthetic Work

The synthesis of tobramycin-catecholate conjugates and structurally similar control conjugates was outlined in this thesis. To fully explore how siderophore moieties can be utilized to increase the efficacy of aminoglycosides, more conjugates should be made with a variety of different approaches. These approaches should focus to synthesize conjugates with higher binding affinities for iron.

One approach should be synthesizing tobramycin conjugates with 2-chloro-3,4-dihydroxybenzoic acid as the catechol component instead of the 3,4-dihydroxybenzoic acid that was used for TOB-CAT conjugates[2]. This is the catechol conjugate utilized by cefiderocol, the addition of the chlorine electron withdrawing group makes the hydroxy groups more acidic and consequently the catechol has a higher iron binding affinity[2]. The protocol of how the 2-chloro-3,4-dihydroxybenzoic acid catecholate is added to make cefiderocol can be adapted to conjugate it to tobramycin via a carbon tether[2].

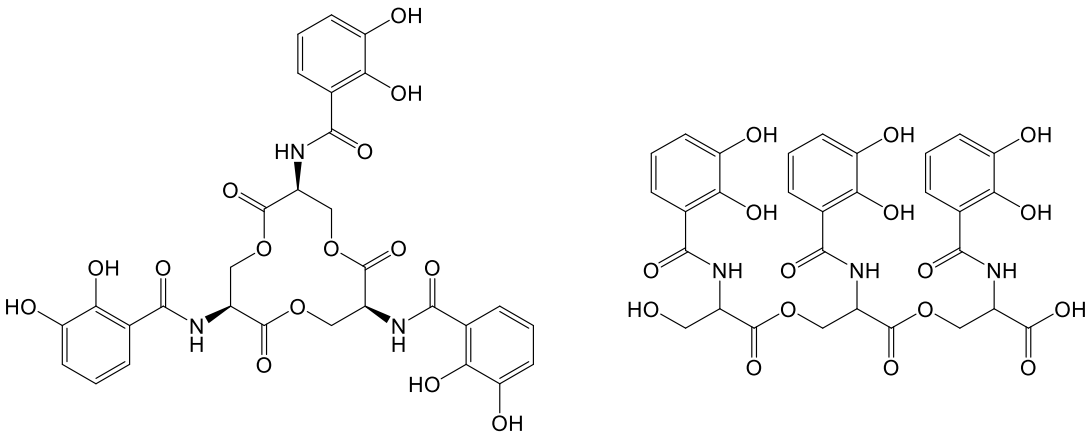

Figure 46. The chemical structures of Enterobactin (left) and Desferri-ferrioxamine (right)[3].

Another approach to increase the binding affinity for iron of the conjugates is by increasing the number of binding ligands per molecule of tobramycin. The higher number of binding ligands a short distance from each other would increase the binding affinity of the conjugate, due to the chelate effect and accessibility of the ligands to form a hexadentate complex with iron[4]. One such method might be to install desferri-ferrioxamine B via a carbon tether to tobramycin[3]. The three catecholate binding ligands of desferri-ferrioxamine B would likely have a higher binding affinity for Fe^{3+} than just the single catecholate of **1a** due to the proximity of the three catecholate ligands. Desferri-ferrioxamine B is a linear form of enterobactin, and due to this it might form a specific iron-enterobactin complex with a specific shape that might be need for proper recognition by receptor proteins[3]. A possible negative from this approach might be that conjugates become too large and impede their ability to use the transporter protein.

In this research only the addition of the catecholate iron binding ligand was explored. There are other binding ligands for iron that are utilized in bacterial siderophores that could also

be used for this Trojan Horse method of antibiotic modification. Some of the more common ligands that can be utilized are hydroxamates and carboxylates[4]. These ligands generally have slightly lower binding affinity compared to catecholates, therefore substituting the catecholates with these other ligands might result in conjugates with a lower iron binding affinity[4]. On the other hand, the complexes that the hydroxamate and carboxylate ligands make with iron might be necessary for the recognition and transport by certain transport proteins. These approaches will provide additional paths to explore how aminoglycoside-siderophore can used with the Trojan Horse model of antibiotics modification.

6.3 REFERENCES

1. Fair, R. J. *et al.* Singly Modified Amikacin and Tobramycin Derivatives Show Increased rRNA A-Site Binding and Higher Potency against Resistant Bacteria. *ChemMedChem* **9**, 2164–2171 (2014).

2. Aoki, T. *et al.* Cefiderocol (S-649266), A new siderophore cephalosporin exhibiting potent activities against Pseudomonas aeruginosa and other gram-negative pathogens including multi-drug resistant bacteria: Structure activity relationship. *European Journal of Medicinal Chemistry* **155**, 847–868 (2018).

3. Fiedler, H.-P., Krastel, P., Müller, J., Gebhardt, K. & Zeeck, A. Enterobactin: the characteristic catecholate siderophore of Enterobacteriaceae is produced by Streptomyces species. *FEMS Microbiology Letters* **196**, 147–151 (2001).

4. Hider, R. C. & Kong, X. Chemistry and biology of siderophores. *Natural Product Reports* **27**, 637–657 (2010).

Chapter 7: Supporting Information

7.1 EXPERIMENTAL SECTION

7.1.1 Synthetic Chemistry

7.1.1.1 General Comments

The reagents and solvents were purchased from commercially available sources and used without purification, unless otherwise noted. Synthesis was performed only performed under anoxic or anhydrous conditions if it was specifically noted. Reactions were monitored with thin-layer chromatography (TLC) on silica gel 60 F254 (0.25mm, Merck) and/or aluminum-backed reverse phase silica gel 60 RP-18 $F_{254}S$ plates (Merck KGaA, Germany) using the indicated solvents. The TLC silica gels were then visualized using ultraviolet light and/or stained with ninhydrin solution (ninhydrin and acetic acid in *n*-butanol). The intermediate compounds were purified using flash chromatography on silica gel 60 (230-400 ASTM mesh) and final compounds were purified on reverse-phase C18 silica gel (Silicyle, USA). 1D and 2D (^{1}H, ^{13}C, COSY, HSQC, HMBC) NMR characterization experiments were performed in either Bruker AMX-500 or Bruker AMX-300 spectrophotometers in the specified deuterated solvents. The chemical shifts (δ) are reported in parts per million with $CDCl_3$ (^{1}H-NMR 7.26ppm, ^{13}C-NMR 77.0ppm) and CD_3OD (^{1}H-NMR 3.31ppm, ^{13}C-NMR 49.3ppm) are used as internal standards. The Matrix-assisted laser desorption ionization (MALDI) mass spectrometry (MS) experiments were carried out on a Burker Daltonics Ultraflex MALDI TOF/TOF mass spectrometer. Electrospray ionization (ESI) MS experiments were carried out on a Varian 500 MS ion trap mass spectrometer.

7.1.1.2 Synthetic Procedure and Characterization of 1,3,2',6',3''-Penta-N-(Tert-Butoxycarbonyl)-Tobramycin (2) and 1,3,2',6',3''-Penta-N-(Tert-Butoxycarbonyl)-Tetra-O-TBDMS-Tobramycin (3)

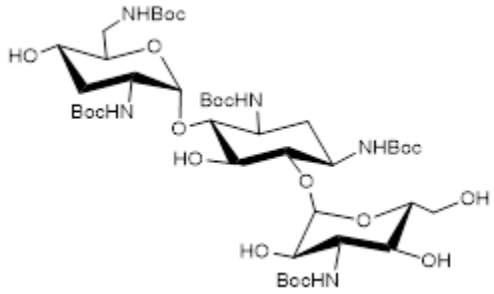

1,3,2',6',3''-Penta-N-(Tert-Butoxycarbonyl)-Tobramycin (2). A stirring solution of tobramycin (2.0 g, 4.3 mmol) in 120 mL of a 2:1 MeOH:H_2O solvent mixture is treated with di-*tert*-butyl decarbonate ($(Boc)_2O$) () and triethylamine () at room temperature. This mixture was stirred overnight at 55 °C. This mixture was then concentrated under reduced pressure which yielded intermediate **3** as white solid. This solid was then used in the next step without further purification. Yield 4.00 g (96%).

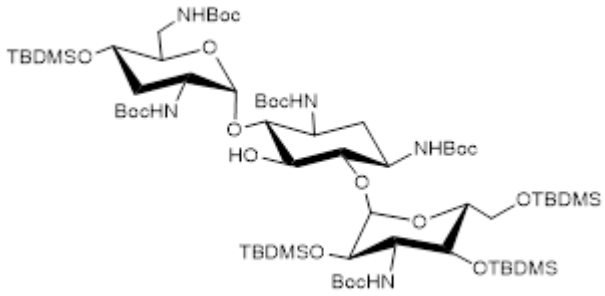

1,3,2',6',3''-Penta-N-(Tert-Butoxycarbonyl)-4',2'',4'',6''-Tetra-O-TBDMS-Tobramycin (3). A stirring solution of **2** (4.1 mmol) in anhydrous DMF (20 mL) was treated with TBDMSCl () and 1-methylimidazole () were added subsequently. The flask was evacuated and flushed with N_2 gas. The reaction mixture was stirred for 4 days under N_2 gas at room temperature. Water (30 mL) is added to the reaction mixture and extracted with ethyl acetate (3x30 mL). These organic layers were combined, then washed with saturated brine and dried with anhydrous sodium sulfate (Na_2SO_4). This mixture was purified by flash chromatography (with a solvent gradient of hexanes/ethyl acetate = 20:1 to 3:1) and concentrated under reduced pressure to yield **3** as a

white solid. Yield: 5.37 g (92%). ^{1}H NMR (300 MHz, CDCl3) δ 5.46 – 5.23 (m, 1H), 5.00 – 4.86 (m, 2H), 4.43 (d, J = 66.4 Hz, 1H), 3.87 (d, J = 10.3 Hz, 2H), 3.78 – 2.95 (m, 13H), 2.79 – 2.64 (m, 1H), 2.11 – 1.98 (m, 1H), 1.72 – 1.51 (m, 2H), 1.48 – 1.38 (m, 45H), 0.94 – 0.85 (m, 36H), 0.14 – 0.03 (m, 24H). ^{13}C NMR (75 MHz, CDCl3) δ 156.30, 155.57, 155.13, 154.67, 99.41, 98.89, 83.95, 81.89, 79.53, 79.44, 78.71, 76.03, 75.33, 72.95, 68.75, 67.52, 63.28, 56.97, 51.02, 50.38, 49.63, 41.50, 34.73, 33.75, 28.58, 28.49, 28.43, 26.12, 26.06, 25.98, 25.77, 18.50, 18.20, 18.12, 17.86, -3.74, -4.16, -4.67, -4.91, -5.14. MALDI TOF-MS *m/e* $[M+Na]^{+}$ calculated for $C_{67}H_{133}N_5O_{19}Si_4Na^{+}$, 1446.859; observed 1446.762.

7.1.1.3 Synthetic Procedure and Characterization of 5-O-(n-bromoalkyl)-1,3,2',6',3''-penta-N-(tert-butoxycarbonyl)-4',2'',4'',6''-tetra-O-TBDMS-tobramycin derivatives (4a-b)

To a stirred solution of compound **5** (0.35 mmol) in hydrated toluene (5 mL), 1,*n*-dibromoalkane (1.05 mmol), and a catalytic amount of tetrabutylammonium hydrogen sulphate (TBAHS) (0.05 mmol) and KOH (1.05 mmol) were added to the mixture subsequently. The reaction mixture was stirred at room temperature overnight. Water (30 mL) is added to the reaction mixture and extracted with ethyl acetate (3x30 mL). These organic layers were combined, then washed with saturated brine and dried with anhydrous sodium sulfate (Na_2SO_4). This mixture was purified by flash chromatography (with a solvent gradient of hexanes/ethyl acetate = 10:1 to 3:1) and concentrated under reduced pressure to yield **4a-b** as a white solid.

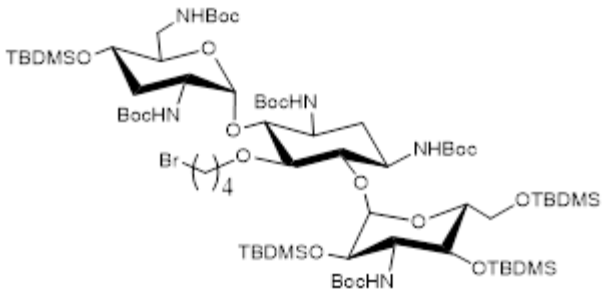

5-O-(4-bromoalkyl)-1,3,2',6',3''-penta-N-(tert-butoxycarbonyl)-4',2'',4'',6''-tetra-O-TBDMS-tobramycin. Yield: 60%. ^{1}H NMR (500 MHz, $CDCl_3$) δ 5.18 (s, 1H), 5.12 (s, 1H), 5.00 – 4.98 (m, 1H), 4.76 (s, 1H), 4.52 (s, 1H), 4.15 – 4.13 (m, 2H), 3.85 – 3.36 (m, 14H), 3.25 – 3.22 (m, 3H), 2.47 (s, 1H), 2.03 – 1.98 (m, 1H), 1.93 – 1.87 (m, 2H), 1.69 – 1.65 (m, 2H), 1.51 – 1.42 (m, 45H), 0.95 – 0.86 (m, 36H), 0.15 – -0.03 (m, 24H). ^{13}C NMR (126 MHz, $CDCl_3$) δ 155.69, 155.65, 155.47, 154.72, 154.59, 97.85, 96.49, 85.90, 79.95, 79.41, 79.27, 79.11, 78.78, 75.41, 72.67, 72.26, 71.57, 67.98, 67.05, 63.22, 57.14, 50.49, 48.82, 48.31, 41.61, 36.64, 36.03, 35.61, 34.62, 34.47, 33.72, 29.47, 29.22, 29.01, 28.60, 28.48, 28.41, 26.09, 25.97, 25.76, 25.24, 18.46, 18.28, 18.07, 17.89, -3.42, -3.76, -4.22, -4.91, -4.93, -5.06, -5.17, -5.20. MALDI TOF-MS *m/e* $[M+Na]^+$ calculated for $C_{71}H_{140}BrN_5O_{19}Si_4Na^+$, 1580.829; observed 1580.907.

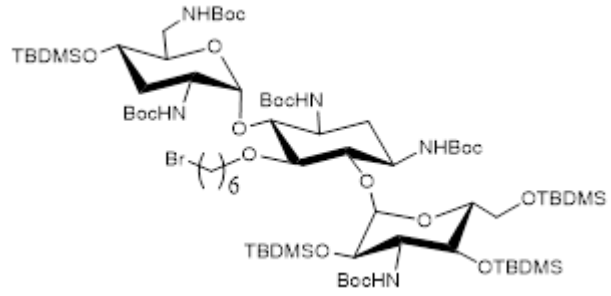

5-O-(6-bromoalkyl)-1,3,2',6',3''-penta-N-(tert-butoxycarbonyl)-4',2'',4'',6''-tetra-O-TBDMS-tobramycin. Yield: 71%. ^{1}H NMR (300 MHz, $CDCl_3$) δ 5.25 – 5.03 (m, 3H), 4.86 (s, 1H), 4.54 (s, 1H), 4.35 – 4.02 (m, 3H), 3.88 – 3.16 (m, 11H), 2.52 (d, J = 12.8 Hz, 1H), 2.07 – 1.98 (m, 1H), 1.90 – 1.81 (m, 2H), 1.68 – 1.58 (m, 1H), 1.65 – 1.54 (m, 2H), 1.51 (s, 1H), 1.48 – 1.40 (m, 45H), 1.43 – 1.17 (m, 6H), 1.10 – 1.02 (m, 1H), 0.96 (s, 9H), 0.92 – 0.84 (m, 27H), 0.22 – 0.12 (m, 6H), 0.11 – 0.02 (m, 18H). ^{13}C NMR (75 MHz, $CDCl_3$) δ155.76, 155.66, 155.46, 154.75,

154.58, 97.72, 96.42, 85.75, 79.89, 79.70, 79.37, 79.20, 78.78, 75.25, 73.17, 72.65, 71.56, 68.06, 67.00, 63.16, 57.25, 50.55, 48.90, 48.34, 41.68, 35.98, 35.72, 33.74, 33.52, 32.82, 32.59, 32.50, 30.42, 28.63, 28.50, 28.43, 27.27, 26.13, 26.00, 25.80, 25.33, 18.49, 18.32, 18.10, 17.92, -3.46, -3.77, -4.19, -4.87, -5.02, -5.15, -5.18, -5.28. MALDI TOF-MS *m/e* $[M+Na]^+$ calculated for $C_{73}H_{144}BrN_5O_{19}Si_4Na^+$, 1608.859; observed 1608.878

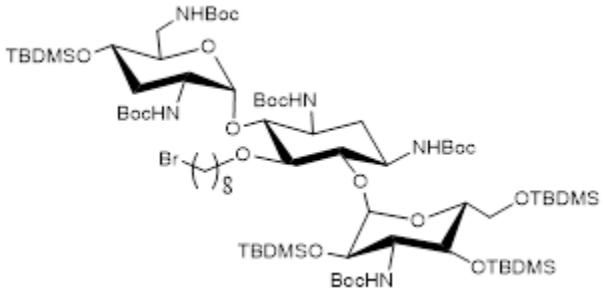

5-O-(8-bromoalkyl)-1,3,2',6',3''-penta-N-(tert-butoxycarbonyl)-4',2'',4'',6''-tetra-O-TBDMS-tobramycin. Yield: 74%. ^{1}H NMR (300 MHz, $CDCl_3$) δ 5.25 – 5.03 (m, 3H), 4.80 (s, 1H), 4.53 (s, 1H), 4.35 – 4.02 (m, 3H), 3.88 – 3.16 (m, 11H), 2.49 (d, J = 12.8 Hz, 1H), 2.07 – 1.98 (m, 1H), 1.90 – 1.81 (m, 2H), 1.68 – 1.58 (m, 1H), 1.65 – 1.54 (m, 2H), 1.51 (s, 1H), 1.48 – 1.40 (m, 45H), 1.38 – 1.17 (m, 10H), 1.10 – 1.02 (m, 1H), 0.96 (s, 9H), 0.92 – 0.84 (m, 27H), 0.22 – 0.12 (m, 6H), 0.11 – 0.02 (m, 18H).^{13}C NMR (75 MHz, $CDCl_3$) δ 155.57, 154.60, 96.47, 90.91, 85.79, 79.96, 79.42, 79.25, 73.25, 68.00, 63.16, 57.23, 50.50, 48.87, 48.27, 35.71, 33.99, 32.85, 30.63, 29.82, 28.77, 28.65, 28.52, 28.42, 28.19, 26.15, 26.02, 25.80, 18.52, 18.35, 18.12, 17.93, -3.77, -4.18, -4.94, -5.05, -5.18. . MALDI TOF-MS *m/e* $[M+Na]^+$ calculated for $C_{75}H_{148}BrN_5O_{19}Si_4Na^+$, 1636.889; observed 1636.944

7.1.1.4 Synthetic Procedure and Characterization of 5-O-(n-azidoalkyl)-1,3,2',6',3''-penta-N-(tert-butoxycarbonyl)-4',2'',4'',6''-tetra-O-TBDMS-tobramycin derivatives (5a-c).

To a stirring solution of **4a-b** (1 equiv.) in anhydrous DMF (5 mL), NaN_3 (20 equiv.) were added. The reaction mixture then stirred for 3h at 70 °C under a nitrogen atmosphere. The reaction mixture was concentrated under reduced pressure. The concentrated mixture was then re-dissolved in ethyl acetate (30 mL), washed with water (3x30 mL) and saturated brine (30 mL), and dried with anhydrous sodium sulfate (Na_2SO_4). This mixture was concentrated under reduced pressure and purified by flash chromatography (with a solvent gradient of hexanes/ethyl acetate = 10:1 to 3:1) and concentrated under reduced pressure to yield **5a-b** as a white solid.

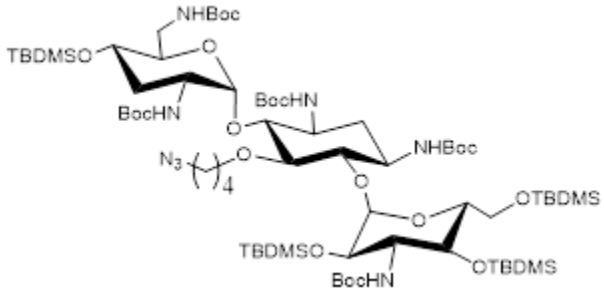

5-O-(4-azidoalkyl)-1,3,2',6',3''-penta-N-(tert-butoxycarbonyl)-4',2'',4'',6''-tetra-O-TBDMS-tobramycin. Yield: 93%. ^{1}H NMR (300 MHz, $CDCl_3$) δ 5.26 (d, J = 24.7 Hz, 1H), 5.17 (d, J = 11.2 Hz, 1H), 4.82 (s, 1H), 4.53 (s, 1H), 4.14 (dd, J = 38.5, 13.5 Hz, 3H), 3.83 – 3.76 (m, 4H), 3.54 (d, J = 6.7 Hz, 9H), 3.25 (d, J = 7.0 Hz, 3H), 2.51 (d, J = 12.8 Hz, 1H), 2.12 – 1.99 (m, 1H), 1.61 (q, J = 7.2 Hz, 4H), 1.49 – 1.43 (m, 45H), 1.17 – 1.06 (m, 1H), 0.98 (s, 9H), 0.93 – 0.86 (m, 27H), 0.19 (d, J = 2.3 Hz, 6H), 0.15 – 0.07 (m, 18H). ^{13}C NMR (75 MHz, $CDCl_3$) δ 155.69, 155.47, 154.75, 154.60, 154.26, 97.87, 96.42, 85.91, 79.96, 79.42, 79.27, 79.15, 78.73, 75.43, 72.65, 72.47, 71.57, 67.97, 67.10, 63.25, 57.14, 51.41, 50.51, 48.84, 48.30, 41.60, 35.92, 35.64, 28.61 - 28.37, 27.59, 26.12 - 25.42, 18.46, 18.28, 18.07, 17.90, -3.48, -3.77, - 4.23, -4.37, -4.70, -4.90, -5.11, -5.24. MALDI TOF-MS *m/e* $[M+Na]^+$ calculated for $C_{71}H_{140}N_8O_{19}Si_4Na^+$, 1543.919; observed 1544.168.

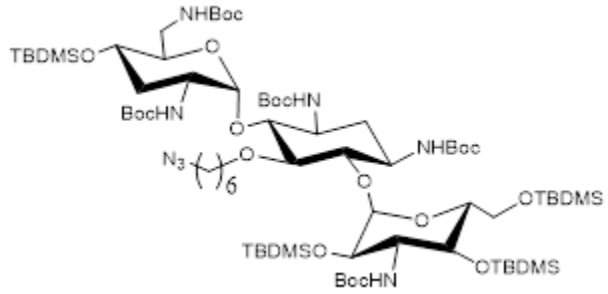

5-O-(6-azidoalkyl)-1,3,2',6',3''-penta-N-(tert-butoxycarbonyl)-4',2'',4'',6''-tetra-O-TBDMS-tobramycin. Yield: 92%. ^{1}H NMR (300 MHz, $CDCl_3$) δ 5.31 (d, J = 24.8 Hz, 1H), 5.12 (d, J = 11.7 Hz, 1H), 4.84 (s, 1H), 4.57 (s, 1H), 4.23 (dd, J = 38.5, 13.3 Hz, 3H), 3.78 – 3.65 (m, 4H), 3.64 (d, J = 6.7 Hz, 9H), 3.21 (d, J = 7.0 Hz, 3H), 2.51 (d, J = 12.8 Hz, 1H), 2.07 – 1.99 (m, 1H), 1.63 (q, J = 7.2 Hz, 4H), 1.49 – 1.45 (m, 45H), 1.34 – 1.25 (m, 4H), 1.23 – 1.02 (m, 1H), 0.95 (s, 9H), 0.92 – 0.88 (m, 27H), 0.19 (d, J = 2.2 Hz, 6H), 0.13 – 0.06 (m, 18H) ^{13}C NMR (75 MHz, $CDCl_3$) δ 155.65, 154.84, 96.34, 85.86, 79.95, 79.56, 79.43, 75.26, 72.83, 71.55, 67.78, 63.19, 57.42, 50.50, 48.98, 48.34, 41.67, 35.71, 28.68, 28.52, 28.47, 27.59, 26.12, 26.02, 25.83, 18.52, 18.29, 18.13, 17.94, -3.38, -3.75, -4.19, -4.81, -4.86, -4.98, -5.07, -5.12. MALDI TOF-MS *m/e* $[M+Na]^+$ calculated for $C_{73}H_{144}N_8O_{19}Si_4Na^+$, 1571.949; observed 1572.154

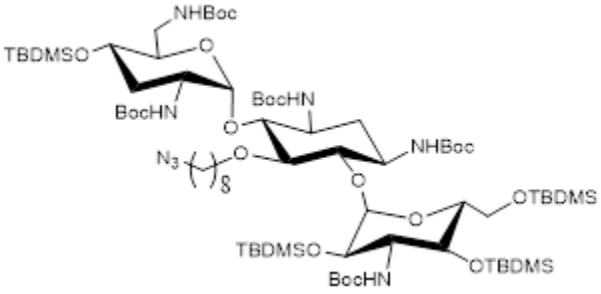

5-O-(8-azidoalkyl)-1,3,2',6',3''-penta-N-(tert-butoxycarbonyl)-4',2'',4'',6''-tetra-O-TBDMS-tobramycin. Yield: 95%. ^{1}H NMR (300 MHz, $CDCl_3$) δ 5.21 (d, J = 24.9 Hz, 1H), 5.07 (d, J = 11.6 Hz, 1H), 4.82 (s, 1H), 4.55 (s, 1H), 4.18 (dd, J = 38.7, 13.7 Hz, 3H), 3.84 – 3.70 (m, 4H), 3.57 (d, J = 6.8 Hz, 9H), 3.27 (d, J = 7.0 Hz, 3H), 2.51 (d, J = 12.8 Hz, 1H), 2.07 – 1.99 (m, 1H), 1.61 (q, J = 7.2 Hz, 4H), 1.49 – 1.45 (m, 45H), 1.36 – 1.29 (m, 8H), 1.12 – 1.04 (m, 1H), 0.98 (s, 9H), 0.92 – 0.88 (m, 27H), 0.19 (d, J = 2.2 Hz, 6H), 0.13 – 0.06 (m, 18H).^{13}C NMR (75 MHz, $CDCl_3$) δ 163.05, 159.99, 142.53,

135.63, 126.63, 108.40, 101.66, 94.27, 90.01, 79.43, 66.81, 62.81, 51.48, 48.90, 43.04, 33.93, 32.99, 30.62, 29.17, 28.85, 28.67, 28.54, 28.44, 26.74, 26.17, 26.03, 25.82, 25.68, 22.43, 18.37, -3.46, -3.78, -4.16, -4.24, -4.86, -4.98, -5.08, -5.16. MALDI TOF-MS *m/e* $[M+Na]^+$ calculated for $C_{75}H_{148}N_8O_{19}Si_4Na^+$, 1599.979; observed 1600.046

7.1.1.5 Synthetic Procedure and Characterization of 5-O-(n-aminoalkyl)-1,3,2',6',3''-penta-N-(tert-butoxycarbonyl)-4',2'',4'',6''-tetra-O-TBDMS-tobramycin derivatives (6a-c).

To a stirring solution of **6a-c** (1 equiv.) in MeOH (20 mL), palladium hydroxide ($Pd(OH)_2$) (3 equiv.) is added to the mixture. The reaction flask is then evacuated and flushed with H_2 gas. The reaction mixture is stirred at room temperature for 3 h under a H_2 gas environment. The solution is then filtered on a bed of Celite® and washed with MeOH. The resulting solution was concentrated under reduced pressure. This mixture was concentrated under reduced pressure and purified by flash chromatography (with a solvent gradient of DCM/MeOH = 100:1 to 20:1) and concentrated under reduced pressure to yield **6a-b** as a white solid.

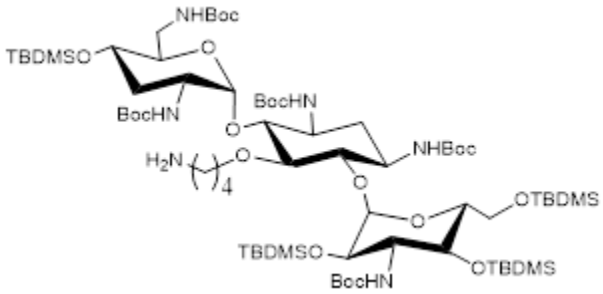

5-O-(4-aminoalkyl)-1,3,2',6',3''-penta-N-(tert-butoxycarbonyl)-4',2'',4'',6''-tetra-O-TBDMS-tobramycin. Yield: 92%. ^{1}H NMR (400 MHz, $CDCl_3$) δ 5.25 – 5.09 (m, 3H), 4.81 (s, 1H), 4.58 (s, 1H), 4.18 – 4.11 (m, 2H), 3.88 – 3.72 (m, 4H), 3.65 – 3.45 (m, 8H), 3.38 – 3.34 (m, 1H), 3.29 – 3.15 (m, 3H), 2.86 – 2.81 (m, 1H), 2.76 – 2.71 (m, 1H), 2.47 (s, 1H), 2.04 – 1.97 (m, 1H), 1.62 – 1.53 (m, 4H), 1.47 –

1.43 (m, 45H), 1.12 – 1.03 (m, 1H), 0.96 (s, 9H), 0.91 – 0.88 (m, 27H), 0.18 (d, J = 4.2 Hz, 6H), 0.11 – 0.05 (m, 18H).^{13}C NMR (101 MHz, $CDCl_3$) δ 155.53, 154.80, 96.24, 85.86, 79.95, 79.58, 79.45, 75.24, 72.85, 71.56, 67.90, 63.22, 57.40, 50.59, 48.90, 48.29, 41.45, 35.71, 28.68, 28.52, 28.48, 27.59, 26.12, 26.02, 25.81, 18.52, 18.29, 18.11, 17.94, -3.38, -3.75, -4.19, -4.81, -4.86, -4.98, -5.07, -5.12. MALDI TOF-MS *m/e* $[M+Na]^+$ calculated for $C_{71}H_{142}N_6O_{19}Si_4Na^+$, 1517.929; observed 1518.605

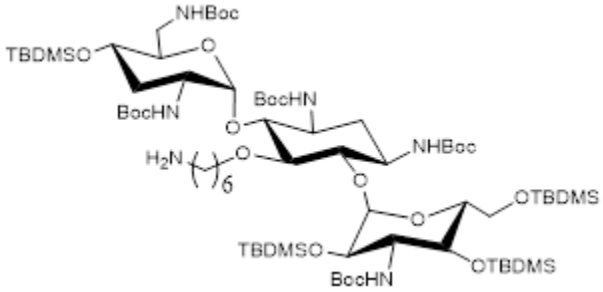

5-O-(6-aminoalkyl)-1,3,2',6',3''-penta-N-(tert-butoxycarbonyl)-4',2'',4'',6''-tetra-O-TBDMS-tobramycin. Yield: 90%. ^{1}H NMR (400 MHz, $CDCl_3$) δ 5.25 – 5.08 (m, 3H), 4.57 (s, 1H), 4.29 – 4.09 (m, 3H), 3.86 – 3.77 (m, 2H), 3.76 – 3.70 (m, 2H), 3.64 – 3.48 (m, 6H), 3.38 – 3.19 (m, 6H), 2.83 (t, J = 7.3 Hz, 2H), 2.47 (d, J = 12.5 Hz, 1H), 2.03 – 1.98 (m, 1H), 1.60 – 1.52 (m, 4H), 1.48 – 1.42 (m, 45H), 1.37 – 1.30 (m, 4H), 1.11 – 1.03 (m, 1H), 0.96 (s, 9H), 0.92 – 0.87 (m, 27H), 0.17 (s, 6H), 0.12 – 0.04 (m, 18H).^{13}C NMR (101 MHz, $CDCl_3$) δ 155.50, 154.72, 96.28, 85.83, 79.95, 79.94, 79.44, 79.25, 72.63, 67.10, 63.27, 57.35, 50.53, 48.28, 41.04, 35.74, 35.73, 30.32, 28.67, 28.52, 28.47, 26.89, 26.14, 26.03, 25.81, 18.53, 18.33, 18.11, 17.94, -3.40, -3.75, -4.16, -4.84, -5.01, -5.13. MALDI TOF-MS *m/e* $[M+Na]^+$ calculated for $C_{73}H_{146}N_6O_{19}Si_4Na^+$, 1545.959; observed 1546.245

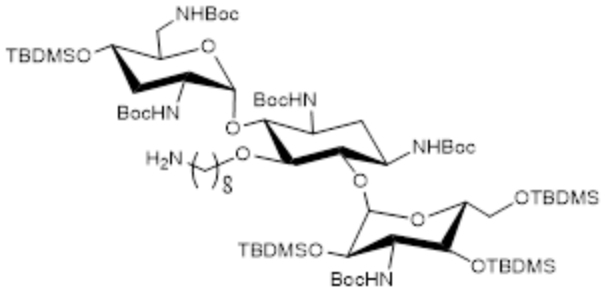

5-O-(8-aminoalkyl)-1,3,2',6',3''-penta-N-(tert-butoxycarbonyl)-4',2'',4'',6''-tetra-O-TBDMS-tobramycin. Yield: 88%. ^{1}H NMR (400 MHz, $CDCl_3$) δ 5.24 (s, 1H), 5.13 – 5.05 (m, 1H), 4.80 (s, 1H), 4.57 (s, 1H), 4.31 – 4.07 (m, 3H), 3.85 – 3.70 (m, 4H), 3.65 – 3.45 (m, 7H), 3.41 – 3.18 (m, 6H), 2.83 (t, J = 7.4 Hz, 2H), 2.49 (d, J = 12.5 Hz, 1H), 2.01 (dd, J = 10.1, 5.3 Hz, 1H), 1.60 (p, J = 6.8 Hz, 4H), 1.48 – 1.42 (m, 45H), 1.29 (d, J = 8.9 Hz, 8H), 1.05 (d, J = 6.4 Hz, 1H), 0.97 (s, 9H), 0.92 – 0.86 (m, 27H), 0.17 (s, 6H), 0.09 (dd, J = 14.3, 5.1 Hz, 18H). ^{13}C NMR (101 MHz, $CDCl_3$) δ 155.59, 154.78, 154.60, 97.83, 96.47, 85.79, 79.44, 79.26, 72.72, 63.16, 57.28, 50.51, 48.89, 48.34, 41.19, 35.63, 30.63, 29.90, 29.18, 28.66, 28.53, 28.45, 26.15, 26.04, 26.02, 25.81, 18.52, 18.35, 18.12, 17.93, -3.36, -3.76, -4.15, -4.84, -5.05, -5.18. MALDI TOF-MS *m/e* $[M+Na]^+$ calculated for $C_{73}H_{146}N_6O_{19}Si_4Na^+$, 1573.989; observed 1574.943.

7.1.1.6 Synthetic Procedure and Characterization of Methyl 3,4-Dihydroxybenzoate (8).

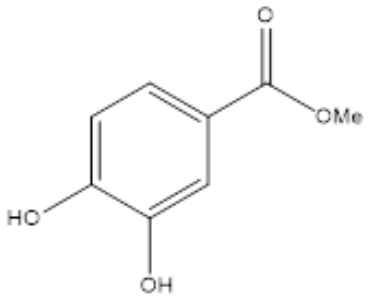

To a stirring solution of 3,4-dihydroxybenzoic (1 equiv.) in MeOH (20 mL), a catalytic amount of H_2SO_4 (0.05 equiv.) is added to the solution. The reaction mixture is refluxed (60 °C) overnight and the solution is then concentrated under reduced pressure. The residue was purified by purified by flash chromatography (with a solvent gradient of DCM/MeOH = 100:1 to 20:1) and concentrated under reduced pressure to yield **8** as a white solid. Yield: 92%. ^{1}H NMR (400 MHz, MeOD) δ 7.43 (m, J = 8.1, 1.6 Hz, 2H), 6.83 – 6.80 (m, 1H), 4.94 (s, 2H), 3.84 (s,

3H).^{13}C NMR (101 MHz, MeOD) δ 167.47, 150.31, 144.79, 122.24, 121.19, 116.01, 114.45, 50.86. ESI TOF-MS *m/e* $[M+Na]^+$ calculated for $C_{10}H_{12}O_4Na^+$, 219.059; observed

7.1.1.7 Synthetic Procedure and Characterization of Methyl 3,4-Bis[(4-Methoxybenzyl)oxy]benzoate (9).

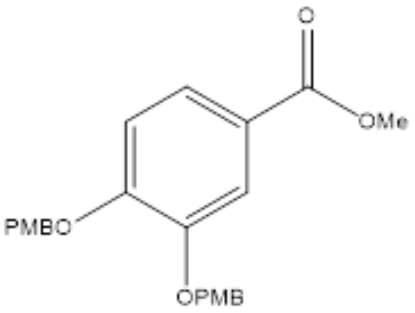

A stirring solution of **8** (1 equiv.) in anhydrous DMF (5 mL) is treated with p-methoxybenzyl chloride (PMB-Cl) (3 equiv.), K_2CO_3 (3 equiv.), and 18-crown-6 ether (1 equiv.). The reaction mixture was stirred overnight at 55°. Water (30 mL) is added to the reaction mixture and extracted with ethyl acetate (3x30 mL). These organic layers were combined, then washed with saturated brine and dried with anhydrous sodium sulfate (Na_2SO_4). This mixture was purified by flash chromatography (with a solvent gradient of hexanes/ethyl acetate = 10:1 to 3:1) and concentrated under reduced pressure to yield **9** as a white solid. Yield: 89%. ^{1}H NMR (300 MHz, $CDCl_3$) δ 7.72 – 7.65 (m, 2H), 7.44 – 7.35 (m, 4H), 6.99 – 6.88 (m, 5H), 5.13 (d, J = 1.6 Hz, 4H), 3.90 (s, 3H), 3.81 (s, 6H). ^{13}C NMR (75 MHz, $CDCl_3$) δ 166.82, 159.47, 159.43, 153.05, 148.38, 129.26, 129.03, 128.92, 128.59, 123.98, 122.92, 115.58, 113.97, 113.92, 113.27, 71.01, 70.62, 55.25, 52.00. ESI TOF-MS *m/e* $[M+Na]^+$ calculated for $C_{24}H_{24}O_6Na^+$, 431.149; observed 431.1451.

7.1.1.8 Synthetic Procedure and Characterization of Methyl 3,4-Bis[(4-Methoxybenzyl)oxy]benzoic Acid (10).

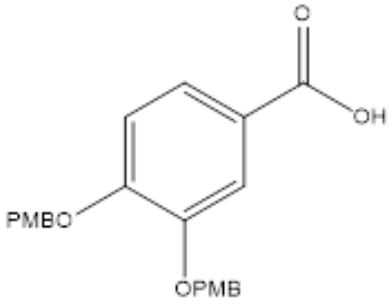

Intermediate **9** was dissolved in a 1.3:1 solvent mixture of THF (13 mL) and MeOH (10 mL). To this mixture, aqueous 2M NaOH (2 equiv.) was added, and the mixture was stirred for 2h while being refluxed. The solvent was evaporated under reduced pressure and then re-dissolved in MeOH (5 mL). To the solution 1M HCl was added until a neutralize pH is reached. The resulting solution was concentrated under reduced pressure and was purified using flash chromatography (with a solvent gradient of DCM/MeOH = 100:1 to 20:1) and concentrated under reduced pressure to yield **10** as a white solid. Yield: 95%. ^{1}H NMR (400 MHz, $CDCl_3$) δ 7.73 – 7.69 (m, 2H), 7.41 – 7.35 (m, 4H), 6.99 – 6.90 (m, 5H), 5.16 (d, J = 14.3 Hz, 4H), 3.84 (s, 6H). ^{13}C NMR (101 MHz, $CDCl_3$) δ 170.19, 159.43, 153.74, 148.39, 129.19, 128.97, 128.91, 128.83, 128.48, 124.85, 121.74, 116.07, 114.01, 113.94, 113.34, 71.06, 70.70, 55.29. ESI TOF-MS *m/e* $[M+Na]^+$ calculated for $C_{23}H_{22}O_6Na^+$, 417.409; observed 417.1299.

7.1.1.9 Synthetic Procedure and Characterization of Compound 7a-c.

Intermediate **10** (1 equiv.) and Mukaiyama reagent (1.5 equiv.) was added to a two-necked flask connected to a condenser. The two regents were dissolved in THF (5mL) and then Et_3N was (3 equiv.) was added subsequently. The flask was evacuated with a vacuum and flushed with N_2 gas. This mixture was left to stir for 15min at room temperature before intermediate **6a-c**, dissolved THF, is added to the flask. This mixture stirred for 5h at reflux under a N_2 gas

environment. The concentrated mixture was then re-dissolved in ethyl acetate (30 mL), washed with water (3x30 mL) and saturated brine (30 mL), and dried with anhydrous sodium sulfate (Na_2SO_4). This mixture was concentrated under reduced pressure and purified by flash chromatography (with a solvent gradient of hexanes/ethyl acetate = 10:1 to 3:1) and concentrated under reduced pressure to yield **7a-b** as a white solid.

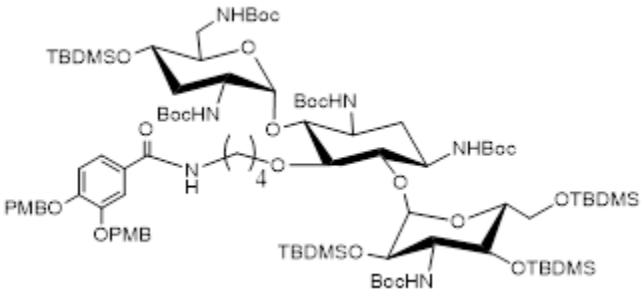

Compound 7a. Yield: 41%. ^{1}H NMR (300 MHz, $CDCl_3$) δ 7.65 (d, *J* = 2.0 Hz, 1H), 7.41 – 7.34 (m, 5H), 7.02 (d, *J* = 8.4 Hz, 1H), 6.92 – 6.87 (m, 4H), 6.60 (s, 1H), 5.25 (s, 1H), 5.19 (d, *J* = 2.8 Hz, 1H), 5.13 (s, 4H), 5.04 (s, 1H), 4.81 (s, 1H), 4.56 (s, 1H), 4.18 (s, 3H), 3.82 (s, 6H), 3.79 – 3.71 (m, 3H), 3.64 – 3.54 (m, 5H), 3.43 (d, *J* = 10.4 Hz, 5H), 3.28 (d, *J* = 6.1 Hz, 2H), 2.48 (s, 1H), 1.98 (d, *J* = 11.8 Hz, 1H), 1.85 (s, 1H), 1.60 (s, 2H), 1.48 – 1.40 (m, 45H), 1.28 – 1.23 (m, 2H), 0.94 (d, *J* = 3.7 Hz, 9H), 0.91 – 0.85 (m, 27H), 0.14 – 0.03 (m, 24H). ^{13}C NMR (75 MHz, $CDCl_3$) δ 166.76, 159.31, 155.64, 155.51, 155.44, 155.15, 154.84, 154.74, 151.44, 148.79, 129.21, 129.14, 129.01, 128.94, 127.81, 119.94, 114.12, 113.86, 113.85, 113.78, 99.98, 96.35, 85.70, 79.99, 79.68, 79.52, 79.30, 79.25, 79.23, 78.65, 75.38, 72.93, 72.50, 71.74, 70.92, 70.78, 67.97, 67.39, 63.30, 57.12, 55.28, 50.57, 48.83, 48.33, 41.61, 39.93, 36.00, 35.91, 35.70, 35.66, 30.98, 29.73, 29.69, 29.57, 28.65, 28.53, 28.49, 27.51, 26.13, 26.03, 25.80, 18.53, 18.33, 18.10, 17.94, -3.42, -3.65, -4.22, -4.77, -4.86, -4.92, -5.08, -5.16. MALDI TOF-MS *m/e* $[M+Na]^+$ calculated for $C_{94}H_{162}N_6O_{24}Si_4Na^+$, 1894.059; observed 1895.188.

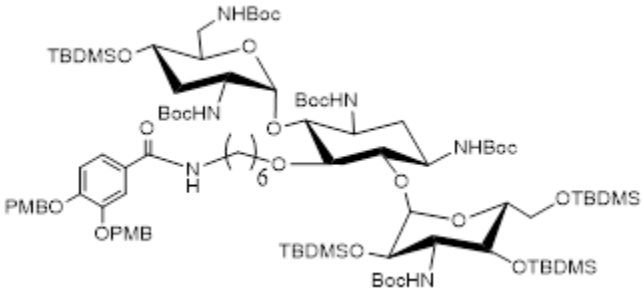

Compound 7b. Yield 36%. ^{1}H NMR (500 MHz, $CDCl_3$) δ 7.54 (d, *J* = 2.1 Hz, 1H), 7.38 – 7.31 (m, 4H), 7.29 – 7.26 (m, 1H), 6.92 – 6.86 (m, 5H), 6.25 (s, 1H), 5.28 – 5.21 (m, 1H), 5.14 (s, 1H), 5.10 (d, *J* = 2.3 Hz, 4H), 5.06 – 5.01 (m, 1H), 4.76 (d, *J* = 14.1 Hz, 1H), 4.51 (s, 1H), 4.26 – 4.06 (m, 3H), 3.80 (s, 6H), 3.78 – 3.75 (m, 1H), 3.70 (d, *J* = 9.8 Hz, 2H), 3.62 (s, 2H), 3.54 (d, *J* = 8.0 Hz, 3H), 3.45 – 3.33 (m, 5H), 3.24 (q, *J* = 10.1, 8.7 Hz, 2H), 2.47 (s, 1H), 2.01 – 1.96 (m, 1H), 1.58 – 1.52 (m, 3H), 1.45 – 1.39 (m, 45H), 1.34 (d, *J* = 6.1 Hz, 4H), 1.25 (s, 2H), 0.94 (s, 9H), 0.89 – 0.85 (m, 27H), 0.16 – 0.13 (m, 6H), 0.09 – 0.02 (m, 18H). ^{13}C NMR (126 MHz, $CDCl_3$) δ 166.85, 159.35, 155.74, 155.49, 154.82, 154.73, 154.66, 154.59, 151.46, 148.88, 129.21, 129.02, 128.90, 128.85, 128.06, 119.82, 114.27, 114.00, 113.88, 113.85, 96.23, 85.81, 79.93, 79.40, 79.38, 79.23, 78.67, 75.23, 73.07, 72.65, 71.60, 71.07, 70.90, 68.03, 67.02, 63.17, 57.19, 55.24, 50.55, 48.79, 48.30, 41.65, 39.94, 36.05, 35.99, 35.93, 35.81, 31.90, 30.44, 29.67, 29.64, 29.48, 28.63, 28.50, 28.41, 27.08, 26.11, 25.99, 25.77, 22.67, 18.49, 18.30, 18.09, 17.91, 14.10, -3.43, -3.78, -4.22, -4.88, -4.92, -5.05, -5.16, -5.18. MALDI TOF-MS *m/e* $[M+Na]^+$ calculated for $C_{96}H_{166}N_6O_{24}Si_4Na^+$, 1922.089; observed 1923.335.

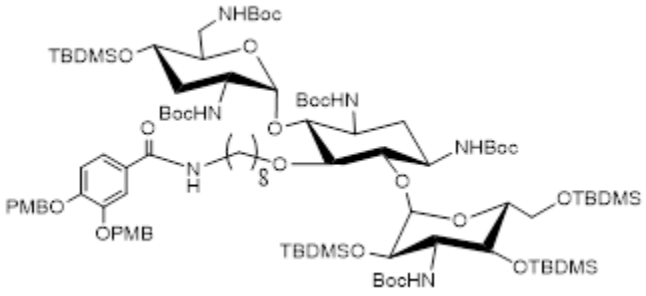

Compound 7c. Yield: 21%.^{1}H NMR (500 MHz, $CDCl_3$) δ 7.50 (d, *J* = 2.1 Hz, 1H), 7.34 (dd, *J* = 19.0, 8.3 Hz, 4H), 7.23 (dd, *J* = 8.2, 2.1 Hz, 1H), 6.91 – 6.86 (m, 5H), 6.12 (t, *J* = 5.5 Hz, 1H), 5.24 (d, *J* = 5.3 Hz, 1H), 5.15 (s, 1H), 5.10 (s, 4H), 5.05 (s, 1H), 4.77 (s, 1H), 4.52 (s, 1H), 4.29 – 4.21 (m, 1H), 4.16 (s, 1H), 4.11 – 4.06 (m, 1H), 3.80 (s, 6H), 3.76 (s, 1H), 3.74 – 3.68 (m, 2H), 3.62 (s, 2H), 3.57 – 3.50 (m, 3H), 3.46 – 3.34 (m, 5H), 3.28 – 3.21 (m, 2H), 2.47 (s, 1H), 2.02 – 1.98 (m, 1H), 1.57 (q, *J* = 7.8 Hz, 3H), 1.45 – 1.40 (m, 45H), 1.34 – 1.25 (m, 10H), 0.95 (s, 9H), 0.89 – 0.85 (m, 27H), 0.15 (d, *J* = 2.3 Hz, 6H), 0.10 – 0.02 (m, 18H). ^{13}C NMR (126 MHz, $CDCl_3$) δ 165.87, 158.36, 154.79, 154.53, 153.75, 153.70, 153.65, 153.57, 150.52, 147.86, 128.20, 127.99, 127.91, 127.80, 127.02, 118.77, 113.31, 112.98, 112.90, 112.87, 95.41, 84.76, 78.93, 78.39, 78.27, 78.23, 77.89, 74.27, 72.25, 71.69, 70.52, 70.12, 69.89, 67.08, 65.86, 62.14, 56.25, 54.25, 49.51, 47.87, 47.37, 40.67, 39.14, 35.00, 34.96, 34.82, 34.71, 30.91, 29.59, 28.82, 28.70, 28.64, 28.34, 27.63, 27.51, 27.41, 26.06, 25.13, 24.99, 24.77, 21.67, 17.49, 17.32, 17.10, 16.91, 13.10, 0.00, -4.41, -4.78, -5.21, -5.89, -5.93, -6.06, -6.17, -6.20. MALDI TOF-MS *m/e* $[M+Na]^+$ calculated for $C_{98}H_{170}N_6O_{24}Si_4Na^+$, 1950.119; observed 1950.793

7.1.1.10 Synthetic Procedure and Characterization of Compound 1a-c

Intermediate **7a-c** was dissolved in a solvent mixture of concentrated HCl/MeOH (2:3) (5 mL). This reaction mixture was stirred for 1h at room temperature, after which it was concentrated under reduced pressure. The residue was then purified using reverse phase flash

chromatography (with a solvent gradient of deionized H_2O) and then concentrated under reduced pressure.

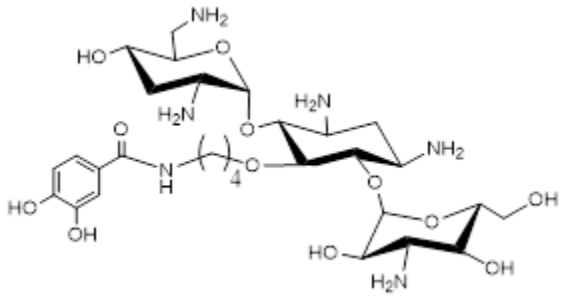

Compound 1a. Yield: 21%. ^{1}H NMR (500 MHz, MeOD) δ 7.29 (d, 1H), 7.22 (d, *J* = 8.7 Hz, 1H), 6.81 (d, *J* = 8.3 Hz, 1H), 5.50 (d, 1H), 5.15 (d, 1H), 4.44 (t, *J* = 9.5 Hz, 1H), 4.21 – 4.17 (m, 1H), 3.99 – 3.95 (m, 1H), 3.90 (t, *J* = 9.3 Hz, 1H), 3.77 (d, *J* = 20.9 Hz, 7H), 3.66 (d, *J* = 9.1 Hz, 4H), 3.57 (dd, *J* = 20.6, 12.8 Hz, 3H), 3.51 (d, *J* = 10.5 Hz, 1H), 3.44 – 3.38 (m, 1H), 3.34 (d, *J* = 6.0 Hz, 1H), 3.24 (s, 2H), 2.47 (d, *J* = 12.2 Hz, 1H), 2.28 – 2.15 (m, 3H), 1.74 – 1.65 (m, 4H). ^{13}C NMR (126 MHz, MeOD) δ 168.38, 152.18, 148.88, 126.54, 120.52, 110.71, 110.55, 100.74, 92.33, 82.24, 81.38, 75.50, 74.44, 74.02, 71.62, 69.13, 65.47, 64.23, 59.90, 55.29, 55.07, 54.96, 49.55, 48.62, 39.33, 39.09, 28.83, 27.94, 26.82, 25.82. MALDI TOF-MS *m/e* $[M+Na]^+$ calculated for $C_{29}H_{50}N_6O_{12}Na^+$, 697.339; observed 697.404.

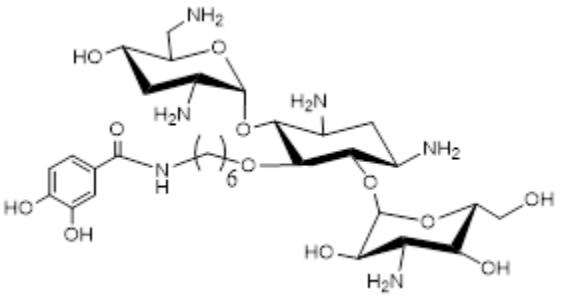

Compound 1b. Yield: 36%. ^{1}H NMR (500 MHz, MeOD) δ 7.27 (d, *J* = 2.1 Hz, 1H), 7.20 (dd, *J* = 8.2, 2.3 Hz, 2H), 6.80 (d, *J* = 8.2 Hz, 2H), 5.46 (d, *J* = 2.7 Hz, 1H), 5.15 (d, *J* = 3.4 Hz, 1H), 4.45 (t, *J* = 9.4 Hz, 2H), 4.21 (d, *J* = 7.6 Hz, 2H), 3.92 (d, *J* = 8.8 Hz, 2H), 3.82 – 3.73 (m, 8H), 3.68 (t, *J* = 9.8 Hz, 5H), 3.59 (d, *J* = 7.3 Hz, 4H), 3.51

(s, 2H), 3.35 (s, 2H), 3.33 (s, 5H), 3.24 (d, *J* = 11.3 Hz, 3H), 2.46 (s, 1H), 2.23 (d, *J* = 6.5 Hz, 4H), 1.65 (d, *J* = 24.9 Hz, 5H), 1.42 (dt, *J* = 12.1, 6.1 Hz, 5H). ^{13}C NMR (126 MHz, MeOD) δ 168.80, 148.61, 144.88, 125.77, 119.07, 114.41, 114.28, 100.75, 92.39, 82.00, 81.48, 75.86, 74.37, 73.89, 71.79, 69.13, 65.46, 64.25, 59.90, 55.02, 49.74, 48.61, 39.20, 39.03, 29.60, 28.99, 28.97, 28.94, 26.41, 25.04. MALDI TOF-MS *m/e* $[M+Na]^+$ calculated for $C_{31}H_{54}N_6O_{12}Na^+$, 725.369; observed 725.375.

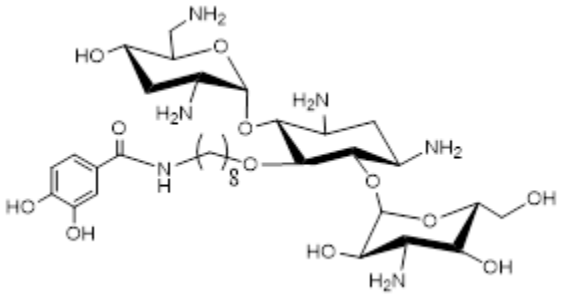

Compound 1c. Yield: 45%. ^{1}H NMR (500 MHz, Methanol-d_4) δ 7.27 (d, *J* = 2.2 Hz, 1H), 7.19 (dd, *J* = 8.3, 2.2 Hz, 1H), 6.80 (d, *J* = 8.3 Hz, 1H), 5.45 (d, *J* = 2.8 Hz, 1H), 5.15 (d, *J* = 3.5 Hz, 1H), 4.42 (t, *J* = 9.5 Hz, 1H), 4.24 – 4.19 (m, 1H), 3.92 – 3.85 (m, 2H), 3.83 – 3.73 (m, 7H), 3.72 – 3.65 (m, 3H), 3.63 – 3.56 (m, 3H), 3.51 (t, *J* = 10.5 Hz, 1H), 3.32 (d, *J* = 2.6 Hz, 1H), 3.30 – 3.22 (m, 10H), 2.48 – 2.43 (m, 1H), 2.26 – 2.18 (m, 3H), 1.63 (dt, *J* = 30.3, 7.2 Hz, 4H), 1.37 (s, 8H). ^{13}C NMR (126 MHz,) δ 168.81, 148.58, 144.85, 125.79, 119.06, 114.40, 114.29, 100.84, 92.45, 81.95, 81.39, 75.81, 74.91, 73.90, 72.29, 69.09, 65.42, 64.11, 59.88, 54.97, 49.66, 48.58, 39.38, 39.03, 29.64, 29.23, 29.06, 28.81, 27.84, 26.42, 25.44. MALDI TOF-MS *m/e* $[M+Na]^+$ calculated for $C_{33}H_{58}N_6O_{12}Na^+$, 753.399; observed 753.468.

7.1.1.11 Synthetic Procedure and Characterization of Compound 12a-c

3,4-dimethoxybenzoic acid (1 equiv.) and Mukaiyama reagent (1.5 equiv.) was added to a two-necked flask connected to a condenser. The two regents were dissolved in THF (5mL) and then Et_3N was (3 equiv.) was added subsequently. The flask was evacuated with a vacuum and flushed with N_2 gas. This mixture was left to stir for 15min at room temperature before intermediate **6a-c**, dissolved THF, is added to the flask. This mixture stirred for 5h at reflux under a N_2 gas environment. The concentrated mixture was then re-dissolved in ethyl acetate (30 mL), washed with water (3x30 mL) and saturated brine (30 mL), and dried with anhydrous sodium sulfate (Na_2SO_4). This mixture was concentrated under reduced pressure and purified by flash chromatography (with a solvent gradient of hexanes/ethyl acetate = 10:1 to 3:1) and concentrated under reduced pressure to yield **7a-b** as a white solid.

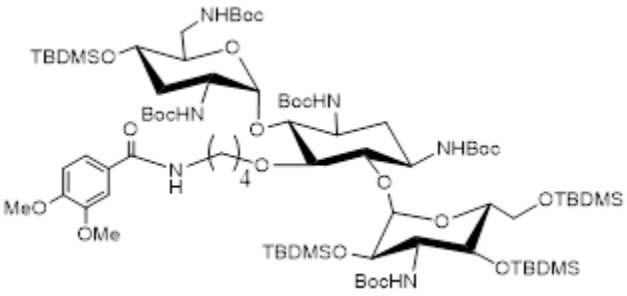

Compound 12a. Yield: 64%. ^{1}H NMR (500 MHz, Chloroform-*d*) δ 7.53 (d, *J* = 2.2 Hz, 1H), 7.42 (d, *J* = 8.3 Hz, 1H), 6.94 (d, *J* = 8.3 Hz, 1H), 6.64 (s, 1H), 5.25 – 5.07 (m, 3H), 4.97 (s, 1H), 4.76 (s, 1H), 4.54 (s, 1H), 4.19 – 4.08 (m, 2H), 3.92 (d, *J* = 5.4 Hz, 6H), 3.82 – 3.71 (m, 3H), 3.69 – 3.65 (m, 1H), 3.61 – 3.51 (m, 4H), 3.47 – 3.35 (m, 4H), 3.29 – 3.23 (m, 2H), 3.15 (s, 1H), 2.46 (s, 1H), 1.97 – 1.92 (m, 1H), 1.72 – 1.54 (m, 4H), 1.44 – 1.39 (m, 45H), 1.09 – 1.01 (m, 1H), 0.92 (s, 9H), 0.86 (d, *J* = 6.3 Hz, 27H), 0.11 – 0.01 (m, 24H). ^{13}C NMR (126 MHz, $CDCl_3$) δ 166.78, 155.68, 155.39, 155.19, 154.79, 154.68, 151.41, 148.77, 127.35, 119.60, 110.61, 110.32, 97.74, 96.22, 85.72, 79.95, 79.70, 79.46, 79.26, 78.48, 75.38, 72.93, 72.49, 71.68, 67.98, 67.85, 67.30, 63.28, 63.28,

57.16, 55.95, 50.60, 48.73, 48.31, 41.61, 39.90, 36.00, 35.92, 29.66, 28.60, 28.48, 28.43, 27.47, 26.08, 25.98, 25.95, 25.75, 18.47, 18.27, 18.05, 17.90, -3.45, -3.70, -4.27, -4.81, -4.91, -4.97, -5.14, -5.20. MALDI TOF-MS *m/e* $[M+Na]^+$ calculated for $C_{80}H_{150}N_6O_{22}Si_4Na^+$, 1681.979; observed 1682.778.

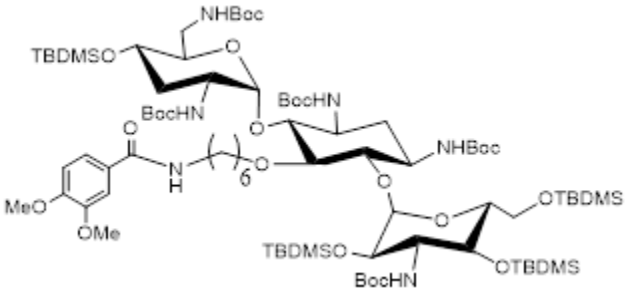

Compound 12b. Yield: 58%. ^{1}H NMR (500 MHz, Chloroform-*d*) δ 7.44 (d, *J* = 2.0 Hz, 1H), 7.31 (dd, *J* = 8.4, 2.1 Hz, 1H), 6.83 (d, *J* = 8.3 Hz, 1H), 6.36 (s, 1H), 5.24 (s, 1H), 5.13 (s, 1H), 5.02 (d, *J* = 10.2 Hz, 1H), 4.72 (s, 1H), 4.51 (s, 1H), 4.22 – 4.05 (m, 3H), 3.90 (d, *J* = 10.6 Hz, 6H), 3.77 – 3.68 (m, 3H), 3.60 (d, *J* = 8.6 Hz, 2H), 3.54 – 3.50 (m, 2H), 3.38 (hept, *J* = 9.2, 8.7 Hz, 5H), 3.23 (q, *J* = 11.2, 8.8 Hz, 2H), 3.17 (s, 1H), 2.44 (d, *J* = 12.5 Hz, 1H), 1.99 – 1.94 (m, 1H), 1.53 (dd, *J* = 23.1, 9.1 Hz, 4H), 1.43 – 1.39 (m, 45H), 1.35 – 1.31 (m, 4H), 1.06 – 0.98 (m, 1H), 0.92 (s, 9H), 0.86 – 0.83 (m, 27H), 0.14 – 0.12 (m, 6H), 0.07 – 0.00 (m, 18H). ^{13}C NMR (126 MHz, $CDCl_3$) δ 166.93, 155.63, 155.47, 154.85, 154.70, 154.58, 151.44, 148.86, 127.58, 119.26, 110.67, 110.18, 97.78, 96.19, 85.81, 79.92, 79.38, 79.22, 78.65, 75.19, 73.07, 72.58, 71.62, 68.01, 68.00, 67.79, 67.00, 63.15, 57.20, 55.96, 55.93, 50.52, 48.74, 48.29, 41.66, 39.91, 36.03, 35.80, 30.36, 29.65, 29.42, 28.60, 28.48, 28.40, 26.99, 26.08, 25.97, 25.75, 18.46, 18.28, 18.06, 17.89, -3.45, -3.80, -4.25, -4.91, -4.94, -5.07, -5.18, -5.21. MALDI TOF-MS *m/e* $[M+Na]^+$ calculated for $C_{82}H_{154}N_6O_{22}Si_4Na^+$, 1710.009; observed 1710.793.

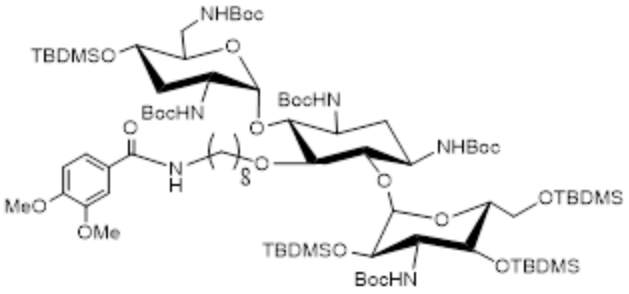

Compound 12c. Yield: 56%. ^{1}H NMR (500 MHz, Chloroform-*d*) δ 7.43 (d, *J* = 2.0 Hz, 1H), 7.27 (d, *J* = 6.1 Hz, 1H), 6.83 (d, *J* = 8.3 Hz, 1H), 6.24 (t, *J* = 5.6 Hz, 1H), 5.22 (s, 1H), 5.13 (s, 1H), 5.04 (d, *J* = 9.6 Hz, 1H), 4.76 (s, 1H), 4.53 (s, 1H), 4.28 – 4.03 (m, 3H), 3.91 (d, *J* = 9.2 Hz, 6H), 3.78 – 3.68 (m, 3H), 3.62 – 3.58 (m, 1H), 3.57 – 3.50 (m, 3H), 3.41 (qt, *J* = 13.4, 7.0 Hz, 5H), 3.23 (q, *J* = 12.1, 8.7 Hz, 2H), 3.15 (s, 1H), 2.45 (s, 1H), 2.03 – 1.96 (m, 1H), 1.59 (p, *J* = 7.3 Hz, 4H), 1.45 – 1.39 (m, 45H), 1.31 – 1.23 (m, 8H), 1.04 (t, *J* = 9.5 Hz, 1H), 0.93 (s, 9H), 0.87 – 0.82 (m, 27H), 0.14 (d, *J* = 2.4 Hz, 6H), 0.09 – 0.01 (m, 18H). ^{13}C NMR (126 MHz, $CDCl_3$) δ 166.97, 155.73, 155.50, 154.76, 154.72, 154.56, 151.49, 148.93, 127.60, 119.07, 110.70, 110.17, 99.98, 97.80, 96.38, 85.76, 79.92, 79.38, 79.27, 79.22, 79.12, 78.88, 75.24, 73.20, 72.69, 71.56, 68.03, 67.82, 66.88, 63.12, 60.34, 57.24, 55.98, 55.95, 50.49, 48.86, 48.36, 41.67, 40.16, 35.93, 35.68, 31.89, 30.56, 29.77, 29.68, 29.66, 29.62, 29.62, 29.30, 28.62, 28.49, 28.47, 28.40, 27.02, 26.11, 26.05, 26.00, 25.97, 25.75, 22.65, 18.47, 18.30, 18.08, 17.89, 14.16, 14.08, -3.42, -3.80, -4.24, -4.92, -4.95, -5.09, -5.18, -5.22. MALDI TOF-MS *m/e* $[M+Na]^+$ calculated for $C_{84}H_{158}N_6O_{22}Si_4Na^+$, 1738.039; observed 1738.872.

7.1.1.12 Synthetic Procedure and Characterization of Compound 11a-c

Intermediate **12a-c** was dissolved in a solvent mixture of concentrated HCl/MeOH (2:3) (5 mL). This reaction mixture was stirred for 1h at room temperature, after which it was concentrated under reduced pressure. The residue was then purified using reverse phase flash

chromatography (with a solvent gradient of deionized H_2O) and then concentrated under reduced pressure.

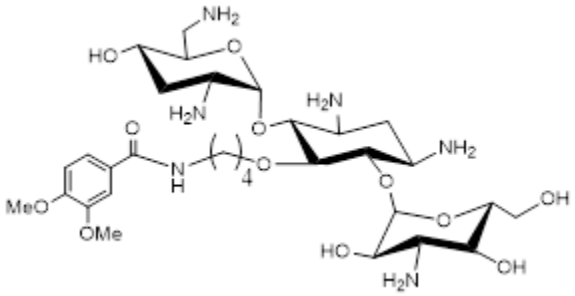

Compound 11a. Yield: 42%. ^{1}H NMR (500 MHz, Methanol-d_4) δ 7.48 (dd, *J* = 8.4, 2.1 Hz, 1H), 7.45 (d, *J* = 2.1 Hz, 1H), 7.02 (d, *J* = 8.4 Hz, 1H), 5.52 (d, *J* = 2.9 Hz, 1H), 5.17 (d, *J* = 3.5 Hz, 1H), 4.41 (t, *J* = 9.5 Hz, 1H), 4.20 – 4.16 (m, 1H), 3.99 – 3.95 (m, 1H), 3.92 (d, *J* = 9.3 Hz, 1H), 3.88 (d, *J* = 4.5 Hz, 6H), 3.82 – 3.72 (m, 7H), 3.69 – 3.56 (m, 6H), 3.51 (t, *J* = 10.5 Hz, 1H), 3.46 – 3.42 (m, 1H), 3.37 (t, *J* = 6.3 Hz, 1H), 3.26 – 3.22 (m, 1H), 2.47 – 2.43 (m, 1H), 2.25 – 2.18 (m, 3H), 1.78 – 1.67 (m, 4H). ^{13}C NMR (126 MHz, MeOD) δ 168.38, 152.18, 148.88, 126.54, 120.52, 110.71, 110.55, 100.74, 92.33, 82.24, 81.38, 75.50, 74.02, 71.62, 69.13, 65.47, 64.23, 59.90, 55.29, 55.07, 54.96, 49.55, 48.62, 48.41, 39.33, 39.09, 28.83, 27.94, 26.82, 25.82. MALDI TOF-MS *m/e* $[M+Na]^+$ calculated for $C_{31}H_{54}N_6O_{12}Na^+$, 725.369; observed 725.4.

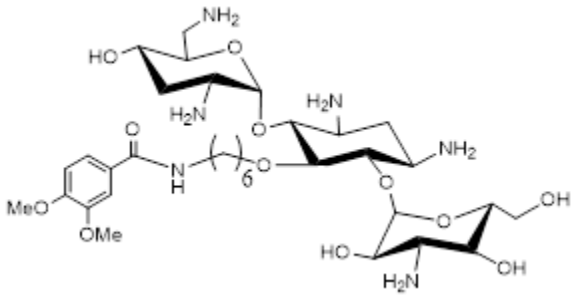

Compound 11b. Yield: 36%. ^{1}H NMR (500 MHz,) δ 8.37 – 8.23 (m, 1H), 7.48 (d, *J* = 8.2 Hz, 1H), 7.46 (s, 1H), 7.02 (d, *J* = 7.9 Hz, 1H), 5.49 (s, 1H), 5.18 (d, *J* = 3.2 Hz, 1H), 4.46 (t, *J* = 8.6 Hz, 1H), 4.27 – 4.23 (m, 1H), 3.94 (t, *J* = 8.4 Hz, 2H), 3.88 (d, *J* = 5.7 Hz, 6H), 3.86 – 3.76 (m, 7H), 3.72 (d, *J* = 8.7 Hz, 3H), 3.65 – 3.61 (m, 2H),

3.56 – 3.52 (m, 1H), 3.38 (t, *J* = 6.4 Hz, 2H), 3.27 (s, 1H), 2.52 (d, *J* = 11.2 Hz, 1H), 2.26 (d, *J* = 10.4 Hz, 3H), 1.71 – 1.63 (m, 4H), 1.49 – 1.38 (m, 4H). ^{13}C NMR (126 MHz, MeOD) δ 168.28, 151.99, 148.77, 126.66, 120.50, 110.68, 110.51, 100.92, 92.43, 82.05, 81.35, 75.55, 74.84, 73.92, 72.38, 69.05, 65.37, 64.10, 59.89, 55.29, 55.13, 54.97, 49.65, 48.65, 39.35, 39.13, 29.67, 29.12, 28.74, 27.56, 26.61, 25.19. MALDI TOF-MS *m/e* $[M+Na]^+$ calculated for $C_{33}H_{58}N_6O_{12}Na^+$, 753.399; observed 753.3.

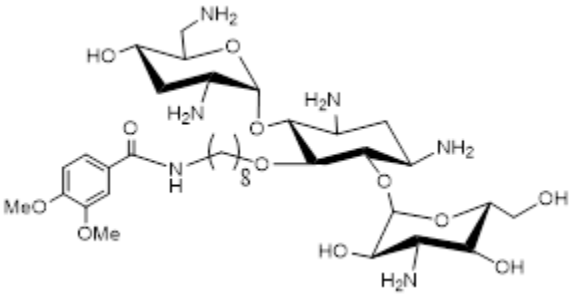

Compound 11c. Yield: 36%. ^{1}H NMR (500 MHz,) δ 8.27 (d, *J* = 30.1 Hz, 0H), 7.46 – 7.42 (m, 2H), 7.00 (d, *J* = 8.1 Hz, 1H), 5.45 (s, 1H), 5.16 (d, *J* = 3.3 Hz, 1H), 4.46 (t, *J* = 8.5 Hz, 1H), 4.24 (d, *J* = 6.4 Hz, 1H), 3.91 (d, *J* = 9.3 Hz, 2H), 3.87 (d, *J* = 3.0 Hz, 6H), 3.83 – 3.74 (m, 7H), 3.68 (d, *J* = 9.5 Hz, 3H), 3.60 (d, *J* = 7.2 Hz, 2H), 3.51 (t, *J* = 10.4 Hz, 1H), 3.35 (t, *J* = 6.8 Hz, 2H), 3.25 (d, *J* = 11.6 Hz, 1H), 2.48 (d, *J* = 11.9 Hz, 1H), 2.29 – 2.20 (m, 3H), 1.64 (d, *J* = 25.5 Hz, 4H), 1.39 (s, 8H). ^{13}C NMR (126 MHz, MeOD) δ 168.30, 152.04, 148.82, 126.67, 120.41, 110.65, 110.51, 100.90, 92.50, 81.99, 81.33, 75.71, 75.09, 73.94, 72.53, 69.07, 65.40, 64.10, 59.90, 55.20, 55.08, 54.97, 49.63, 48.63, 39.57, 39.09, 29.74, 29.35, 29.16, 28.96, 28.71, 27.53, 26.56, 25.55. MALDI TOF-MS *m/e* $[M+Na]^+$ calculated for $C_{35}H_{62}N_6O_{12}Na^+$, 781.429; observed 781.4.

7.2 MICROBIOLOGY

7.2.1 Bacterial Isolates

The bacterial isolates used for the microbiological studies were obtained from the American Type Culture Collection (ATCC), the Canadian National Intensive Care Unit (CAN-ICU) study, and the Canadian Ward Surveillance (CANWARD) studies[1–3]. The reference strains are supplied by ATCC and the clinical isolates are supplied from the CAN-ICU and CANWARD studies. Multiple medical centres from all regions of Canada participated in the CAN-ICU and CANWARD studies[1–3]. Bacterial isolates were submitted from emergency rooms, surgical wards, and intensive care units (ICUs) from these participating medical centres[1–3]. Presumed "clinically significant" bacterial isolates were recovered from blood, urine, wound/tissue, and respiratory specimens[1–3]. All isolates were transported to the reference laboratory (Health Science Centre, Winnipeg, Canada), subcultured onto appropriate media and classified as either MDR, XDR, or pan-drug resistant bacteria[1–3].

7.2.2 Minimum Inhibitory Concentration Determination

The in vitro antibacterial activities of agents were determined by microbroth dilution susceptibility test in accordance with the Clinical and Laboratory Standards Institute (CLSI) guidelines[4]. The antibacterial compounds were made into stock solutions with concentrations of 10.24 or 5.12 mg/mL in either deionized water or DMSO depending on solubility of the compounds, and stored in a -20 °C. The stock solutions of imipenem and meropenem were made the day of testing to prevent compound breakdown. The minimum inhibitory concentrations (MICs) of the tested antibacterial agents were determined by serial dilution of the agent in

Mueller–Hinton broth (MHB) or iron deficient cation adjusted MHB (ID-CAMHB) in 96-well plates, followed by inoculation of selected bacterial strains to an approximate final concentration of 5×10^5 CFU/mL. The ID-CAMHB was prepared according to CLSI guidelines. After inoculation of the 96-well plates with the bacterial solutions, the plates are incubated in aerobic conditions at 37 °C for 18 h prior to reading.

7.2.3 Antibacterial Combination Screening

Combinations of antibiotics with other antibiotics or adjuvants have been a long used clinical tactic to improve an antibiotic's activity[5]. The checkerboard method was used to determine the interactions of the combined antibacterial agents[5–7]. These checkerboard assays were conducted using 96-well plates, where the first agent is serially two-folded diluted along the x-axis and the second agent is serially two-folded diluted along the y-axis. The max concentrations of these agents should be two-fold higher than the MIC of the agents. The result of this is that each well contains a unique combination of the two antibacterial agents. Then 50 μL of MHB is added to each well. Subsequently, 50 μL of a standardized bacterial culture was added to the plates bringing the final volume of each well to 100 μL. The bacterial culture was standardized to 0.5 McFarland turbidity in saline, diluted 1:50 in MHB and left to grow overnight prior to the checkerboard assay. Finally, the plates were incubated in aerobic conditions at 37 °C for 18 h prior to reading.

The fractional inhibitory concentration indices (FICI) are used to quantify the interaction of the combined antibacterial agents against the tested bacterial strain[5–8]. The FICI is the sum of the FICs of the antibacterial agents, which are determined from the checkerboard assays[5–8]. The

FICs of the antibacterial agents are calculated by the [MIC of agent in combination]/[MIC of agent alone][5–8]. FICI values of ≤0.5, >0.5 to <4.0, and ≥4.0 represents synergistic, not significant, and antagonistic interactions between the antibacterial agents, respectively[5–8].

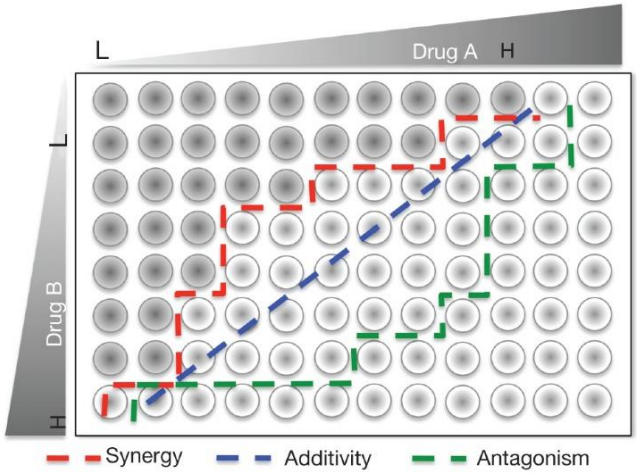

$$FICI = [FIC]_A + [FIC]_B = \left(\frac{MIC_{Combined}}{MIC_{Aalone}}\right) + \left(\frac{MIC_{Combined}}{MIC_{Balone}}\right)$$

Figure 42. (a) An illustration of a microbroth checkerboard assay used to determine the FIC index of drugs[5]. (b) The equation used to determine the FIC index (FICI), used to quantitatively assess combinations[5].

7.2.4 Outer Membrane Permeabilization Assay

1-N-phenylnapthylamine (NPN), a fluorescent probe that is impermeable to the outer membrane was used to assess the synthesized conjugate's ability to permeabilize the outer membrane permeabilization of wild type *P. aeruginosa* (PAO1)[9]. NPN weakly fluoresces in aqueous solutions, but strongly fluoresces in hydrophobic environments[9]. Thus, this ability of

NPN allows for a strong fluorescent signal to be observed when exposed to the phospholipids of a broken bacterial membrane as a result of membrane permeabilizing agents[9]. *P. aeruginosa* PAO1 cells at mid-logarithmic phase (A_{600} = 0.4–0.5) were harvested, washed, and resuspended in 5 mM HEPES buffer at pH 7.2. To the cell suspension, NPN and sodium azide were added to a final concentration of 10μM, the resulting suspension was then incubated for 30min at room temperature in darkness. Compound **1a** was then added to the suspension to form varying final concertation of 1a, and the resulting fluorescence change was recorded at a continuous interval on a FlexStation 3 (Molecular Devices, Sunnyvale, USA) microplate reader at the excitation wavelength of 350 nm and emission wavelength of 420 nm. Polymyxin B nonapeptide (PMBN) was used as a positive control as it is a well known and clinically relevant outer membrane permeabilizer[10]. Cell suspension with NPN and untreated with compound **1a** was used as the negative control, and special reading was subtracted from experimental data to account for any background fluorescence.

7.3 REFERENCES

1. Zhanel, G. Antimicrobial susceptibility of 22746 pathogens from Canadian hospitals: results of the CANWARD 2007–11 study. *Journal of Antimicrobial Chemotherapy* **68**, i7–i22 (2013).

2. G, Z. G. Prevalence of Antimicrobial-Resistant Pathogens in Canadian Hospitals: Results of the Canadian Ward Surveillance Study (CANWARD 2008). *Antimicrobial Agents and Chemotherapy* **54**, 4684–4693 (2010).

3. G, Z. G. Antimicrobial-Resistant Pathogens in Intensive Care Units in Canada: Results of the Canadian National Intensive Care Unit (CAN-ICU) Study, 2005-2006. *Antimicrobial Agents and Chemotherapy* **52**, 1430–1437 (2008).

4. Clinical and Laboratory Standards Institute (CLSI). *Performance Standards for Antimicrobial Susceptibility Testing*. (Clinical and Laboratory Standards Institute, 2016).

5. Kalan, L. & Wright, G. D. Antibiotic adjuvants: multicomponent anti-infective strategies. *Expert Reviews in Molecular Medicine* **13**, e5 (2011).

6. Bellio, P., Fagnani, L., Nazzicone, L. & Celenza, G. New and simplified method for drug combination studies by checkerboard assay. *MethodsX* **8**, 101543 (2021).

7. Gani, O., Aysen, B., Yasemin, Z. & Iclal, B. Synergy Tests by E Test and Checkerboard Methods of Antimicrobial Combinations against Brucella melitensis. *Journal of Clinical Microbiology* **43**, 140–143 (2005).

8. Meletiadis, J., Pournaras, S., Roilides, E. & Walsh, T. J. Defining fractional inhibitory concentration index cutoffs for additive interactions based on self-drug additive

combinations, Monte Carlo simulation analysis, and in vitro-in vivo correlation data for antifungal drug combinations against Aspergillus fumigatus. *Antimicrob Agents Chemother* **54**, 602–9 (2010).

9. Muheim, C. Increasing the permeability of Escherichia coli using MAC13243. *Sci Rep* **7**, 17629 (2017).

10. Tsubery, H., Ofek, I., Cohen, S. & Fridkin, M. Structure−Function Studies of Polymyxin B Nonapeptide: Implications to Sensitization of Gram-Negative Bacteria. *Journal of Medicinal Chemistry* **43**, 3085–3092 (2000)

7.4 TABLES

Table 7.4.1. Minimal inhibitory concentration (MIC) (μg/mL) of compounds **1a-c** against Gram-positive bacteria.

	Minimum Inhibitory Concentration (MIC) (μg/mL)			
Bacterial Strains	**TOB**	**1a**	**1b**	**1c**
***S. aureus* ATCC 29213**	≤0.25	128	16	128
MRSA ATCC 33592	0.5	>128	128	>128
***E. faecalis* ATCC 29212**	8	>128	>128	>128
E. faecium ATCC 27270	16	>128	>128	>128

MRSA: methicillin-resistant *Staphylococcus aureus*; TOB: tobramycin.

7.5 NMR SPECTRA

Appendix 1. ^{1}H spectrum of **6a** in $CDCl_3$

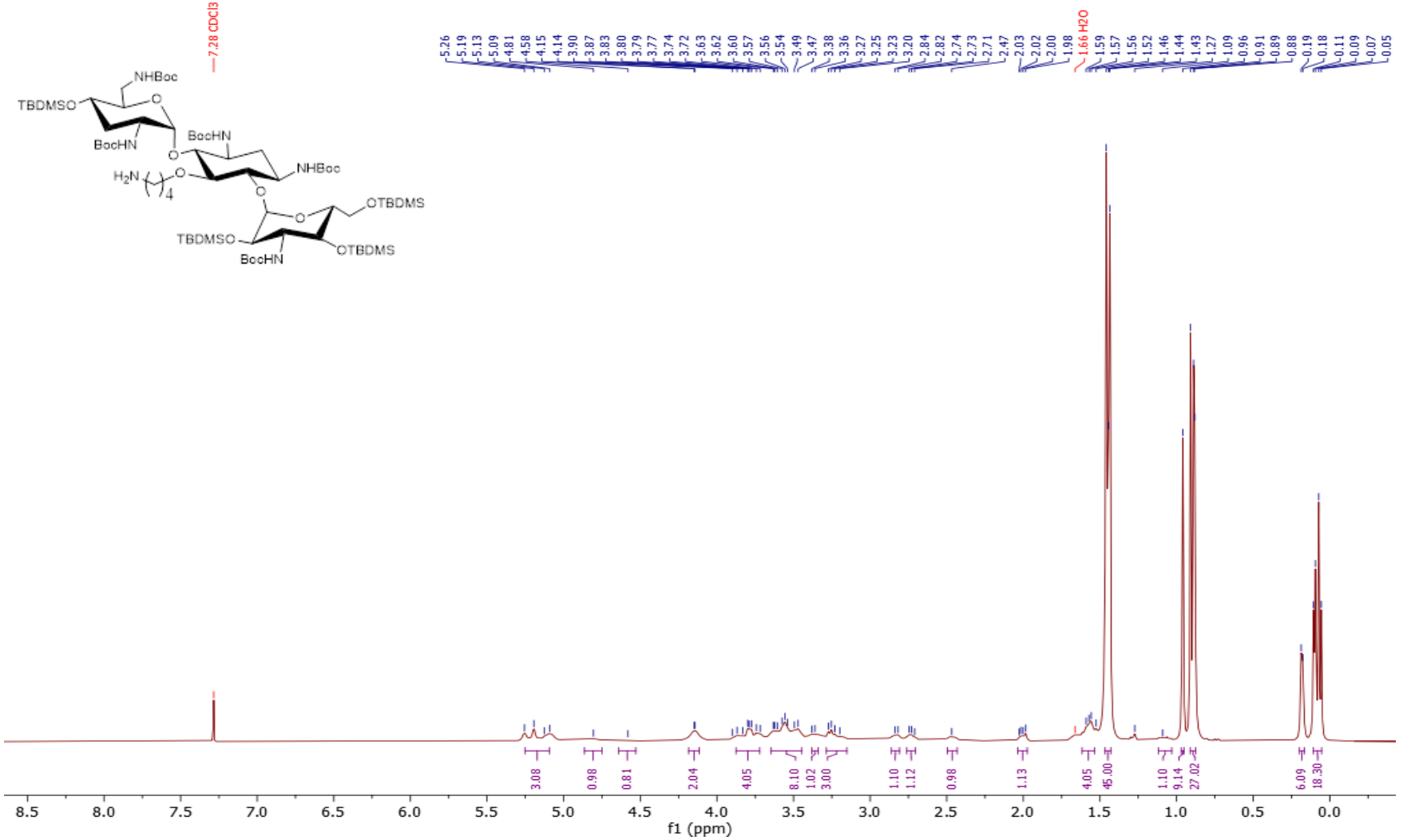

Appendix 2. ^{13}C spectrum of **6a** in $CDCl_3$

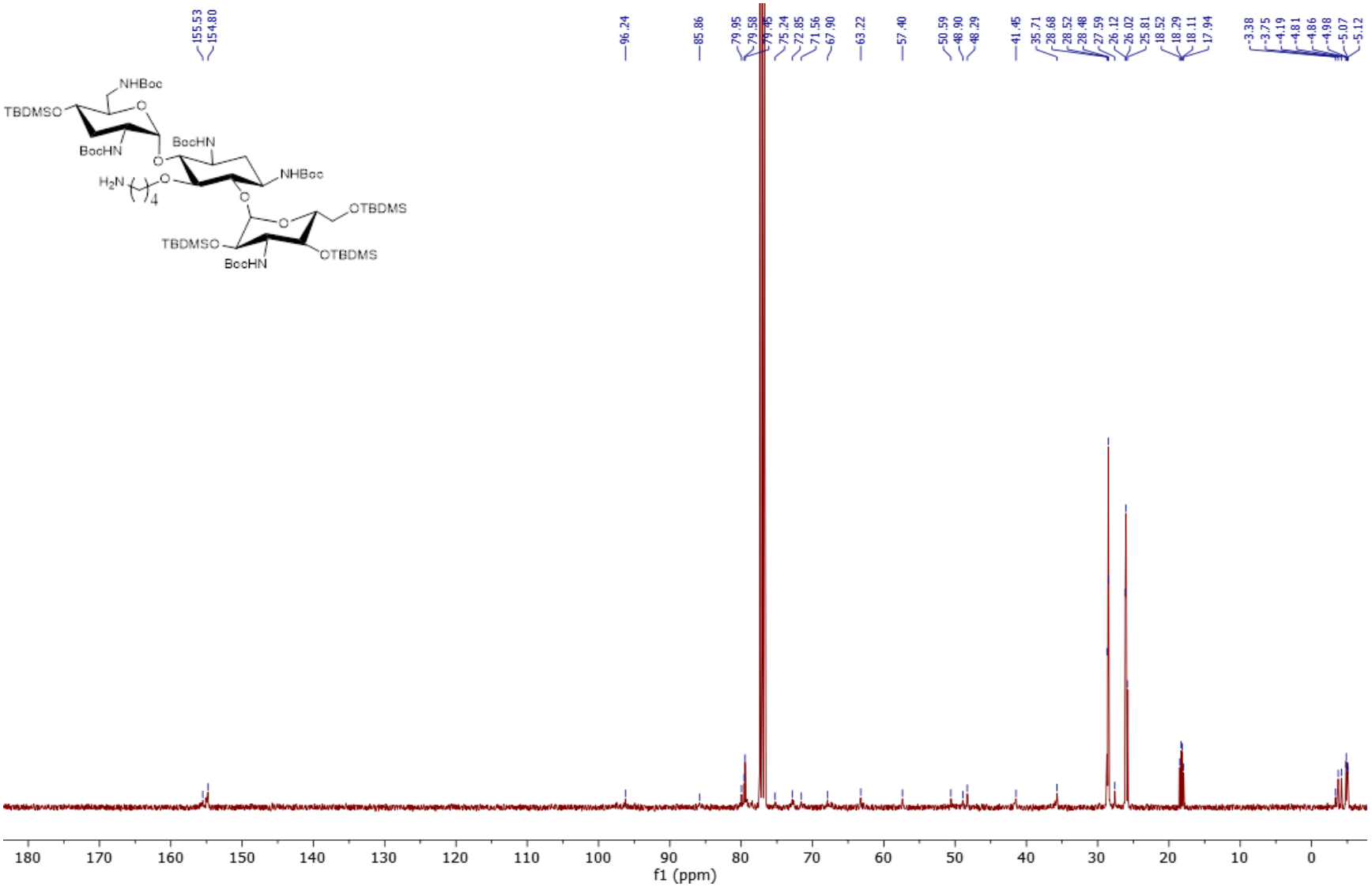

Appendix 3. ^{1}H spectrum of **6b** in $CDCl_3$

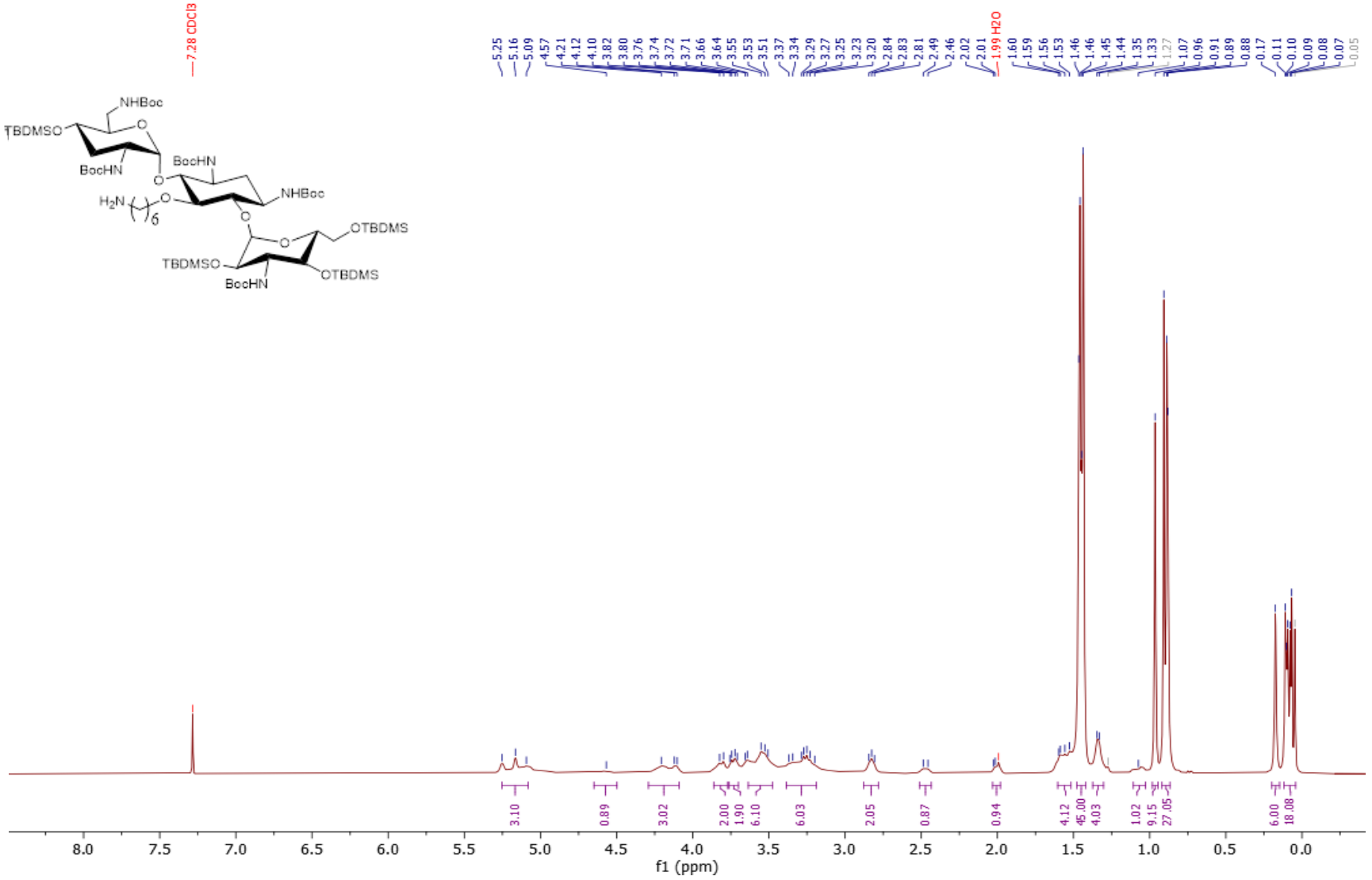

Appendix 4. ^{13}C spectrum of **6b** in $CDCl_3$

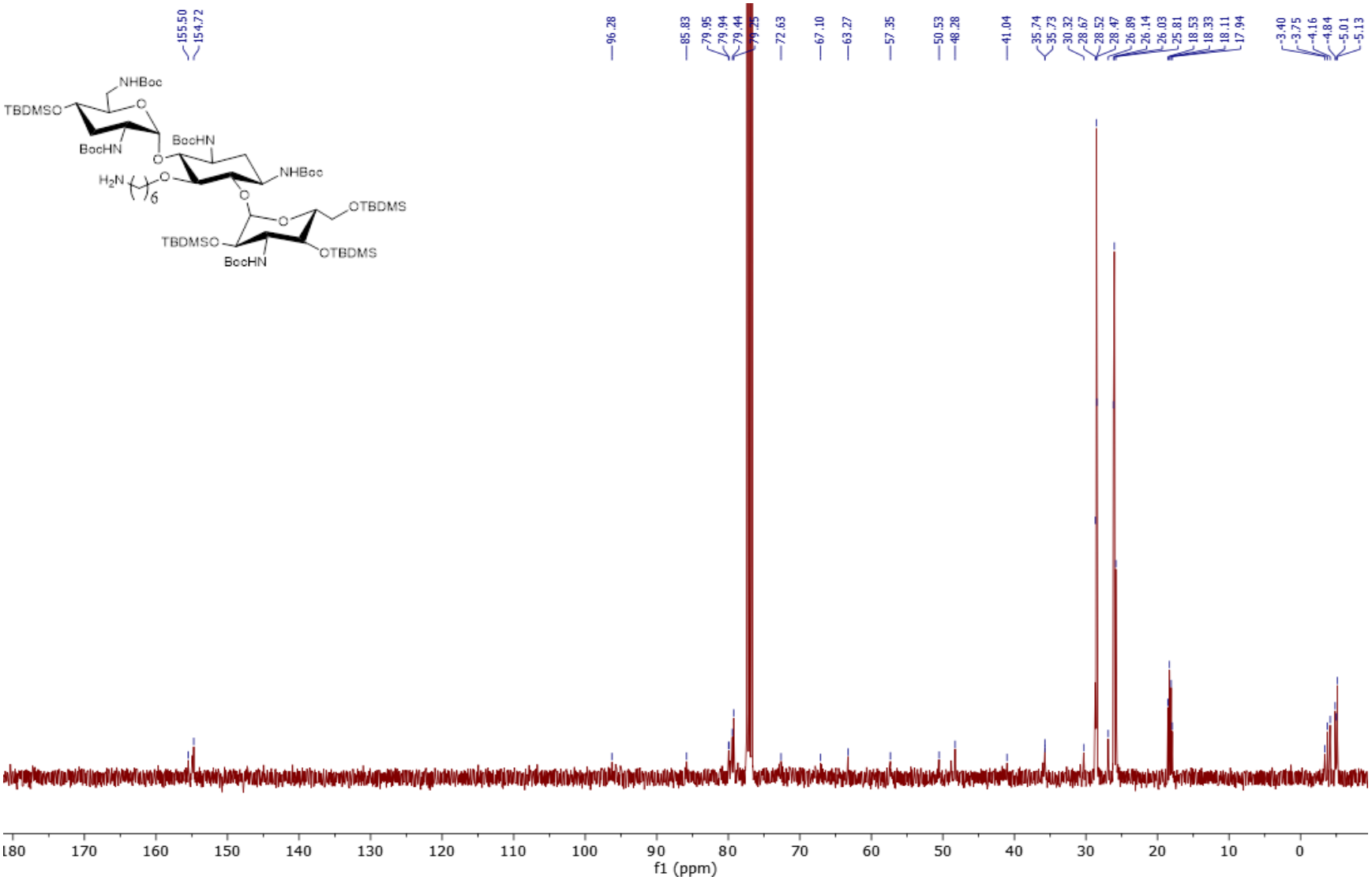

Appendix 5. ^{1}H spectrum of **6c** in $CDCl_3$

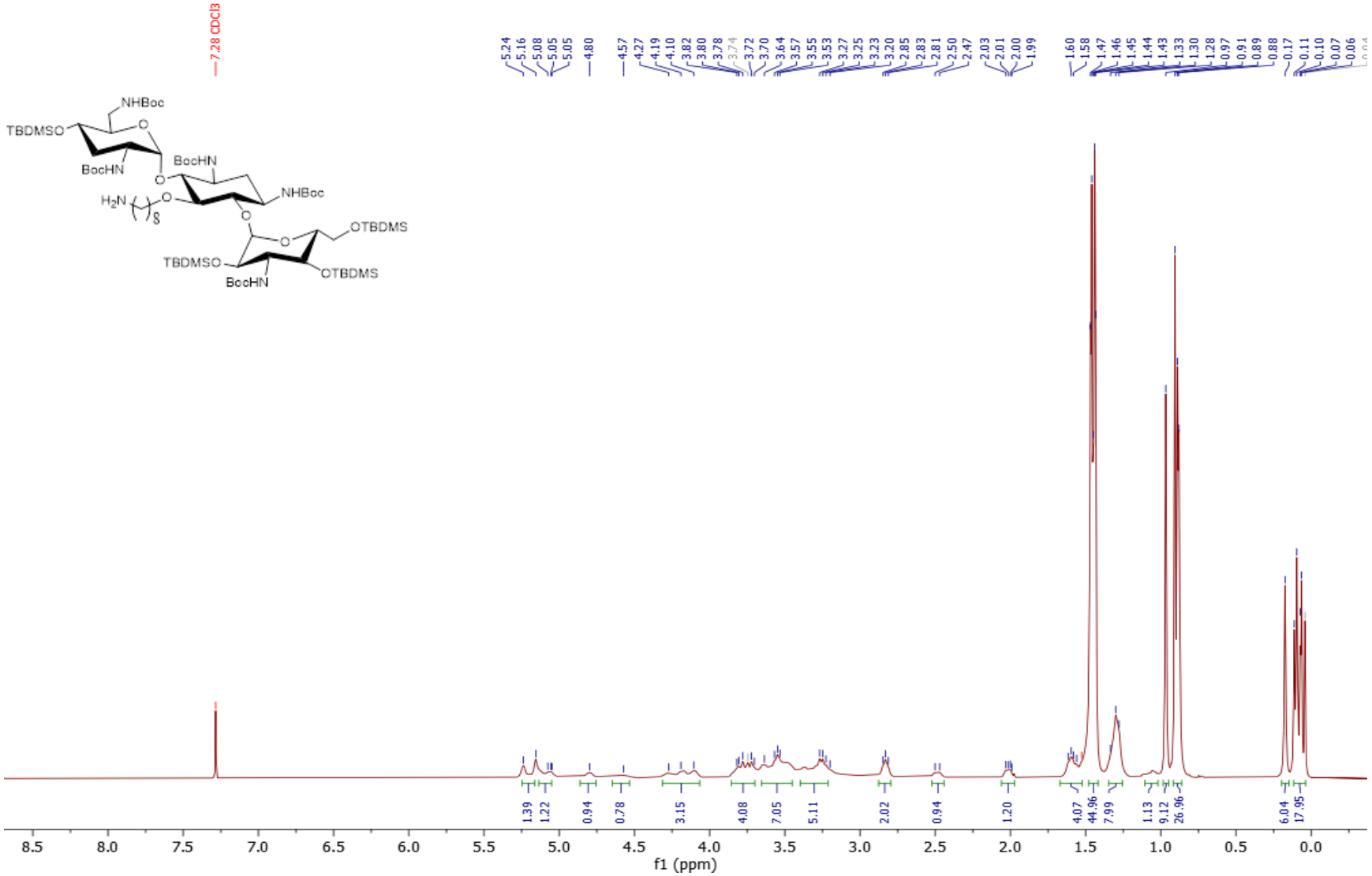

Appendix 6. ^{13}C spectrum of **6c** in $CDCl_3$

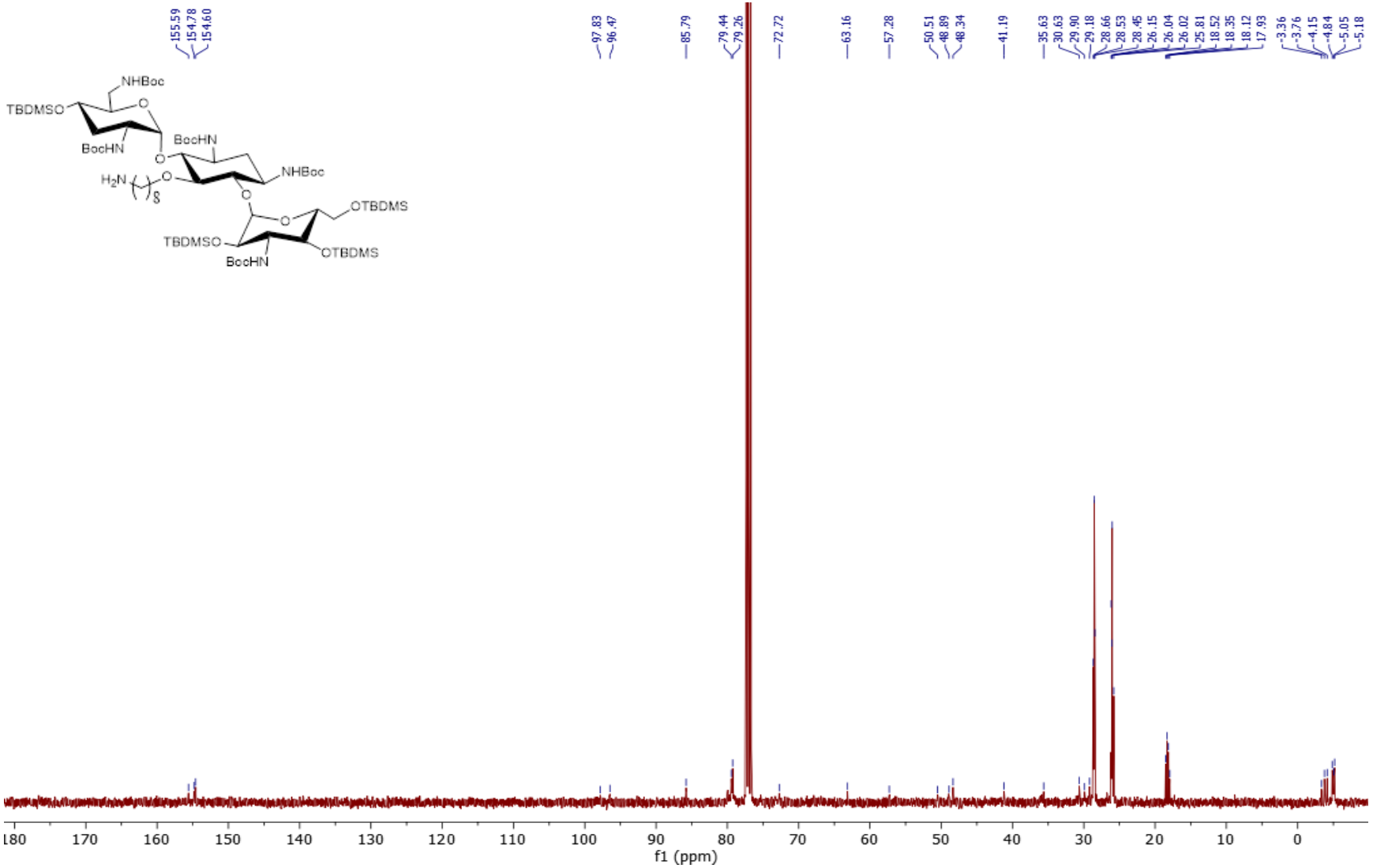

Appendix 7. ^{1}H spectrum of **8** in MeOD

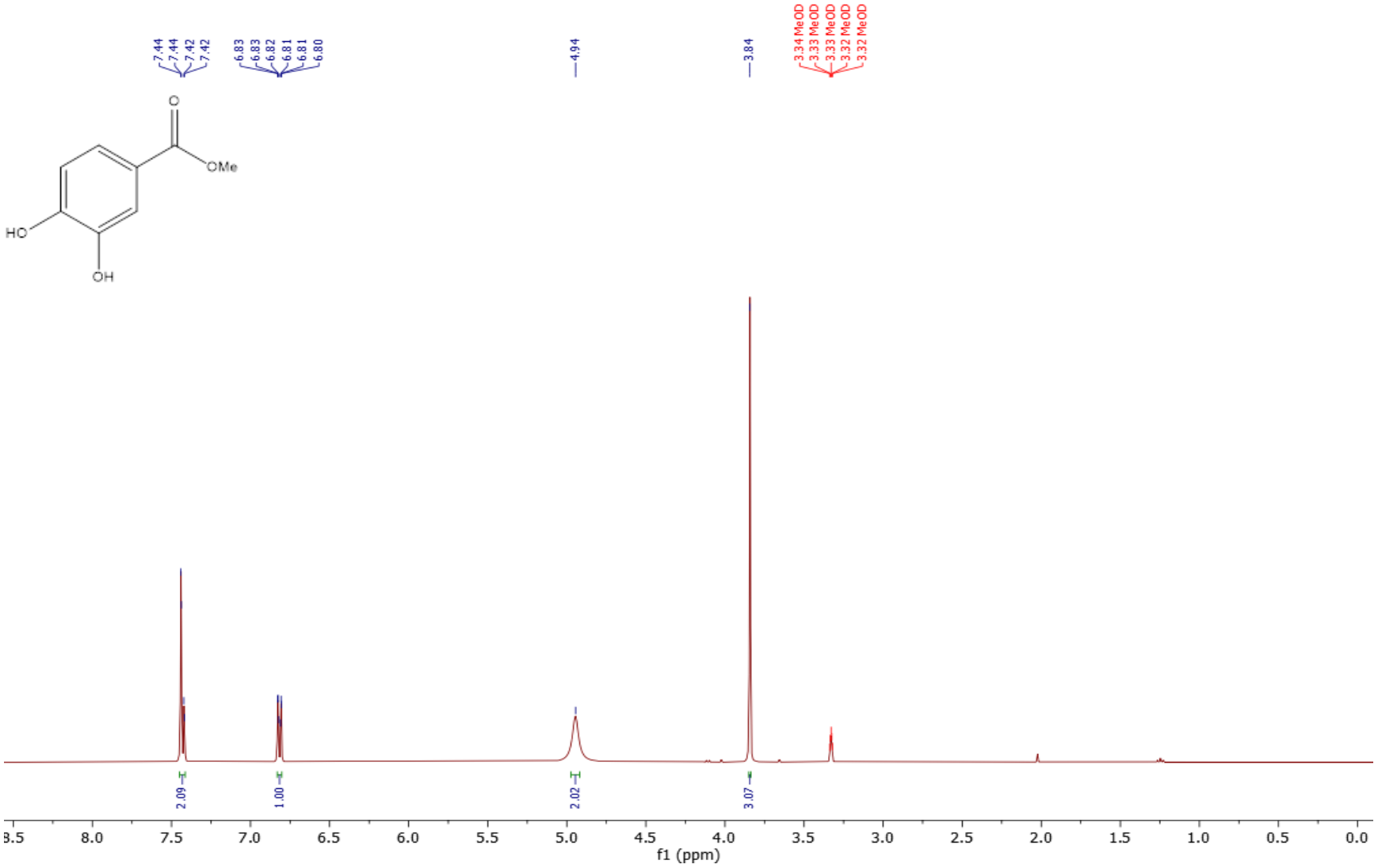

Appendix 8. ^{13}C spectrum of **8** in MeOD

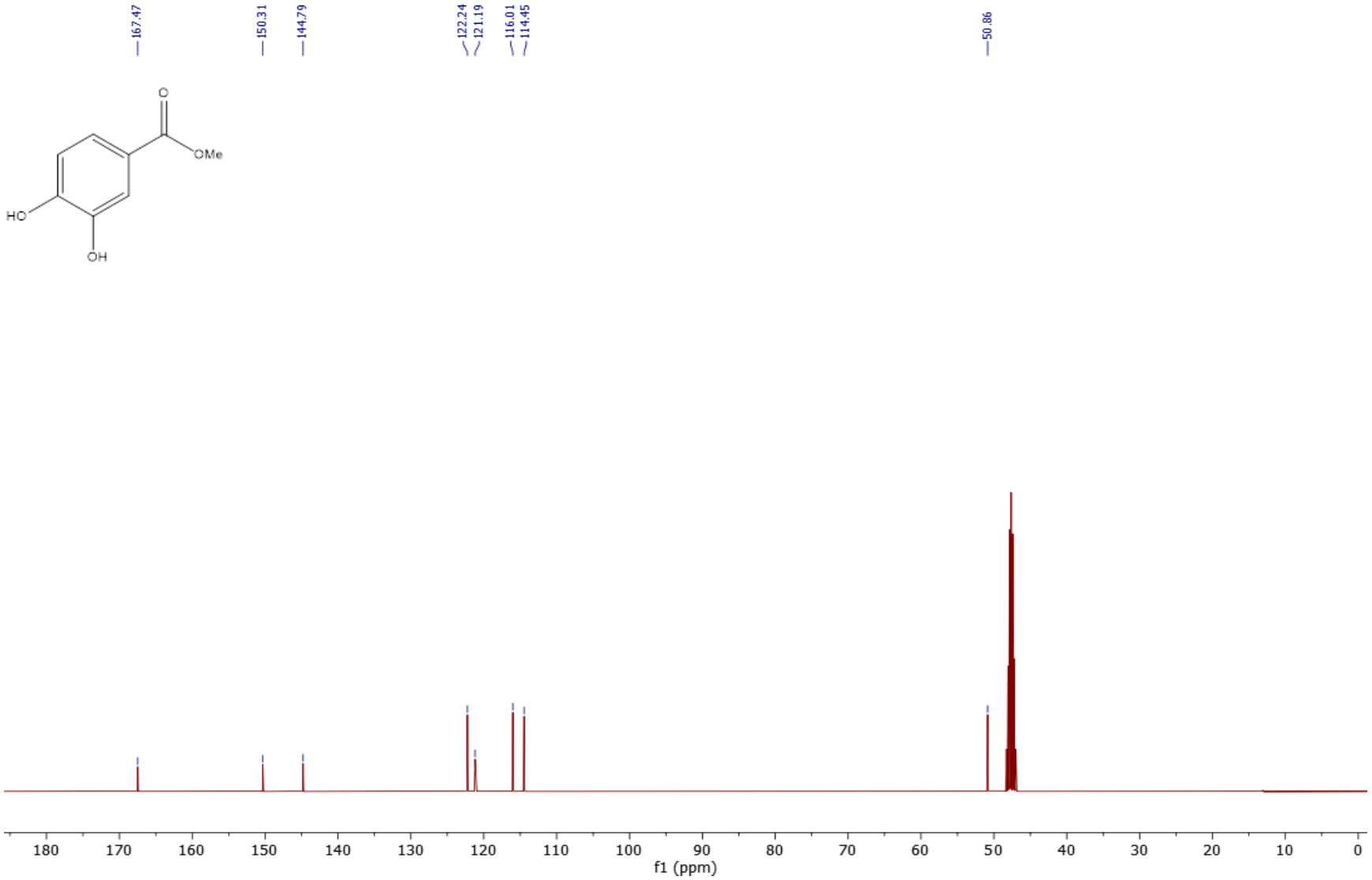

Appendix 9. ^{1}H spectrum of **9** in $CDCl_3$

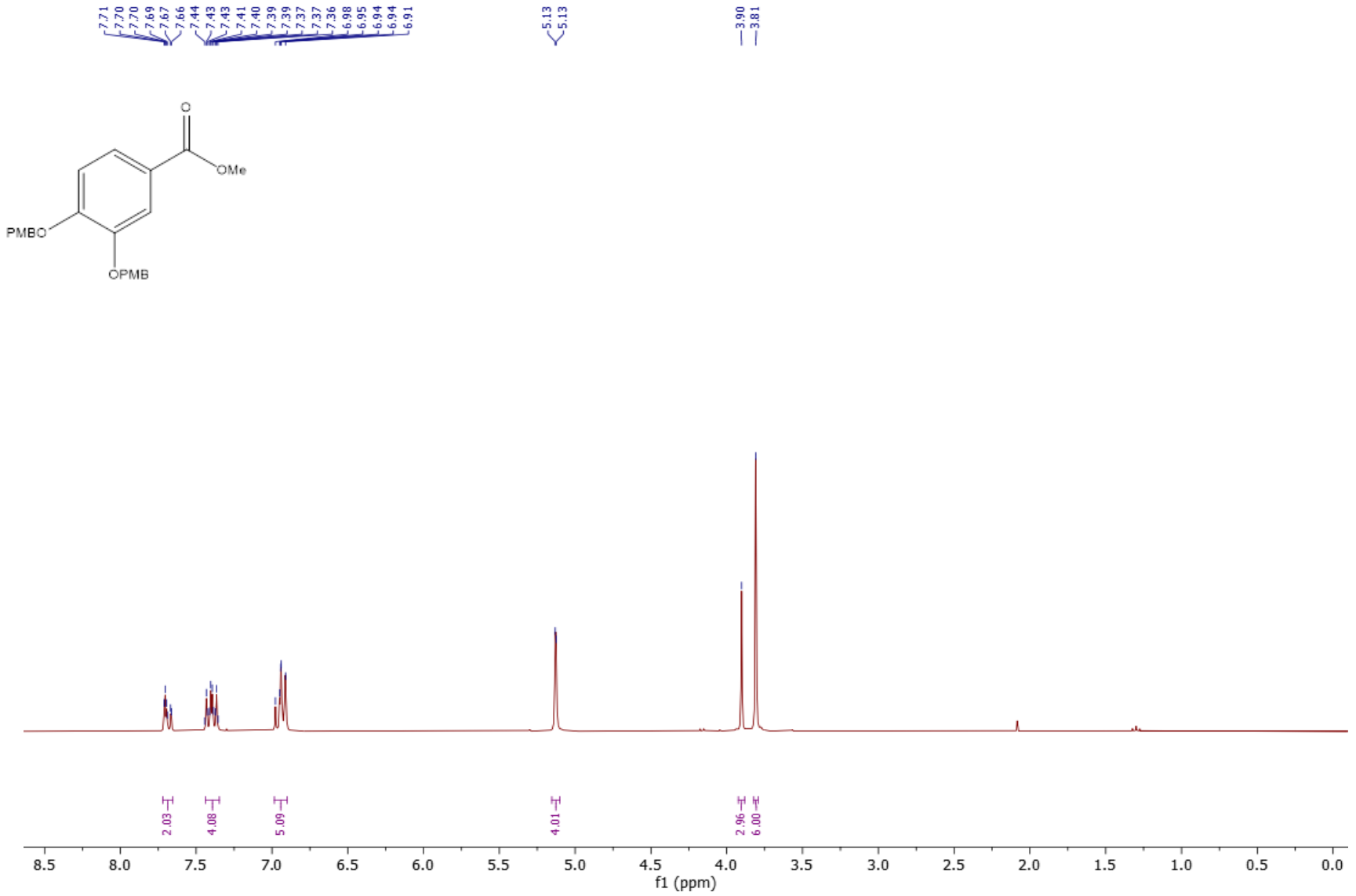

Appendix 10. ^{13}C spectrum of **9** in $CDCl_3$

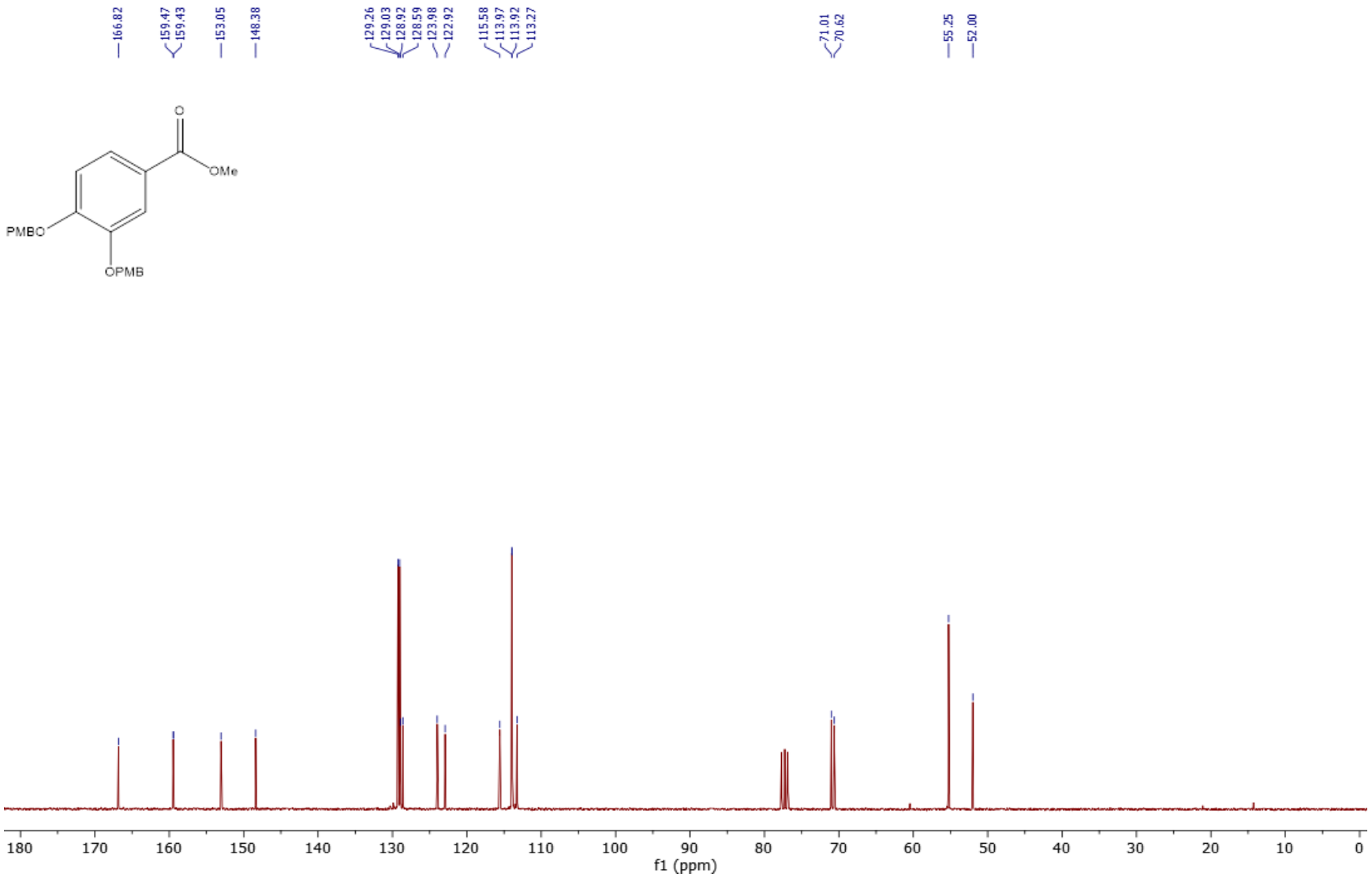

Appendix 11. ^{1}H spectrum of **10** in $CDCl_3$

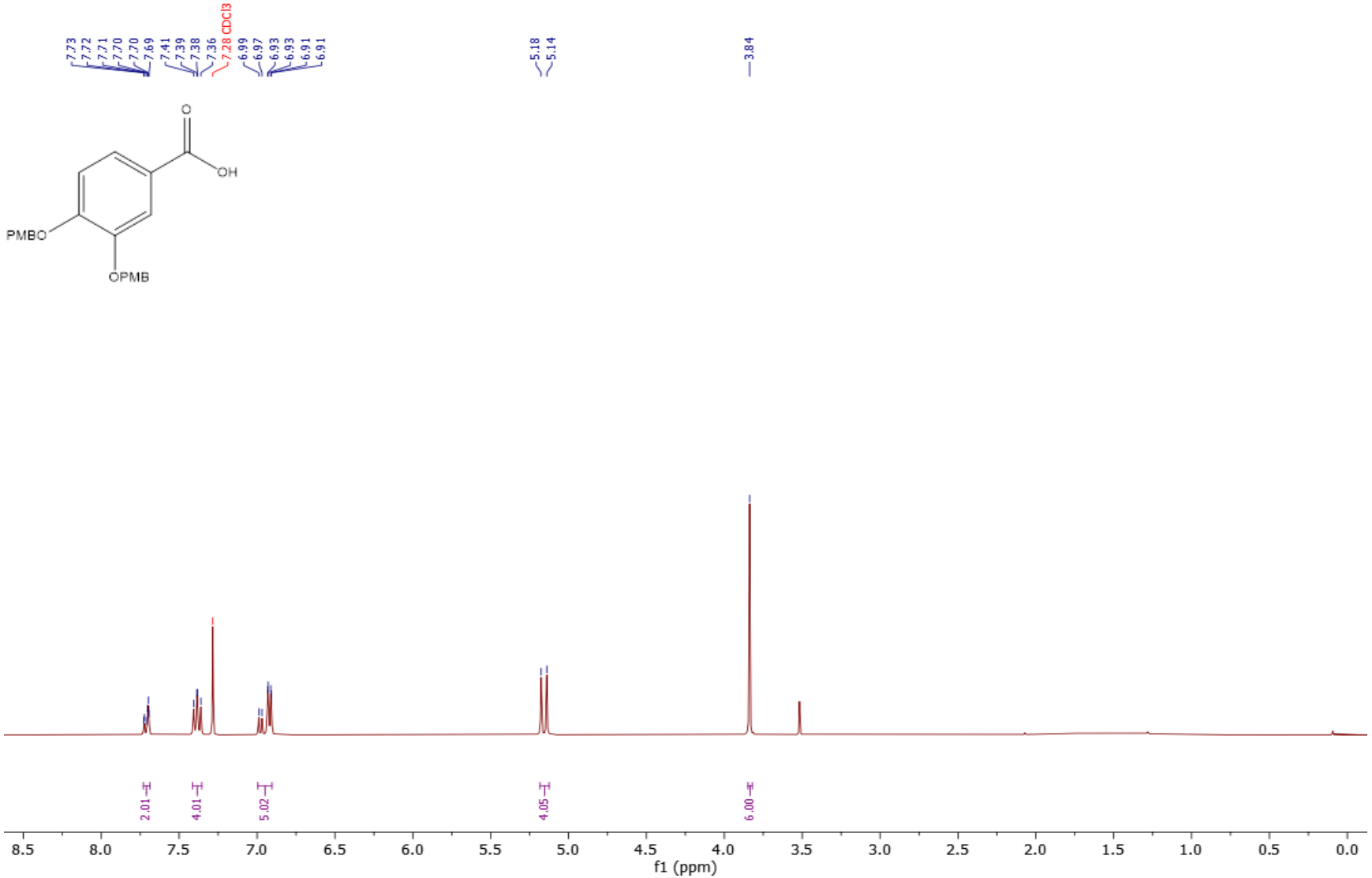

Appendix 12. ^{13}C spectrum of **10** in $CDCl_3$

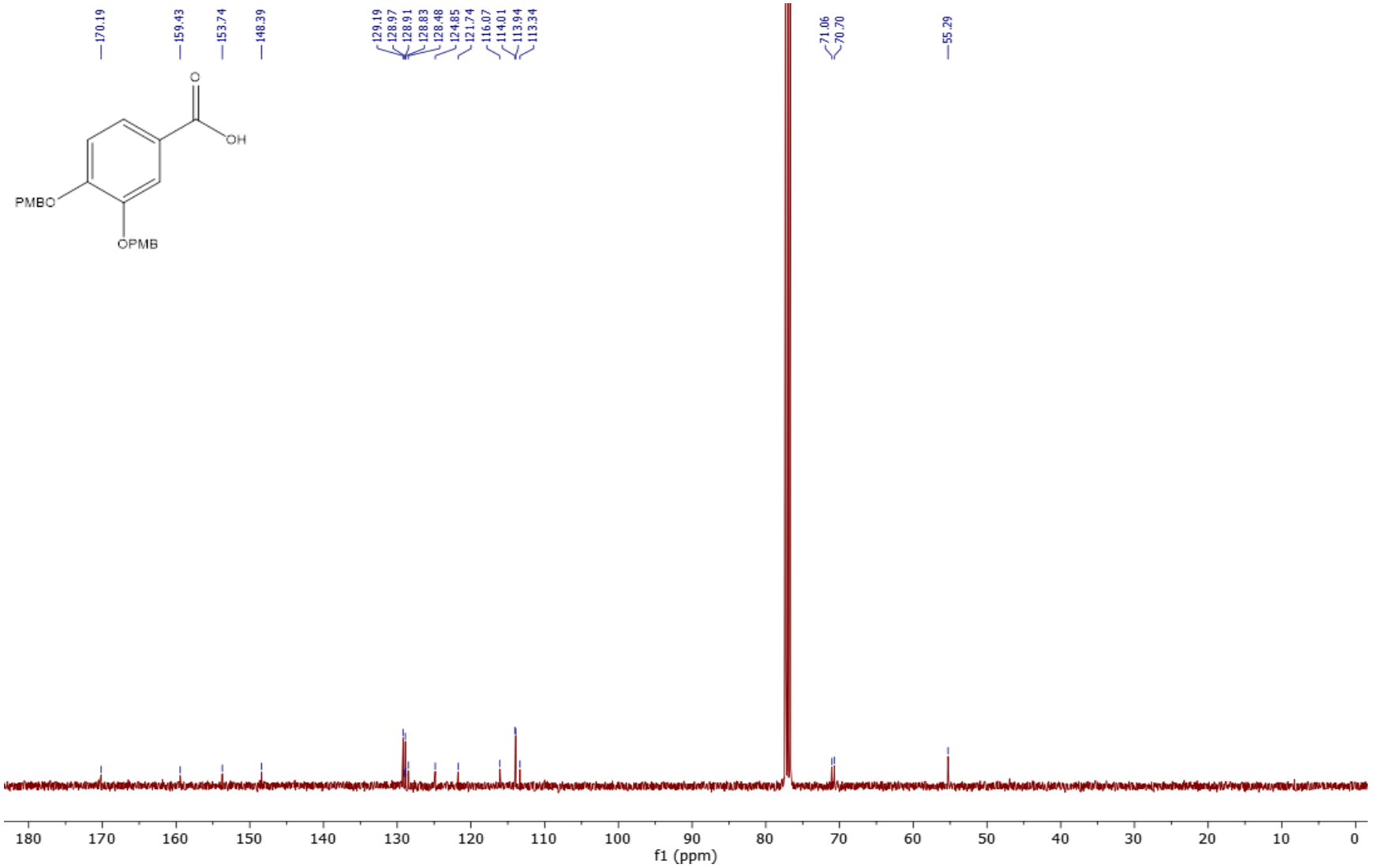

Appendix 13. ^{1}H spectrum of **7a** in $CDCl_3$

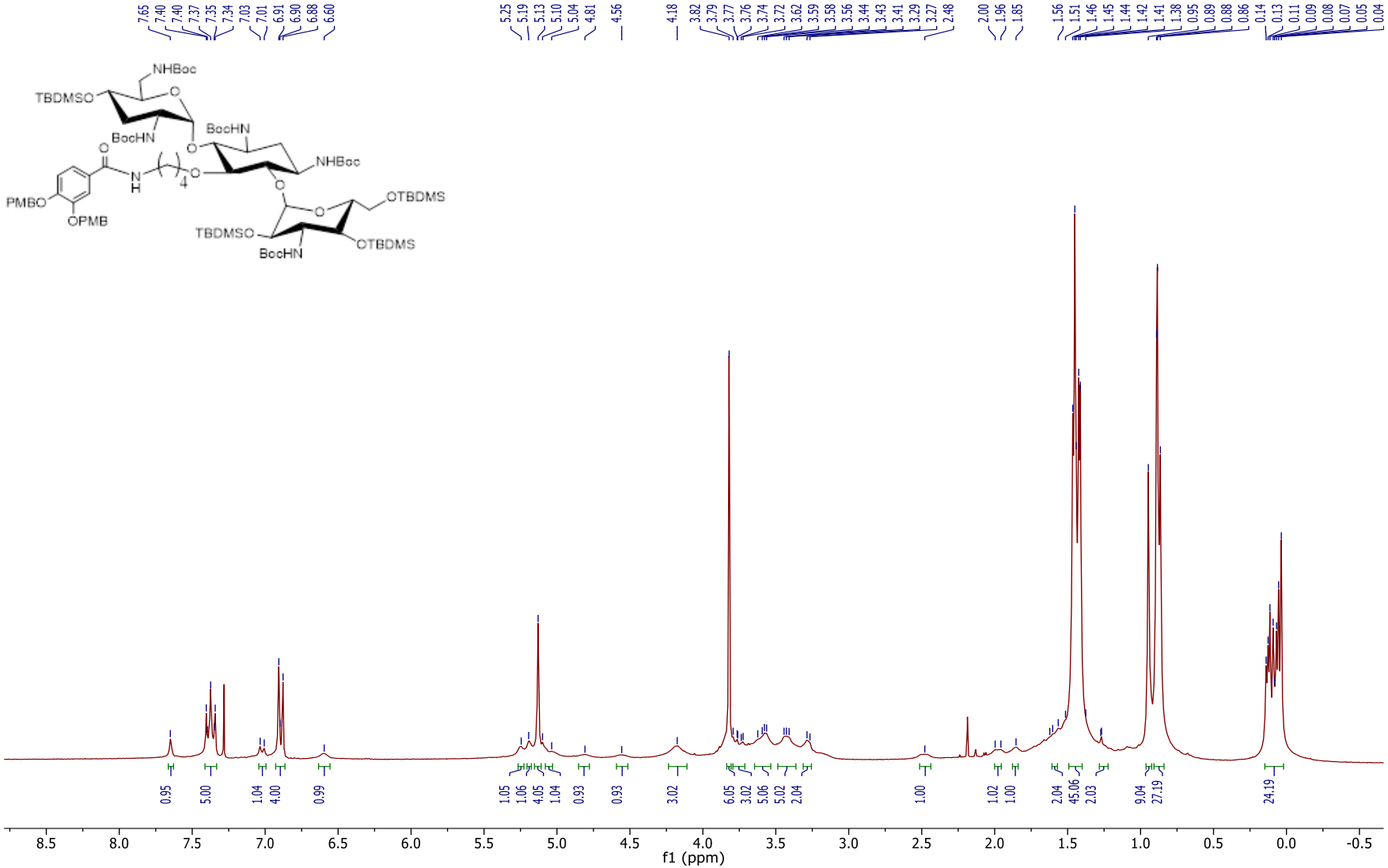

Appendix 14. ^{13}C spectrum of **7a** in $CDCl_3$

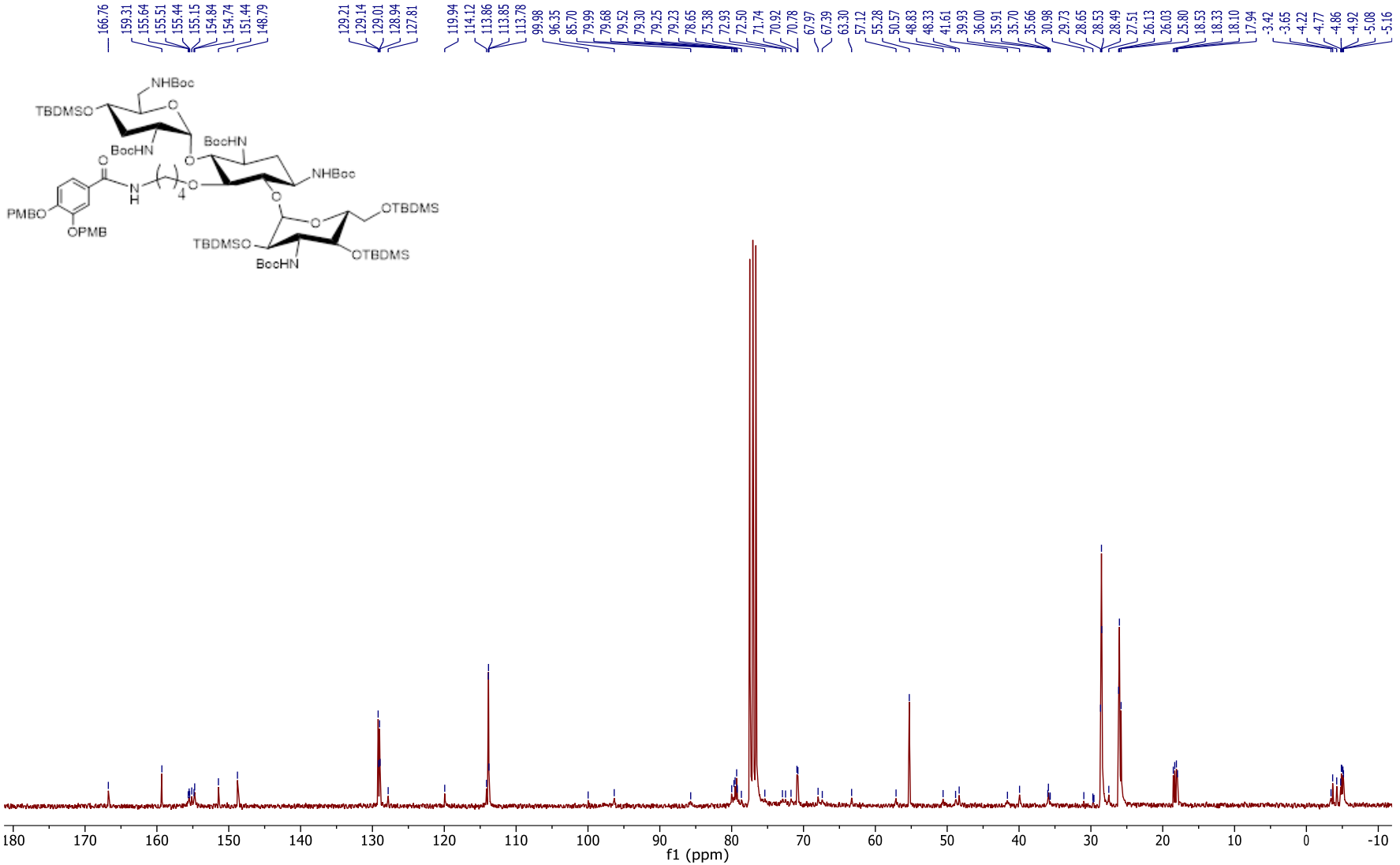

Appendix 15. ^{1}H spectrum of **7b** in $CDCl_3$

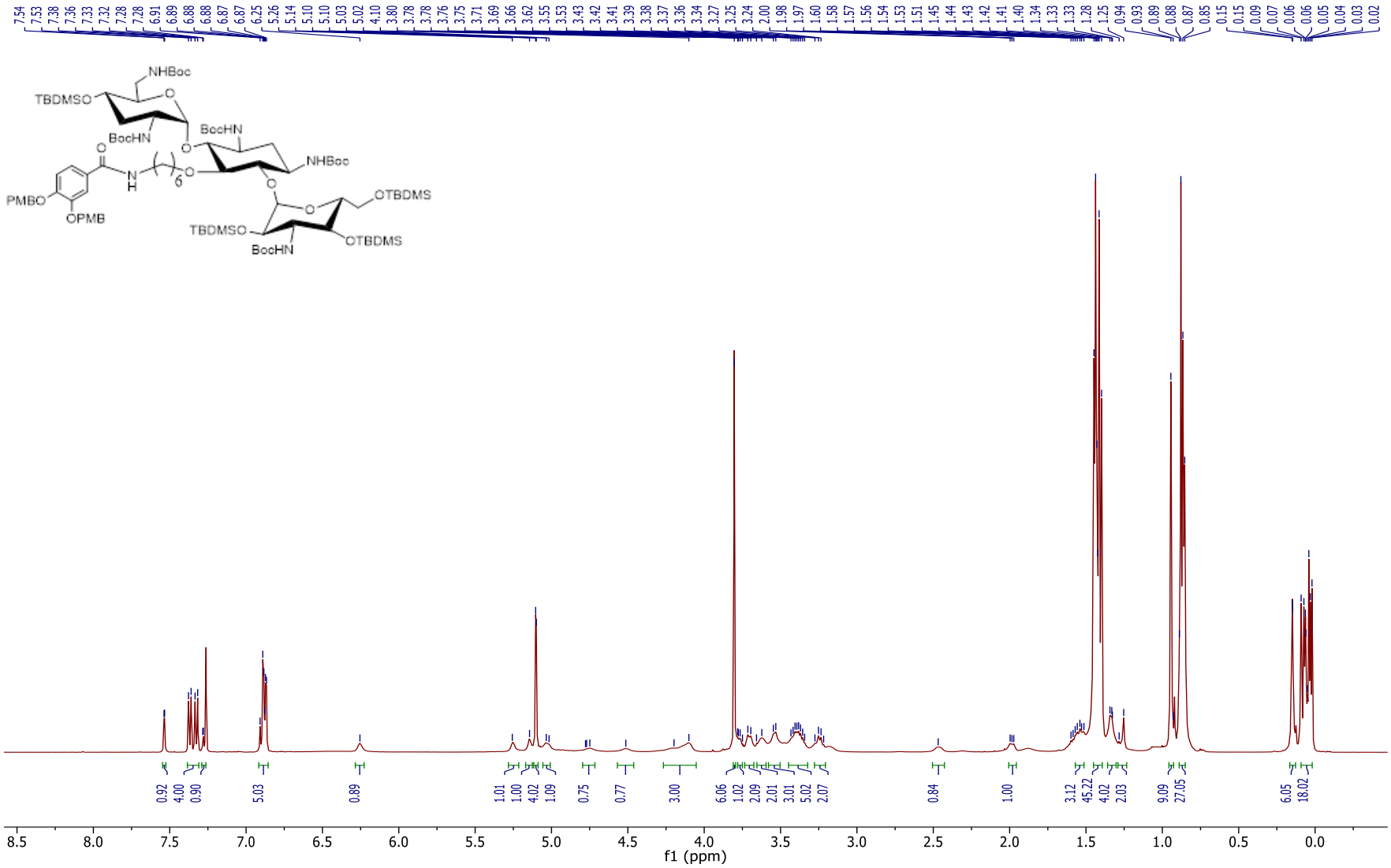

Appendix 16. ^{13}C spectrum of **7b** in $CDCl_3$

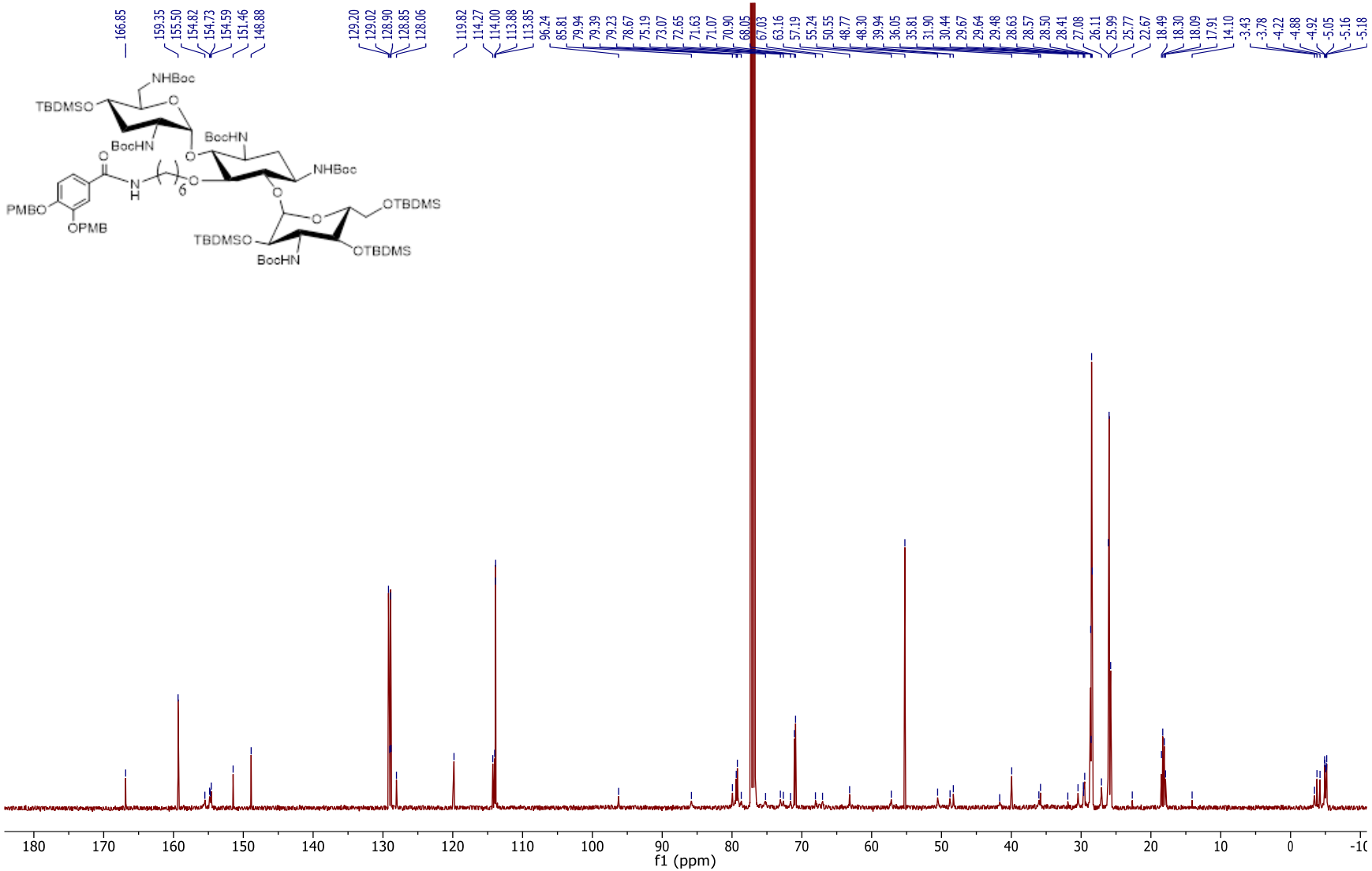

Appendix 17. ^{1}H spectrum of **7c** in $CDCl_3$

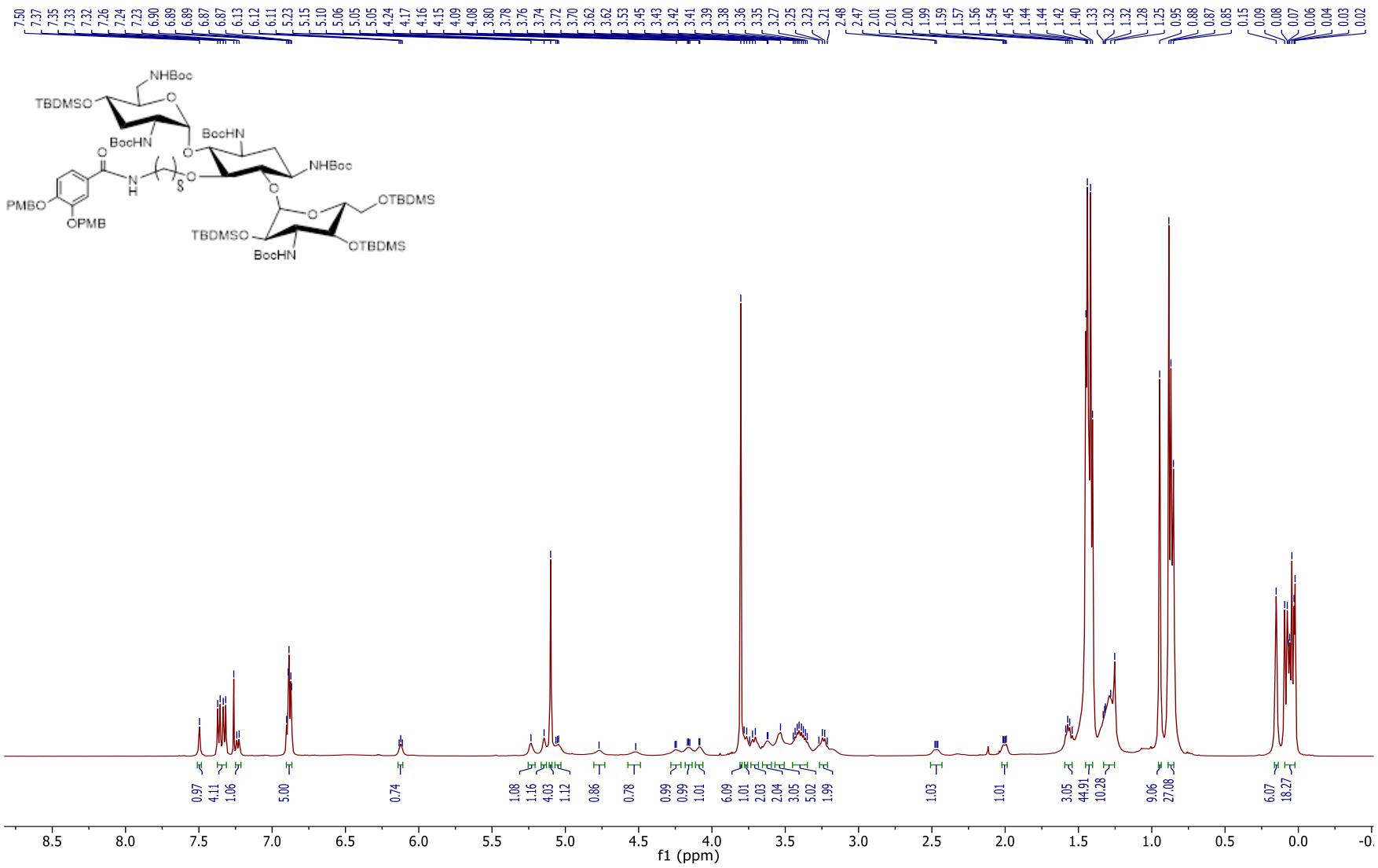

Appendix 18. ^{13}C spectrum of **7c** in $CDCl_3$

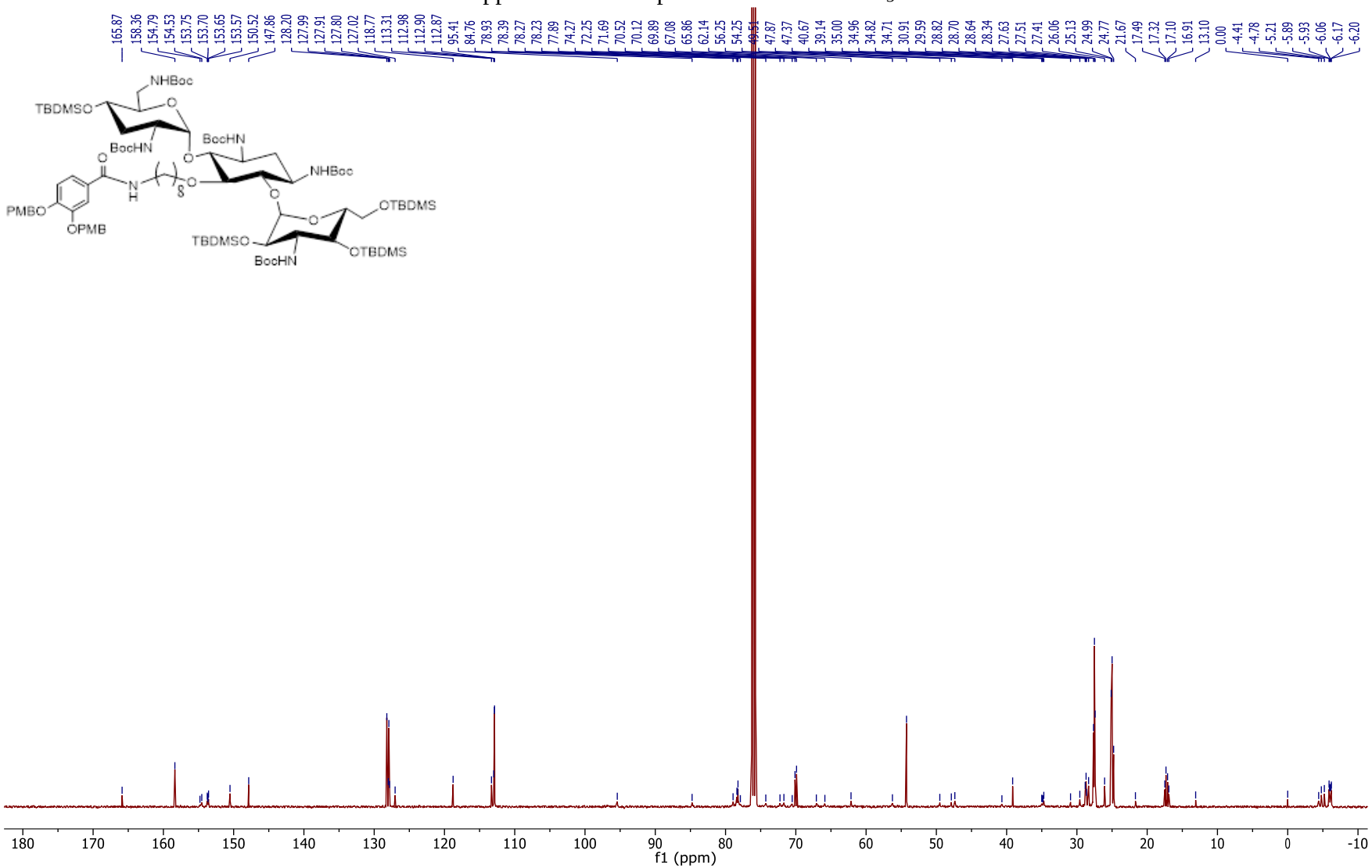

Appendix 19. ^{1}H spectrum of **1a** in $CDCl_3$

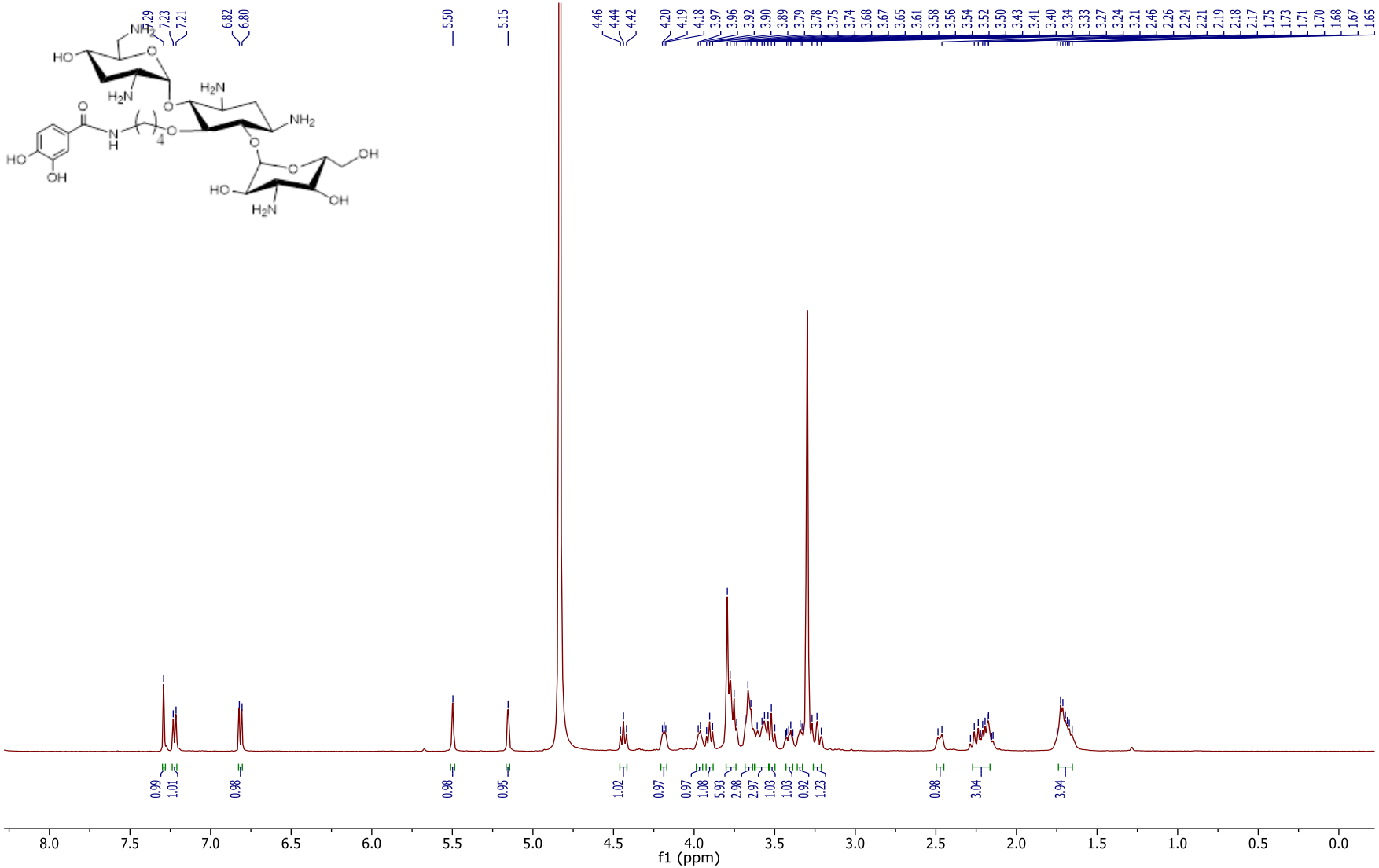

Appendix 20. ^{13}C spectrum of **1a** in MeOD

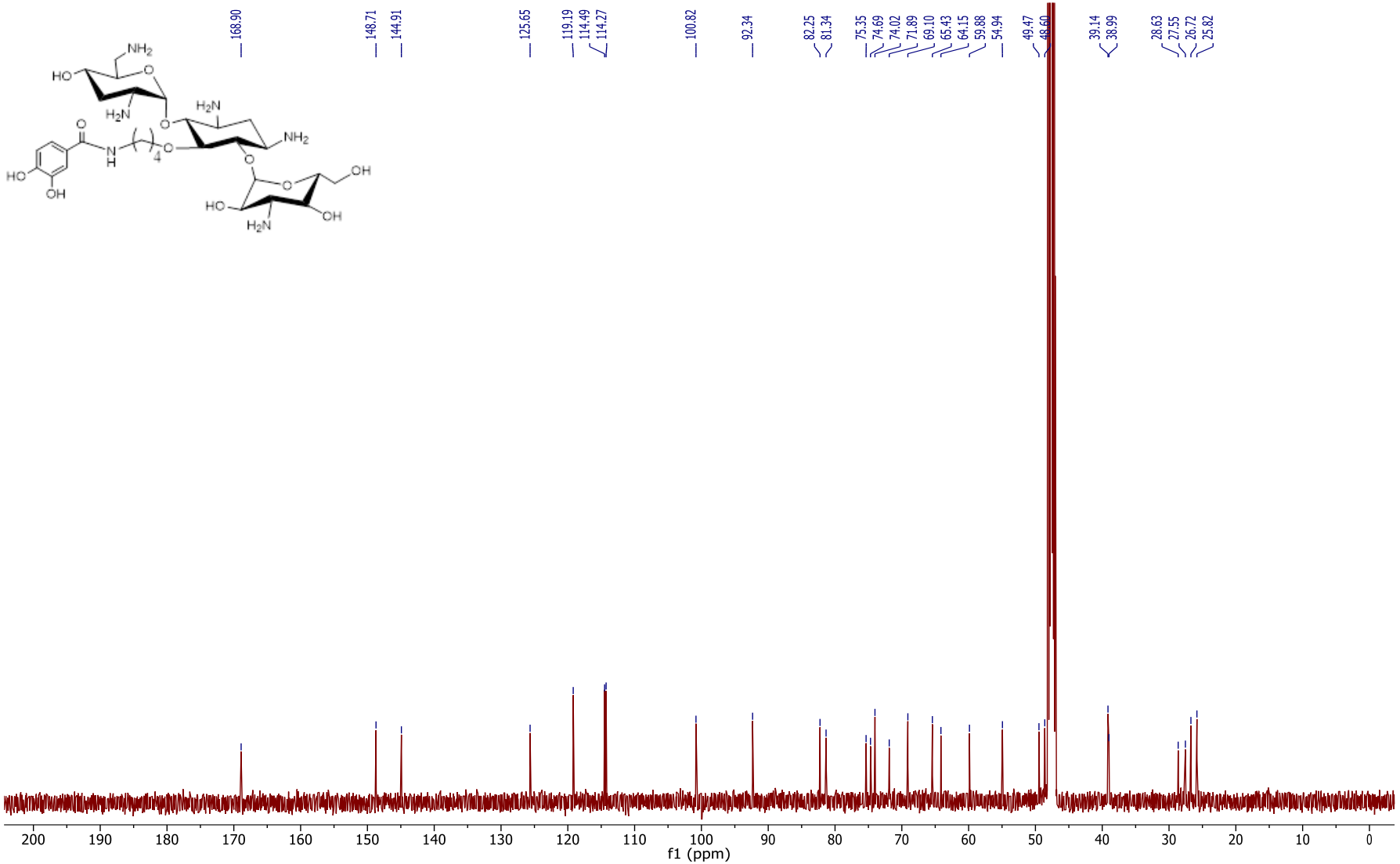

Appendix 21. ^{1}H spectrum of **1b** in MeOD

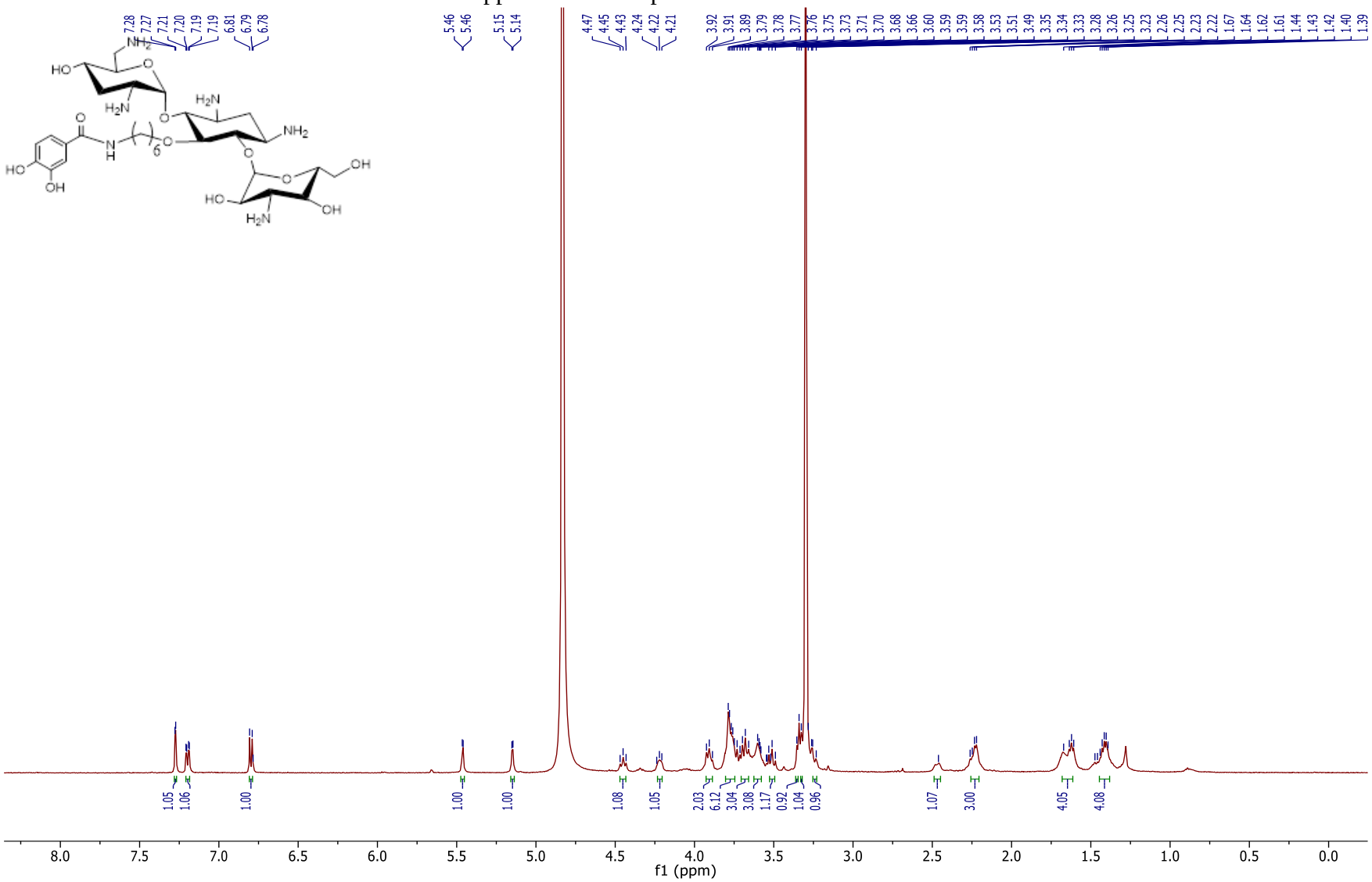

Appendix 22. ^{13}C spectrum of **1b** in MeOD

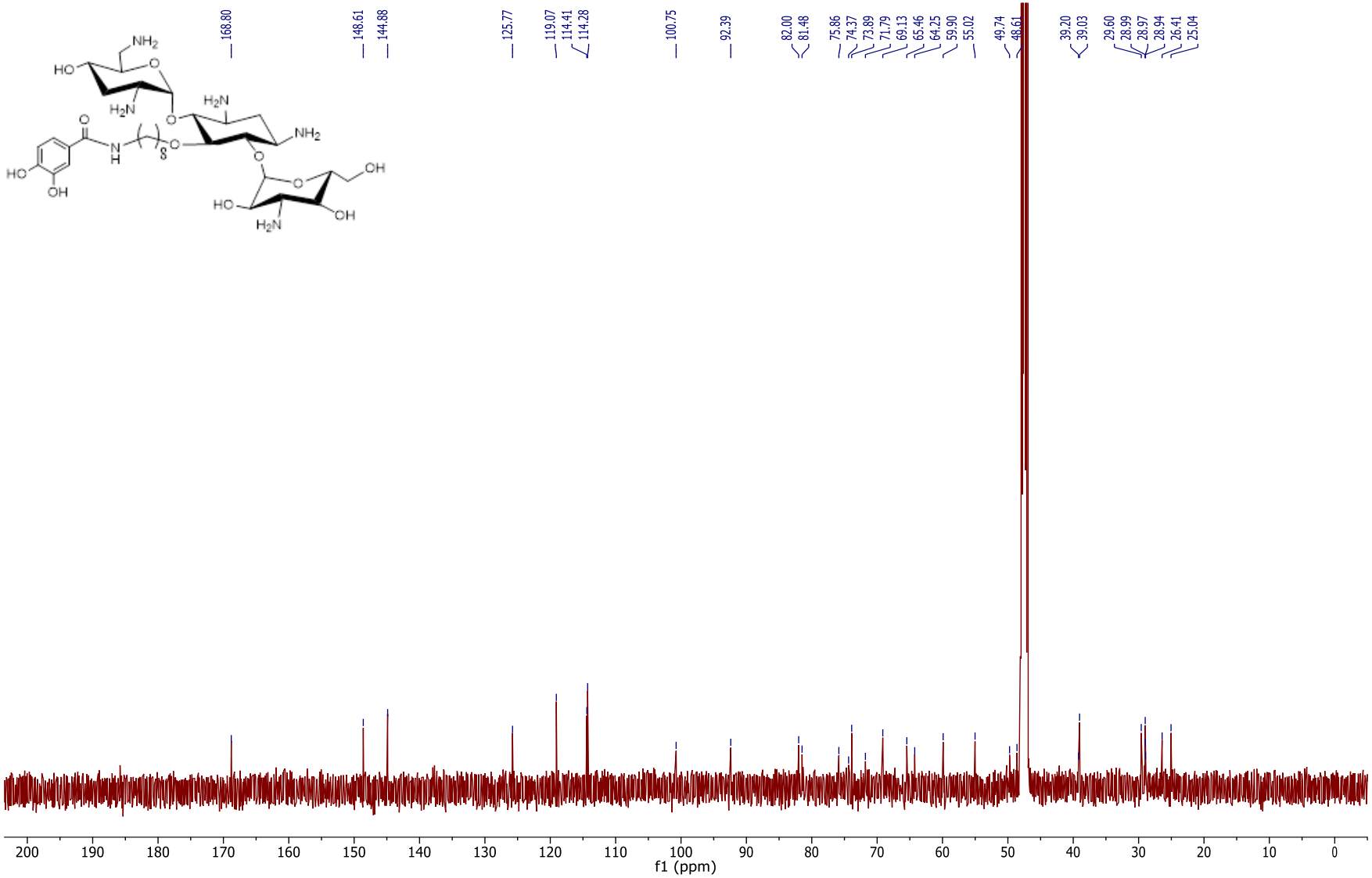

Appendix 23. ^{1}H spectrum of **1c** in MeOD

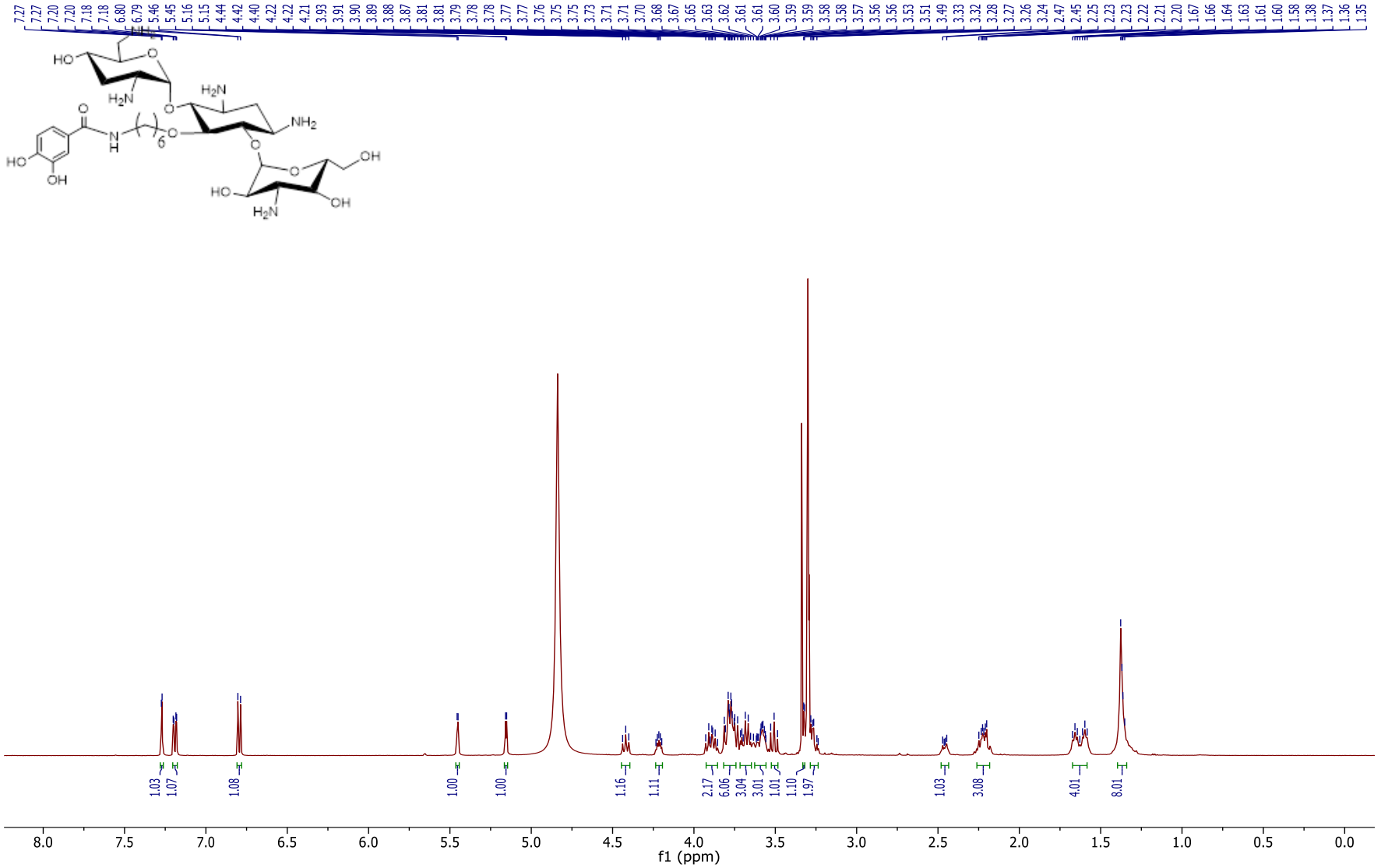

Appendix 24. ^{13}C spectrum of **1c** in MeOD

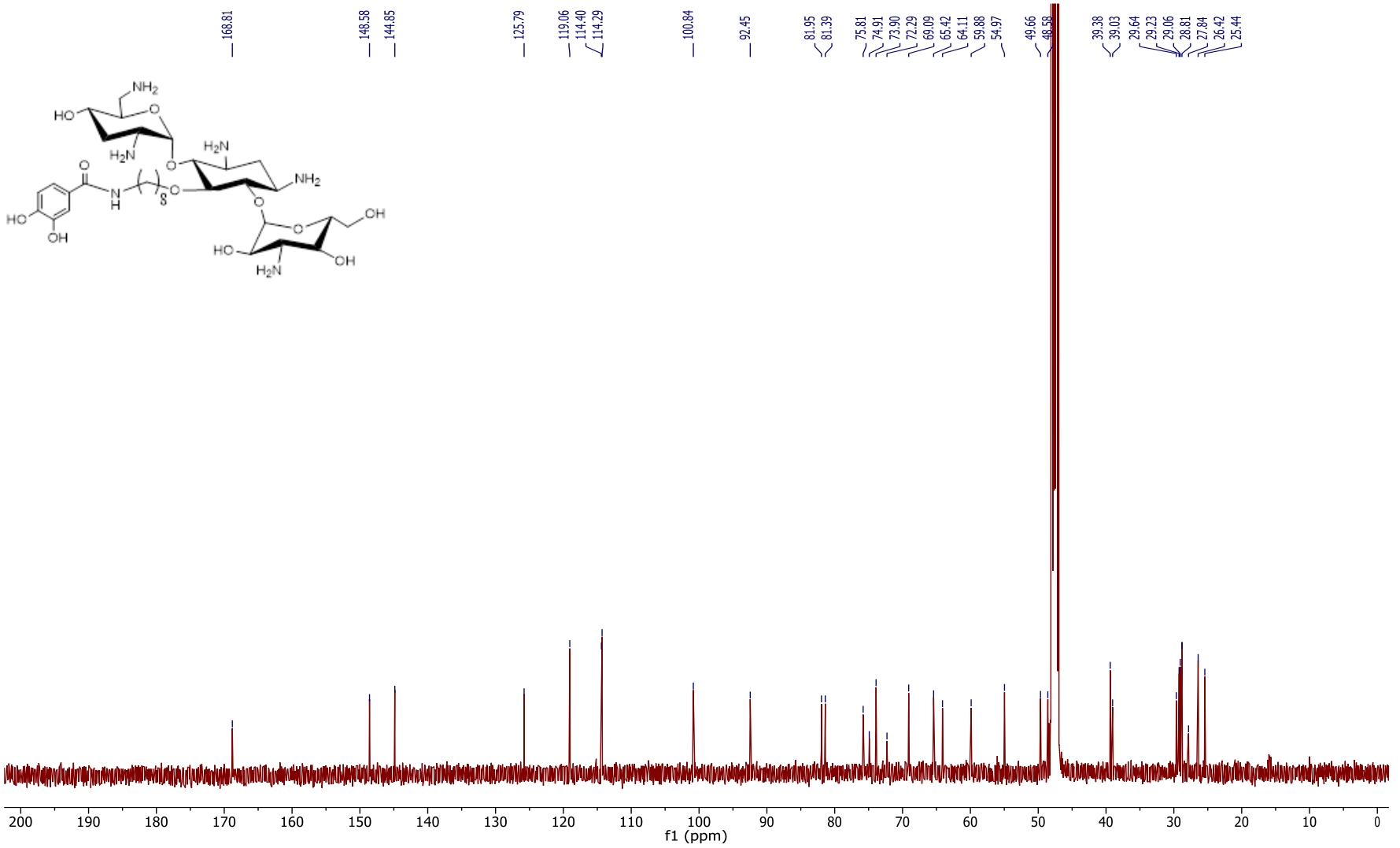

Appendix 25. ^{1}H spectrum of **12a** in $CDCl_3$

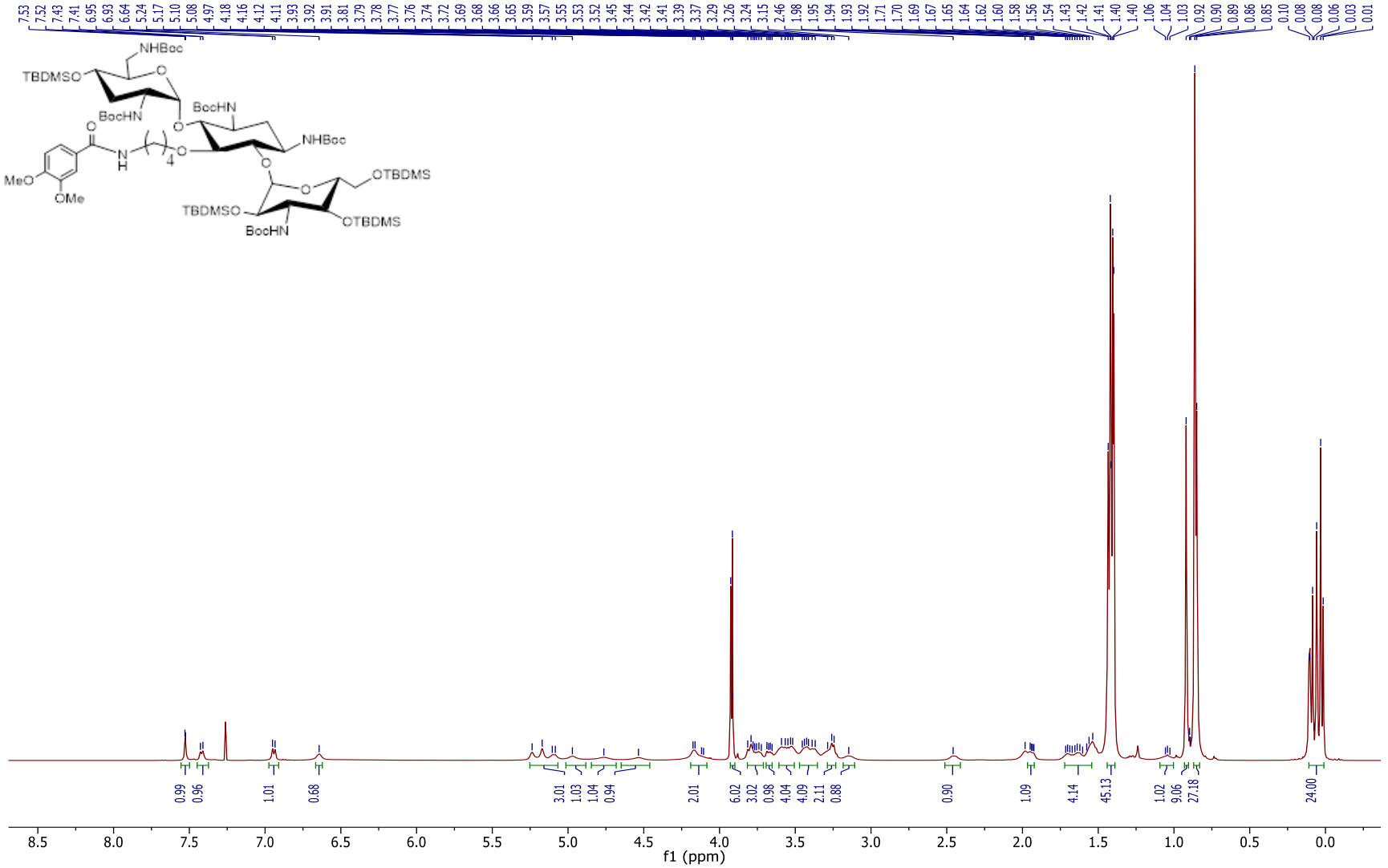

Appendix 26. ^{13}C spectrum of **12a** in $CDCl_3$

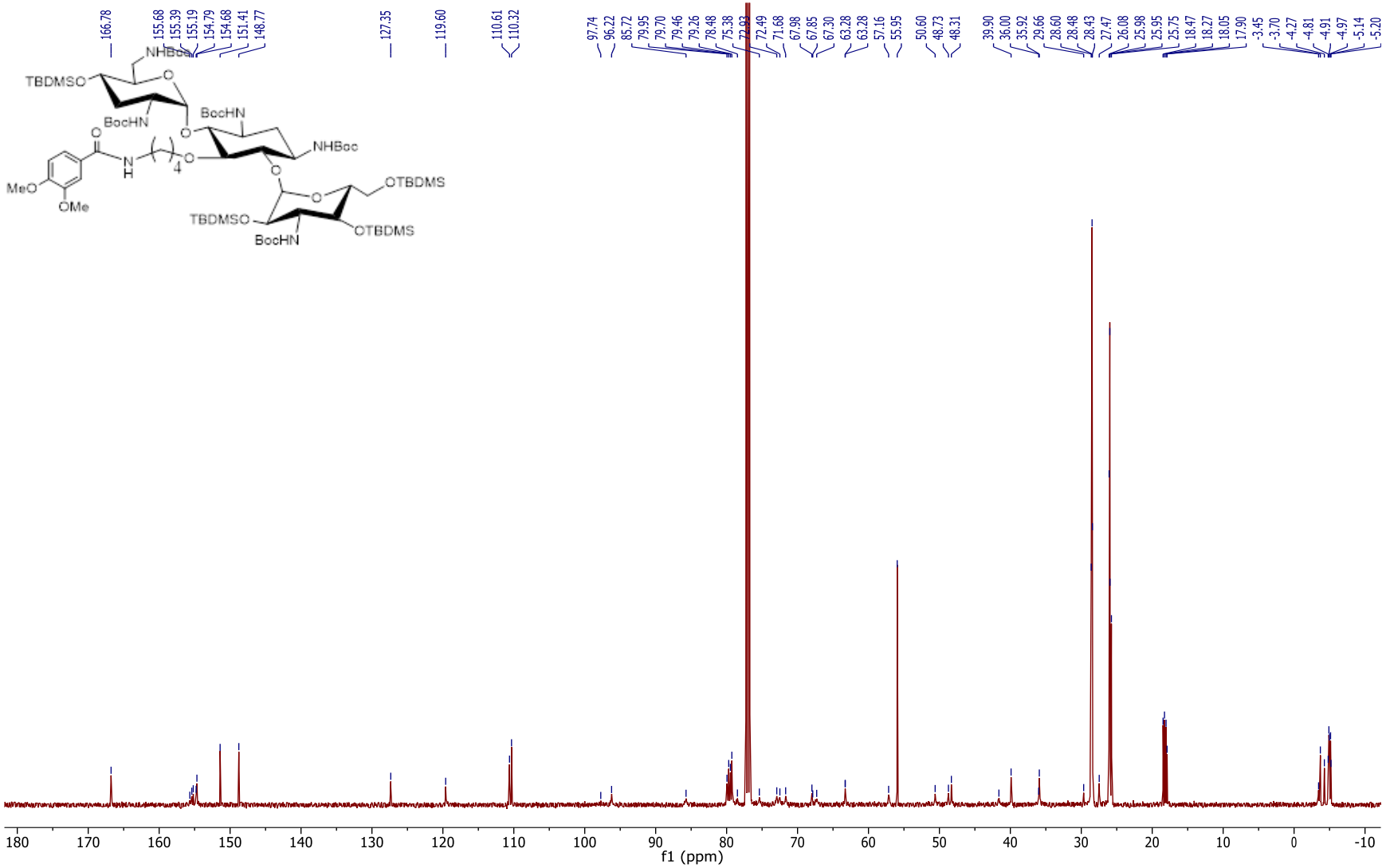

Appendix 27. ^{1}H spectrum of **12b** in $CDCl_3$

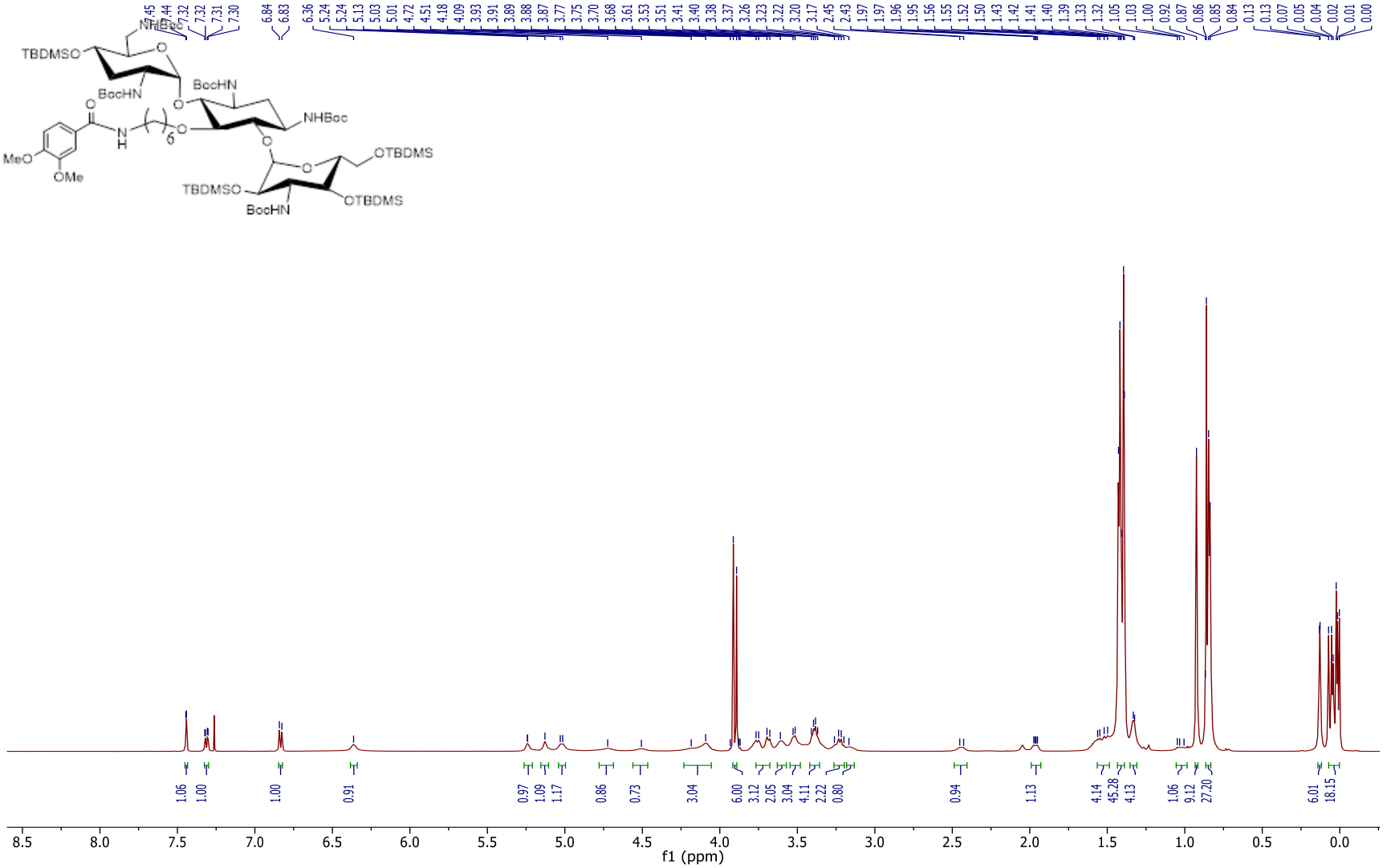

Appendix 28. ^{13}C spectrum of **12b** in $CDCl_3$

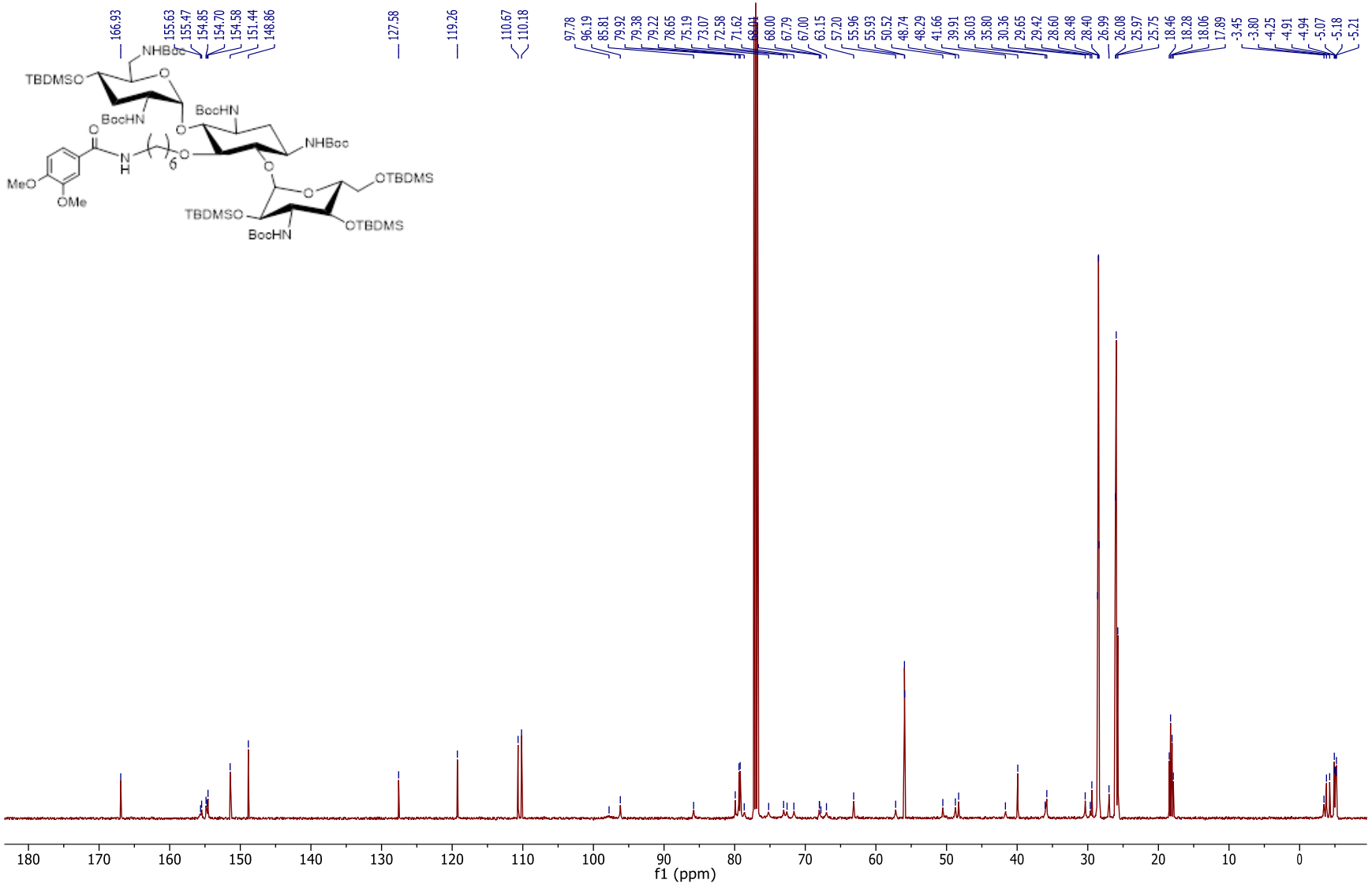

Appendix 29. ^{1}H spectrum of **12c** in $CDCl_3$

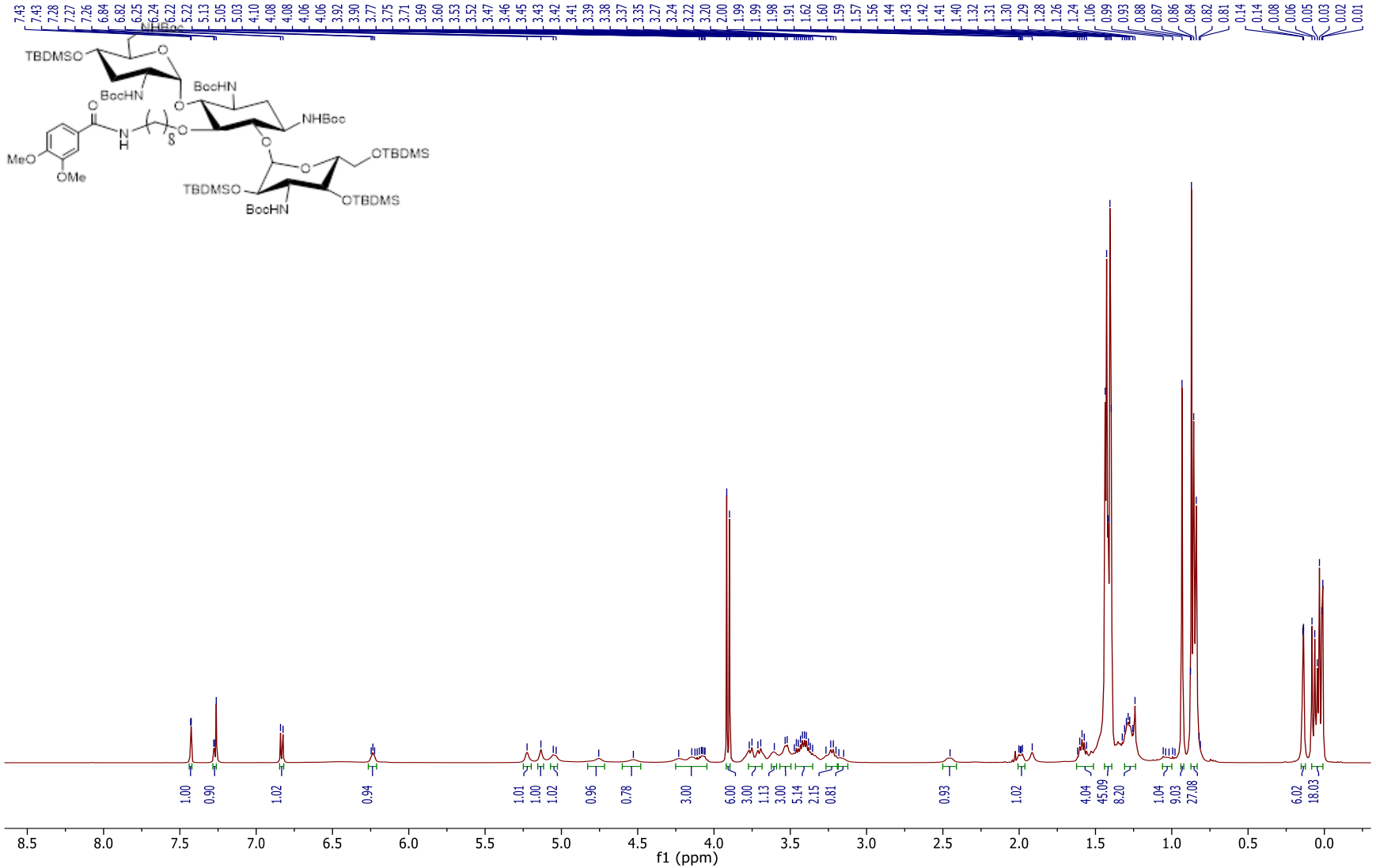

Appendix 30. ^{13}C spectrum of **12b** in $CDCl_3$

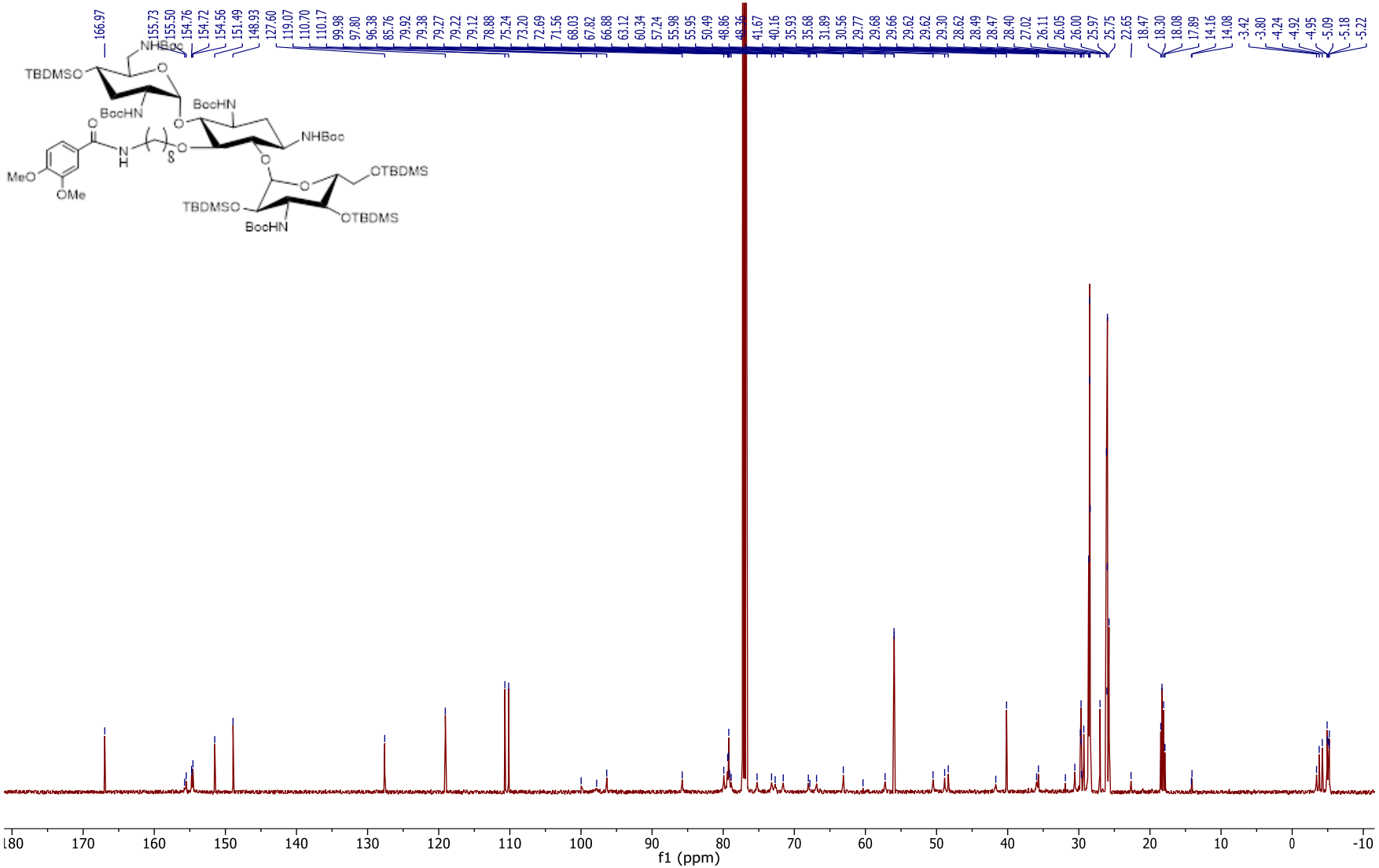

Appendix 31. ^{1}H spectrum of **11a** in MeOD

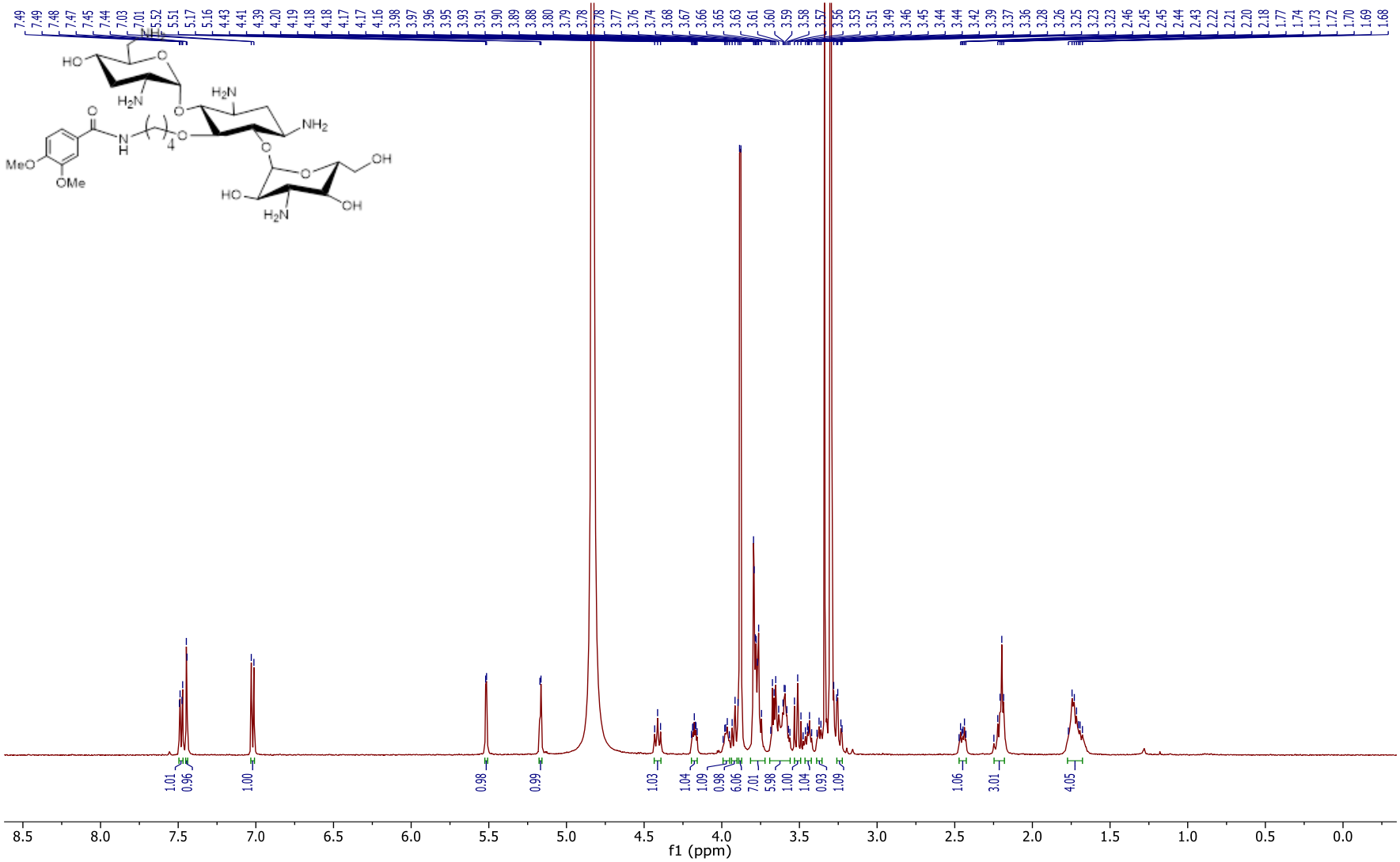

Appendix 32. ^{13}C spectrum of **11a** in MeOD

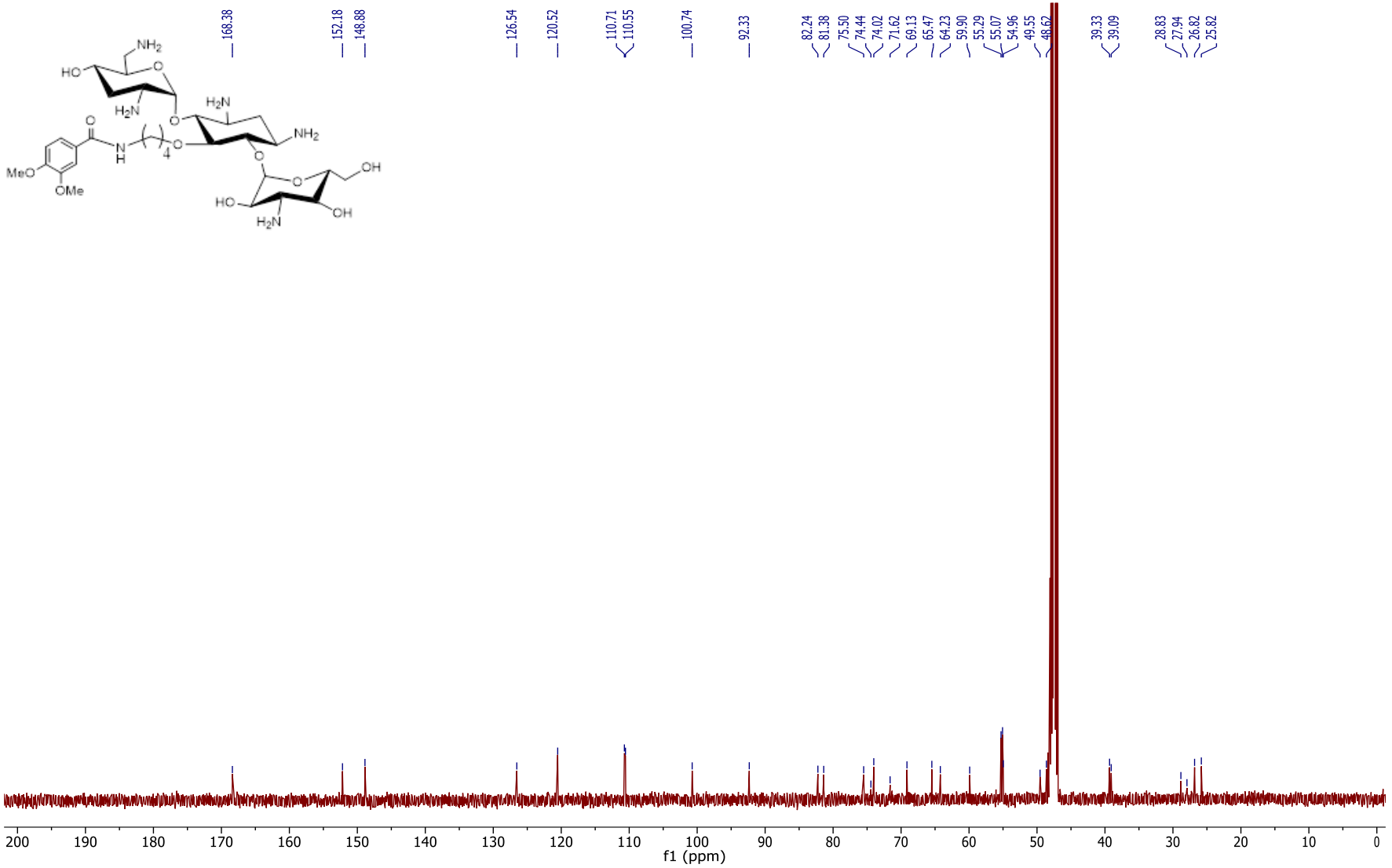

Appendix 33. ^{1}H spectrum of **11b** in MeOD

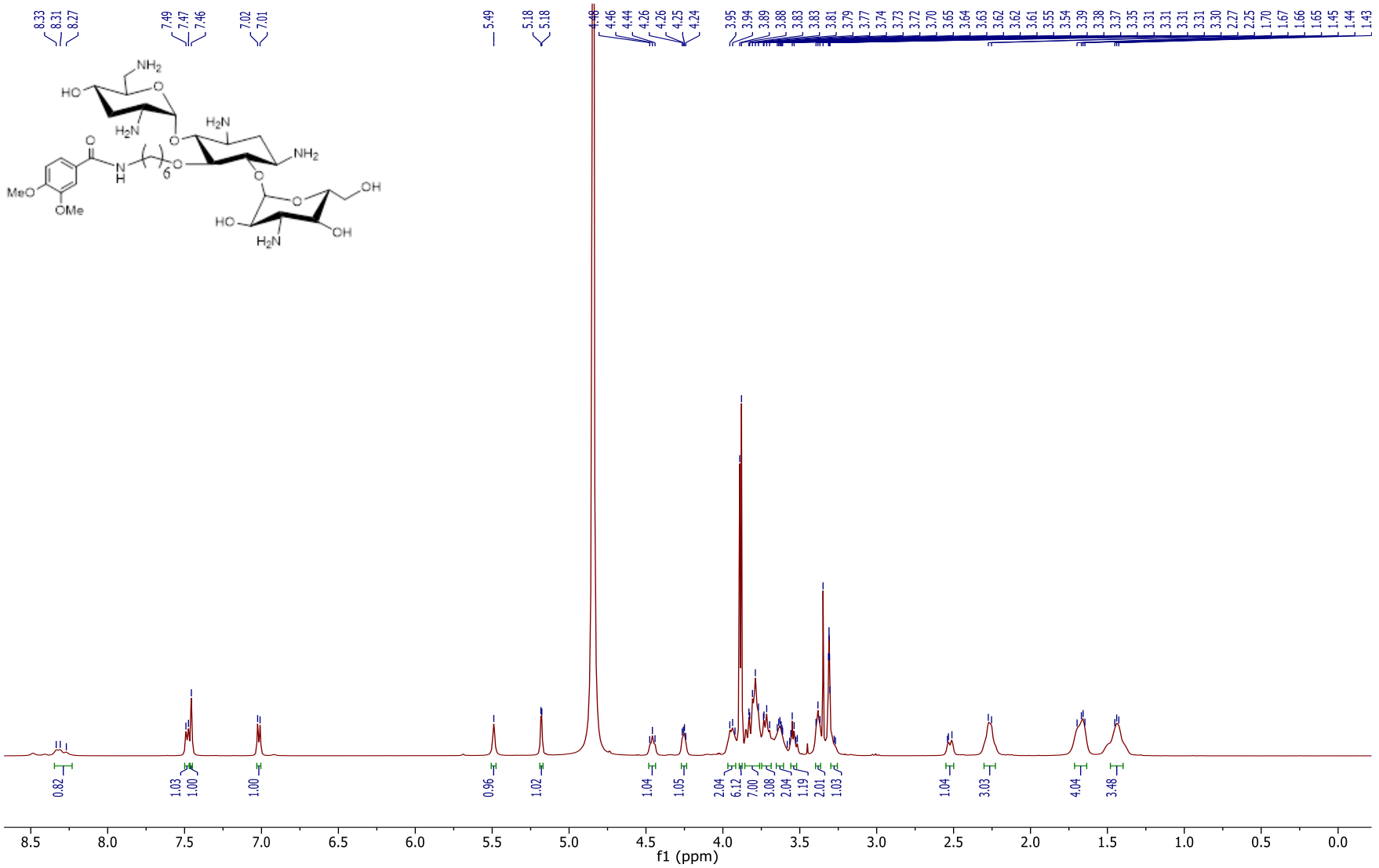

Appendix 34. ^{13}C spectrum of **11b** in MeOD

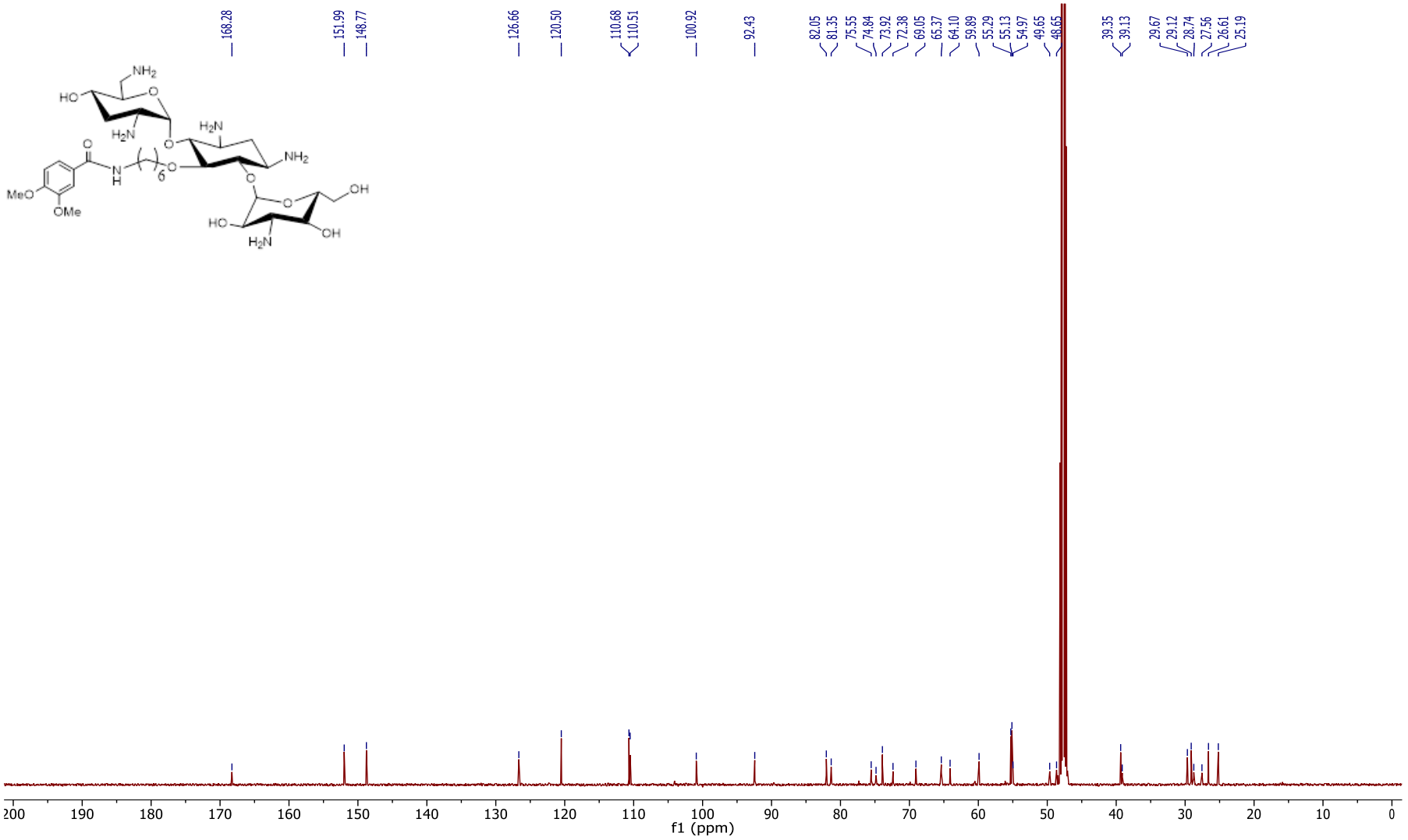

Appendix 35. ^{1}H spectrum of **11c** in MeOD

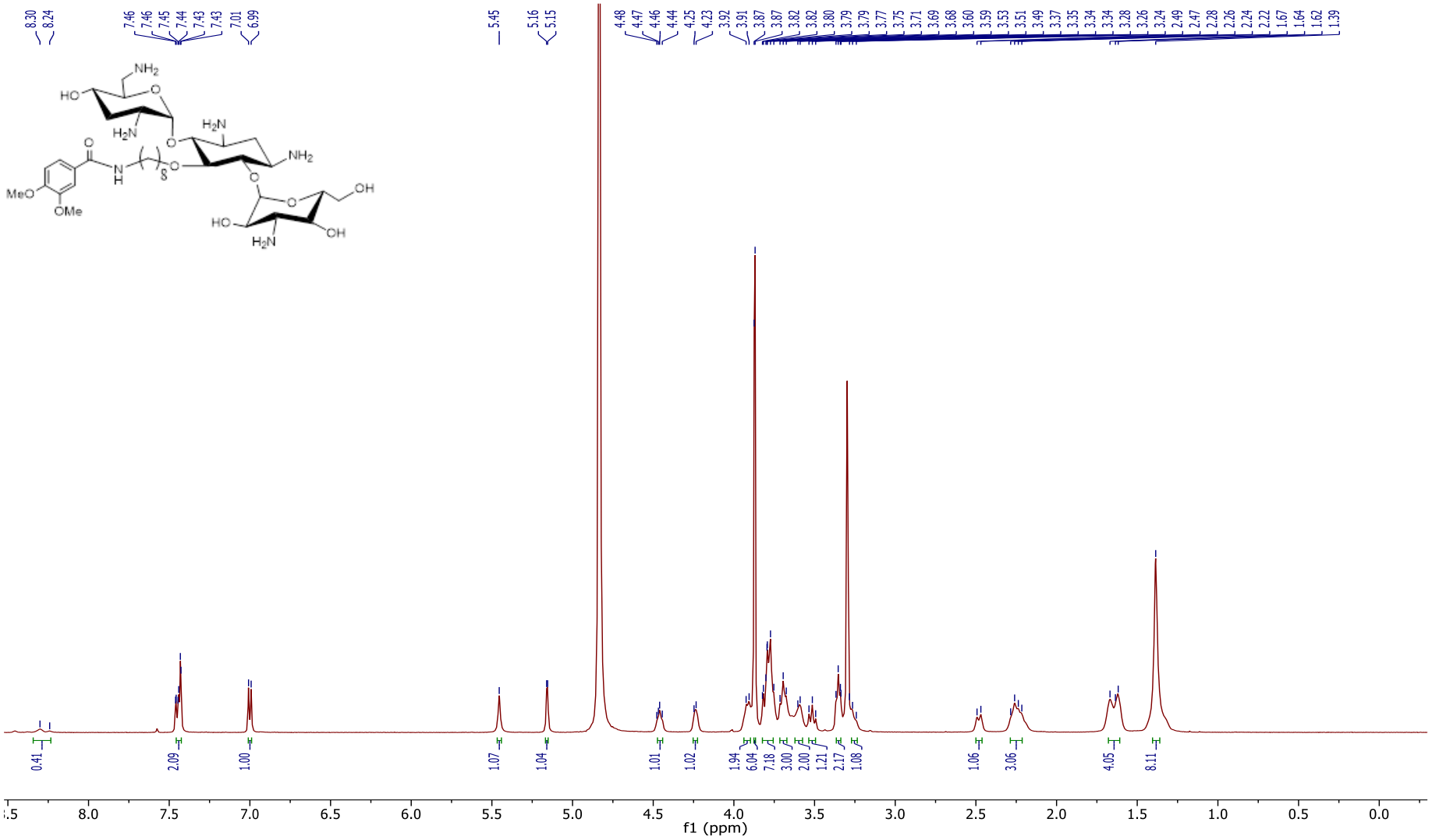

Appendix 36. ^{13}C spectrum of **11c** in MeOD

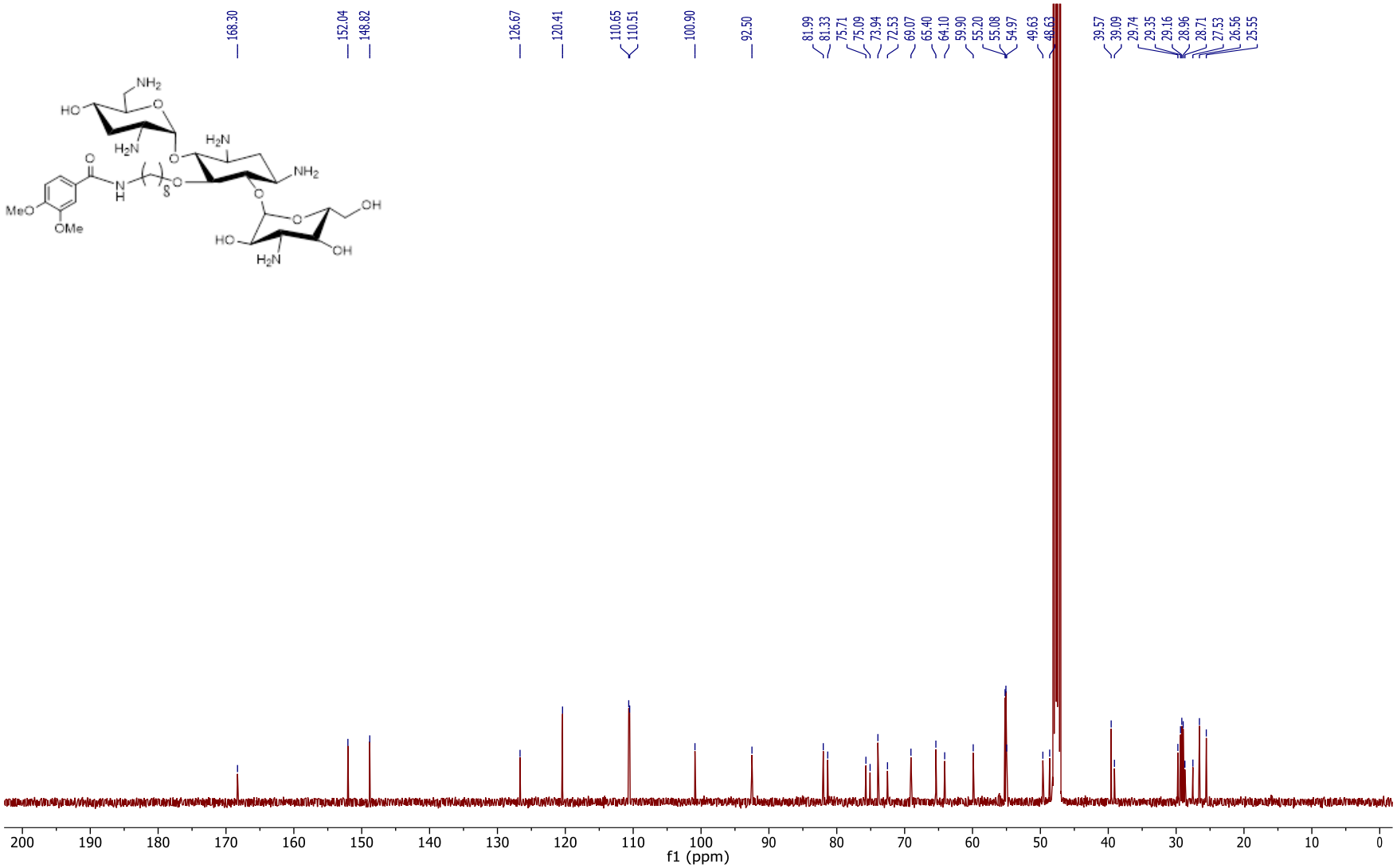

7.6 NMR SPECTRA

Appendix 37. MALDI Mass Spectrum of **6a**

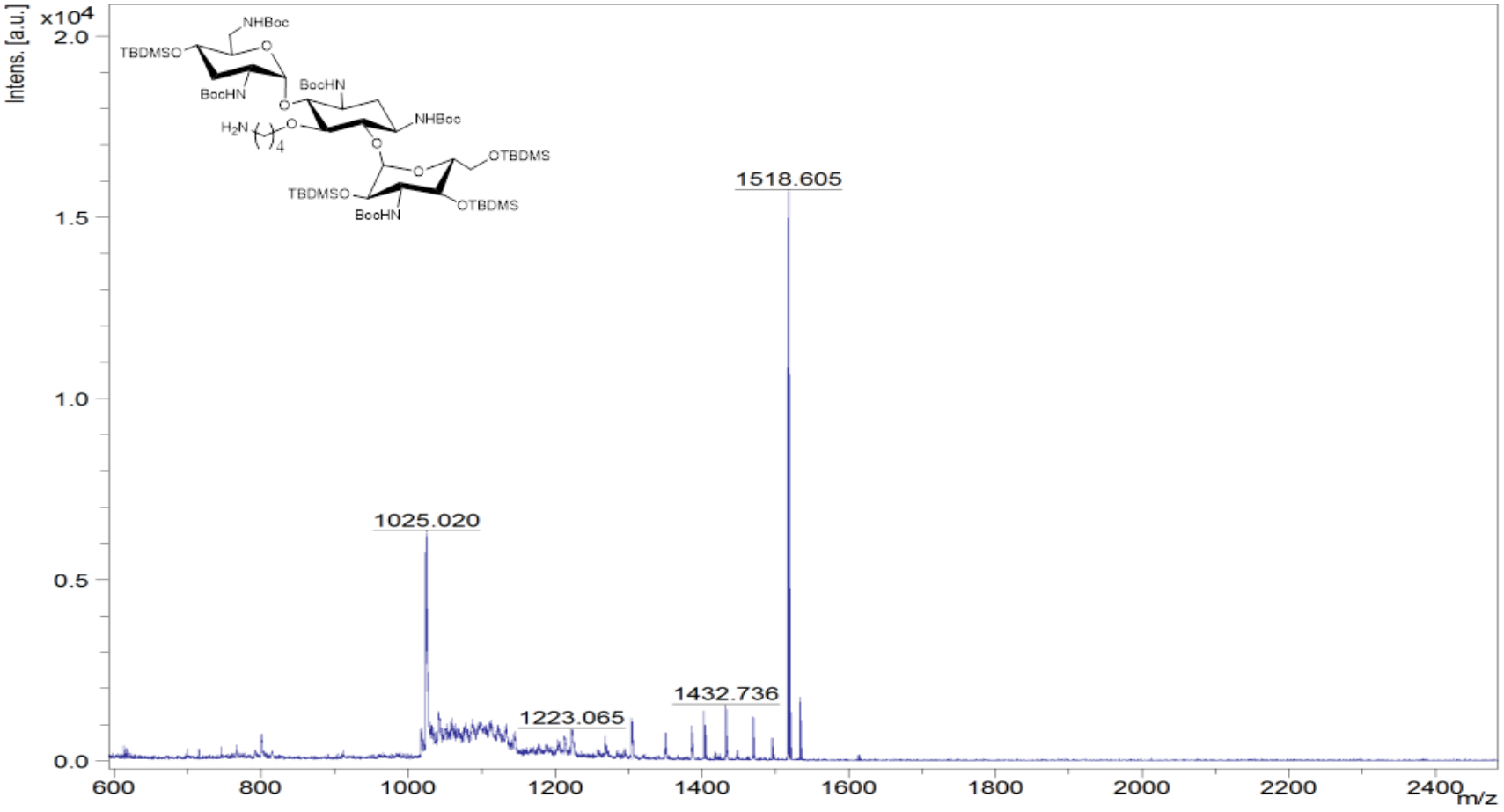

Appendix 38. MALDI Mass Spectrum of **6b**

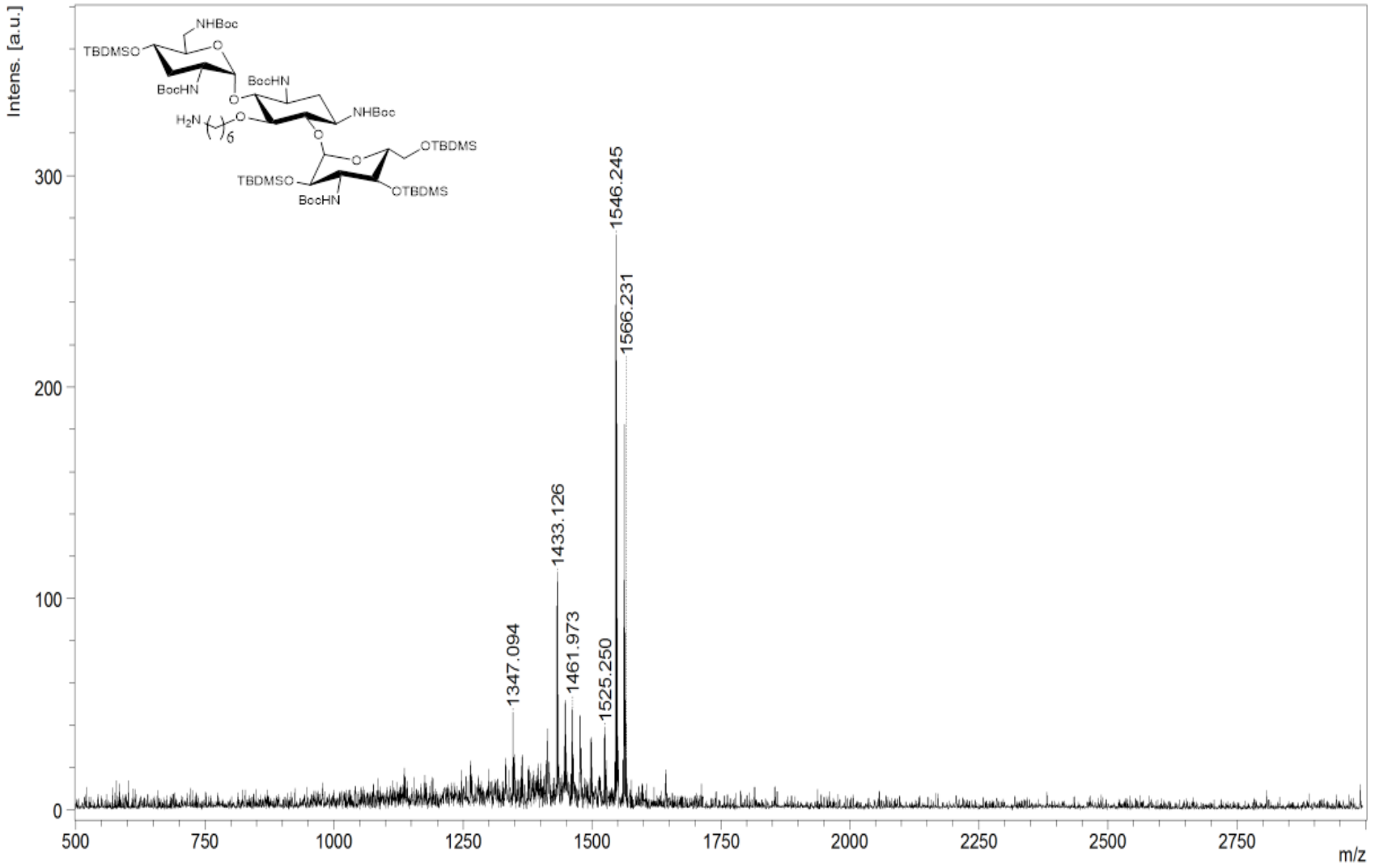

Appendix 39. MALDI Mass Spectrum of **6c**

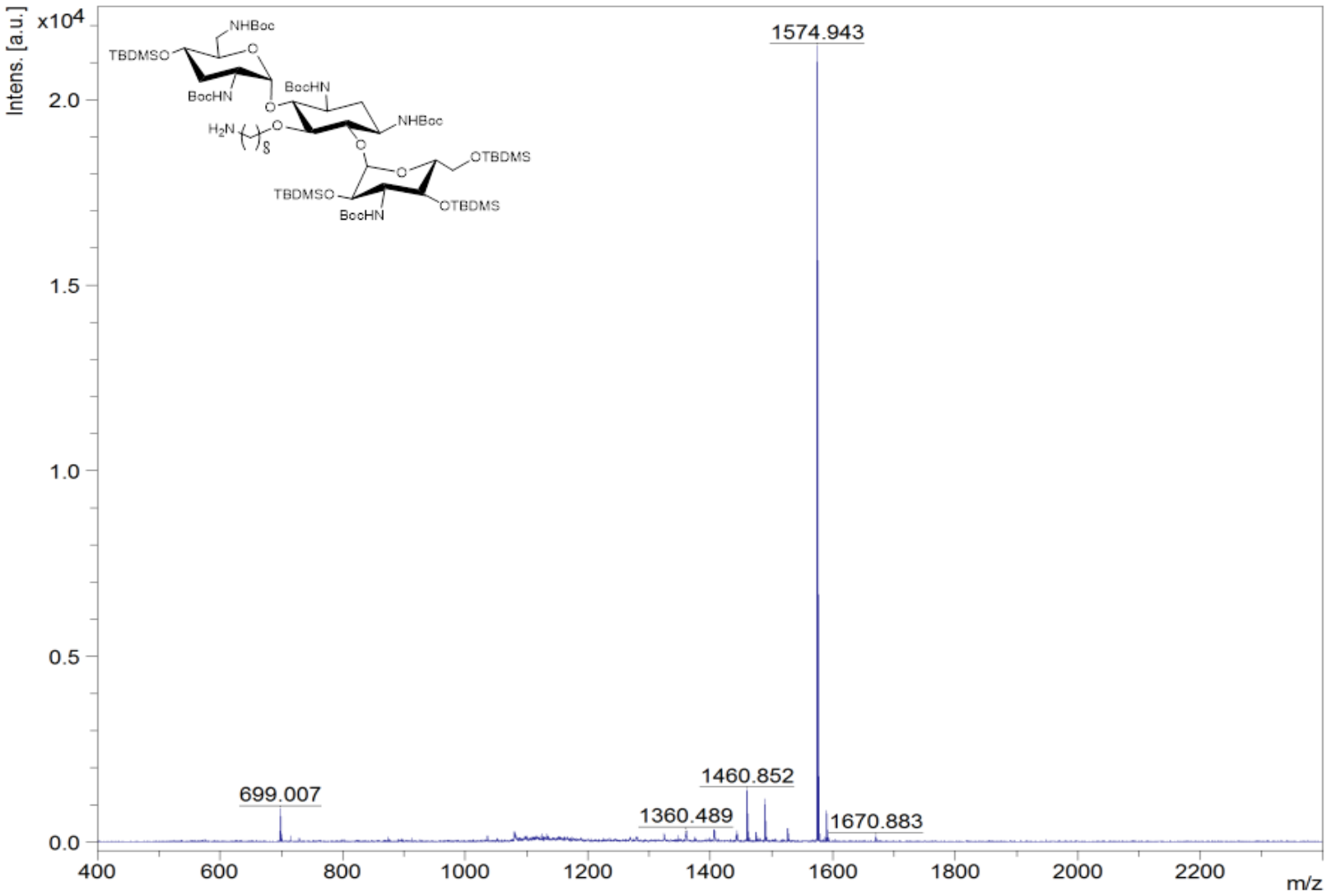

Appendix 40. ESI Mass Spectrum of **9**

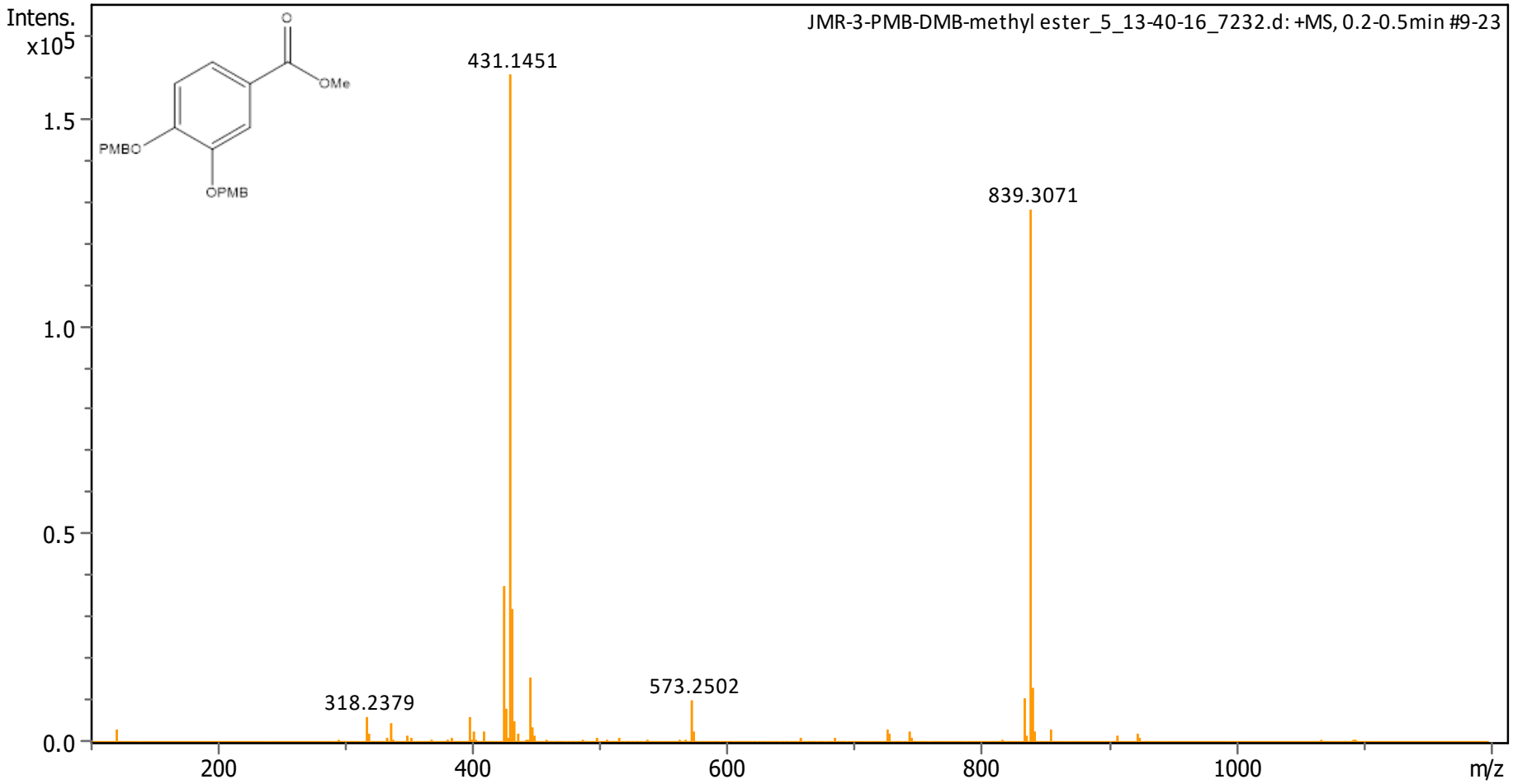

Appendix 41. ESI Mass Spectrum of **10**

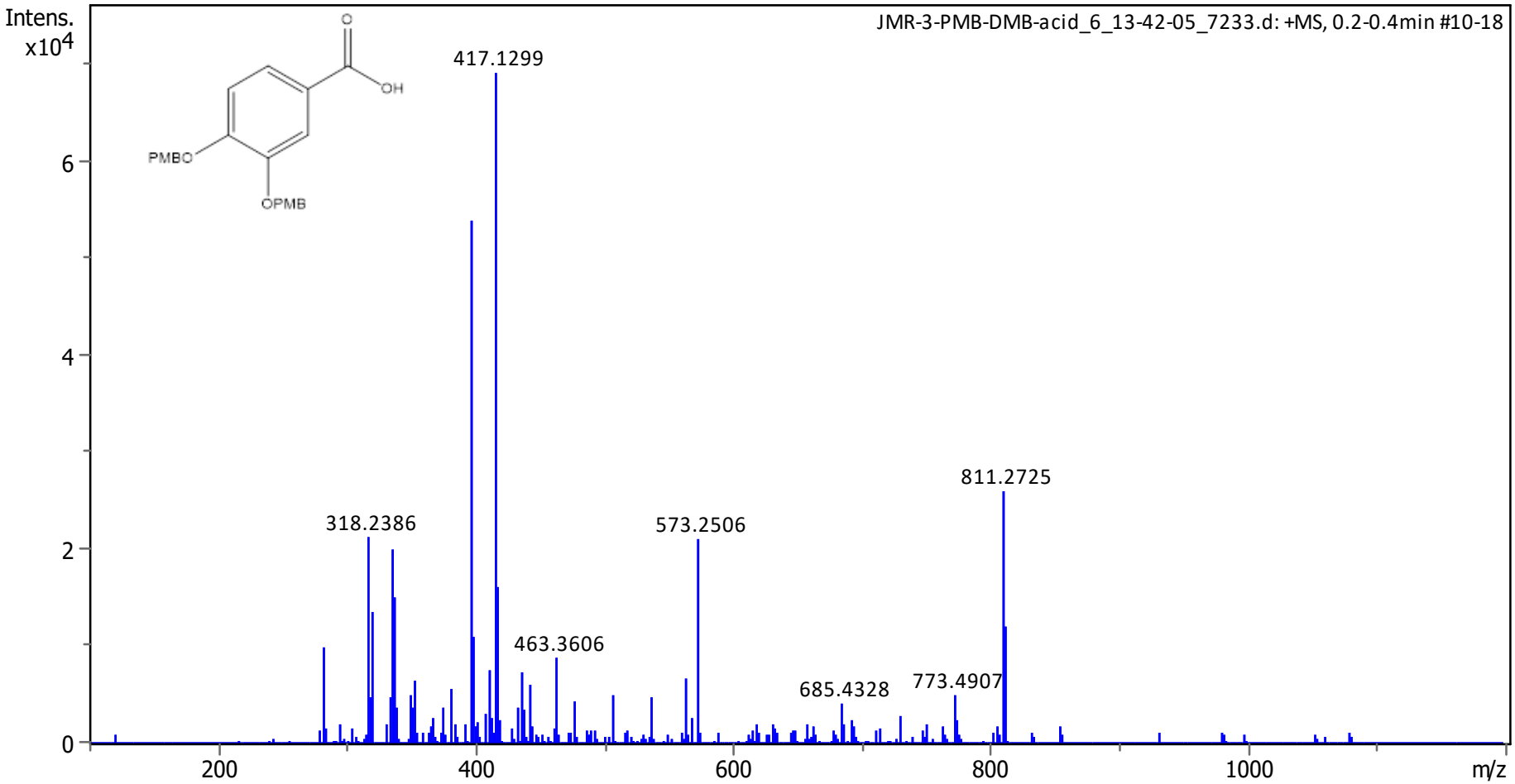

Appendix 42. MALDI Mass Spectrum of **7a**

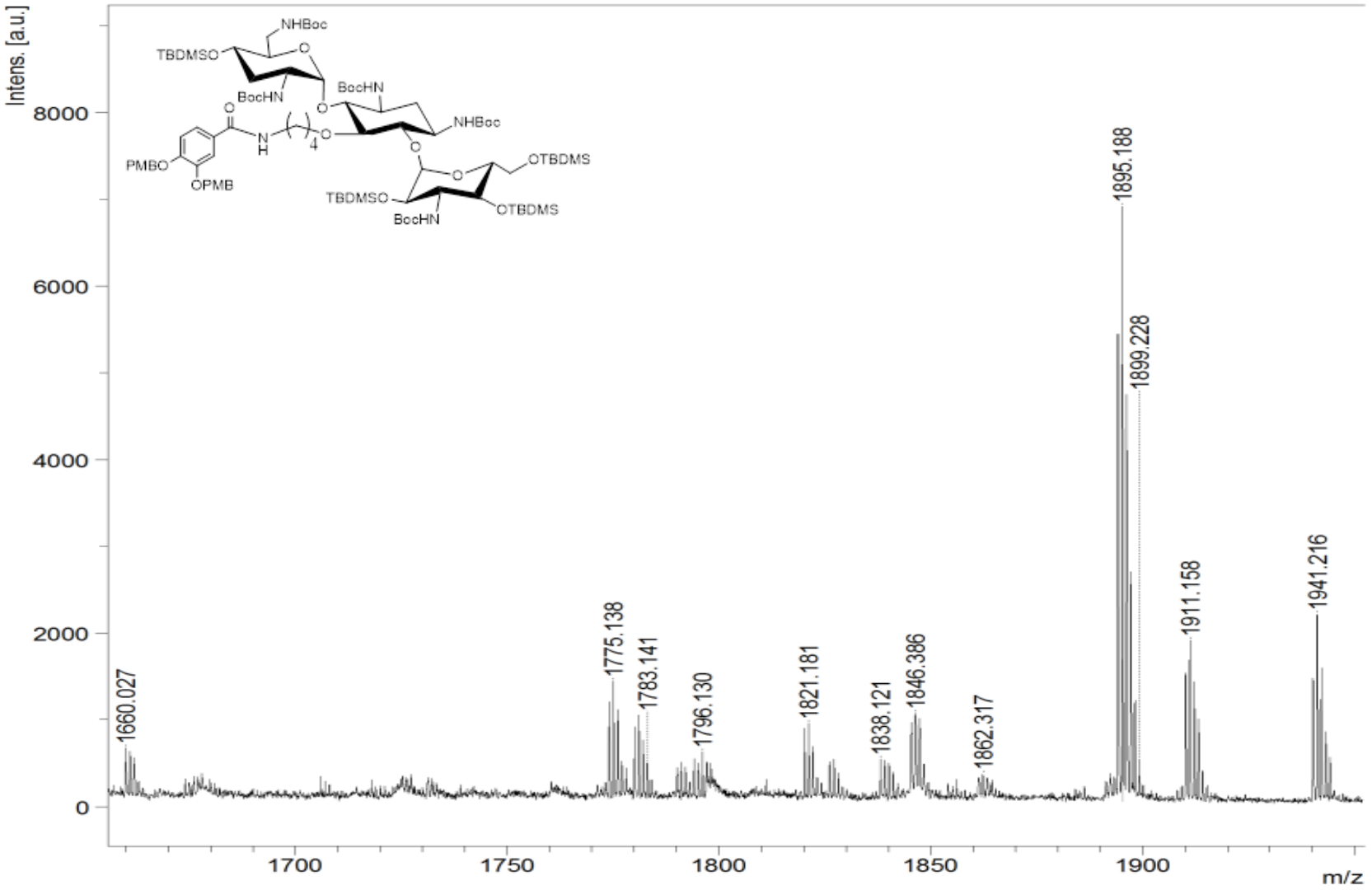

Appendix 43. MALDI Mass Spectrum of **7b**

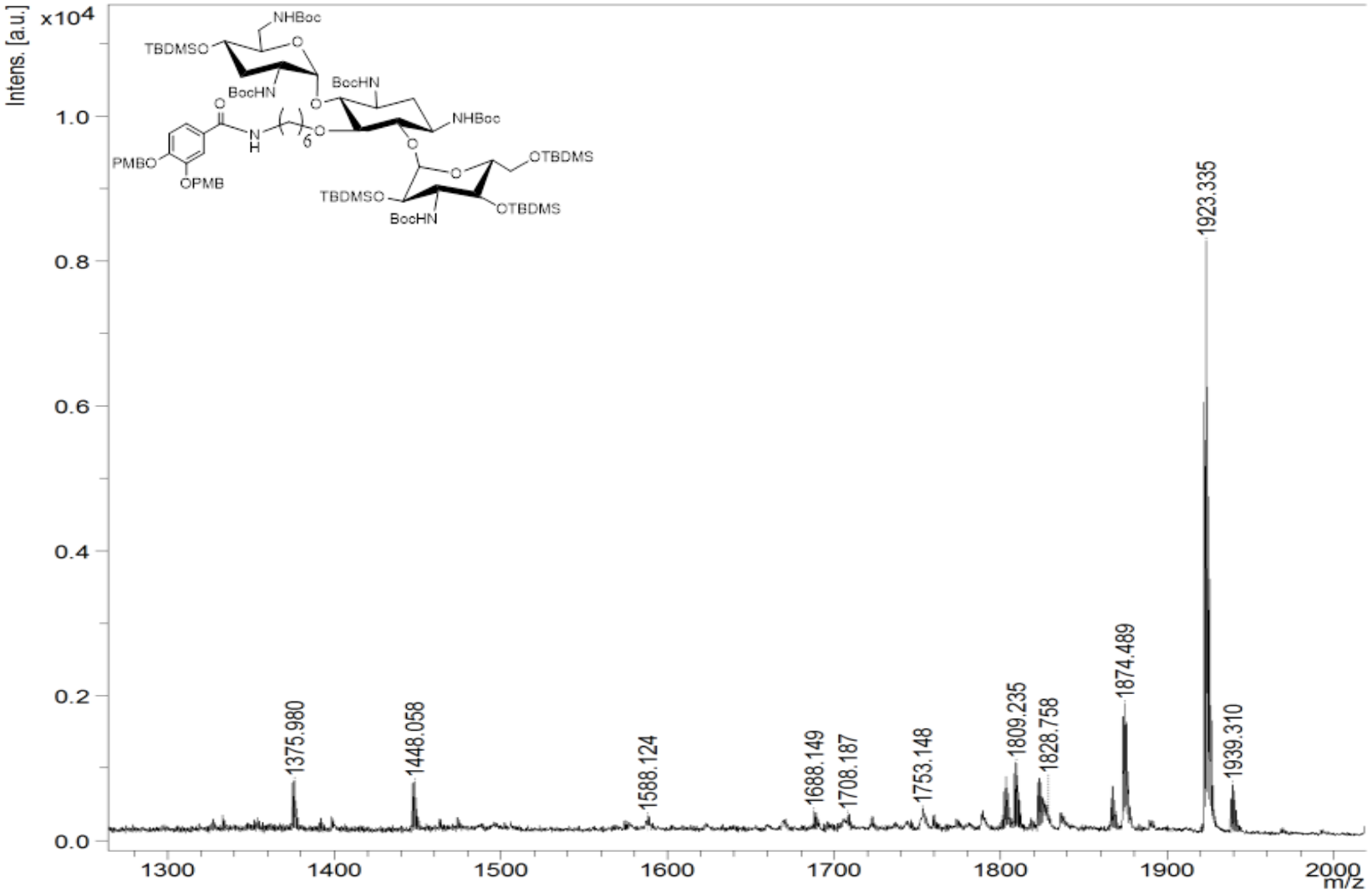

Appendix 44. MALDI Mass Spectrum of **7c**

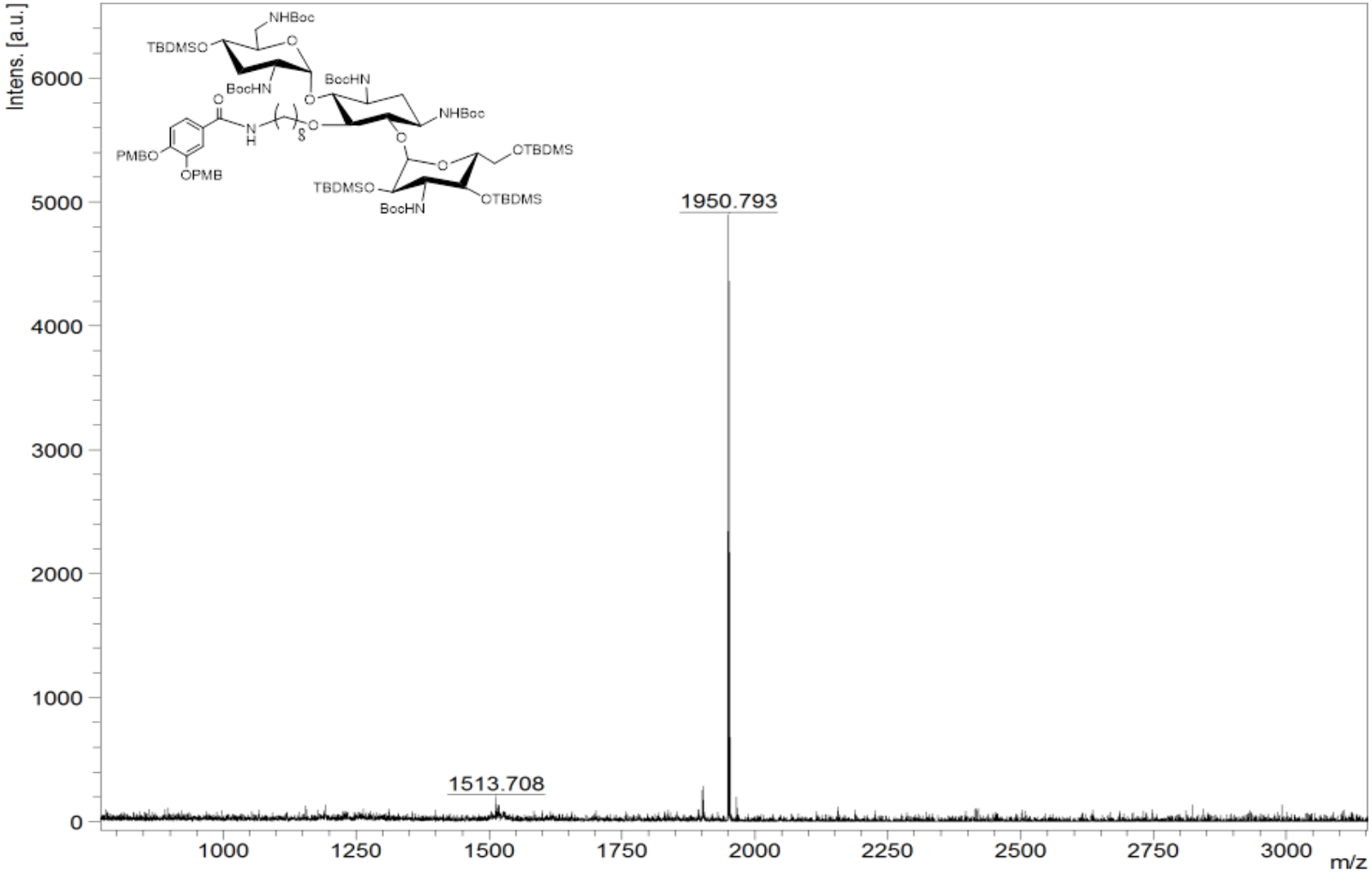

Appendix 45. MALDI Mass Spectrum of **1a**

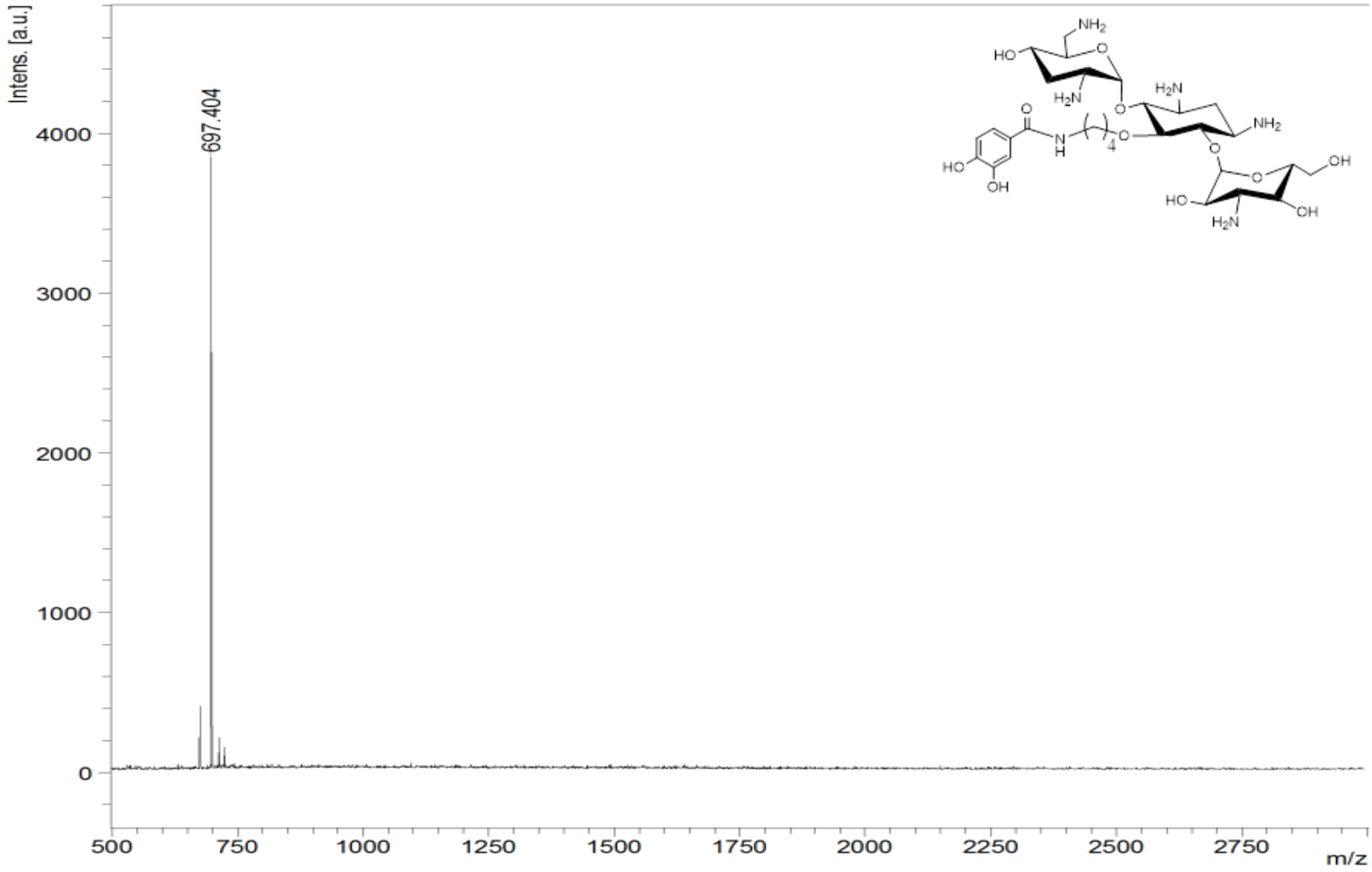

Appendix 46. MALDI Mass Spectrum of **1b**

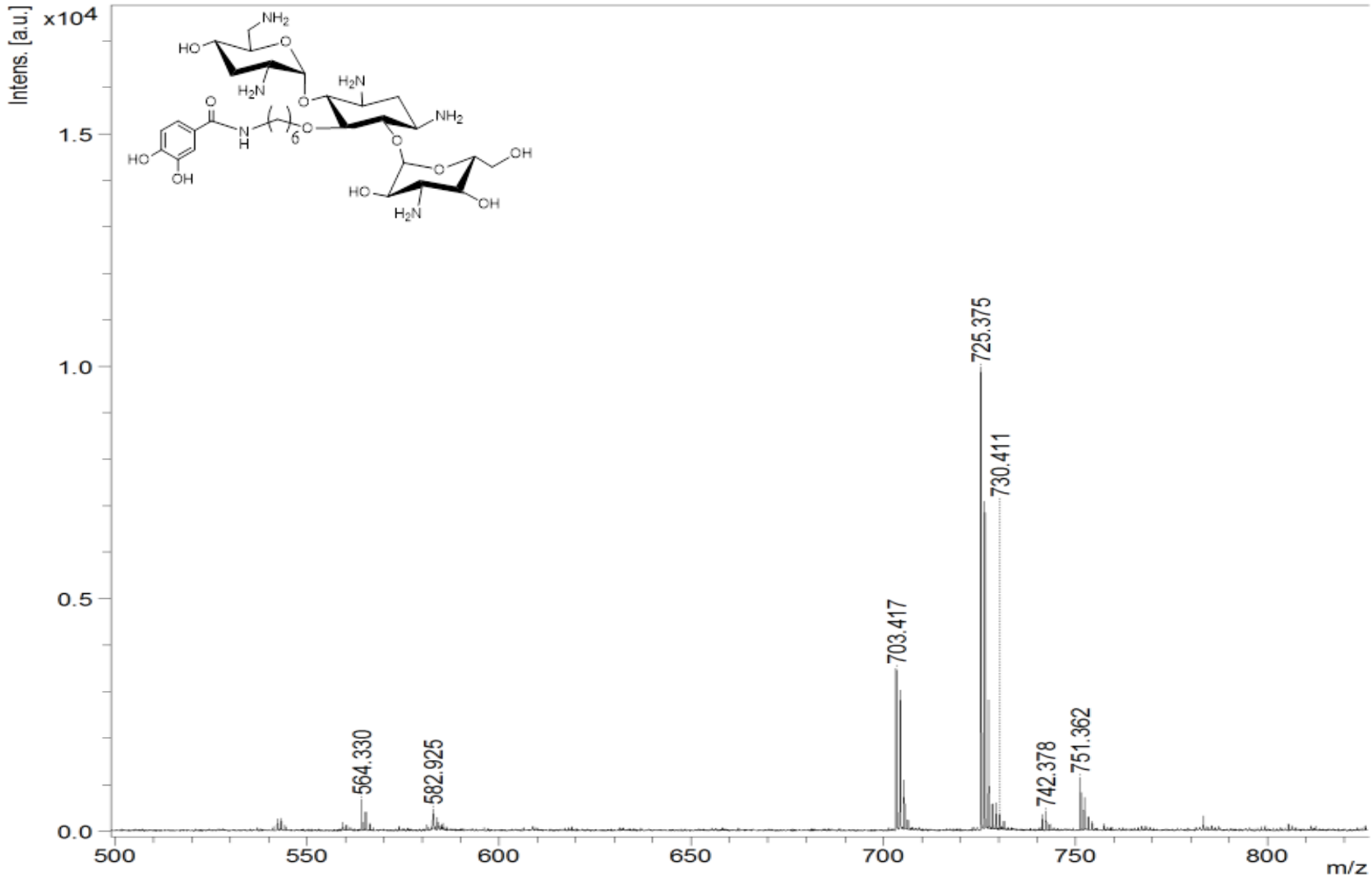

Appendix 47. MALDI Mass Spectrum of **1c**

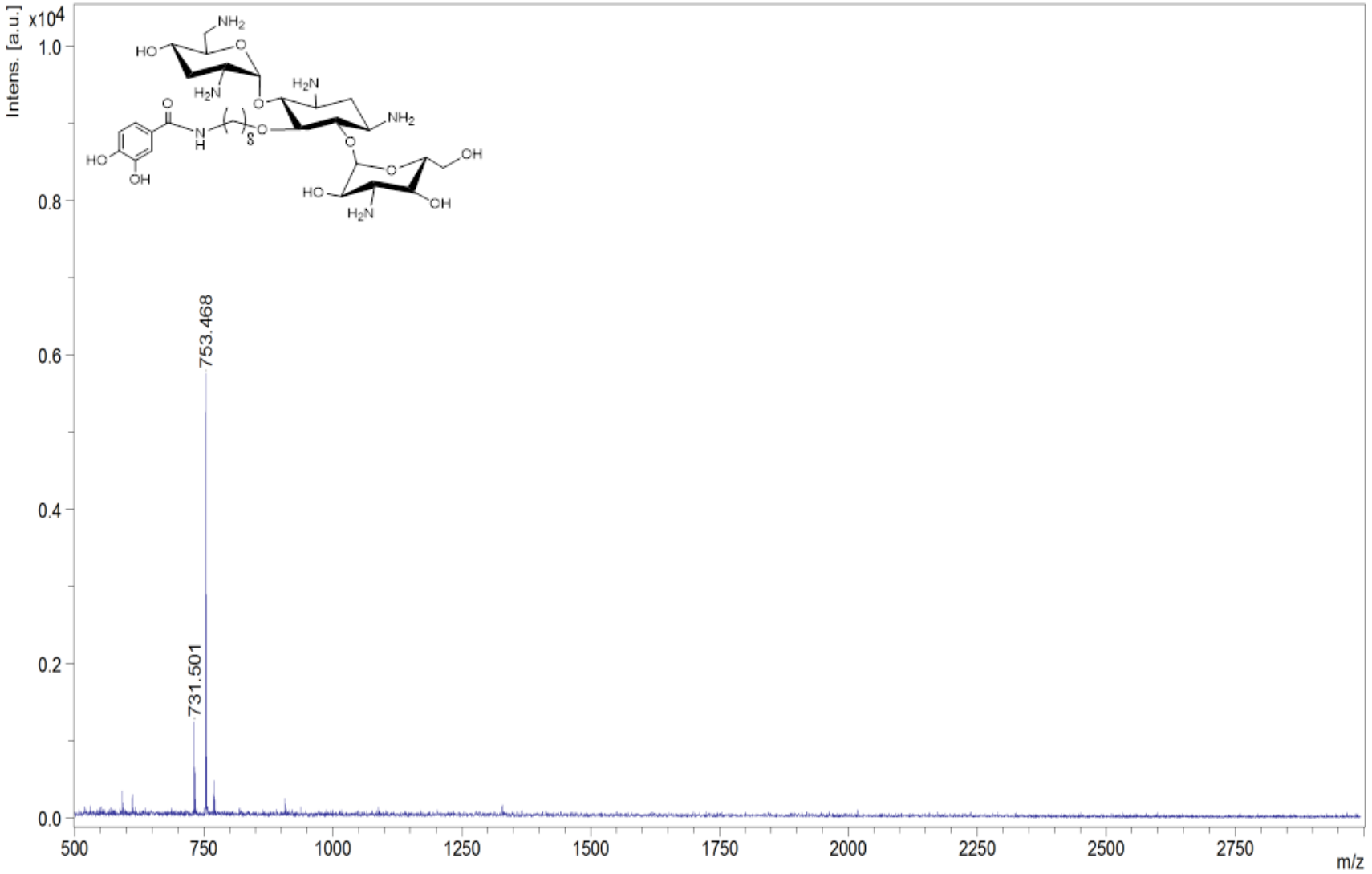

Appendix 48. MALDI Mass Spectrum of **12a**

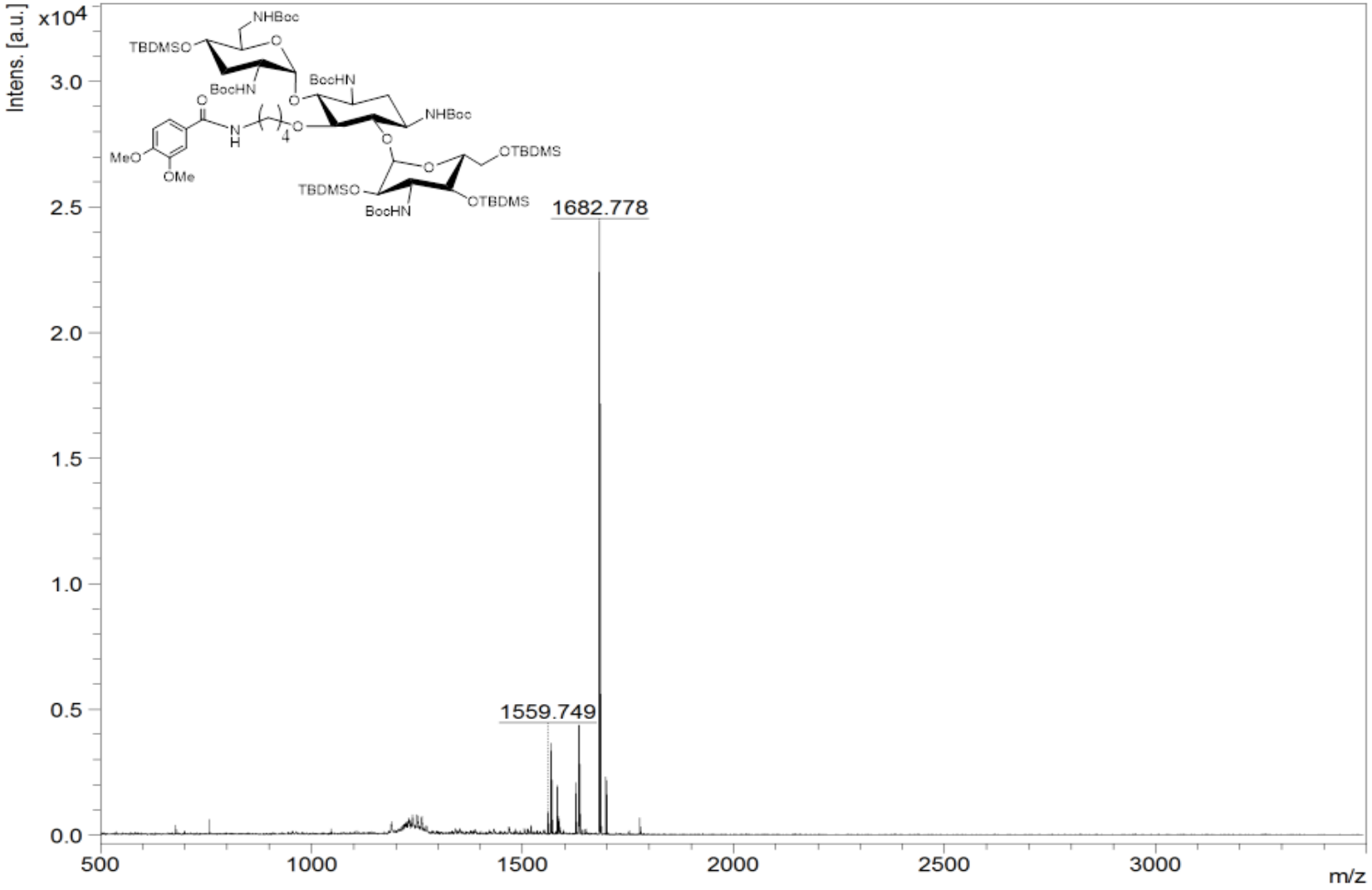

Appendix 49. MALDI Mass Spectrum of **12b**

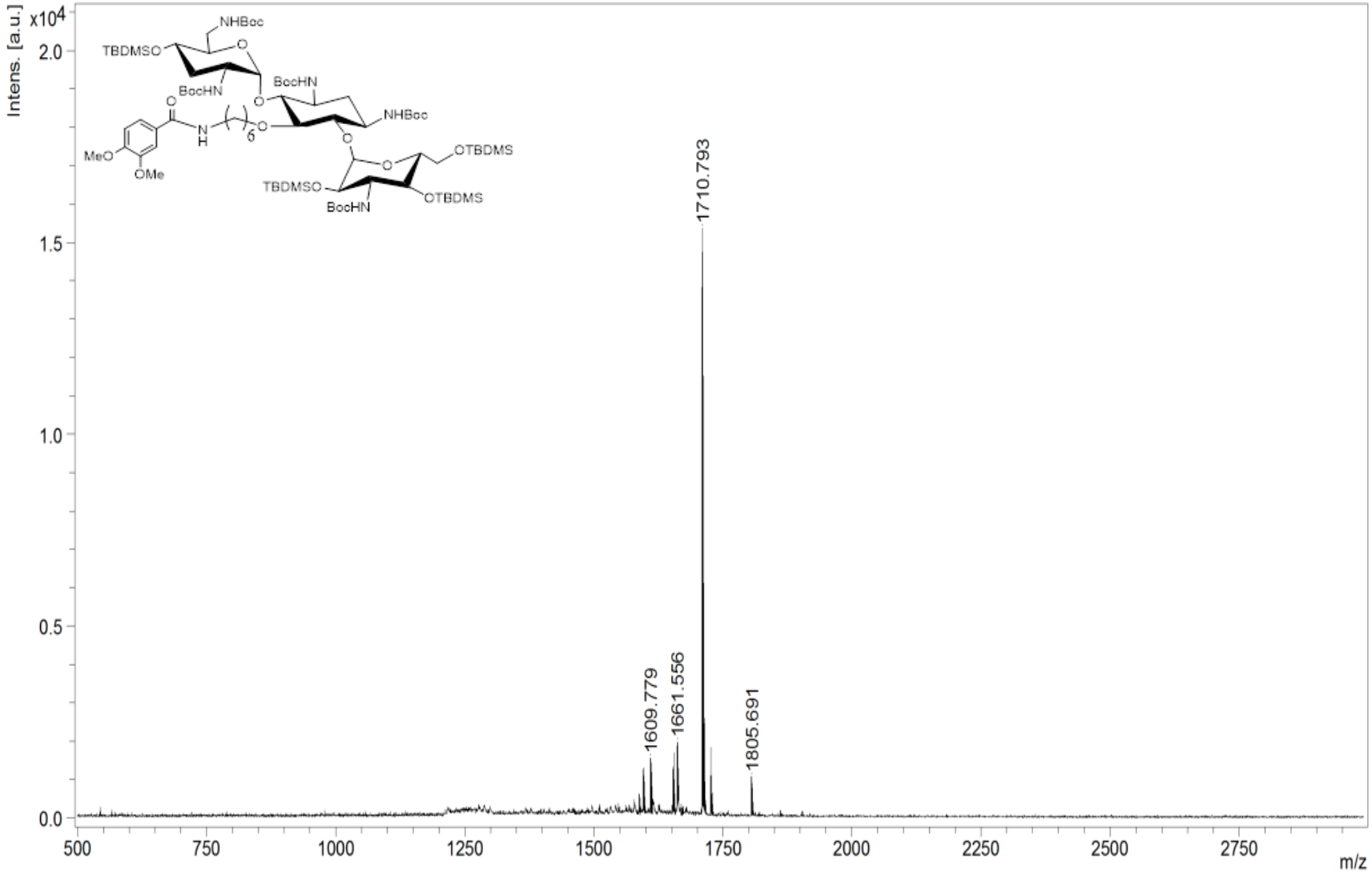

Appendix 50. MALDI Mass Spectrum of **12c**

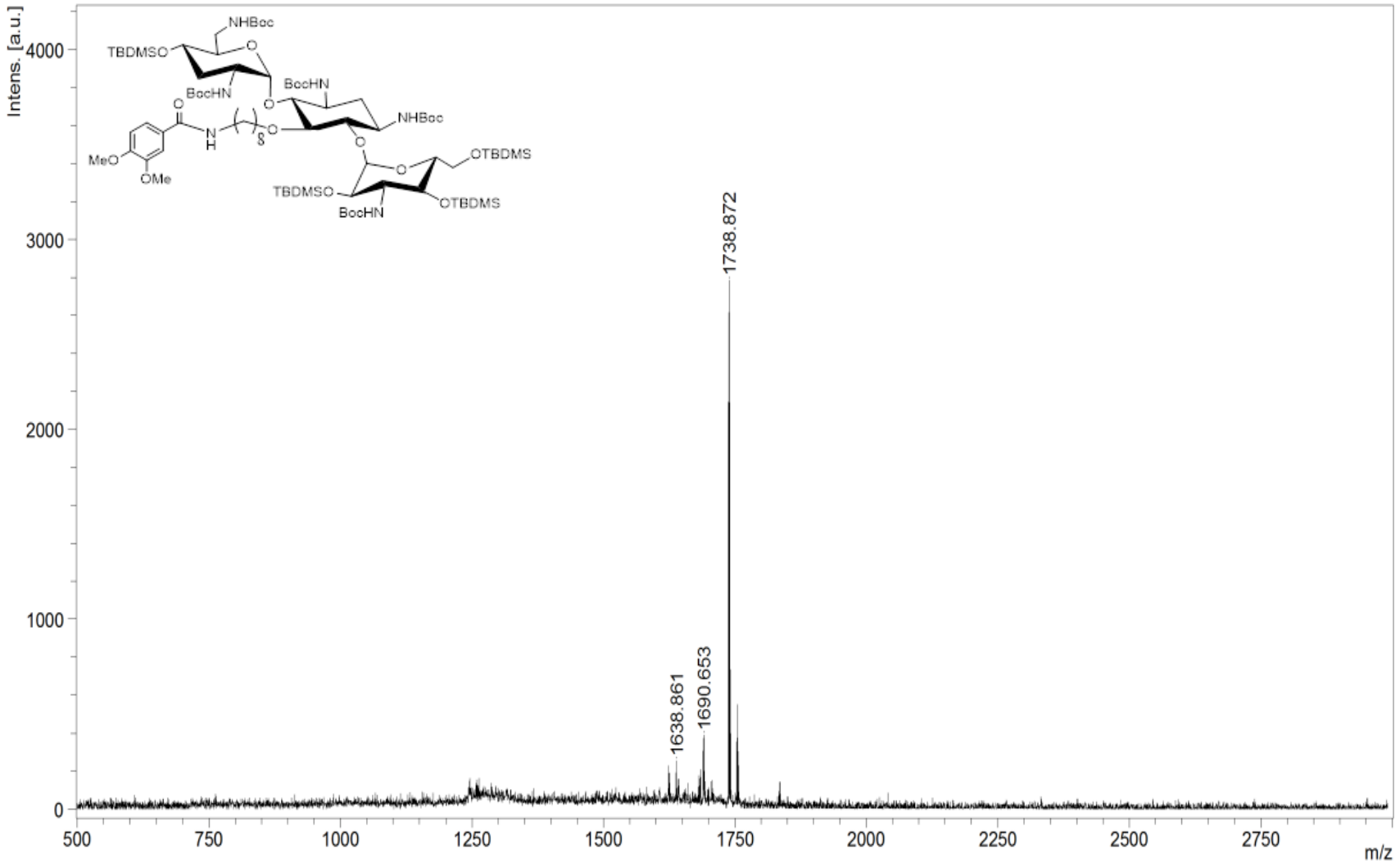

Appendix 51. MALDI Mass Spectrum of **11a**

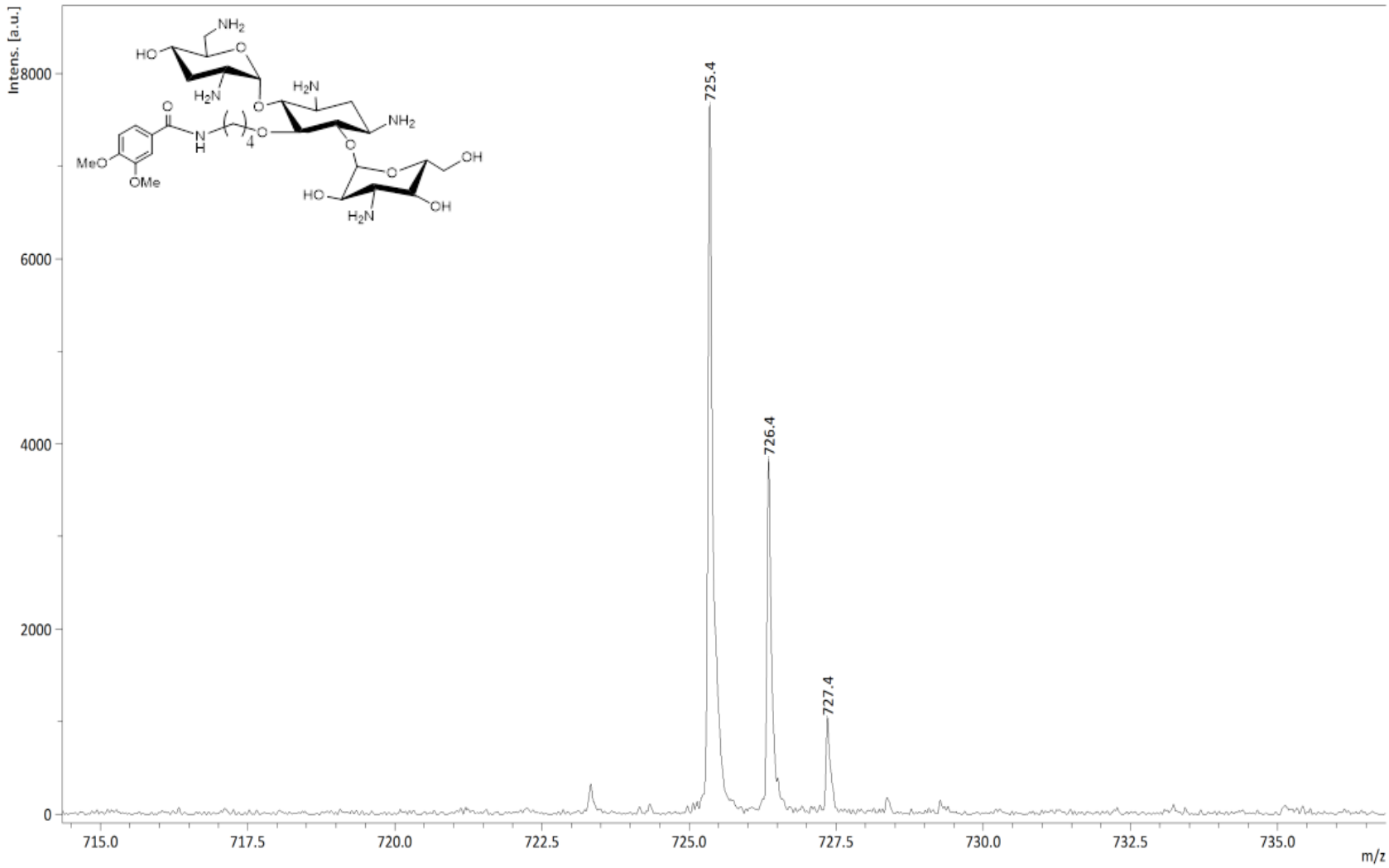

Appendix 52. MALDI Mass Spectrum of **11b**

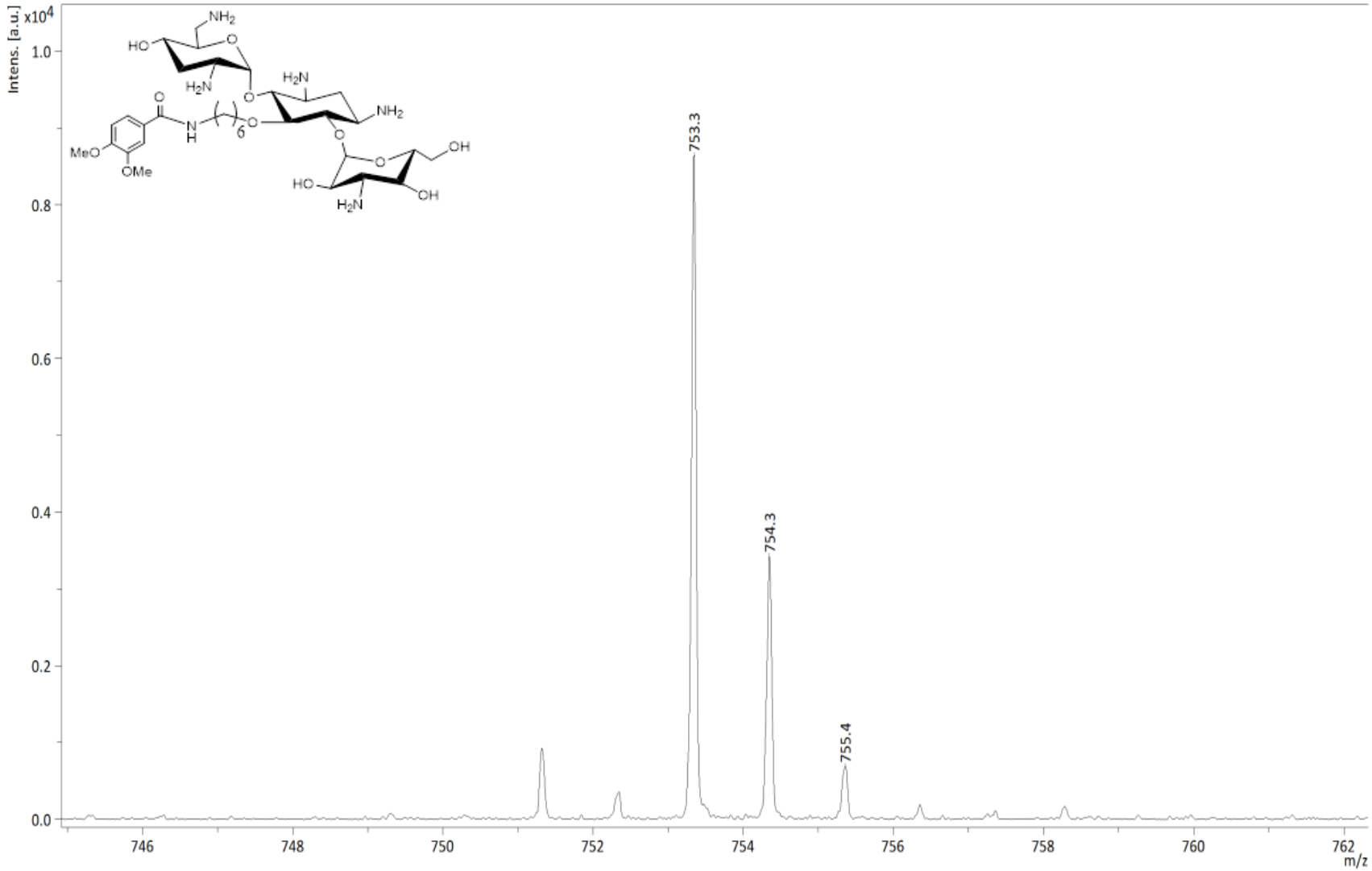

Appendix 53. MALDI Mass Spectrum of **11c**